On Robustness of Motion Control Systems

by

Quang Phuc Ha, B.E. (Ho Chi Minh City), Ph.D. (Moscow)

Department of Electrical and Electronic Engineering

Submitted in fulfilment of the requirements for the degree of
Doctor of Philosophy

The University of Tasmania

December 1996

To the memory of my mother, Trần thị Mười

Statement of Originality

This thesis contains no material which has been accepted for the award of any other degree or diploma in any tertiary institution. To the best of my knowledge and belief, the thesis contains no material previously or written by another person, except when due reference is made in the text.

Quang Phuc Ha

Acknowledgments

Firstly, I would like to thank Dr Michael Negnevitsky for his appreciable guidance and support as a supervisor. I am particularly grateful to Professor Thong Nguyen, Head of the Electrical and Electronic Engineering Department at the University of Tasmania, for his valuable advice and consistent encouragement during my work. I would also like to thank all the academic staff; John Brodie, Peter Watt, Richard Langman, Bob Wherrett, Greg Thé, Dr David Lewis, Dr Habib Talhami, Dr Zhihong Man, and technical staff; Glenn Mayhew, Russell Twining, David Craig, Steven Avery, Alec Cosic, Bernard Chenery, and especially the departmental secretary, Mrs Judy Bonsey, for their kind assistance and friendship. Many thanks go to my fellow postgraduate students, especially Andrew Innes and Richard Andrews for reading through some of my manuscript papers. I thankfully appreciate financial assistance from the Department and the Faculty of Engineering while undertaking my study. Lastly, I would like to extend my thanks and also dedicate this work to my wife, Nguyễn thị Ngọc Hòa, and my father, Hà Thông, for their love, care, and support.

Abstract

Robustness and intelligence are becoming increasingly important in motion control systems. In multi-mass electromechanical systems, the estimation of damping capability and design of robust controllers are among very important aspects. In this thesis, conventional control methods coupled with fuzzy logic and neural networks are used to address these issues.

First, damping capability of multi-mass electromechanical systems is estimated. The maximal damping and complete damping cases are determined using the generalised model for a multi-mass electromechanical system. To eliminate the load variation influence and reduce elastic vibrations, robust modal control is proposed with observer-based state feedback and feedforward compensation.

The use of fuzzy logic dealing with uncertainties is investigated. Good transient performance is obtained, even in the case of changing plant parameters, by fuzzy tuning of the proportional-integral (PI) controller parameters. It is shown that PI controllers with fuzzy tuning can be used in cascade control in a two-mass system. Fuzzy tuning schemes, based on expert knowledge, can be applied to sliding mode control to accelerate the reaching phase and reduce chattering for robustness enhancement.

In robust modal control, taking into account uncertainties in the plant parameters and disturbance rate of change, an improvement of observer robustness is achieved via a fuzzy tuning scheme of the predictive coefficient. Insensitivity to load variations is enhanced by continuously tuning the feedforward compensation coefficients. These fuzzy tuning schemes can be applied to robust modal control of multi-mass systems in the presence of uncertainties. Since tuning is a continuous process, exponential membership functions are used. However, with Gaussian or sigmoidal membership

functions, similar results can also be obtained. Observer robustness achieved by fuzzy tuning is demonstrated to be suitable for incipient fault detection in dynamic systems.

Neural network-based techniques to the problem concerned are also presented. It is shown that a neural net controller can replace the role of a feedforward controller or a fuzzy logic controller. Moreover, a neural net-based controller can be used as a classifier for recognising the error and derivative-of-error patterns, and providing an appropriate control action to improve tracking performance. The proposed controller can be used in a two-mass system without *a priori* knowledge of the plant. Neuro-fuzzy approach is introduced with a feedforward compensation from an observer-based control loop and robust enhancement from a neural network model.

Tuning is a human experience to increase robustness. Fuzzy tuning is shown to be efficient thanks to the possibility of adopting this experience. Neurotuning with learning capability will be a subject for further research.

Contents

Thesis Organisation and List of Publications

Thesis Organisation

This thesis is organised into eight chapters. The first chapter introduces the aim of this work, recent strategies to achieve robust enhancement in motion control systems, and its contributions to the topic. Chapter 2 is devoted to the estimation of damping capability of multi-mass electromechanical systems, considering also the influence of varying electro-magnetic and electromechanical time-constants, and of viscous friction. Chapter 3 is involved in the robust modal control technique covering the design of a combined observer for the states and disturbances, a feedforward controller, and a robust controller. Chapter 4 outlines primary concepts of fuzzy logic and fuzzy logic control and illustrates the design of a fuzzy logic controller for an overhead crane model. Chapter 5 is concerned with the use of fuzzy logic to tune the controller parameters in proportional-integral control and the control action in sliding mode control. Chapter 6 applies fuzzy tuning schemes resulting in explicit expressions to adjust the robust modal control parameters for improving system robustness. Chapter 7 employs the ability of a neural network to approximate an input/output relation, to classify the patterns of error and its derivative, and to learn the inverse dynamics for robust enhancements in motion control systems. Finally, Chapter 8 provides a summary of main results of this thesis and suggests some avenues for future research.

Supporting Publications

This research resulted in a number of journal and conference papers listed below:

1. Journal papers:

[1] Ha, Q.P., "A robust sliding mode controller with fuzzy tuning," *IEE Electronics Letters*, Vol. 32, No. 17, pp. 1626-1628, August 1996.

[2] Ha, Q.P., "PI controllers with fuzzy tuning," *IEE Electronics Letters*, Vol. 32, No. 11, pp. 1043-1044, May 1996.

[3] Ha, Q.P. and Negnevitsky, M., "Robust controllers with fuzzy tuning", *Australian Journal of Intelligent Information Processing Systems*, Vol. 3, No 3, pp. 33-40, 1996.

[4] Alferov, V.G. and Ha, Q.P., "A digital observer device with prediction," *Elektromekhanika*, No 3, pp. 71-76, March 1992. *In Russian.*
English abstract in INSPEC no. 431647, Institution of Electrical Engineers.

[5] Alferov, V.G. and Ha, Q.P., "Using the root-locus method and dominant root pairs for dynamic properties estimation," *Elektrotekhnika*, No 6, pp. 29-32, June 1993. *In Russian.*
English abstract in COMPENDEX no.378346, Engineering Info. Inc.
English translation by Allerton Press, Inc.: *Soviet Electrical Engineering*, 1993, No 6, pp. 35-40.

[6] Alferov, V.G. and Ha, Q.P., "Design of a modal control system for servo drive," *Elektrichestvo*, No 6, pp. 48-54, June 1993. *In Russian.*
English abstract in INSPEC no. 4515187, Institution of Electrical Engineers.

[7] Alferov, V.G. and Ha, Q.P., "DC-motor position drives with robust modal control," *Elektrichestvo*, No 9, pp. 17-24, September 1995. *In Russian.*
English abstract in INSPEC no. 5140507, Institution of Electrical Engineers.

[8] Ha, Q.P. and Alferov, V.G., "On the problem of parameter sensitivity in control system of DC motor position drive," *Elektrichestvo*, No. 1, pp. 47-53, January 1996. *In Russian.*

2. Chapter in a book:

[9] Ha, Q.P. and Negnevitsky, M., "Fuzzy tuning in motion control", in *Applications of Artificial Intelligence in Engineering XI*, Computational Mechanics Publications, R.A. Adey, G. Rzevski, and A. K. Sunol (Eds.), Southampton, UK, 1996, 734p.

3. Refereed international conference papers:

[10] Ha, Q.P. and Negnevitsky, M., "Neural network-based controller for servo drives," in *Proceedings of the IEEE 22nd International Conference on*

Industrial Electronics, Control, and Instrumentation (IECON 96), Taipei, Taiwan, Vol. 2, pp. 904-909, August 1996.

[11] Palis, F., Buch, A., Ladra U., Kurrich R., Ha, Q.P., and Negnevitsky, M., "Robust control using neuro-fuzzy approach", in *Proceedings of the International Conference on Electrical Drives and Power Electronics (EDPE 96)*, Kosice, Slovakia, Vol. 1, pp. 194-198, October 1996.

[12] Ha, Q.P., Negnevitsky, M. and Man, Z., "Sliding mode control with fuzzy tuning", in *Proceedings of the IEEE 4th Australian and New Zealand Conference on Intelligent Information Systems (ANZIIS 96)*, Adelaide, Australia, pp. 216-219, October 1996.

[13] Palis, F., Buch, A., Ladra U., Kurrich R., Ha, Q.P., and Negnevitsky, M.,"Fuzzy and neurocontrol of drive systems with changing parameters and load", in *Proceedings of the European Power Electronics Symposium on Electric Drive Design and Applications (EPE 96)*, Nancy, France, pp. 183-186, June 1996.

[14] Ha, Q.P. and Negnevitsky, M., "Neural network application for the position drive of a swinging load", in *Proceedings of the International Conference on Modelling, Simulation and Optimization (IASTED 96)*, Gold Coast, Australia, May 1996.

[15] Ha, Q.P. and Negnevitsky, M., "Fuzzy tuning in robust modal control," in *Proceedings of the 1st International Discourse on Fuzzy Logic and the Management of Complexity (FLAMOC 96)*, Sydney, Australia, Vol. 2, pp. 160-164, January 1996.

[16] Negnevitsky, M., Ha, Q.P., L.P. Chee and T.H. Ting, "A fuzzy logic controller for an overhead crane", in *Proceedings of the 1st International Discourse on Fuzzy Logic and the Management of Complexity (FLAMOC 96)*, Sydney, Australia, Vol. 2, pp. 171-175, January 1996.

[17] Ha, Q.P. and Negnevitsky, M., "Root locus application for damping capability estimation of multi-mass electromechanical systems," in *Proceedings of the IEEE 21st International Conference on Industrial Electronics, Control, and Instrumentation (IECON 95)*, Orlando, USA, vol. 1, pp. 633-638, November 1995.

[18] Ha, Q.P. and Negnevitsky, M., "A digital predictive observer for incipient fault detection," in *Proceedings of the IEE 3rd International Conference on*

Advances in Power System, Operation & Management (APSCOM 95), HongKong, vol. 1 , pp. 183-188, November 1995.

[19] Ha, Q.P. and Negnevitsky, M., "A robust modal controller with fuzzy tuning for multi-mass electromechanical systems," in *Proceedings of the IEEE 3rd Australian and New Zealand Conference on Intelligent Information Systems (ANZIIS 95)*, Perth, Australia, pp. 214-219, November 1995.

[20] Ha, Q.P. and Negnevitsky, M., "New trends in control theory and their reflection in electrical engineering education," in *Proceedings of the Pacific Region Conference on Electrical Engineering Education (PRCEEE 95)*, Victoria, Australia , pp. 109-112, February 1995.

[21] Ha, Q.P., Negnevitsky, M., and Palis, F., "Cascade PI controllers with fuzzy tuning", to appear in *Proceedings of the 6th IEEE International Conference on Fuzzy Systems (FUZZ-IEEE 97)*, Barcelona, Spain, July 1997.

[22] Ha, Q.P., Negnevitsky, M. and Man, Z., "Dominant pole-based controller for maximal damping of multi-mass systems", to appear in *Proceedings of the 2nd Asian Control Conference (ASCC 97)*, Seoul, Korea, July 1997.

[23] Man, Z., Yu, X. H., and Ha, Q.P., "Adaptive control using fuzzy basis function expansion for SISO linearisable nonlinear systems", to appear in *Proceedings of the 2nd Asian Control Conference (ASCC 97)*, Seoul, Korea, July 1997.

[24] Man, Z., Yu, X.H., and Ha, Q.P., "A study of uncertainty bound for rigid robot control systems", to appear in *Proceedings of the 2nd Asian Control Conference (ASCC 97)*, Seoul, Korea, July 1997.

[25] Ha, Q.P. and Negnevitsky, M., "Continuous variable structure systems with fuzzy tuning", submitted to *the 5th IEEE Australian and New Zealand Conference on Intelligent Information Systems ANZIIS'97* , Dunedin, New-Zealand, November 1997.

4. Refereed national conference papers:

[26] Ha, Q.P., "A neural network-based controller for multi-mass electromechanical systems," in *Proceedings of the Australian Universities Power Engineering Conference (AUPEC 96)*, Melbourne, Australia, Vol. 1, pp. 31-36, October 1996.

[27] Ha, Q.P., "Root locus method application for damping capability estimation of multi-mass electromechanical systems," in *Preprints of the CONTROL'95 Conference*, Melbourne, Australia, vol. 1, pp. 255-259, October 1995.

[28] Ha, Q.P. and Palis, F., "Fuzzy logic application in a robust modal controller for position drives," in *Proceedings of the 30th Universities Power Engineering Conference (UPEC 95)*, London, UK, vol.1, pp. 85-89, September 1995.

[29] Ha, Q.P., "A digital predictive observer with fuzzy tuning for multi-mass electromechanical systems," in *Proceedings of the Australian Universities Power Engineering Conference (AUPEC 95)*, Perth, Australia, vol. 3, pp. 422-427, September1 995.

[30] Ha, Q.P., "A dynamic feedforward controller with fuzzy tuning for electromechanical systems," in *Proceedings of the Australian Universities Power Engineering Conference (AUPEC 95)*, Perth, Australia, vol. 3, pp. 428-433, September 1995.

[31] Ha, Q.P. and Alferov, V.G., "Robust modal controller for position drives," in *Preprints. of the Electrical Engineering Congress (EEC 94)*, Sydney, Australia, pp. 609-614, November 1994.

[32] Alferov, V.G., Ha, Q.P., and Khusainov, R.M., "Drive control systems with a disturbance observer," in *Industrial application of electric drives on the perspective element base*, N.F. Ilynsky (Ed.), Moscow, Russia, pp. 93-99, May 1992. *In Russian.*

Chapter 1

Introduction

The emergency of motion control field started since 1970's through the application of control theory to power electronics by the use of microprocessors to drive electrical motors. Motion control is currently accepted as an established and prominent field of technology covering control engineering, computer science and mechanical engineering (Harashima [1]). Two main issues in motion control systems are robustness against parameter variations and disturbances, and the intelligent capability to adjust the control system itself to environment changes and task requirements. This thesis is an attempt to combine conventional methods and recently developed techniques, namely fuzzy logic and neural network, to address the problem of robustness enhancement in electromechanical systems or, in general, dynamic systems. Towards that aim some control strategies are involved as follows.

1.1 Robust Control

Robustness is the property of a dynamic system being insensitive to significant plant uncertainties. Dorato in [2] noted that although solutions to this classical control problem have been proposed for a long time, the actual term "robust control" first appeared in a conference paper by Davidson in 1973. Robust controllers have been explored extensively in literature in the last two decades (Dorato *et al.* [3], Tsypkin [4]). Robust control has been widely applied to enhance performance of dynamic systems subject to any sources of uncertainty and changing environments. Various methods of modern control theory have been developed for the analysis and design of these systems. In addition to impressive progress in the theory and applications of

optimal control and adaptive control, since the middle of 1970's intensive efforts have been dedicated to robust control which deals with the design of fixed controllers. Robust stability of dynamic systems has been of interest since the seminal paper by Kharitonov [5]. The most popular in robust control is the H-infinity method, originated by Zames in 1979, based on frequency optimisation (Kwakernaak [6]). The variable structure system with sliding-mode method, first introduced by Emelyanov [7] and then developed by Utkin [8], is also effective for robust control. Robust control methods are now useful for applications because of the prolific computational resources for implementing control algorithms and associated electronic devices. As an application to electromechanical systems, robust modal control proposed by Ha [9], a state feedback method, is under investigation in this thesis. Moreover, with a partially known environment some artificial intelligent tools are incorporated to the control system to improve robustness.

1.2 Intelligent control

Qualitatively, a system which includes the ability to sense its environment, process the information to reduce uncertainty, and generate and execute control action for several situations constitutes an intelligent control system (Kumar & Mani [10]). Advances in the areas of artificial intelligence have demonstrated a potential for new approaches to the control of complex systems under changing environments and performance criteria, unmeasurable disturbances and component failure. Artificial intelligence tools, such as expert system, fuzzy logic, and neural network are expected to usher a new area in motion control in the coming decades. In the early 1970's a way of structuring software that closely matches the human thinking process, called "expert system" was born and has found wide applications in many areas (Bose [11]). In a real-time expert system-based control the input signals, accessed from the sensors, are processed and control signals for the system are generated. As to "fuzzy logic", since the seminal paper by Zadeh on fuzzy sets in 1965 [12], fuzzy systems have developed explosively, attracting many researchers from around the world. One of the landmark in this development is the genesis of fuzzy logic control in 1972 (Chang & Zadeh [13]). The key principle underlying fuzzy logic control is based on a logical model which represents the thinking process that an operator might go through to control the system manually. Fuzzy logic control can be considered as one of the intelligent techniques where engineering is reflected in the controllers. The viability of fuzzy logic control has been demonstrated through widespread applications (Schwartz *et al.*

[14]). On the other hand, much attention was recently focused on a new branch of artificial intelligence, called artificial neural network or "neural network." The artificial neural network tends to simulate the biological neural network by electronic computation circuits. The neural network technology was gradually evolving since the 1950's but only since the beginning of the 1990's has this artificial intelligence tool captivated the attention of practically the whole scientific community (Widrow & Lehr [15]). Indeed, its field of applications is covering process control, diagnostics, identification, character recognition, robot vision, flight scheduling, etc. (Bose [11]). As new trends in control theory, these artificial intelligence tools have found their way into tertiary institutions for engineering education (Ha & Negnevitsky [16]) and are believed to touch almost every engineering application by the early next century. In this thesis, fuzzy logic and neural network are used for the purpose of tuning the controller parameters or providing an appropriate control action through a learning process to improve robustness and tracking performance of servo systems.

1.3 Robustness via Fuzzy Tuning

Controller parameter tuning is a popular engineering experience. Human skill is normally utilised to tune the controller parameters to achieve required control performances. In the design of a knowledge-based feedback controller it is desirable to embed the expert skill of the designers so that the controller can make decisions on the choice of appropriate control algorithm. Till now, the proportional-integral-derivative (PID) controllers have been the most popular in industry. For these controllers, autotuners, which include methods of extracting process dynamics from experiments and control design methods, have been commercially available since 1981 (Astrom *et al.* [17]). The application of auto-tuning formulae has brought intelligent insights into the conventional controllers. In the field of electrical drives, proportional-integral (PI) controllers with the auto-calibration method, inspired by the symmetric optimum principles, can be used to tune the controller parameters (Voda & Landau [18]). Based on a point of the plant frequency characteristics, autotuning or auto-calibration of controller parameters in the presence of uncertainties is effective provided that there is knowledge of the process involved. Truly effective autotuning schemes for conventional controllers, in general, are restricted to a linear process or a class of nonlinear process with the presumed range of operation. Using the state space technique, a robust modal controller (Ha & Alferov [19]) with fixed parameters cannot cope well with a large range of uncertainty or nonlinear dynamics. In order to

account for sensor noise, model uncertainties, and severe nonlinearity, the linguistic characteristics of fuzzy logic with some engineering heuristics provide a good approach to the uncertainty problem (Tseng & Hwang [20]). In this thesis, tuning the conventional controllers is accomplished through fuzzy approximate reasoning techniques with some tuning schemes applied for continuously changing the coefficients of a cascaded PI controller, a digital predictive observer, a dynamic feedforward controller, and a robust modal controller (Ha & Negnevitsky [21]), or changing the control action in a sliding mode controller (Ha *et al.* [22]).

1.4 Neural Network Application for Control Performance Enhancement

In recent years there has been a growing interest in applying artificial neural networks to dynamic systems identification, prediction and control. The use of neural networks is characterised by the capability of learning from examples or patterns. Thus, it enables, through a training process, modelling and predicting the behaviour of complex systems, and providing an appropriate control action to achieve desired performance, without *a priori* information about the systems' structures or parameters. Neural network approaches can be used to a variety of applications in identification, prediction and control systems (Pham & Xing [23]). The advantages of a neural network controller over a conventional one are that (i) a much larger amount of sensory information can be efficiently used in planning and executing a control action, (ii) the collective processing ability to respond more quickly to complex sensory inputs, and the most important, (iii) a good adaptation can be achieved through learning (Psaltis *et al.* [24]). Almost all the neural network controllers could be regarded as inverse controllers as they are all based on modelling the inverse dynamics of the plant. The well-established structures for neural network controllers using an inverse model are supervised control (Werbos [25]), direct inverse control (Miller *et al.* [26]), model reference control (Narenda & Parthasarathy [27]), and internal model control (Hunt & Sbarbaro [28]). In addition to these inverse model-based controllers, there are also other neural controllers originating from conventional approaches, for example, those based on variable structure technique (Colina-Morles & Mort [29]), the robust control strategy (Rovithakis & Christodoulou [30]), the model predictive method (Evans *et al.* [31]), and the parallel adaptive PID-like controller (Lee *et al.* [32]). In this thesis a neural network approach is used for improving robust performance of motion control systems on the basis of an observer-based controller (Palis, Ha *et al.* [33]). Another neural network-based controller is

proposed here for not modelling the system inverse dynamics but classifying the patterns of the control error and its derivative, and correspondingly, providing an appropriate control action to achieve a good tracking performance (Ha & Negnevitsky [34]).

1.5 Thesis contributions

Throughout this thesis, issues relating to robustness of motion control systems are addressed. First, the estimation of damping capability of multi-mass electromechanical systems is addressed. The critical values of the mass ratio are found. The cases of maximal damping and complete damping are determined. The influence of parameter variations and viscous friction is investigated by using multi-parameter root loci. It is shown in Ha & Negnevitsky [35] that damping capability is more affected by variations in viscous friction on the load shaft than on the motor shaft. For a design procedure to eliminate the load variation influence and reduce elastic vibrations a robust modal controller is proposed by Ha & Alferov [20], [36] with feedback signals from the system states and observer-based feedforward compensation form the disturbance estimate. The use of fuzzy logic as a powerful tool dealing with uncertainties is investigated through explicit expressions of fuzzy tuning schemes. The reference response is well-damped with adequately fast dynamics and the maximum deviation of the disturbance response is reduced, even in the case of changing plant parameters, by using a fuzzy tuning scheme for conventional PI controllers (Ha & Negnevitsky [37]). It is shown in Ha *et al.* [38] that PI controllers with fuzzy tuning can be used with cascade control principles in multi-mass systems. Taking into account uncertainties in the plant parameters and unknown input rate of change, an improvement of observer robustness is achieved via a fuzzy tuning scheme of the predictive coefficient (Ha [39]). Insensitivity to load variations is enhanced with the dynamic feedforward compensation coefficients continuously tuned by fuzzy logic (Ha [40]). These fuzzy tuning schemes can be applied to robust modal control (Ha & Negnevitsky [41]) or sliding mode control (Ha *et al.* [22]) of multi-mass electromechanical systems for vibration suppression and load rejection in the presence of plant parameter and load uncertainties. Since tuning is a continuous process exponential membership functions are used. However, with Gaussian or sigmoidal membership functions, similar results can also be obtained, as reported in Ha & Negnevitsky [42]. Robustness achieved through a fuzzy tuning scheme for an unknown input observer is demonstrated to be suitable for incipient fault detection in

power system, eg. in a synchronous generator (Ha & Negnevitsky [43]). Neural network approaches to the problems involved are preliminarily presented at the closing of the thesis. It is shown that the a neural network can replace the role of a feedforward controller in Palis, Ha *et al.* [33] or a fuzzy logic controller in Ha & Negnevitsky [34]. In addition, a neural net-based controller can be used as an classifier for recognising the control error and derivative-of-error patterns and providing an appropriate control action to improve tracking performance (Ha & Negnevitsky [44]). The proposed controller can be used in a multi-mass system without a priori knowledge of the controlled plant (Ha [45]). For further investigation, a neuro-fuzzy technique might be a solution to the problem of extracting from the error signal all the necessary information for a high quality control strategy regardless of the plant structure and changing environments. It is believed that an architecture for neurotuning may bring intelligent features into the tuning process and thus, make dynamic systems cope well with any uncertain factors or severe nonlinearity. Tuning is a human experience to increase robustness. Fuzzy tuning is shown to be efficient thanks to the capability of adopting this experience. Neurotuning may be a subject for further research.

Chapter 2

Multi-Mass Electromechanical Systems: Damping Capability Estimation

In industrial applications, many electromechanical systems can be modelled as consisting of a motor and a load connected with a flexible shaft. A multi-mass system, in practice, can be the model of a rolling mill, a flexible link arm, a large-scale space structure, a launch vehicle during the ascent phase, an automobile wheel steering system, or a mass-spring-damper system, in general. Damping analysis and torsional oscillation suppression in an electromechanical system (EMS) are classical problems. However, control issues of flexible structures have gained increasing attention, especially in space technology where recent efforts are required to maintain high precision positioning of ever lighter and more flexible structures (Gawronski [46]), and in robotics where the control of multi-inertia manipulators will be an important problem in the future of motion control (Lin [47]). Thus, the analysis and design of these systems are timely and worth being investigated. The thesis starts with the estimation of damping capability of electromechanical systems served as the common plant for some controller design procedures discussed in the following chapters.

2.1 Introduction

Special interest has recently been paid to EMS damping capability (see, e.g., Klepikov & Samarskii [48], Alferov & Ha [49], and Dhaouadi *et al.* [50]). In some industrial applications torsional loads on electrical drive systems may cause undesirable vibrational effects and lower the dynamic performance of the drive. The suppression of elastic vibration is a challenging problem. In many cases this vibration is not only undesirable but also the origin of system instability. Damping factor of these systems should be taken into account when designing a controller. Analysing the mutual effects of the electrical and mechanical parts on damping issues of an

electromechanical system were an interesting subject in Soviet literature in 1980's (see, e.g., Kljuchev [51], Ol'khovikov *et al.* [52], and Zadarozhny & Zemljakov [53]). The conventional approach to the estimation of EMS dynamics relies on the location of the roots of the system characteristic equation in the complex plane. While approximate relations between these roots and the system parameters are developed in Ol'khovikov *et al.* [52], the calculated results are valid only at certain values of the damping factor. The interaction of electrical and mechanical parts of EMS's is analysed via the root distribution of the characteristic equation in Zadarozhny & Zemljakov [53]. However, the influence of the parameter variation on the roots of the characteristic equation is not considered. The frequency response is used in Klepikov & Samarskii [48] to explain the EMS dynamic properties but the parameters at the critical case are not directly determined. In Alferov & Ha [49], the analytical relations between the optimal time-constants and the mass ratio are given, and the root dependence on parameter variation is examined using the classical Evans root locus method. However this application is limited to the two-mass case without considering friction. In this chapter the proposed technique is extended to a general n-mass system with the determination of the system parameters at the critically-damped case. First, the general model for an n-mass electromechanical system is constructed. By using the dynamic stiffness concept proposed by Kljuchev [54], the motor's electromagnetic process is described by a first order transfer function. The characteristic equation of a generalised multi-mass EMS is obtained in dimensionless space. By introducing some definitions and identifying the coefficients of the characteristic equation, sufficient conditions for the maximal damping case are derived. The root locus of the two-mass, three-mass EMS's are provided at different values of the mass ratio to confirm the mathematical analysis. Friction on the motor shaft and load shaft is taken into account using the multi-parameter root loci. Damping capability of some practical multi-mass EMS's are analysed for illustration. The results are based mainly on Ha & Alferov [49], Ha [55], and Ha & Negnevitsky [35].

2.2 Generalised model for a multi-mass electromechanical system

Motion control systems can be defined as high-performance servo drives for rotational or translational control of torque, speed, and/or position. For such purposes there are DC motor drives, variable-reluctance stepper drives, and brushless DC motor drives available at present. In [56], Lorenz *et al.* noted that the principle of field

orientation, first evolved in the early 1970's in Germany, has allowed the induction motor to move beyond the variable-speed control of volts per hertz drives, and bridged the difference between an AC servo and a DC servo characteristics. For example, with field-oriented control (vector control) an AC servo motor can be designed to have the same transfer function as DC servo motors (Harashima [1]). This approves the Soviet electromechanical engineering viewpoint of describing the electromagnetic process in a generalised model using the dynamic stiffness of a speed-torque characteristics.

2.2.1 Dynamic stiffness of a linearised speed-torque characteristics

Consider the well-known differential equation of a DC motor:

$$R_a i_a + L_a \frac{di_a}{dt} = K_b \omega, \tag{2.1}$$

where i_a and ω are the motor current and speed, and R_a, L_a, and K_b are the armature circuit resistance, inductance, and motor back emf constant, respectively. With the developed torque $T = K_t i_a$, where K_t is the motor torque constant, the dynamic relation speed-torque can be represented by the following transfer function:

$$G_m(s) = \frac{T(s)}{\omega(s)} = \frac{\beta}{1 + T_a s}, \tag{2.2}$$

where $T_a = \frac{L_a}{R_a}$ is the motor electromagnetic time-constant, $\beta = \frac{K_b K_t}{R_a}$ is the stiffness of the motor speed-torque characteristics, and s is the Laplace operator. Since the DC motor speed-torque characteristics is linear, the value of β is found as

$$\beta = \left| \frac{dT(\omega)}{d\omega} \right|. \tag{2.3}$$

In the same way, by linearising the motor speed-torque characteristics around its operation point P, as shown in Figure 2.1, and using the dynamic stiffness β of the linearised speed-torque characteristics (2.3), the general model for a motor electromagnetic process can be given by Kljuchev [54]:

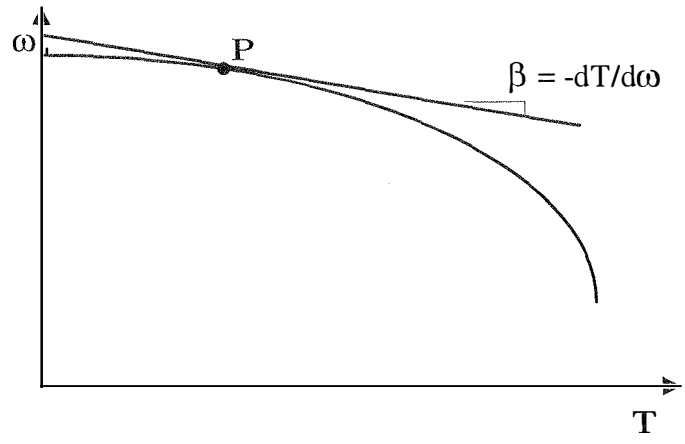

Figure 2.1. Dynamic stiffness of a linearised speed-torque characteristics.

$$G_m(s) = \frac{\Delta T(s)}{\Delta \omega(s)} = \frac{\beta}{1 + T_e s}, \tag{2.4}$$

where T_e is the motor electromagnetic time-constant.

2.2.2 An n-mass electromechanical system model

In some fields of robotics such as space robot manipulators, robust control techniques are required to obtain a stable and quick motion response. Since the robot total weight is limited due to the allowable transport capability of space rockets, the stiffness of the manipulator flexible structures is reduced and its motion tends to vibrate because of the system small stiffness. To simplify the mathematical description, a model of multiple mass spring system of Figure 2.2 is introduced for modelling the dynamic behaviour of a flexible link arm. An industrial steel rolling mill can be represented by the same structure. The state equations describing such a system can be written as (a dot denotes the time derivative):

$$\dot{T} = \frac{1}{T_e} T + \frac{\beta}{T_e} (\omega_{ref} - \omega_1),$$

$$\dot{\omega}_1 = \frac{1}{J_1} (T - T_{12}),$$

$$\dot{T}_{12} = K_{12} (\omega_1 - \omega_2),$$

$$\begin{aligned}
\dot{\omega}_2 &= \frac{1}{J_2}(T_{12} - T_{23}), \\
&\cdots\cdots \\
\dot{T}_{n-1,n} &= K_{n-1,n}(\omega_{n-1} - \omega_n), \\
\dot{\omega}_n &= \frac{1}{J_n}(T_{n-1,n} - T_L),
\end{aligned} \tag{2.5}$$

where J_1 and ω_1 are the motor moment of inertia and speed,

J_i and ω_i, $(i = 2,\ldots,n)$ are the i -th moment of inertia and speed,

$K_{i,i+1}$ $(i = 1,\ldots,n-1)$ are the stiffness of the coupling shaft between the i -th and $(i+1)$-th masses, and

T, T_L, and $T_{i,i+1}$ are the motor torque, disturbance torque, and elastic torque (or reaction torque in Nomura *et al.* [57]) of the i -th shaft, respectively. Note that all the viscosities B_i $(i = 1,\ldots,n)$ of the i -th mass, and $B_{i,i+1}$ $(i = 1,\ldots,n-1)$ of the i -th shaft are omitted here, they will be considered in Section 2.6. The block diagram an n -mass electromechanical system is shown in Figure 2.3 in the case neglecting the load disturbance $(T_L = 0)$. The compensation of the load torque influence, e.g. arm disturbance rejection in a multi-mass resonant system (Matsuoka *et al.* [58]), will be discussed in the following chapters.

2.3 EMS characteristic equation in dimensionless space

In this section the characteristic equation of the structure of Figure 2.3 is derived in dimensionless space.

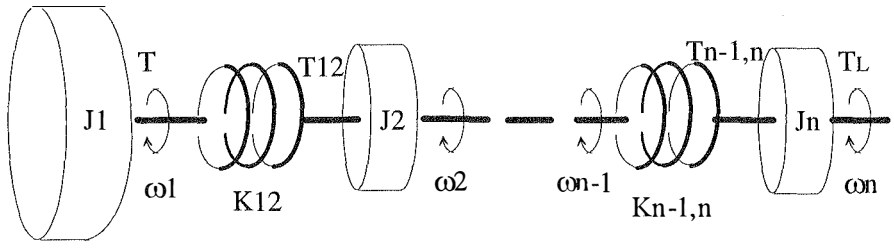

Figure 2.2. Multiple mass spring system.

2.3.1 EMS characteristic equation

Consider first the two-mass system. An equivalent manipulation gives the simplified block diagram, as shown in Figure 2.4, with

$$G_1(s) = \frac{\omega_1(s)}{T(s)} = \frac{T_{12}(s)}{T(s)} \Big/ \frac{T_{12}(s)}{\omega_1(s)} = \frac{1}{J_1 s} \frac{s^2 + \Omega_N^2/\gamma}{s^2 + \Omega_N^2}, \tag{2.6}$$

where

$$\Omega_N = \left(K_{12} \frac{J_1 + J_2}{J_1 J_2} \right)^{1/2} \tag{2.6a}$$

is the two-mass system natural resonant frequency, and

$$\gamma = \frac{J_\Sigma}{J_1} = \frac{J_1 + J_2}{J_1} \tag{2.6b}$$

is the mass ratio in this case. The characteristic equation of the system of Figure 2.4 is found as

$$\Delta(s) = 1 + T_e s + \beta G_1(s) = 0. \tag{2.7}$$

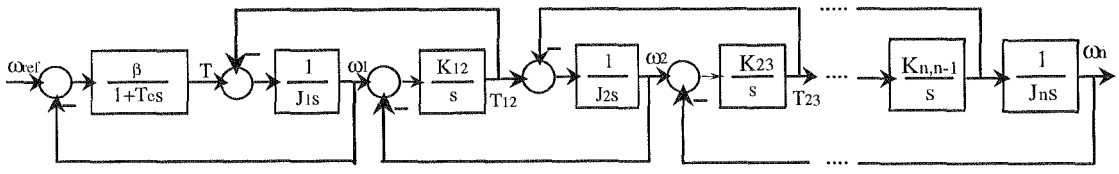

Figure 2.3. An n-mass electromechanical system model.

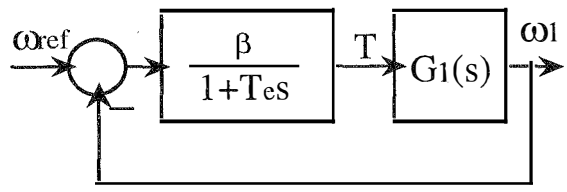

Figure 2.4. Equivalent block diagram.

In the case of a two-mass EMS, (2.7) can be put in the form:

$$\Delta_2(s) = T_e T_m s^4 + T_m s^3 + (\gamma + T_e T_m \Omega_N^2) s^2 + T_m \Omega_N^2 s + \Omega_N^2 = 0, \tag{2.8}$$

where $T_m = \frac{J_\Sigma}{\beta} = \frac{\gamma J_1}{\beta}$ is the system electromechanical time-constant. The same procedure can be applied to a three-mass system with

$$G_1(s) = \frac{\omega_1(s)}{T(s)} = \frac{1}{J_1 s} \frac{s^4 + b_1 \Omega_N^2 s^2 + \Omega_N^4/\gamma}{s^4 + a_1 \Omega_N^2 s^2 + \Omega_N^4}, \tag{2.9}$$

where

$$\Omega_N = \left(K_{12} K_{23} \frac{J_\Sigma}{J_1 J_2 J_3} \right)^{1/4} \tag{2.9a}$$

is the three-mass natural resonant frequency,

$$\Omega_{12} = \left(K_{12} \frac{J_1 + J_2}{J_1 J_2} \right)^{1/2}, \; \Omega_{23} = \left(K_{23} \frac{J_2 + J_3}{J_2 J_3} \right)^{1/2} \tag{2.9b}$$

are the first and second mode resonant frequencies,

$$\gamma = \frac{J_\Sigma}{J_1} = \frac{J_1 + J_2 + J_3}{J_1} \tag{2.9c}$$

is the mass ratio, and

$$a_1 = \frac{\Omega_{12}^2 + \Omega_{23}^2}{\Omega_N^2}, \; b_1 = \frac{\Omega_{12}^2/\gamma_{12} + \Omega_{23}^2}{\Omega_N^2}, \; \gamma_{12} = \frac{J_1 + J_2}{J_1}. \tag{2.9d}$$

The three-mass system characteristic equation can then be obtained:

$$\begin{aligned} \Delta_3(s) = {} & T_e T_m s^6 + T_m s^5 + (\gamma + a_1 \Omega_N^2 T_e T_m) s^4 + a_1 \Omega_N^2 T_m s^3 + \\ & + (\gamma b_1 + T_e T_m \Omega_N^2) \Omega_N^2 s^2 + \Omega_N^4 T_m s + \Omega_N^4 = 0. \end{aligned} \tag{2.10}$$

The characteristic equation of an n-mass electromechanical system model can be derived in the same way. For a chain of resonant blocks, the transfer function $G_1(s)$ can be written in the form

$$G_1(s) = \frac{\omega_1(s)}{T(s)} = \frac{1}{J_1 s} \frac{N(s)}{D(s)}, \tag{2.11}$$

with $D(s) = s^{2(n-1)} + a_1\Omega_N^2 s^{2(n-2)} + a_2\Omega_N^4 s^{2(n-3)} + \ldots + a_{n-2}\Omega_N^{2(n-2)} s^2 + \Omega_N^{2(n-1)}$,

$$N(s) = s^{2(n-1)} + b_1\Omega_N^2 s^{2(n-2)} + b_2\Omega_N^4 s^{2(n-3)} + \ldots b_{n-2}\Omega_N^{2(n-2)} s^2 + \Omega_N^{2(n-1)} / \gamma,$$

where

$$a_i > 0,\ b_i > 0,\ i = 1, 2, \ldots, n-2,$$

$$\Omega_N = \left(K_{12}K_{23}\ldots K_{n-1,n} \frac{J_\Sigma}{J_1 J_2 \ldots J_n} \right)^{1/2(n-1)} \tag{2.12}$$

is the natural resonant frequency,

$$J_\Sigma = J_1 + J_2 + \ldots + J_n, \tag{2.13}$$

is the total moment of inertia, and

$$\gamma = \frac{J_\Sigma}{J_1} \tag{2.14}$$

is the mass ratio. The characteristic equation of the n-mass electromechanical system model of Figure 2.3 can then be obtained:

$$\begin{aligned}\Delta_n(s) &= J_1 s(1 + T_e s) D(s) + \beta N(s) = \\ &= T_e T_m s^{2n} + T_m s^{2n-1} + (\gamma + a_1\Omega_N^2 T_e T_m) s^{2(n-1)} + a_1\Omega_N^2 T_m s^{2n-3} + (\gamma b_1 + a_2\Omega_N^4 T_e T_m) s^{2(n-2)} + \ldots \\ &+ (\gamma b_{n-3} + a_{n-2}\Omega_N^{2(n-2)} T_e T_m) s^4 + a_{n-2}\Omega_N^{2(n-2)} T_m s^3 + (\gamma b_{n-2} + \Omega_N^{2(n-1)} T_e T_m) s^2 + \Omega_N^{2(n-1)} T_m s + \Omega_N^{2(n-1)} = 0,\end{aligned} \tag{2.15}$$

where the system electromechanical time-constant is defined as:

$$T_m = \frac{J_1 + J_2 + \ldots + J_n}{\beta} = \frac{\gamma J_1}{\beta}. \tag{2.16}$$

2.3.2 Dimensionless space

In the remainder of this chapter the following per-unit notation, proposed by Kljuchev [54], is employed:

$$p = \frac{s}{\Omega_N},\ \tau_e = \Omega_N T_e,\ \tau_m = \Omega_N T_m. \tag{2.17}$$

The n-mass EMS characteristic equation then has the form:

$$\Delta_n(p) = \tau_e\tau_m p^{2n} + \tau_m p^{2n-1} + (\gamma + a_1\tau_e\tau_m)p^{2(n-1)} + a_1\tau_m p^{2n-3} + (\gamma b_1 + a_2\tau_e\tau_m)p^{2(n-2)} + \ldots$$
$$+ (\gamma b_{n-3} + a_{n-2}\tau_e\tau_m)p^4 + a_{n-2}\tau_m p^3 + (\gamma b_{n-2} + \tau_e\tau_m)p^2 + \tau_m p + 1 = 0. \tag{2.18}$$

For a two-mass EMS system ($n = 2$, $a_1 = 1$, $b_1 = 0$) the characteristic equation in dimensionless space is obtained:

$$\Delta_2(p) = \tau_e\tau_m p^4 + \tau_m p^3 + (\gamma + \tau_e\tau_m)p^2 + \tau_m p + 1 = 0, \tag{2.19}$$

and for a three-mass system ($n = 3$):

$$\Delta_3(p) = \tau_e\tau_m p^6 + \tau_m p^5 + (\gamma + a_1\tau_e\tau_m)p^4 + a_1\tau_m p^3 + (\gamma b_1 + \tau_e\tau_m)p^2 + \tau_m p + 1 = 0, \tag{2.20}$$

where a_1 and b_1 are given in (2.9d) with $2<a_1$, $0<b_1<2$.

2.3.3 EMS with a negligible electromagnetic inertia

The electromagnetic process in some DC and AC servo motors usually have a negligible inertia and thus, results in very small values of τ_e ($\tau_e \cong 0$). In this case, the n-mass EMS characteristic equation (2.18) is rewritten as

$$\Delta_n(p) = \tau_m p^{2n-1} + \gamma p^{2(n-1)} + a_1\tau_m p^{2n-3} + \gamma b_1 p^{2(n-2)} + \ldots + \gamma b_{n-3} p^4 + a_{n-2}\tau_m p^3 + \gamma b_{n-2} p^2 + \tau_m p + 1 = 0, \tag{2.21}$$

and particularly, for a two-mass system

$$\Delta_2(p) = \tau_m p^3 + \gamma p^2 + \tau_m p + 1 = 0, \tag{2.22}$$

and for a three-mass system

$$\Delta_3(p) = \tau_m p^5 + \gamma p^4 + a_1 \tau_m p^3 + \gamma b_1 p^2 + \tau_m p + 1 = 0. \tag{2.23}$$

2.4 Maximal damping conditions

The discussion on the estimation of damping properties of an EMS starts with some definitions.

2.4.1 Definitions

In general, the characteristic equation (2.17) of an n-mass EMS has n pairs of roots $p_i = -\sigma_i + j\Omega_i$ and $\overline{p}_i = -\sigma_i - j\Omega_i$, $i = 1,...,n$, where $j^2 = -1$, and σ_i and Ω_i are non-negative real numbers. Each pair of roots can be either complex-conjugate or real. For estimating damping properties of an EMS the following concepts are introduced:

Definition 2.1. Damping factor of a pair of complex-conjugate roots, $p_i = -\sigma_i + j\Omega_i$ and $\overline{p}_i = -\sigma_i - j\Omega_i$, is the value

$$\delta_i = \frac{\sigma_i}{\sigma_i^2 + \Omega_i^2} = \cos\Phi_i, \tag{2.24}$$

where Φ_i is the angle illustrated in Figure 2.5.

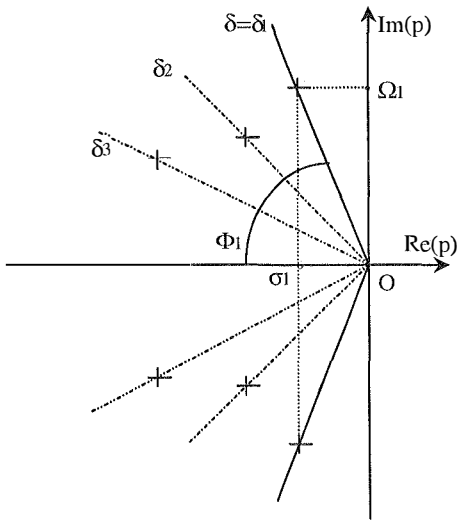

Figure 2.5. Multi-mass system damping factor

Definition 2.2. (Alferov & Ha [49]) *Damping factor of a multi-mass system* is the minimal value of damping factors δ_i (Figure 2.5):

$$\delta = \min_{1 \le i \le n}(\delta_i). \tag{2.25}$$

Definition 2.3. Dominant roots of a multi-mass system are the pair of complex-conjugate roots of the characteristic equation (2.18) that correspond to the system damping factor (2.25).

Definition 2.4. Maximal damping of an electromechanical system is the case when the electrical and mechanical parts have a common damping factor (Strelkov [59]). A maximal damping case of an n-mass electromechanical system of Figure 2.3 occurs when all the complex-conjugate roots of the characteristic equation (2.18) have the same damping factor.

Definition 2.5. Complete damping of an electromechanical system is the case when all the roots of the characteristic equation (2.18) are located on the negative real axis. It can be a special case of maximal damping when the common damping factor is equal to unity.

Definition 2.6. Critical value γ_{cr} of the mass ratio of an electromechanical system is a the value of the mass ratio γ at which complete damping corresponds to a multiple root of the characteristic equation.

2.4.2 Maximal damping of an n-mass EMS

Theoretical calculations and experiments indicate that maximal damping of a two-mass EMS depends on the mass ratio γ. The critical value of γ is found equal to 5 for the case considering the electromagnetic time constant τ_e or equal to 9 for the case neglecting τ_e as given in Kljuchev [54]. The root loci for two-mass EMS's and analytic expressions for system parameters at maximal damping are given in Alferov & Ha [49]. The question arises as to whether these results can be extended to the general case of n masses.

Theorem 2.1. (Maximal damping) A maximal damping case for an n-mass EMS of Figure 2.3 with the characteristic equation (2.18) and the mass ratio γ defined in (2.14) is possible at the following system parameters:

$$\tau_m = \tau_m^* = \sqrt{\frac{3n^2(\gamma-1)}{n^2-1}},\ \tau_e = \tau_e^* = \frac{1}{\tau_m^*}, \tag{2.26}$$

and the maximal damping factor in this case is

$$\delta = \delta^* = \frac{1}{2}\sqrt{\frac{3(\gamma-1)}{n^2-1}}. \tag{2.27}$$

Proof: In the general case, a maximal damping case can be found at a multiple root $-\left(\delta \pm j\sqrt{1-\delta^2}\right)/\tau$ of the EMS characteristic equation (2.18). Thus, the system parameters at possible maximal damping can be obtained by identifying the coefficients of (2.18) and the expansion of $(\tau^2 p^2 + 2\delta\tau p + 1)^n$. The following equations are obtained:

$$\begin{cases} \tau_e\tau_m = \tau^{2n}, \\ \tau_m = 2n\delta\tau^{2n-1}, \\ \gamma + a_1\tau_e\tau_m = n\tau^{2(n-1)} + 2\delta^2 n(n-1)\tau^{2(n-1)}, \\ a_1\tau_m = 2\delta n(n-1)\tau^{2n-3} + \dfrac{4}{3}\delta^3 n(n-1)(n-2)\tau^{2n-3}, \\ \dots \\ \tau_m = 2n\delta\tau, \end{cases} \tag{2.28}$$

where a feasible solution can be found at

$$\begin{cases} \tau_e\tau_m = \tau = 1, \\ \tau_m = 2n\delta, \\ \gamma = 1 + 4(n^2-1)\delta^2/3. \end{cases}$$

Thus, for a given mass ratio $\gamma > 1$, the EMS time-constants at maximal damping are found dependent on γ as in (2.26) with the damping factor given in (2.27).

Theorem 2.2. (Complete damping) A complete damping case for an n-mass EMS of Figure 2.3 with the characteristic equation (2.18) is possible at a critical value of the mass ratio

$$\gamma = \gamma_{cr} = \frac{4n^2 - 1}{3}, \tag{2.29}$$

when the system time-constants are given by

$$\tau_m = \tau_{m,cr} = \sqrt{1 + 3\gamma} = 2n, \; \tau_e = \tau_{e,cr} = \frac{1}{\tau_{m,cr}}. \tag{2.30}$$

Proof: The complete damping case is possible when the system damping factor $\delta = 1$. Assigning unity for the left hand side of (2.27) gives the critical value of the mass ration as in (2.29). Substituting this value into (2.26) gives the critical values of the time-constants (2.30).

Theorem 2.3. (Case $\tau_e \cong 0$) A maximal damping case for an n-mass EMS of Figure 2.3 with the characteristic equation (2.21), when the electromagnetic time-constant τ_e is negligible, is possible at the following electromechanical time-constant

$$\tau_m = \tau_m^* = \gamma^{\frac{2n-1}{4n-4}}, \tag{2.31}$$

and the maximal damping factor is found to be

$$\delta = \delta^* = \frac{\sqrt{\gamma} - 1}{2(n-1)}. \tag{2.32}$$

The critical value of the mass ratio at complete damping for this case is

$$\gamma_{cr} = [1 + 2(n-1)]^2. \tag{2.33}$$

Proof: In the case $\tau_e \cong 0$, a possible maximal damping case takes place when the characteristic equation (2.20) has a $(n-1)$-multiple root at $-\left(\delta \pm j\sqrt{1-\delta^2}\right)/\tau$ and a real root at $-1/\tau$. Thus, the system parameters can be obtained by identifying the

coefficients of (2.21) and the expansion of $(\tau p+1)(\tau^2 p^2+2\delta\tau p+1)^{n-1}$. The following equations are obtained

$$\begin{cases} \tau_m = \tau^{2n-1}, \\ \gamma = \tau^{2(n-1)} + 2\delta(n-1)\tau^{2(n-1)}, \\ \cdots \\ \tau_m = \tau + 2(n-1)\delta\tau, \end{cases}$$

where a feasible solution is found at $\tau = \gamma^{\frac{1}{4(n-1)}}$ and thus, the value of the electromechanical time-constant is obtained as in (2.31) with the maximal damping factor δ^* given by (2.32). The value of δ^* achieves unity at complete damping when the mass ratio γ is equal to its critical value given in (2.33).

Remark 2.1
From (2.29) and (2.33), there is a possibility of complete damping in a two-mass EMS ($n=2$) when the mass ratio is equal to 5 taking into account electromagnetic inertia, and to 9 neglecting τ_e. The result is well-documented in Soviet literature (Kljuchev [51]).

Remark 2.2
For a three-mass EMS ($n=3$), the critical value of the mass ratio γ_{cr} is found by the same formulae to be 35/3 considering τ_e, and 25 when $\tau_e \cong 0$ (Ha [55]).

2.5 Root loci of multi-mass electromechanical systems

In this section, the influence of the system parameter variations on damping capability is investigated using the classical root locus method. In order to plot the root distribution of a characteristic equation $\Delta(s)=0$, depending on a varying parameter K, following the Evans root locus principles (Kuo [60]), it is required to put the equation $\Delta(s)=0$ into the form

$$\Delta(s) = 1 + KG(s) = 0, \tag{2.34}$$

where $G(s)$ is a rational function of s. For an n-mass EMS of Figure 2.3, the characteristic equation (2.18) in dimensionless space can be brought into the form

(2.34), where the varying parameter is the electromechanical time-constant τ_m. In fact, (2.18) can be rewritten

$$\begin{aligned}\Delta_n(p) &= \gamma(p^{2(n-1)} + b_1 p^{2(n-2)} + \ldots + b_{n-3}p^4 + b_{n-2}p^2) + 1 + \tau_m(\tau_e p^{2n} + p^{2n-1} + a_1\tau_e p^{2(n-1)} + \\ &+ a_1 p^{2n-3} + a_2\tau_e p^{2(n-2)} + \ldots + a_{n-2}\tau_e p^4 + a_{n-2}p^3 + \tau_e p^2 + p) = \\ &= \gamma(p^{2(n-1)} + b_1 p^{2(n-2)} + \ldots + b_{n-3}p^4 + b_{n-2}p^2) + 1 + \tau_m p(\tau_e p + 1)(p^{2(n-1)} + \\ &+ a_1 p^{2(n-2)} + a_2 p^{2(n-3)} + \ldots + a_{n-2}p^2 + 1) = 0.\end{aligned}$$

The root locus equation is then obtained as

$$\Delta_n(p) = 1 + \tau_m \frac{p(\tau_e p + 1)(p^{2(n-1)} + a_1 p^{2(n-2)} + a_2 p^{2(n-3)} + \ldots + a_{n-2}p^2 + 1)}{\gamma(p^{2(n-1)} + b_1 p^{2(n-2)} + \ldots + b_{n-3}p^4 + b_{n-2}p^2) + 1} = 0. \quad (2.35)$$

2.5.1 Root loci of two-mass electromechanical systems

For a two-mass system, the root locus equation (2.35) becomes

$$\Delta_2(p) = 1 + \tau_m \frac{p(\tau_e p + 1)(p^2 + 1)}{\gamma p^2 + 1} = 0. \quad (2.36)$$

Using (2.27) and (2.26), the maximal damping factor δ^* and corresponding time-constants τ_m^* and τ_e^* are found dependent on the mass ratio γ:

$$\delta^* = \frac{\sqrt{\gamma - 1}}{2}, \quad \tau_m^* = 2\sqrt{\gamma - 1}, \quad \tau_e^* = \frac{1}{2\sqrt{\gamma - 1}}, \quad (2.37)$$

with the critical value γ_{cr}=5 given by (2.29). Figure 2.6 shows the root locus of two-mass systems with the mass ratio γ=3<γ_{cr}, and $\tau_e = 0.2 < \tau_e^*$ (Figure 2.6(a)), $\tau_e = \tau_e^* = 0.7$ (Figure 2.6(b)), and $\tau_e = 1 > \tau_e^*$ (Figure 2.6(c)). Maximal damping corresponds to a multiple root of the characteristic equation. Hence, it takes place at minimax or saddle points of the root locus (Kuo [60]) as observed in Figure 2.6(b). The location of these points is given in Alferov & Ha [49]:

$$p_s = \frac{1}{2}\left(-\sqrt{\gamma - 1} \pm j\sqrt{5 - \gamma}\right), \quad (2.38)$$

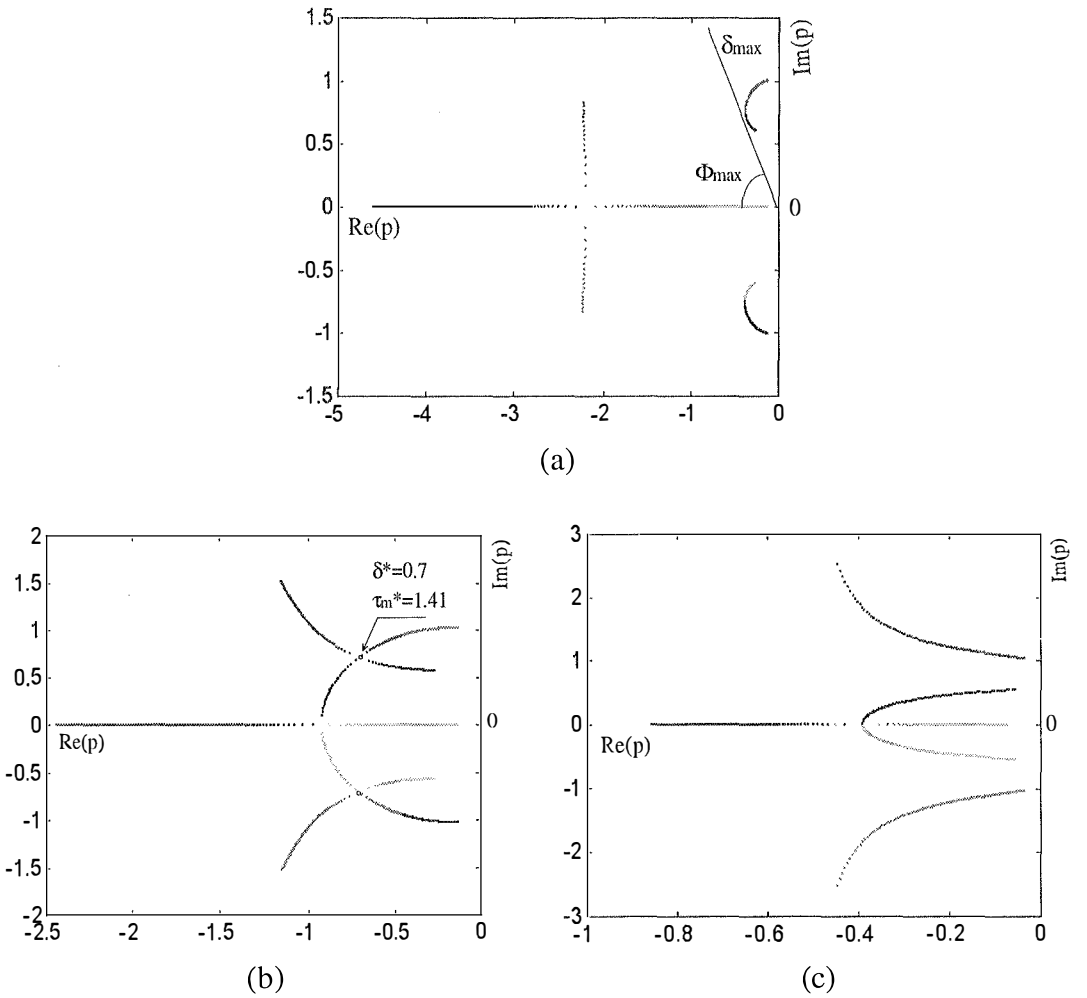

Figure 2.6. Two-mass EMS root locus with $\gamma=3<\gamma_{cr}$: (a) $\tau_e = 0.2 < \tau_e^*$, (b) $\tau_e = \tau_e^* = 0.7$, and (c) $\tau_e = 1 > \tau_e^*$.

where the mass ratio $\gamma<\gamma_{cr}=5$. Complete damping of two-mass systems when $\gamma<\gamma_{cr}$ is not obtained except in the critical case ($\gamma=\gamma_{cr}=5$, $\tau_e = \tau_{e,cr} = 0.25$). This special case is depicted in Figure 2.7 where a multiple root is found at $p=-1$. The two-mass EMS root loci with $\gamma=10>\gamma_{cr}$ and $\tau_e = 0.1 < \tau_e^*$, $\tau_e = \tau_e^* = 0.167$, and $\tau_e = 1 > \tau_e^*$ are shown in Figure 2.8(a), Figure 2.8(b), and Figure 2.8(c), respectively. If the mass ratio is greater than $\gamma_{cr}=5$, complete damping is possible at small values of the electromagnetic time-constant (Figure 2.8(a)). As shown in Figure 2.8(b), maximal damping in the case $\gamma>\gamma_{cr}$ coincides with complete damping which occurs at the two saddle points (Alferov & Ha [49]):

$$p_{s1} = -\frac{1}{2}\left(\sqrt{\gamma-1}-\sqrt{\gamma-5}\right),\ p_{s2} = -\frac{1}{2}\left(\sqrt{\gamma-1}+\sqrt{\gamma-5}\right). \qquad (2.39)$$

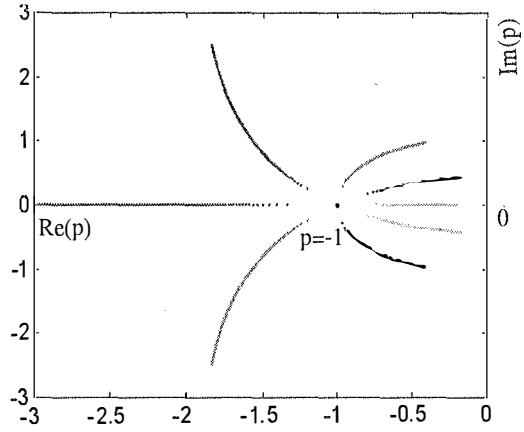

Figure 2.7. Two-mass EMS root locus with $\gamma=\gamma_{cr}=5$ and $\tau_e = \tau_{e,cr} = 0.25$.

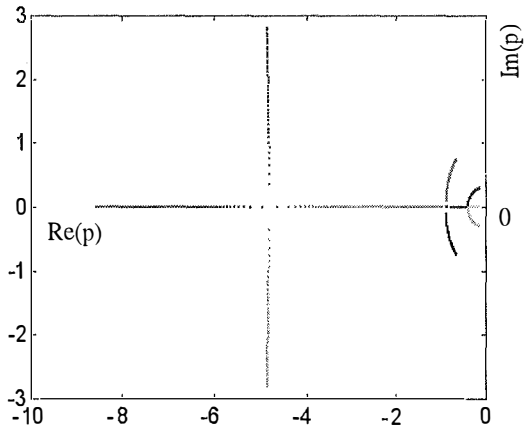

(a)

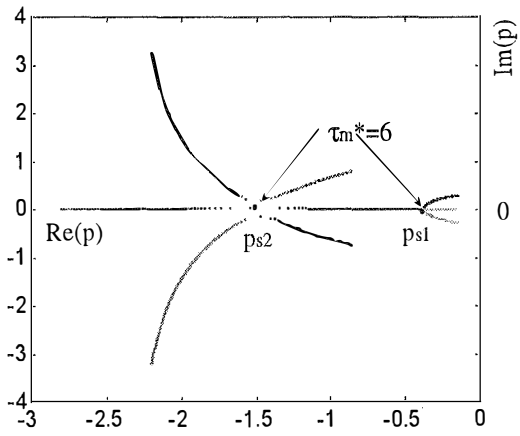

(b)

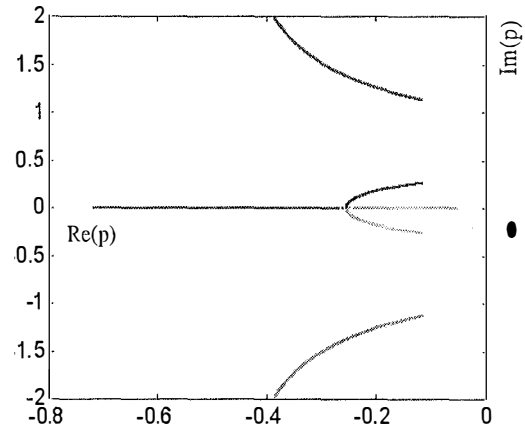

(c)

Figure 2.8. Two-mass EMS root locus with $\gamma=10>\gamma_{cr}$: (a) $\tau_e = 0.1 < \tau_e^*$, (b) $\tau_e = \tau_e^* = 0.167$, and (c) $\tau_e = 1 > \tau_e^*$.

The root locus equation for two-mass systems when $\tau_e \cong 0$ is written as

$$\Delta_2(p) = 1 + \tau_m \frac{p(p^2+1)}{\gamma p^2 + 1} = 0. \tag{2.40}$$

Equations (2.31), (2.32) give the maximal damping parameters

$$\tau_m^* = \gamma^{\frac{3}{4}}, \ \delta^* = \frac{\sqrt{\gamma}-1}{2}, \tag{2.41}$$

with the critical value γ_{cr}=9 obtained from (2.33). The root locus with the mass ratio γ=4<γ_{cr}, γ=γ_{cr}=9, and γ=13>γ_{cr} is shown in Figure 2.9(a), Figure 2.9(b), and Figure 2.9(c), respectively. Complete damping of a two-mass EMS with negligible τ_e takes place at large values of the mass ratio $\gamma \geq \gamma_{cr} = 9$. The values of the electromechanical time-constant τ_m at complete damping can be determined from (2.40) and the saddle points (Alferov & Ha [49]):

$$p_{s1} = -\left[\frac{\gamma - 3 + \sqrt{(\gamma-1)(\gamma-9)}}{2\gamma}\right]^{1/2}, \ p_{s2} = -\left[\frac{\gamma - 3 - \sqrt{(\gamma-1)(\gamma-9)}}{2\gamma}\right]^{1/2}. \tag{2.42}$$

At small values of the mass ratio γ (γ<5 for τ_e>0, or γ<9 for $\tau_e \cong 0$), two-mass EMS damping is incomplete and maximal damping corresponds to the value δ_{max} at the tangent from the coordinate origin with the root locus branch containing the dominant roots (Figures 2.6(a) and 2.9(a)) (Alferov & Ha [49]).

2.5.2 Root loci of three-mass electromechanical systems

For three-mass systems, (2.35) is written as following

$$\Delta_3(p) = 1 + \tau_m \frac{p(\tau_e p + 1)(p^4 + a_1 p^2 + 1)}{\gamma(p^4 + b_1 p^2) + 1} = 0, \tag{2.43}$$

where $a_1$and b_1 are given in (2.9b). The maximal damping factor δ^* and corresponding time-constants τ_m^* and τ_e^* are determined using theorem 2.1 and equations (2.27) and (2.26):

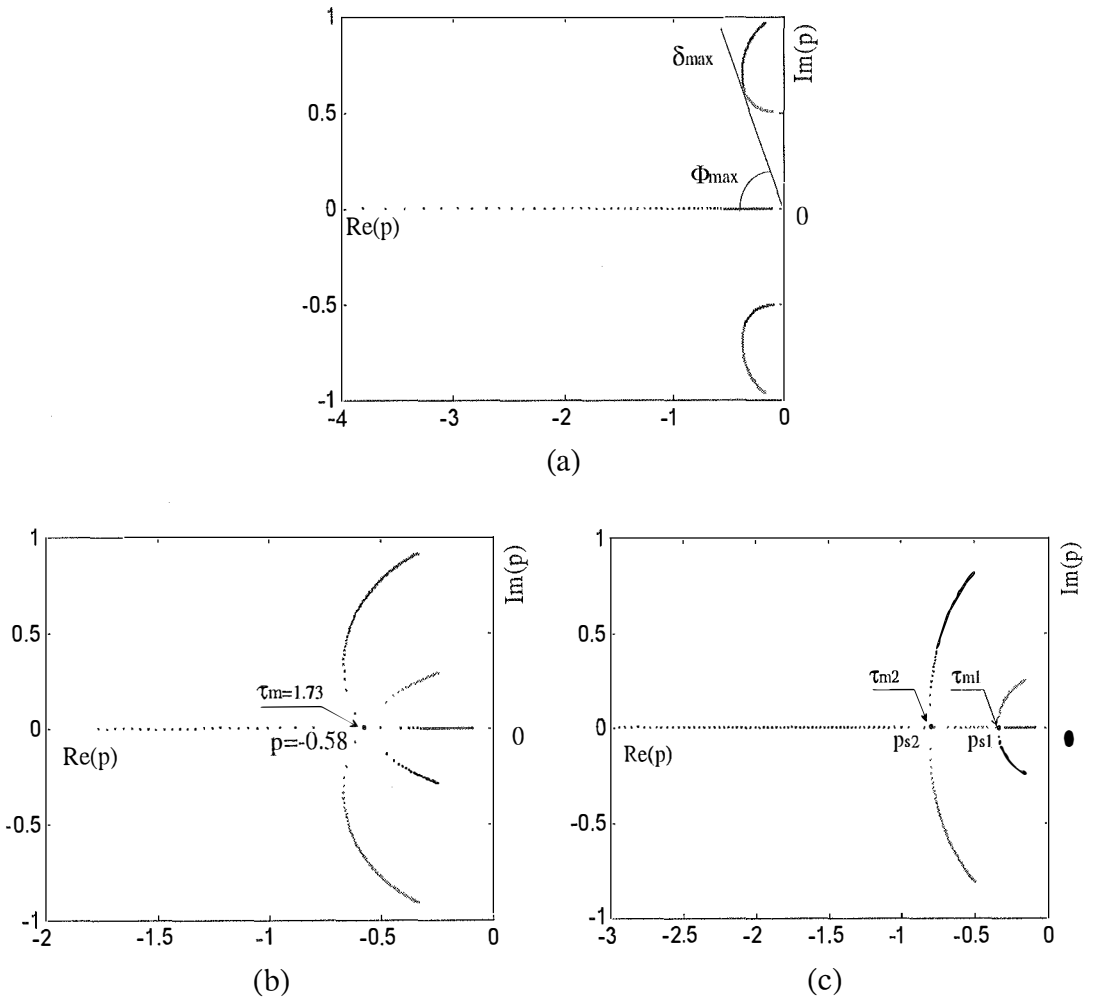

Figure 2.9. Two-mass EMS root locus with $\tau_e \cong 0$: (a) $\gamma=4<\gamma_{cr}$, (b) $\gamma=\gamma_{cr}=9$, and (c) $\gamma=13>\gamma_{cr}$.

$$\delta^* = \frac{1}{4}\sqrt{\frac{3}{2}(\gamma-1)},\ \tau_m^* = \frac{3}{2}\sqrt{\frac{3}{2}(\gamma-1)},\ \tau_e^* = \frac{1}{\tau_m^*}, \tag{2.44}$$

and the critical value $\gamma_{cr}=35/3$ obtained from (2.29) (Ha [55]). The root locus for the case $\gamma=7<\gamma_{cr}$ is shown in Figure 2.10 where incomplete damping is observed. In the critical case, and $\gamma=\gamma_{cr}=35/3$ and $\tau_e = \tau_{e,cr} = 0.167$, a multiple root $p=-1$ is found at $\tau_m = \tau_{m,cr} = 6$ as depicted in Figure 2.11. The root loci for the case $\gamma=15>\gamma_{cr}$with $\tau_e = 0.13 > \tau_e^*$, $\tau_e = \tau_e^* = 0.146$, and $\tau_e = 0.2 > \tau_e^*$ are represented in Figure 2.12(a), 2.12(b), and 2.12(c).

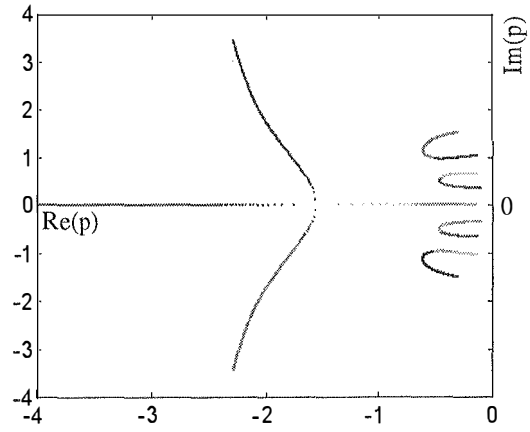

Figure 2.10. Three-mass EMS root locus with $\gamma=7<\gamma_{cr}$.

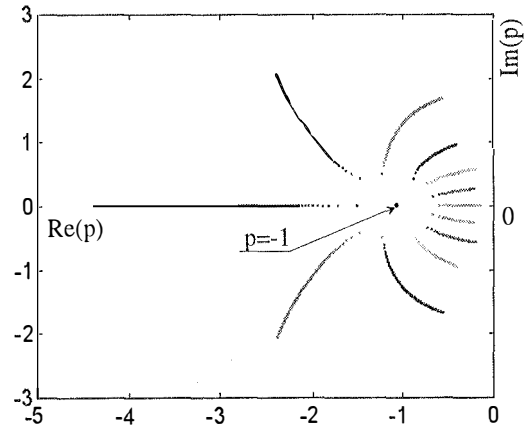

Figure 2.11. Three-mass EMS root locus with $\gamma=35/3=\gamma_{cr}$.

While damping capability in three-mass systems increases at small values of the electromagnetic time-constant τ_e, complete damping is impossible except in the critical case. When $\tau_e \cong 0$, the three-mass EMS root locus equation (2.41) is written as:

$$\Delta_3(p) = 1 + \tau_m \frac{p(p^4 + a_1 p^2 + 1)}{\gamma(p^4 + b_1 p^2) + 1} = 0. \qquad (2.45)$$

Theorem 2.3 and equations (2.31), (2.32) give the maximal damping parameters:

$$\tau_m^* = \gamma^{5/8},\ \delta^* = \frac{\sqrt{\gamma} - 1}{4}. \qquad (2.46)$$

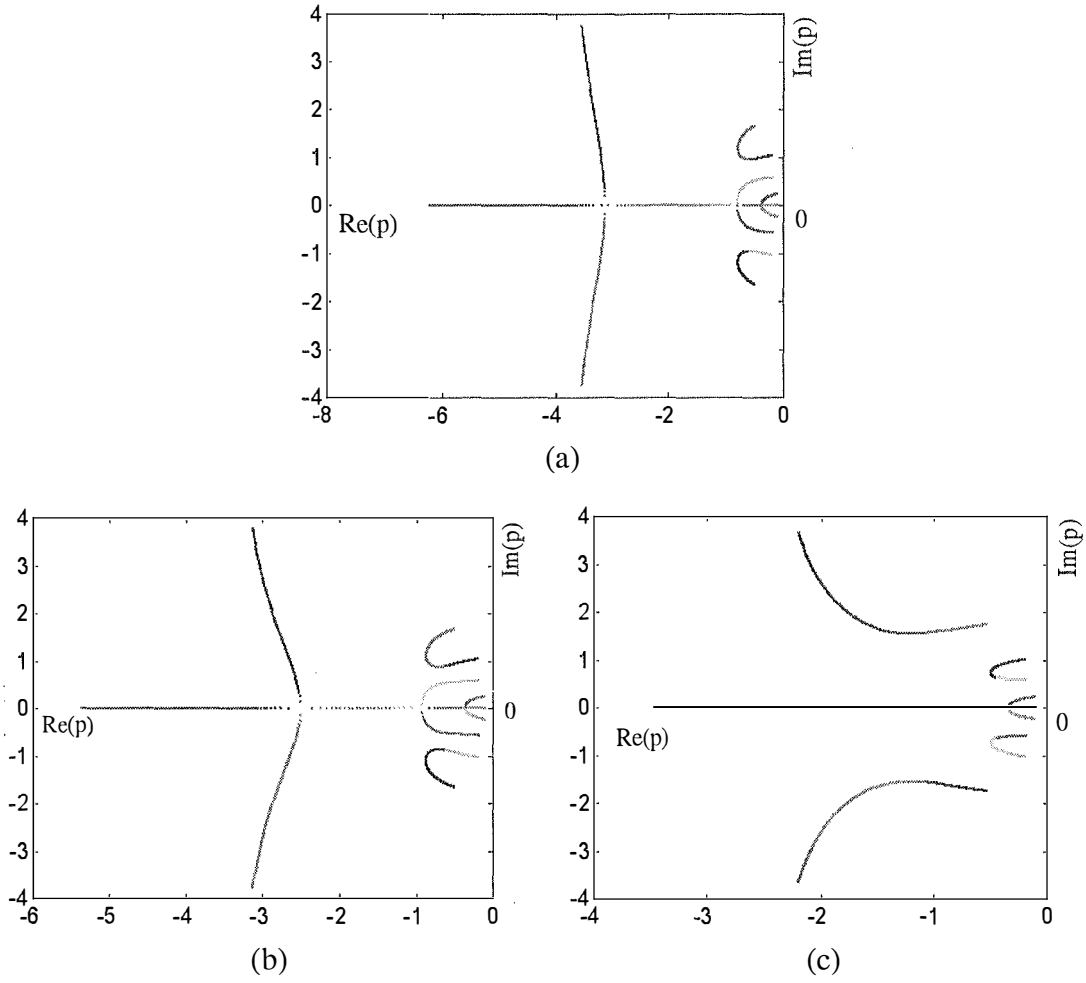

Figure 2.12. Three-mass EMS root locus with γ=15: (a) $\tau_e = 0.13 > \tau_e^*$, (b) $\tau_e = \tau_e^* = 0.146$, and (c) $\tau_e = 0.2 > \tau_e^*$.

The critical value of the mass ratio is found from (2.31) to be γ_{cr}=25 with complete damping possible at $\tau_m = \tau_{m,cr} = 7.48$. Figure 2.13(a) and 2.13(b) show the root locus with γ=9<γ_{cr} and γ=25=γ_{cr}. The root locus for the case γ=36>γ_{cr} is depicted in Figure 2.14(a) and 2.14(b) with different values of a_1 and b_1. It is observed that with $\gamma > \gamma_{cr}$ complete damping is possible at some values of a_1 and b_1 (Figure 2.14(b)).

2.5.3 EMS multi-parameter root loci

When operating, electromechanical systems are subject to parameter variations. The influence of parameter perturbations on the characteristic equation roots can be examined by using a family of root loci with several varying parameters.

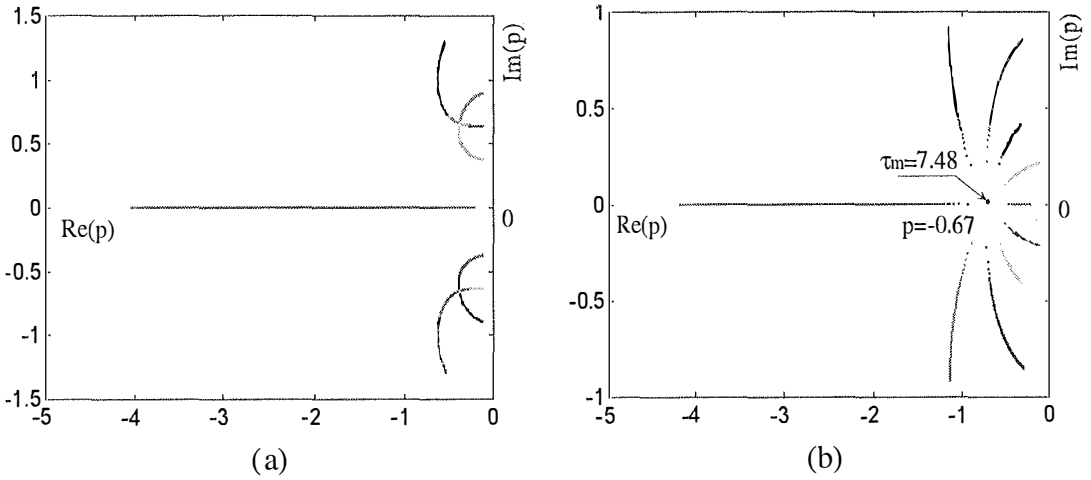

Figure 2.13. Three-mass EMS root locus when $\tau_e \cong 0$: (a) $\gamma=9<\gamma_{cr}$, and (b) $\gamma=25=\gamma_{cr}$.

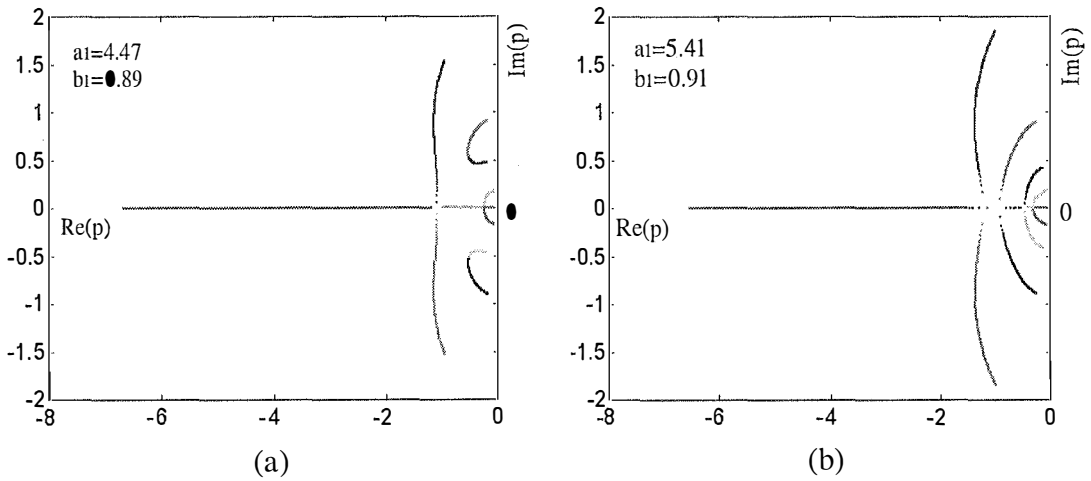

Figure 2.14. Three-mass EMS root locus with $\tau_e \cong 0$ and $\gamma=36$: (a) $a_1=4.47$, $b_1=0.89$; (b) $a_1=5.41$, $b_1=0.91$.

Based on the sharpest possible bounds provided by the well-known Kharitonov polynomials [5], the robust root locus method, proposed by Barmish & Tempo [61], exploits a two-dimensional gridding of a bounded set of the complex plane for generating the multi-parameter root loci. A computational technique for the robust root locus is described in Tong & Sinha [62]. Applying the robust root locus method requires that each coefficient of the nominator and denominator of the function $G(s)$

in (2.34) depends on one and only one perturbation parameter in order to result in an interval characteristic polynomial (Barmish & Tempo [61]). To maintain the physical meaning in parameter variations and to avoid the conservative requirement on the relations of the monic characteristic equation coefficients with the perturbation vector, the classical multi-parameter root locus method is used in this section. The influence of variations of the load moment of inertia J_n and dynamic stiffness β of the motor speed-torque characteristics is considered in terms of root loci with varying values of the mass ratio γ and electromechanical time-constant τ_m. The multi-parameter root loci for the two-mass case with $\tau_e \cong 0$ are shown in Figure 2.15, where complete damping can be observed on the negative real axis with some values of τ_m.

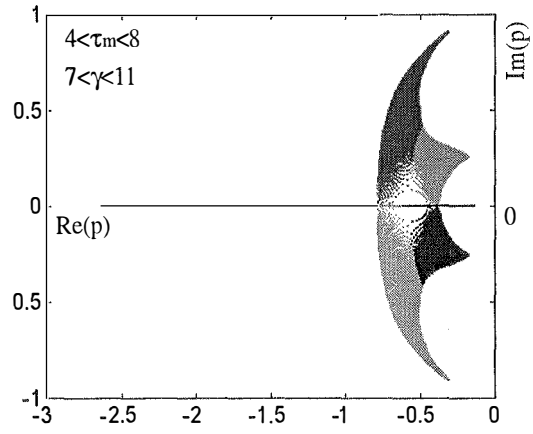

Figure 2.15. Two-mass EMS multi-parameter root loci with $\tau_e \cong 0$, τ_m = var., γ = var.

Taking into account the electromagnetic inertia, the loci when $\tau_e = 0.25$, τ_m = var., γ = var. are shown in Figure 2.16(a) and when $\gamma = 5$, τ_e = var., τ_m = var. in Figure 2.16(b). Damping capability increases at smaller values of τ_e. The three-mass system root loci with varying γ and τ_m are shown in Figure 2.17(a) when $\tau_e = 0.167$ and 2.17(b) when $\tau_e \cong 0$. While complete damping is possible only in the critical case considering the electromagnetic inertia, it can be achieved at $\gamma > \gamma_{cr}$ and some values of τ_m with $\tau_e \cong 0$. The sparse region around the real axis (Figures 2.15-2.16) or at the centre of the root loci (Figure 2.17) indicates that the roots of the characteristic equation and hence, the system dynamic properties, at maximal damping are sensitive to parameter variations, eg. changes in the mass ratio, the electromechanical and

electromagnetic time-constants. This is explained by the fact that these roots are multiple [56]. The dense region near the imaginary axis implies that the dominant roots of a multi-mass EMS are less sensitive to varying environments and can be used for the purpose of model reduction when designing a robust controller for these systems. It should be noted that this root region contrast is not specified with the robust root locus method.

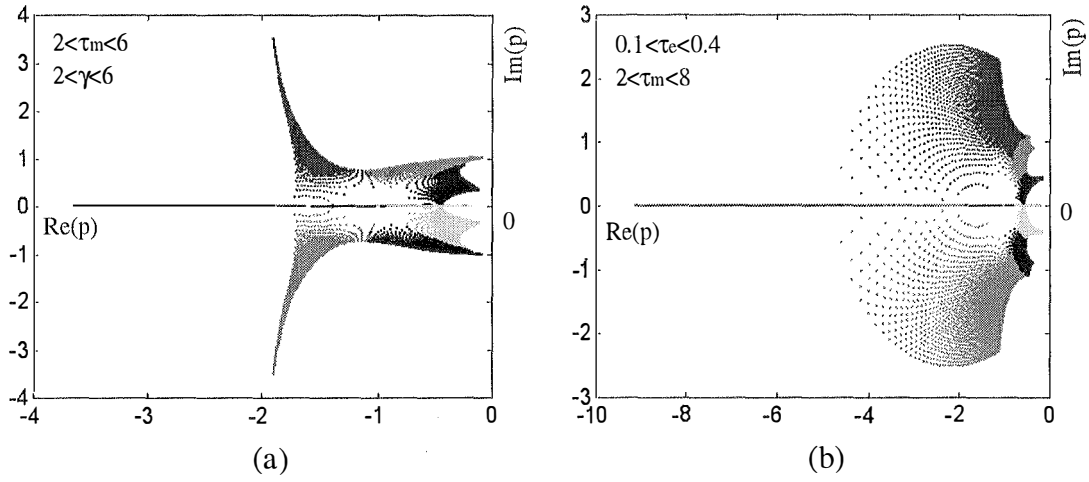

Figure 2.16. Two-mass EMS multi-parameter root loci with
(a) $\tau_e = 0.25$, τ_m = var., γ = var.; (b) $\gamma = 5$, τ_e = var., τ_m = var.

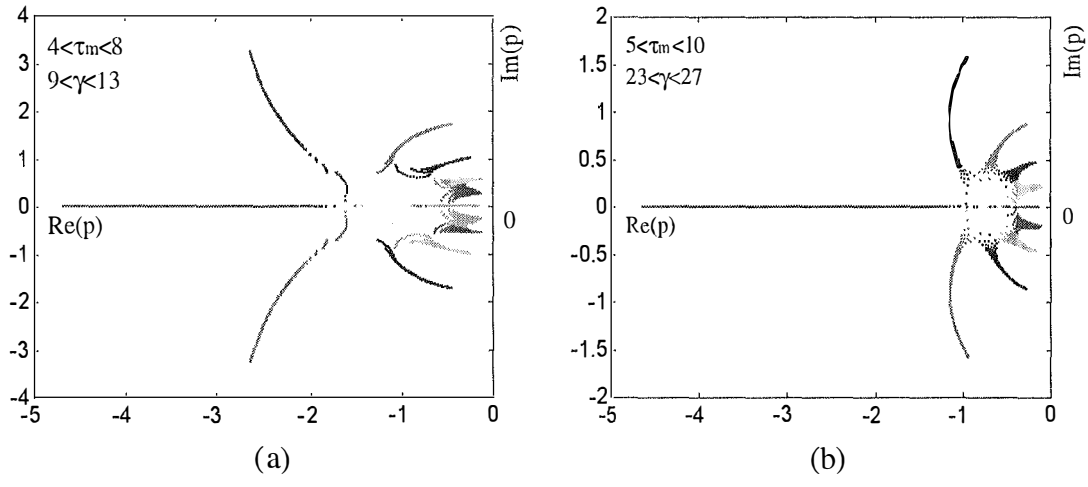

Figure 2.17. Three-mass EMS root loci with τ_m = var., γ = var.:
(a) $\tau_e = 0.167$, (b) $\tau_e \cong 0$.

2.6 Viscous friction influence

Although friction maybe a desirable property, as it is for brakes, it is generally an impediment for servo control. The field of control has long incorporated sophisticated investigations of other contributions, eg. multi-mass dynamics, to the forces of motion (Armstrong-Helouvry *et al.* [63]). The influence of viscous friction on two-mass EMS damping capability is considered using the mass-spring-damper model shown in Figure 2.18(a) with the block diagram of Figure 2.18(b). The state equations with $T_L = 0$ can be written as:

$$\begin{aligned}
\dot{T} &= -\frac{1}{T_e}T - \frac{\beta}{T_e}(\omega_{ref} - \omega_1), \\
\dot{\omega}_1 &= \frac{1}{J_1}(T - T_{12} - B_1\omega_1), \\
\dot{T}_{12} &= K_{12}(\omega_1 - \omega_2) + B_{12}\left[\frac{1}{J_1}(T - T_{12} - B_1\omega_1) - \frac{1}{J_2}(T_{12} - B_2\omega_2)\right], \\
\dot{\omega}_2 &= \frac{1}{J_2}(T_{12} - B_2\omega_2),
\end{aligned} \tag{2.47}$$

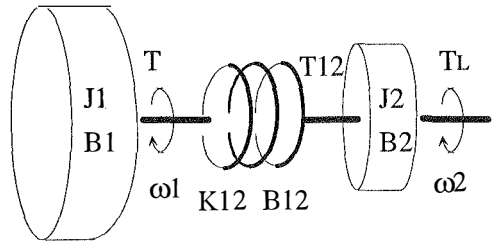

(a)

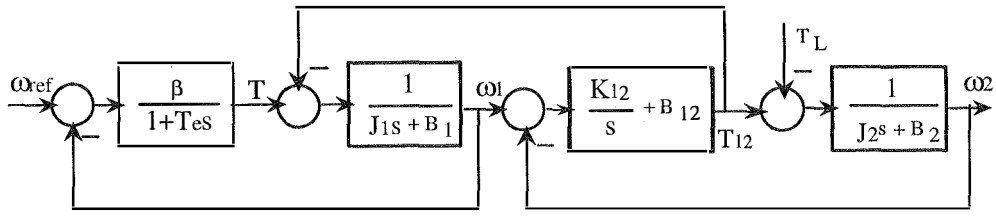

(b)

Figure 2.18. Two-mass system with viscosities:
(a) spring-mass-damper model, (b) block diagram.

where B_1, B_2, and B_{12} are viscous friction coefficients of motor, load, and the coupling shaft, respectively. The system characteristic equation can be found as:

$$\Delta_2(s) = T_e T_m s^4 + \left[T_e\left(\frac{B_1}{J_1} + \frac{B_2}{J_2} + B_{12}\left(\frac{1}{J_1} + \frac{1}{J_2}\right)\right) + 1 \right] T_m s^3 +$$
$$+ \left[T_m\left(\frac{B_1}{J_1} + \frac{B_2}{J_2} + B_{12}\left(\frac{1}{J_1} + \frac{1}{J_2}\right)\right) + T_e T_m \left(\frac{B_1 B_2 + B_{12}(B_1 + B_2)}{J_1 J_2} + \Omega_N^2\right) + \gamma \right] s^2 +$$
$$+ \left[\frac{(B_1 B_2 + (B_1 + B_2) B_{12}) T_m + (B_2 + B_{12}) J_\Sigma}{J_1 J_2} + (T_e \frac{B_1 + B_2}{J_\Sigma} + 1)\Omega_N^2 T_m \right] s + (\frac{B_1 + B_2}{\beta} + 1)\Omega_N^2 = 0, \tag{2.48}$$

where the natural frequency Ω_N and the mass ratio γ are given in (2.6a) and (2.6b). By introducing further per-unit coefficients

$$\beta_1 = \frac{B_1}{\beta},\ \beta_2 = \frac{B_2}{\beta},\ \mu = \frac{B_{12}\Omega_N}{K_{12}},\ \text{and}\ \nu = \frac{B_2 \Omega_N}{K_{12}}, \tag{2.49}$$

the two-mass EMS characteristic equation (2.48) can be written in dimensionless space as follows:

$$\Delta_2(p) = \tau_e \tau_m p^4 + [\mu \tau_e \tau_m + (\beta_1 + \frac{\beta_2}{\gamma - 1})\gamma \tau_e + \tau_m] p^3 +$$
$$+ [(1 + \beta_1 + \frac{\beta_2}{\gamma - 1})\gamma + \mu \tau_e (\beta_1 + \beta_2) + (\tau_e + \mu)\tau_m + \beta_1 \beta_2 \frac{\gamma^2}{\gamma - 1} \frac{\tau_e}{\tau_m}] p^2 +$$
$$+ [\mu + \nu + \tau_m + (\tau_e + \mu)(\beta_1 + \beta_2) + \beta_1 \beta_2 \frac{\gamma^2}{\gamma - 1} \frac{1}{\tau_m}] p + \beta_1 + \beta_2 + 1 = 0. \tag{2.50}$$

The root locus equation of the form (2.36) can be derived for the case considering viscous friction on the first shaft (motor) ($B_1 \neq 0$, $B_2 = B_{12} = 0$):

$$\Delta_2(p) = 1 + \tau_m \frac{p(\tau_e p + 1)(p^2 + 1)}{(\gamma p^2 + 1)(\tau_e \beta_1 p + 1 + \beta_1)} = 0, \tag{2.51}$$

and the case considering the viscous friction pair on the second shaft (load) and the coupling shaft ($B_1 = 0$, $B_2 \neq 0$, $B_{12} \neq 0$):

$$\Delta_2(p) = 1 + \tau_m \frac{p(\tau_e p + 1)(p^2 + \mu p + 1)}{\gamma p^2 + 1 + \beta_2(\tau_e p + 1)(\frac{\gamma}{\gamma - 1} p^2 + \mu p + 1) + (\mu + \nu)p} = 0. \quad (2.52)$$

The multi-parameter root loci for a two-mass EMS at $\gamma = \gamma_{cr}$=5 with varying viscous friction coefficient B_1 are shown in Figure 2.19. As can be seen, viscous friction on the motor shaft makes the dominant roots move closer to the imaginary axis and the other two roots further in the left hand side of the complex plane. Thus, two-mass EMS dynamics is sensitive to friction B_1.

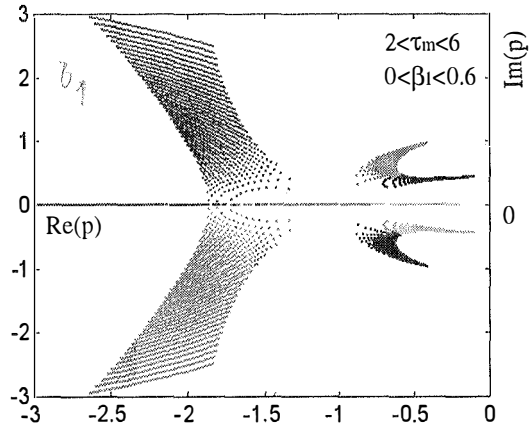

Figure 2.19. Two-mass EMS root loci with viscous friction on the motor shaft (γ=5, τ_e=0.25).

The root loci with varying viscous friction coefficient B_2 on the load shaft are depicted in Figure 2.20(a). It is inherent that two-mass EMS dominant roots are less sensitive to viscous friction B_2 on the load shaft than to viscous friction B_1 on the motor shaft. The influence of varying friction coefficient B_{12} on the coupling shaft is represented in Figure 2.20(b) when $B_2 = 0$, and in Figure 2.20(c) when $B_2 \neq 0$. The root loci indicates that friction on the coupling shaft has similar effects as friction on the motor shaft, i.e. sensitivity to any variations. EMS dynamics is observed not as sensitive to viscous friction on the load shaft as to friction on the motor or coupling shaft. However, damping capability of the system is more affected with friction on the load shaft. As shown in Figure 2.20(a) and 2.20(c), complete damping does not exist with the presence of viscous friction B_2.

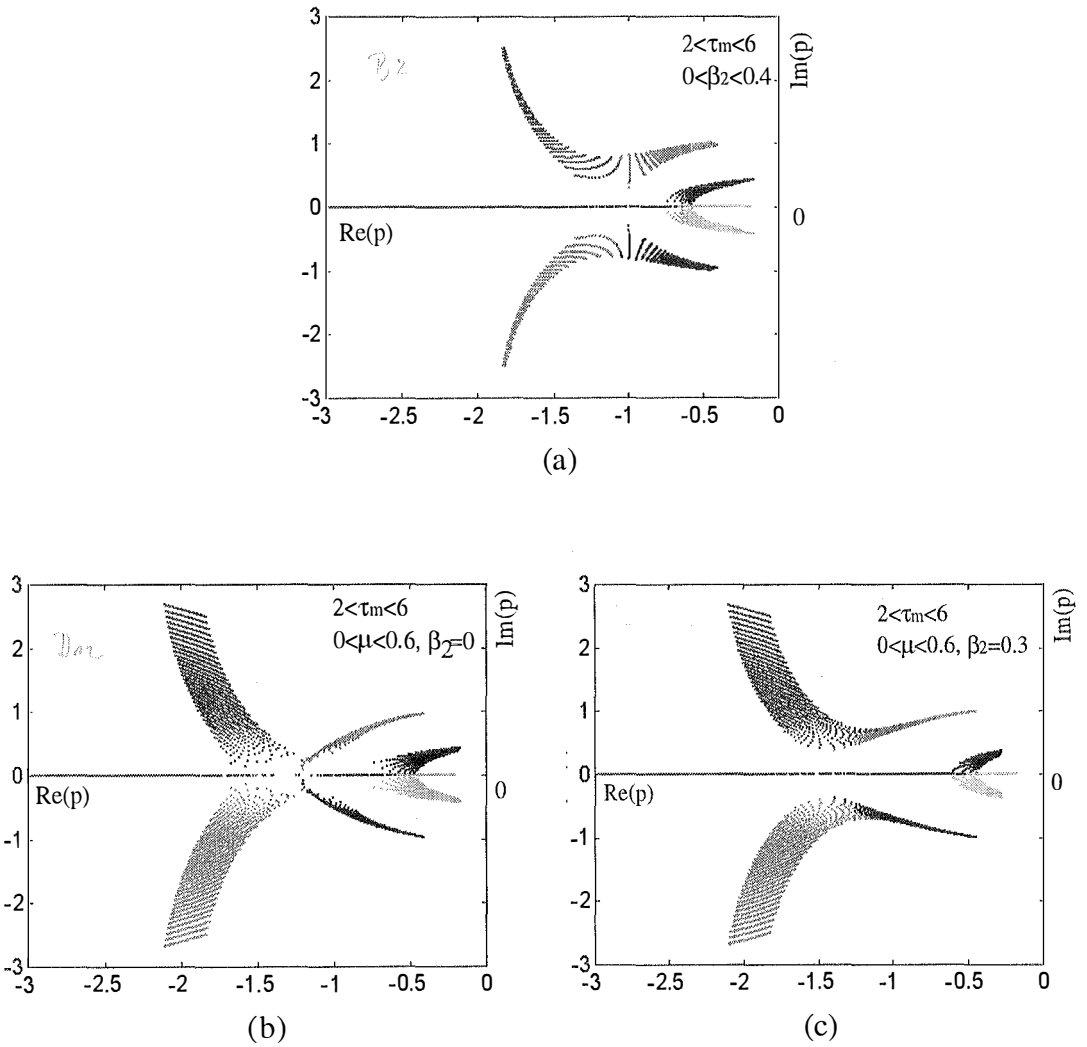

Figure 2.20. Root loci with viscous friction on the load and coupling shaft (γ=5, τ_e=0.25):
(a) B_1=0, $B_2 \neq 0$, $B_{12} = 0$; (b) B_1=0, $B_2 = 0$, $B_{12} \neq 0$; (c) B_1=0, $B_2 \neq 0$, $B_{12} \neq 0$.

In some industrial applications such as steel rolling mills or metal-cutting machines, viscous friction on the load and coupling shaft may cause undesirable self-excited oscillations. The root loci at larger values of the mass ratio γ show that this influence is reduced as the mass ratio increases.

2.7 Illustrative examples

Example 2.1: (Ha & Negnevitsky [35]) Consider first the three-mass rolling system reported in Hori *et al.* [64] with the following specifications: moments of inertia J_1=4.6758×10^4 kgm^2, J_2=1.2383×10^4 kgm^2, and J_3 = 9.4584×10^2 kgm^2; coupling shaft stiffness's K_{12} = 2.2164×10^8 Nm/rad, and K_{23}=1.2485×10^7 Nm/rad; the electromagnetic time-constant T_e=0.002sec. Equations (2.9a) to (2.9d) give the system parameters: the mass ratio γ=1.286, natural frequency Ω_N=132$rad/\sec$ (f_N=21Hz), first and second mode resonant frequencies Ω_{12}=112$rad/\sec$ (f_{12}=17.8Hz) and Ω_{23}=156$rad/\sec$ (f_{23}=24.8Hz), and a_1=2.115, b_1=1.843, γ_{12}=1.286. The system is a model of the steel rolling mills where the roll is coupled to the driving motor by long shafts and gear boxes. The finite but small elasticity of the shafts gets magnified and has a vibrational effect on the load speed. This vibration is not only undesirable but also the origin of the system instability in many cases. The discussion above mentioned can be used to estimate damping capability of this system. The possible maximal damping of the system is determined using theorem 2.1 and the conditions (2.44) which give the following values: δ^*=0.16 at τ_m^*=0.98 and τ_e^*=1.02. The root locus with τ_e = 0.264 and τ_m variable has the form of Figure 2.10. The dominant roots branches, located closed to the imaginary axis, are shown in Figure 2.21. These branches correspond to the first and second mode of the system. Note that with a small value of the mass ratio γ = 1.286 << γ_{cr}=35/3, torsional mechanical vibration in this rolling mill system is a serious problem.

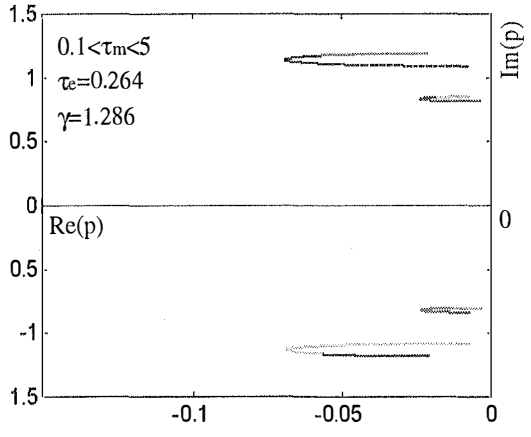

Figure 2.21. Root locus of a three-mass rolling mill system with τ_e=0.264 and τ_m= var.

Example 2.2: Consider a two-mass antenna drive system reported in Alferov & Ha [49]. The system parameters are given as follows: the electromagnetic and electromechanical time-constants T_e=0.03sec, T_m=0.116sec, moments of inertia J_1=0.814kgm^2, J_2=0.012kgm^2, and coupling shaft stiffness (modulus of rigidity) K_{12}=0.21Nm/rad. The system original is a servo drive for an antenna with paraboloidal surface. The open-loop plant has the structure of Figure 2.18(b), where the viscous friction coefficient B_{12} is uncertain but considerable. The natural frequency and the mass ratio are calculated from (2.6a) and (2.6b): Ω_N=4.21$rad/\sec$, γ=1.015. With a small value of the mass ratio, the system is expected to have self-excited oscillations. In fact, the maximal damping condition (2.37) gives δ^*=0.061 at τ_m^*=0.244, τ_e^*=4.09. The possible maximal damping factor is found very small and the viscous friction B_{12} on the coupling shaft is an uncertain factor affecting damping capability of the system. This influence can be examined by the root locus with varying viscous friction coefficient μ. The root locus of the form (2.52) with β_2 =0, μ=var., τ_e=0.139, and τ_m=0.489 is shown in Figure 2.22. If the value of the viscous friction coefficient B_{12} is around $6.3\times10^{-4}Nm.s/rad$ then μ is calculated to be 0.0126. Note that viscous friction in this case slightly increases the system damping factor from δ=0.003 to 0.009. However, the mass ratio γ is almost unity, vibrational effects are the main origin of instability in this system. This explains why it is very sensitive to load disturbances (for example, the influence of wind on the antenna paraboloidal surface) and parameter variations.

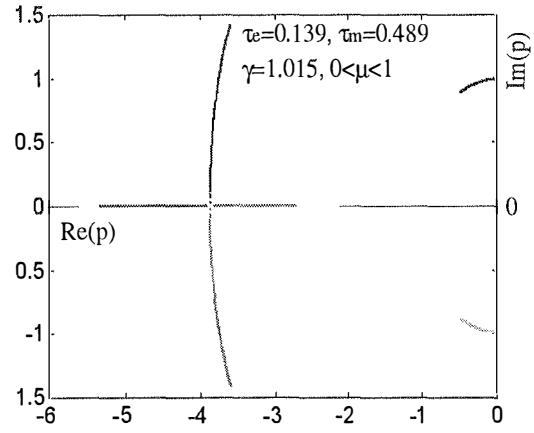

Figure 2.22. Root locus of a two-mass antenna servo system with β_2 =0, τ_e=0.139, τ_m=0.489, and varying viscous friction on the coupling shaft μ= var.

2.8 Summary

In this chapter, the problem of estimating maximal damping capability in multi-mass electromechanical systems was systematically addressed. The concept of dynamic stiffness of a linearised speed-torque characteristics, proposed by Kljuchev, is used for modelling the electromagnetic process of a motor. Thus, an n-mass flexible structure dynamics can be represented by a general block diagram. By introducing the per-unit notation, the characteristic equation of n-mass systems can then be written in dimensionless space, depending only on the mass ratio and the electromagnetic and electromechanical time-constants in relative units.

The main contribution here is that the conditions for maximal damping and complete damping are determined in the general case. The values of the electromagnetic and electromechanical time-constants at maximal damping are found depending on the mass ratio γ. Hence, the critical value of the mass ratio γ_{cr} and the corresponding system time-constants at complete damping can be derived. For two-mass systems, γ_{cr} is obtained equal to 5 in the case considering electromagnetic inertia τ_e, or equal to 9 in the case neglecting τ_e, a result widely-known in Soviet literature. For three-mass systems, the critical value of the mass ratio is 35/3 taking electromagnetic inertia into account, or 25 in the case $\tau_e \cong 0$. There exists a theoretical possibility for maximal damping, or complete damping if the flexible structure is not so complicated (eg. $n = 2$) and the electromagnetic time-constant is small enough. However, at maximal damping large values of the mass ratio γ are required.

One important feature is the use of the classical root locus method to illustrate the cases of maximal and complete damping in two-mass and three-mass electromechanical systems considering or neglecting motor's electromagnetic inertia. The influence of variations in the electromechanical time-constant τ_m (eg. changes in load inertia or dynamic stiffness of motor's speed-torque characteristics) on the root distribution of the system characteristic equation is directly observed on root locus plots. The multi-parameter root loci take into consideration other changing factors such as the electromagnetic time-constant and the mass ratio. It is obvious that at maximal or complete damping, which corresponds to a multiple root of the characteristic equation, the system dynamic behaviour is extremely sensitive to varying parameters. With a given mass ratio γ, dominant root branches of the system

root loci are observed not affected by parameter variations as much as the branches containing other roots.

The influence of viscous friction exerted on the motor, load, and coupling shafts is considered in dimensionless space using multi-parameter root loci. It is shown that two-mass system dynamics is more sensitive to friction on the motor and coupling shaft than friction on the load shaft. However, maximal damping of the system is seriously affected by friction on the load shaft. The oscillatory influence of viscous friction on the load and coupling shaft in two-mass systems is reduced at large values of the mass ratio.

A three-mass rolling mill system and a two-mass antenna servo drive system are used for the illustration purpose. In practice, the mass ratio value of electromechanical systems is usually much smaller than the critical value, as illustrated in the examples. The problem of increasing the damping capability in these systems becomes considerably important, especially for vibration suppression and the achievement of robustness to load and parameter variations. Furthermore, it should be noted that the generalised model (2.4) is applied to electric motors only under linearised conditions of the speed-torque characteristics.

Chapter 3

Robust Modal Control: an Overview

In multi-mass electromechanical systems, the suppression of elastic oscillations and rejection of external disturbances are challenging problems. The influence of parameter and load variations, and nonlinearities may also deteriorate the system performance to an intolerable extent. Thus, these systems require a controller that can achieve specified signal levels in the face of uncertainty, or a robust controller. This chapter is devoted to the development of such a control method for electrical drive systems, especially for flexible structures.

3.1 Introduction

Dote in [65] noted that there has been a great effort in applying modern control techniques in motor control. Feedback control covers a large area in these applications. In high performance electrical drives, for example in the area of robotics, tool machines, and electrical servos, it is required to develop a controller that can provide high accuracy, fast response, and insensitivity to system parameter variations, changing load, torque disturbance and nonlinearities. Various control methods addressing these problems have been developed: loop gain shaping (Bailey & Hui [66]), state feedback control (De Vegte [67]), linear quadratic control (Anderson & Moore [68]), model reference and adaptive control (Astrom [69]), H_∞ robust control (Kwakernaak [6]), and variable structure systems with sliding mode (Utkin [7], DeCarlo *et al.* [70]). (The issues relating to controllers using artificial intelligence tools, such as fuzzy logic or neural networks will be discussed in the following chapters). The conventional proportional-integral controllers cannot meet these requirements simultaneously. Adaptive controllers are effective to the control of the drive system whose model parameters are uncertain but sometimes it gives undesirable response [65]. The variable structure system method provides parameter insensitivity once the system is in the sliding mode but chattering is a problem.

Furthermore, when the system uncertainty is larger than one taken into account in the design, the sliding mode does not exist (Furuta [71]).

For applications in flexible structures, among the above methods, linear state feedback is of particular interest due to its design simplicity and its ability to assign a desired eigenstructure or *modes* to the closed loop system. That is why the method is also referred to as modal control (Kuzovkov [72]). The objective of modal control is to determine the feedback gain matrix in the linearised state equation in such a way that all the poles of the closed loop system are desirably placed in the complex plane and thus, its transient response has a desired shape. In modal control, knowledge of the state variables is required. However, in practice, not all of these variables are readily measurable. On the other hand, the influence of external disturbances may deteriorate the steady-state performance of the control system and should be compensated for. Hence, it is required to incorporate observers with a modal controller to provide estimates of the unmeasurable state variables for pole-placement feedback control, and estimates of the disturbances for feedforward compensation control. Moreover, the eigenvalue assignment is dependent on entries of state matrices, and thus, modal control is sensitive to system parameters. Therefore, robustness of pole assignment techniques should be taken into consideration. This chapter addresses these problems using an approach called *robust modal control.* Its material is based on the works by Ha [9], Ha & Alferov [19, 91], Alferov & Ha [73, 75, 36], and also in Alferov, Ha & Khusainov [74]. The design of a continuous and discrete-time robust modal controller with its applications in electromechanical systems are discussed in the following sections. Pros and cons of the proposed method and further suggestions will conclude this chapter.

3.2 Modal control

3.2.1 Linearised model

Modal control requires a linear approximation of the controlled object dynamics. For a broad class of motion control systems the dynamic behaviour of the system variations about operation point values can be approximated by a time-invariant linear differential equation, or equivalently, a state model of the form:

$$\begin{aligned} \dot{\mathbf{x}}(t) &= \mathbf{A}\mathbf{x}(t) + \mathbf{B}\mathbf{u}(t) + \mathbf{D}\mathbf{v}(t) \\ \mathbf{y}(t) &= \mathbf{C}\mathbf{x}(t) \end{aligned}, \tag{3.1}$$

where $\mathbf{x}(t) \in R^n$ is the state vector, $\mathbf{u}(t) \in R^r$ is the control vector, $\mathbf{v}(t) \in R^q$ is the disturbance vector, and $\mathbf{y}(t) \in R^m$ is the output vector; $\mathbf{A} \in R^{n \times n}$ is the *system matrix*, $\mathbf{B} \in R^{n \times r}$, $\mathbf{C} \in R^{m \times n}$, and $\mathbf{D} \in R^{n \times q}$.

In electrical drives, many systems can be described by, or reduced to the linearised model (3.1). The linear state equations are given in Ha & Alferov [19] for a variety of electric motors used in servo systems. The typical motors widely used in position drives are DC motors. Consider a servo system including a converter, a DC motor, and its mechanism with the angular position as the output. The state and output equation can be written as:

$$\dot{\mathbf{x}}(t) = \begin{bmatrix} -1/T_c & 0 & 0 & 0 \\ 0 & -B_m/J_m & K_b/J_m & 0 \\ 1/R_aT_a & -K_t/R_aT_a & -1/T_a & 0 \\ 0 & 1 & 0 & 0 \end{bmatrix} \mathbf{x}(t) + \begin{bmatrix} K_c/T_c \\ 0 \\ 0 \\ 0 \end{bmatrix} u(t) + \begin{bmatrix} 0 \\ -1/J_m \\ 0 \\ 0 \end{bmatrix} T_L(t), \quad (3.2)$$

$$y(t) = [0 \;\; 0 \;\; 0 \;\; 1]\mathbf{x}(t),$$

where the state vector is chosen as $\mathbf{x}(t) = \left[e_{sp} \;\; \omega \;\; i_a \;\; \theta\right]^T$ (superscript T identifies a transpose), with the supply voltage e_{sp}, the motor speed ω, the armature current i_a, and the position angle θ; the control signal $u(t)$ as the voltage applied to the voltage converter; and the external disturbance as the load torque $T_L(t)$. The coefficient K_c is the converter voltage gain, T_c is the converter time-constant, B_m is the viscous friction coefficient, J_m is the total moment of inertia, K_b is the motor back emf constant, K_t is the motor torque constant, R_a is the total armature resistance, $T_a = L_a/R_a$ is the electromagnetic time-constant, and L_a is the armature inductance. The model can be made simpler if T_c is negligible or a current converter is used (Alferov & Ha [75]).

In servo applications, DC motors are being gradually replaced by permanent magnet synchronous motors, sinusoidal or trapezoidal classes (brushless DC motors) (Jahns [76]), since they have lower inertia, larger power rate, fewer spark problems and lower noise. While there are some differences in construction between the two classes of permanent magnet synchronous machines, a sinusoidal permanent magnet synchronous motor and a brushless DC motor are all synchronous machines with a Y-connected 3-phase stator and a permanent magnet rotor. In field-oriented or vector control (Boldea & Nasar [77]), an independent (or decoupled) control of flux and torque of the motor is accomplished through a coordinated change in the supply

voltage and frequency. In permanent magnet synchronous machines, by field-oriented control, the stator current component i_{ds} in the $d-q$ frame is made equal to zero. The general voltage controlled model for permanent magnet synchronous drives can then be written as:

$$\dot{\mathbf{x}}(t)=\begin{bmatrix} -B_m/J_m & K_t/J_m & 0 \\ -\lambda_m/L_q & -R_s/L_q & 0 \\ 1 & 0 & 0 \end{bmatrix}\mathbf{x}(t)+\begin{bmatrix} 0 \\ 1/L_q \\ 0 \end{bmatrix}V_{qs}(t)+\begin{bmatrix} -p/J_m \\ 0 \\ 0 \end{bmatrix}T_L(t), \qquad (3.3)$$

$$y(t)=[0\ \ 0\ \ 1]\mathbf{x}(t),$$

where the state vector is chosen as $\mathbf{x}(t)=\left[\omega\ \ i_{qs}\ \ \theta\right]^T$, the control voltage as the stator voltage component $V_{qs}(t)$, and the disturbance as the load torque $T_L(t)$, and where λ_m is the magnet flux linkage amplitude, L_q is q-axis stator inductance, R_s is stator resistance, p is the number of pole pairs, and $K_t=3p\lambda_m/2$ is the torque constant. The model for a permanent magnet synchronous motor can be further simplified by using a current source inverter where i_{qs} is a known quantity and serves as a control signal to the motor in Ko *et al.* [78].

For an induction motor with a current regulated Pulse Width Modulator the mathematical model in the rotating reference frame $d-q$ can be linearised by using vector control (Tzou & Wu [79]). In the constant torque region $i_{ds}=const$, the state model of a current-decoupled induction motor is written as [19]:

$$\dot{x}(t)=\begin{bmatrix} -B_m/J_m & K_t/J_m & 0 \\ -\lambda_m/L_q & -1/T_i & 0 \\ 1 & 0 & 0 \end{bmatrix}x(t)+\begin{bmatrix} 0 \\ K_tK_i/L_m \\ 0 \end{bmatrix}i_q^*(t)+\begin{bmatrix} -1/J_m \\ 0 \\ 0 \end{bmatrix}T_L(t), \qquad (3.4)$$

$$y(t)=[0\ \ 0\ \ 1]\mathbf{x}(t),$$

where the state vector $\mathbf{x}(t)$ is chosen as in (3.3) and the control signal $i_q^*(t)$ is the inverter input, and where $K_t=3pL_m^2/2\,L_r$ is the torque constant, K_i is the inverter gain, T_i is the inverter time-constant, L_m is the mutual magnetising inductance, and L_r is the rotor inductance.

Consider the speed control of a two-mass servo drive of Figure 2.18(b). Taking into account the influence of the load torque T_L as the external disturbance, with the state

vector chosen as $\mathbf{x}(t) = [T \;\; \omega_1 \;\; T_{12} \;\; \omega_2]^T$ and the load speed ω_2 as the output, the state model for the system (2.47) can be written as (Ha [9]):

$$\dot{\mathbf{x}}(t) = \begin{bmatrix} \frac{-1}{T_e} & \frac{-\beta}{T_e} & 0 & 0 \\ \frac{1}{J_1} & \frac{-B_1}{J_1} & \frac{-1}{J_1} & 0 \\ \frac{B_{12}}{J_1} & \frac{K_{12}J_1 - B_{12}B_1}{J_1} & \frac{-B_{12}(J_1+J_2)}{J_1J_2} & \frac{B_{12}B_1 - K_{12}J_2}{J_2} \\ 0 & 0 & \frac{1}{J_2} & \frac{-B_2}{J_2} \end{bmatrix} \mathbf{x}(t) + \begin{bmatrix} \frac{\beta}{T_e} \\ 0 \\ 0 \\ 0 \end{bmatrix} \omega_{ref}(t) + \begin{bmatrix} 0 \\ 0 \\ \frac{B_{12}}{J_2} \\ \frac{-1}{J_2} \end{bmatrix} T_L(t), \quad (3.5)$$

$$y(t) = [0 \;\; 0 \;\; 0 \;\; 1]\mathbf{x}(t).$$

3.2.2 Modes, Controllability, and Observability

Recall that the state model for a system depends on the choice of a set of state variables, and thus is not unique. In fact, a new state vector $\mathbf{z}(t)$ can be defined by a nonsingular coordinate transformation $\mathbf{x} = \mathbf{Tz}$ but the eigenvalues of the transformed system matrix $\mathbf{T}^{-1}\mathbf{AT}$ and of $\mathbf{A}$ are the same because the characteristic equation does not change:

$$\left|s\mathbf{I}_n - \mathbf{T}^{-1}\mathbf{AT}\right| = \left|\mathbf{T}^{-1}(s\mathbf{I}_n - \mathbf{A})\mathbf{T}\right| = \left|s\mathbf{I}_n - \mathbf{A}\right| = 0, \quad (3.6)$$

where $\mathbf{I}_n \in R^{n\times n}$ is the identity matrix. Of particular interest is the transformation $\mathbf{U}$ required to diagonalise the system matrix $\mathbf{A}$:

$$\mathbf{U}^{-1}\mathbf{AU} = \Lambda = diag(\lambda_1,\ldots,\lambda_n), \quad (3.7)$$

where λ_i, $i = 1,\ldots,n$, are the roots of the open loop system characteristic equation:

$$\Delta_o(s) = \left|s\mathbf{I}_n - \mathbf{A}\right| = \left|s\mathbf{I}_n - \Lambda\right| = (s-\lambda_1)(s-\lambda_2)\ldots(s-\lambda_n) = \quad (3.8)$$
$$= s^n + a_n s^{n-1} + \ldots + a_2 s + a_1 = 0.$$

It can be derived from (3.6) that $\mathbf{AU} = \mathbf{U}\Lambda$, or

$$\mathbf{A}[\mathbf{u}_1, \ldots, \mathbf{u}_n] = [\mathbf{u}_1, \ldots, \mathbf{u}_n]diag(\lambda_1,\ldots\lambda_n),$$

and by equating the $i-$th columns, we have

$$\mathbf{A}\mathbf{u}_i = \lambda_i \mathbf{u}_i, \quad \text{or} \quad (\lambda_i \mathbf{I}_n - \mathbf{A})\mathbf{u}_i = \mathbf{0}. \tag{3.9}$$

The solution $\mathbf{u}_i$ of (3.9) is the i–th (right) eigenvector of the system matrix $\mathbf{A}$ with respect to the eigenvalue λ_i corresponding to a system *mode*. Thus, the transformation $\mathbf{U}$ diagonalising $\mathbf{A}$ is called the (open loop) *modal matrix*. Assuming that the system (3.1) is free of disturbances ($\mathbf{D} = \mathbf{0}$), with $\mathbf{x} = \mathbf{U}\mathbf{z}$, the transformed state equation is then written as:

$$\dot{\mathbf{z}} = \Lambda \mathbf{z} + \mathbf{U}^{-1}\mathbf{B}\mathbf{u} = \Lambda \mathbf{z} + \mathbf{V}^T\mathbf{B}\mathbf{u}, \quad \mathbf{y} = \mathbf{C}\mathbf{U}\mathbf{z}, \tag{3.10}$$

where $\mathbf{z} = \mathbf{U}^{-1}\mathbf{x} = \mathbf{V}^T\mathbf{x}$ is the modal vector. The i–th columns $\mathbf{v}_i$ of $\mathbf{V} = [\mathbf{v}_1, \ldots, \mathbf{v}_n]$ are the left eigenvectors of $\mathbf{A}$:

$$\mathbf{v}_i^T\mathbf{A} = \lambda_i \mathbf{v}_i^T \quad \text{or} \quad \mathbf{A}^T\mathbf{v}_i = \lambda_i \mathbf{v}_i. \tag{3.11}$$

and satisfy the following properties:

$$\mathbf{v}_i^T\mathbf{u}_j = 0 \quad (i \neq j), \quad \mathbf{v}_i^T\mathbf{u}_i = 1. \tag{3.12}$$

The linear system is *controllable* if and only if $\mathbf{U}^{-1}\mathbf{B}$ has no rows consisting entirely of zero elements, and it is *observable* if and only if $\mathbf{C}\mathbf{U}$ has no columns consisting entirely of zero elements (De Vegte [67]). The concepts of controllability and observability, first introduced by R. E. Kalman [80], play an important role in modal control. Suppose that the i–th row of $\mathbf{U}^{-1}\mathbf{B}$ has only zero elements, then from (3.9) the i–th mode is uncontrollable, since it is not affected by the control. Similarly, suppose that the j–th column of $\mathbf{C}\mathbf{U}$ has only zero elements, then the j–th mode is unobservable, because it does not show up in the output. It is known that the conditions of controllability and observability are expressed in terms of $\mathbf{A}$ and $\mathbf{B}$, and $\mathbf{A}$ and $\mathbf{C}$, respectively (De Vegte [67], Kuzovkov [72]). The following theorem is very popular:

Theorem 3.1: The pair ($\mathbf{A}$, $\mathbf{B}$) is controllable if and only if the rank of the *controllability matrix*

$$\Gamma_C = [\mathbf{B} \;\; \mathbf{A}\mathbf{B} \;\; \mathbf{A}^2\mathbf{B} \ldots \mathbf{A}^{n-1}\mathbf{B}] \tag{3.13}$$

is n. The pair ($\mathbf{C}$, $\mathbf{A}$) is observable if and only if the rank of the *observability matrix*

$$\Gamma_0 = [\mathbf{C}^T \ \mathbf{A}^T\mathbf{C}^T \ \mathbf{A}^{T^2}\mathbf{C}^T \ \ldots \ \mathbf{A}^{T^{n-1}}\mathbf{C}^T] \tag{3.14}$$

is n.

3.2.3 Pole assignment and feedback matrix

For the system (3.1) with $\mathbf{D} = \mathbf{0}$, the state model and *state feedback control* are:

$$\dot{\mathbf{x}} = \mathbf{A}\mathbf{x} + \mathbf{B}\mathbf{u}, \ \ \mathbf{y} = \mathbf{C}\mathbf{x}, \tag{3.15a}$$

$$\mathbf{u} = -\mathbf{K}\mathbf{x}, \tag{3.15b}$$

where $\mathbf{K} \in R^{r\times n}$ is the feedback gain matrix. The objective of state feedback control is to assign the closed-loop eigenvalues of the *closed-loop matrix* $(\mathbf{A} - \mathbf{BK})$ or the roots of the closed-loop characteristic equation

$$\Delta(s) = \left|s\mathbf{I}_n - (\mathbf{A} - \mathbf{BK})\right| = 0. \tag{3.16}$$

The desired characteristic equation is found from the desired closed-loop eigenvalues $\lambda_{c,i}$ $(i = 1,\ldots,n)$:

$$\begin{aligned}\Delta_c(s) &= (s - \lambda_{c,1})(s - \lambda_{c,2})\ldots(s - \lambda_{c,n}) = \\ &= s^n + \alpha_n s^{n-1} + \ldots + \alpha_2 s + \alpha_1 = 0.\end{aligned} \tag{3.17}$$

The choice of the poles $\lambda_{c,i}$ is based the desired transient response of the closed-loop response. There exists many criteria for such a choice. In the field of electrical drives, for example, the popular criteria are the binomial expansion, Butterworth polynomials, magnitude optimum principles, and Graham-Lathrop minimisation of the integral time absolute error (ITAE) (Terekhov [81]). Transient performance and coefficients of normalised polynomials by those criteria are given in Appendix A. A comprehensive comparison between the magnitude and symmetric optimum criterion with others is discussed in Umland & Safiudin [82]. After choosing the desired closed-loop poles, the elements of the feedback matrix $\mathbf{K}$ can be found by equating coefficients in (3.16) and (3.17). In state feedback control, the condition for determining the feedback matrix $\mathbf{K}$ consisting of constant gains is the controllability of the pair $(\mathbf{A}, \mathbf{B})$.

For the single-input case ($n = 1$), the design procedure comprises of two steps: (i) using a coordinate transformation to bring the state model (3.15a) to the *companion form* with

$$\mathbf{A} = \begin{bmatrix} 0 & 1 & \dots & 0 \\ \vdots & & \ddots & \vdots \\ 0 & & & 1 \\ -a_1 & -a_2 & \dots & -a_n \end{bmatrix}, \mathbf{b} = \begin{bmatrix} 0 \\ \vdots \\ 0 \\ 1 \end{bmatrix}, \tag{3.18}$$

and (ii) the feedback row vector $\mathbf{k}^T = [k_1 \;\; k_2 \;\dots\; k_n]$ is then found as

$$\mathbf{k}^T = [\alpha_1 - a_1 \;\; \alpha_2 - a_2 \;\dots\; \alpha_n - a_n], \tag{3.19}$$

where a_i and α_i are the coefficients of the open loop and desired closed-loop characteristic polynomial, respectively. For multiple-input systems, a common technique is to reduce them in effect to single-input ones according to $\mathbf{u} = \mathbf{g}w$, where $\mathbf{g}$ is a vector of constant and w is a new single input. Then

$$\dot{\mathbf{x}} = \mathbf{A}\mathbf{x} + \mathbf{B}\mathbf{u} = \mathbf{A}\mathbf{x} + (\mathbf{B}\mathbf{g})w = \mathbf{A}\mathbf{x} + \mathbf{b}w, \tag{3.20}$$

and $\mathbf{g}$ must be chosen such that $(\mathbf{A}, \mathbf{b})$ is controllable.

An alternative technique for pole assignment is modal control which is based on modal transformation. Consider a single-input system with state feedback:

$$\dot{\mathbf{x}} = \mathbf{A}\mathbf{x} + \mathbf{b}w, \quad w = -\mathbf{k}^T\mathbf{x}. \tag{3.21}$$

By using the modal transformation in (3.10)-(3.12) and feedback from the $i-$th and $j-$th modal variables z_i, z_j with gains k_i, k_j to generate w, the control signal may be written as:

$$w = -k_i z_i - k_j z_j = -k_i \mathbf{v}_i^T\mathbf{x} - k_j \mathbf{v}_j^T\mathbf{x} = -(k_i \mathbf{v}_i^T + k_j \mathbf{v}_j^T)\mathbf{x} = -\mathbf{k}^T\mathbf{x}. \tag{3.22}$$

Applying the orthogonal properties (3.11) to the closed-loop system matrix yields

$$(\mathbf{A} - k_i\mathbf{b}\mathbf{v}_i^T - k_j\mathbf{b}\mathbf{v}_j^T)\mathbf{u}_k = \mathbf{A}\mathbf{u}_k = \lambda_k\mathbf{u}_k \;\; (k \neq i, j). \tag{3.23}$$

This means that the eigenvalues λ_k $(k \neq i, j)$ of the open loop system are not affected by the feedback from the $i-$th and $j-$th modal variables and thus, verifies the following:

Remark: Modal control uses feedback from selected modal variables to change only these eigenvalues to more desirable locations, without affecting the others.

A procedure for calculating the feedback vector $\mathbf{k}^T$ is given as follows (De Vegte [67]):

(i) The feedback gains k_i, k_j in (3.21) to move the eigenvalues λ_i, λ_j of the system (3.20) to the desired $\lambda_{c,i}$, $\lambda_{c,j}$ are

$$k_i = \frac{(\lambda_i - \lambda_{c,i})(\lambda_i - \lambda_{c,j})}{(\mathbf{v}_i^T\mathbf{b})(\lambda_i - \lambda_j)}, \quad k_j = \frac{(\lambda_j - \lambda_{c,j})(\lambda_j - \lambda_{c,i})}{(\mathbf{v}_i^T\mathbf{b})(\lambda_j - \lambda_i)}. \tag{3.24}$$

(ii) The feedback gain k_i to move only λ_i to $\lambda_{c,i}$ (λ_j=$\lambda_{c,j}$, k_j=0) is

$$k_i = \frac{(\lambda_i - \lambda_{c,i})}{(\mathbf{v}_i^T\mathbf{b})}. \tag{3.25}$$

(iii) The generalised form of (3.23) to move λ_1, ..., λ_p to $\lambda_{c,1}$, ..., $\lambda_{c,p}$ is

$$k_i = \frac{\prod_{j=1}^{p}(\lambda_i - \lambda_{c,j})}{(\mathbf{v}_i^T\mathbf{b}) \prod_{j=1,\neq i}^{j=p}(\lambda_i - \lambda_j)}. \tag{3.26}$$

An approach to multiple input systems is also to reduce them in effect to single-input ones. For a plant with r inputs, $\mathbf{B}$ consists of r columns $\mathbf{b}_i$ $(i = 1,\ldots,r)$. The state equation and state feedback control can then be expressed as

$$\dot{\mathbf{x}} = \mathbf{A}\mathbf{x} + \mathbf{B}\mathbf{u} = \mathbf{A}\mathbf{x} + \mathbf{b}_1 u_1 + \ldots + \mathbf{b}_r u_r, \tag{3.27}$$

$$\mathbf{u} = -\mathbf{K}\mathbf{x} \quad u_i = -\mathbf{k}_i^T\mathbf{x}, \quad (i = 1,\ldots,r),$$

where u_i is the i−th element of $\mathbf{u}$ and $\mathbf{k}_i^T$ is the i−th row of $\mathbf{K}$. The input u_i can be used to place the eigenvalues for which $\mathbf{v}_i^T\mathbf{b} \neq 0$. A mode is usually controllable from more than one input, so the design is not unique in a multiple-input system.

3.2.3 Discrete-time modal controller

Similar results can obtained in discrete-time linear systems with a time-invariant state model of the form:

$$\begin{aligned} \mathbf{x}(k+1) &= \mathbf{A}_d\mathbf{x}(k) + \mathbf{B}_d\mathbf{u}(k) + \mathbf{D}_d\mathbf{v}(k) \\ \mathbf{y}(k) &= \mathbf{C}_d\mathbf{x}(k) \end{aligned}, \tag{3.28}$$

where $\mathbf{x}(k) \in R^n$ is the state vector, $\mathbf{u}(k) \in R^r$ is the control vector, $\mathbf{v}(k) \in R^q$ is the disturbance vector, and $\mathbf{y}(k) \in R^m$ is the output vector. The matrices $\mathbf{A}_d \in R^{n\times n}$, $\mathbf{B}_d \in R^{n\times r}$, $\mathbf{C}_d \in R^{m\times n}$, and $\mathbf{D}_d \in R^{n\times q}$ can be obtained from the continuous-time forms in (3.1) using the state transition matrix (Kuo [83]) with a given sampling period T. The cumbersome elaboration on the inverse Laplace transform to obtained the entries of these matrices (Ha & Alferov [91]) can be avoided by using a numerical algorithm.

A modal controller can be designed to assign a desired eigenstructure to the discrete-time system (3.28) with a state feedback strategy:

$$\mathbf{u}(k) = -\mathbf{K}\mathbf{x}(k). \tag{3.29}$$

For a single-input system, while (3.24)-(3.26) can be used to determine the feedback gains, there are some expressions, convenient for calculating $\mathbf{k}^T$. Let

$$\Delta_o(z) = \left|z\mathbf{I}_n - \mathbf{A}_d\right| = z^n + a_n z^{n-1} + \ldots + a_2 z + a_1 = 0 \tag{3.30}$$

and

$$\Delta_c(z) = z^n + \alpha_n z^{n-1} + \ldots + \alpha_2 z + \alpha_1 = 0 \tag{3.31}$$

be the open-loop and desired closed-loop characteristic equations, respectively. The row feedback vector $\mathbf{k}^T$ required to move all the roots of (3.30) to those of (3.31) can be determined (Kuo [83]) by:

$$\mathbf{k}^T = (\alpha - \mathbf{a})^T(\Gamma_C\mathbf{M})^{-1}, \tag{3.32}$$

where $$\alpha = [\alpha_n \;\; \alpha_{n-1} \;\; \ldots \;\; \alpha_1]^T, \quad \mathbf{a} = [a_n \;\; a_{n-1} \;\; \ldots \;\; a_1]^T, \tag{3.33}$$

$$\Gamma_C = [\mathbf{B}_d \;\; \mathbf{A}_d\mathbf{B}_d \;\; \mathbf{A}_d{}^2\mathbf{B}_d \;\ldots\; \mathbf{A}_d{}^{n-1}\mathbf{B}_d] \tag{3.34}$$

is the controllability matrix, and

$$\mathbf{M} = \begin{bmatrix} 1 & a_n & a_{n-1} & \ldots & a_3 & a_2 \\ 0 & 1 & a_n & \ldots & a_4 & a_3 \\ 0 & 0 & 1 & \ldots & a_5 & a_4 \\ \vdots & \vdots & \vdots & \ddots & \vdots & \vdots \\ 0 & 0 & 0 & \ldots & 1 & a_n \\ 0 & 0 & 0 & \ldots & 0 & 1 \end{bmatrix}. \tag{3.35}$$

Another expression, commonly called Ackermann's formula (Ogata [84]), can be used for determining the feedback gain $\mathbf{k}^T$:

$$\mathbf{k}^T = [0 \;\; 0 \ldots 0 \;\; 1]\Gamma_C^{-1}\Delta_c(\mathbf{A}_d), \tag{3.36}$$

where the controllability matrix Γ_C is given in (3.34), and

$$\Delta_c(\mathbf{A}_d) = \mathbf{A}_d^n + \alpha_n\mathbf{A}_d^{n-1} + \ldots + \alpha_2\mathbf{A}_d + \alpha_1\mathbf{I}_n. \tag{3.37}$$

In the multiple-input case, the system response can be speeded up due to the more freedom to choose the control signals but the determination of the state feedback gain matrix $\mathbf{K}$ in (3.29) becomes more complicated. Again, system eigenvalues can be moved one at a time by using (3.27). A tactful approach can be applied for reducing the system to a single-input one by fixing the ratios of the inputs according to $\mathbf{u}(k) = \mathbf{g}w(k)$ as in (3.20), where $\mathbf{g}$ is a constant vector and $w(k)$ is a new single input.

One important feature of a discrete-time modal controller is that it can provide a *deadbeat* step response (which exhibits the minimum possible settling time, no steady-state error, and no ripples between the sampling instants) whereas a continuous-time one cannot. In deadbeat control, the sampling time is the important design parameter which should be carefully chosen taking account of the trade-off between the limited magnitude of control signal due to saturation and the response speed (Ogata [84]).

3.3 Dominant pole-based assignment and sensitivity analysis

In manipulator control, linearisation is performed with respect to some reference states (*node points*), modal control can be applied to make the robot follow a desired trajectory, prescribed by a set of node points, with a dynamic error determined by the assigned eigenstructure in Stepanenko [85]. However, for a system of order n, there are $2n^2$ entries of the closed-loop modal matrix to be determined. For large space structures, neglecting the effect of non-critical modes, the problem of assigning the eigenvalues associated with critical modes (Lu *et al.* [86]) can be solved by direct velocity feedback using collocated actuators and sensors. Since modal control in general does not increase the order of a system, it is not guaranteed that the output or states of the system will follow the input in the steady state regime. When the design objective is to have the system track a certain input, the state feedback schemes should be properly modified (Bortsov *et al.* [87]). In the field of electrical drives, critical modes are decided by dominant roots of the characteristic equation. By assigning only the dominant roots, modal control can take into consideration other performance criteria, for example steady-state requirements (Alferov & Ha [75]), as described in the following section.

3.3.1 Dominant pole-based modal controller

In servo drives, a modal control algorithm which can provide a desired set of closed-loop eigenvalues and some steady-state performance at the same time may lead to an infeasible solution because the number of variables is greater than that of the equations (Kukharenko [88]). This can be avoided by assigning only a pair of dominant poles for satisfactory bandwidth and damping, and choosing the other eigenvalues to the left of this pair in such a way that some performance enhancement can be obtained. In this case the number of variables the feedback gains is equal to the number of equations. As many servo drive systems can be represented by linearised models, the dominant pole-based modal control technique is illustrated through a DC motor position drive of Figure 3.1, where the plant state model is given in (3.2) with a negligible viscous friction coefficient ($B_m = 0$). The modal controller (MC) consists of feedback from the shaft angle θ, speed ω, current i_a, and voltage e_c. The open-loop characteristic equation is

$$\Delta_o(s) = s(s + \frac{1}{T_c})(s^2 + \frac{1}{T_a}s + \frac{1}{T_a T_m}) = 0, \tag{3.39}$$

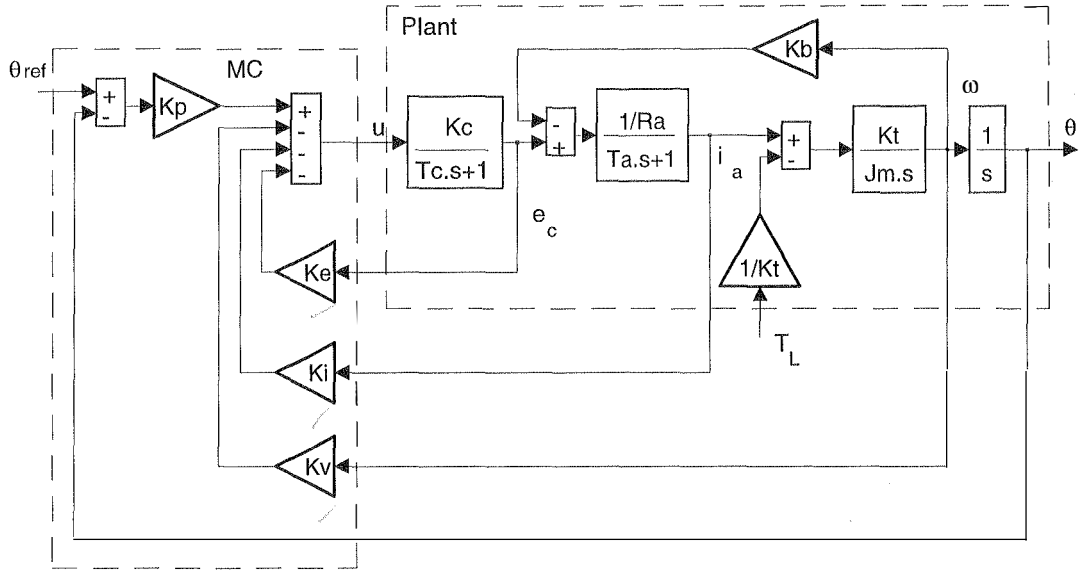

Figure 3.1. Modal control of a DC position drive.

where $T_m = \dfrac{J_m R_a}{K_b K_t}$ is the electromechanical time-constant. The closed-loop characteristic equation can be found by (3.16) with matrices **A** and **b** defined in (3.2) and the feedback vector $\mathbf{k}^T = (K_E \;\; K_V \;\; K_I \;\; K_P)$:

$$\Delta(s) = s^4 + \frac{T_a + T_c + K_c K_E T_a}{T_a T_c} s^3 + \frac{1 + K_c K_E + K_c K_I / R_a + T_c / T_m}{T_a T_c} s^2 + \\ + \frac{1 + K_c K_V / K_b}{T_a T_c T_m} s + \frac{K_c K_P / K_b}{T_a T_c T_m} = 0. \tag{3.40}$$

First, let us assign to $\Delta(s)$ a pair of dominant roots $-\delta\Omega_0 \pm j\Omega_0\sqrt{1-\delta^2}$, where the values of the damping factor δ and resonant frequency Ω_0 are determined according to the required transient performance, for example, overshoot and settling time. The other two roots are assumed to lie far in the left side of the dominant roots in the complex plane and thus, have a negligible effect on the closed-loop dynamics. The desired characteristic polynomial consists of two quadratic terms:

$$\Delta_d(s) = (s^2 + 2\delta\Omega_0 s + \Omega_0^2)(s^2 + \alpha_2 s + \alpha_1), \tag{3.41}$$

where α_1 and α_2 are coefficients determining the location of the rest two roots with $\alpha_2 >> \delta\Omega_0$. By analysing the influence of the feedback gains on the steady-state

errors due to a ramp reference input and a unit step load torque, a procedure for determining the feedback gains K_E, K_V, K_I and K_P can be obtained with improved steady-state performance (Alferov & Ha [75]). First, α_1 and K_I are determined by solving a system of linear equations:

$$\alpha_1 - \frac{K_c}{T_c R_a T_a} K_I = \frac{1}{T_a T_m} + \frac{1}{T_a T_c} - 2\delta\Omega_0 \left(\frac{1}{T_a} + \frac{1}{T_c} - 2\delta\Omega_0\right)$$

$$2\delta\Omega_0\alpha_1 - \frac{K_c}{2T_c R_a T_a}\left(\frac{1}{T_a} + \frac{1}{T_c}\right)K_I = \left(\frac{1}{T_a} + \frac{1}{T_c} - 2\delta\Omega_0\right)\Omega_0^2 - \frac{1}{2T_c T_m T_a}\left(1 + \frac{T_m + T_c}{T_a} + \frac{T_m}{T_c}\right) \tag{3.42a}$$

then the other feedback gains are derived as follows:

$$\begin{aligned} K_E &= 0 \\ K_V &= \frac{K_b}{2K_c}\left[K_c \frac{K_I}{R_a}\frac{T_m}{T_a} + \frac{T_c + T_m}{T_a}\left(1 + K_c \frac{K_I}{R_a}\right) - 1\right] \\ K_P &= \frac{K_b}{K_c} T_a T_c T_m \Omega_0^2 \alpha_1 . \end{aligned} \tag{3.42b}$$

When the vibration tendency in the system is serious, taking account of the maximal damping condition (see Section 2.4.2) the second term in (3.41) is chosen to coincide with the first one. Thus, the design equations for the feedback gains can be found by equating the coefficients of (3.40) and (3.41):

$$\begin{aligned} K_E &= \frac{4\delta\Omega_0 T_a T_c - T_a - T_c}{K_c T_a}, \\ K_I &= \frac{R_a}{K_c}\left[T_a T_c \Omega_0^2 (1 + 4\delta^2) + \frac{T_c}{T_a} - 4\delta\Omega_0 T_c - \frac{T_c}{T_m}\right], \\ K_V &= (4\delta T_a T_c T_m \Omega_0^3 - 1)\frac{K_b}{K_c}, \\ K_P &= \frac{T_a T_c T_m \Omega_0^4 K_b}{K_c}. \end{aligned} \tag{3.43}$$

Note that in (3.43), a damping factor chosen at δ=0.707 corresponds to the choice of closed-loop eigenvalues with the magnitude optimum criterion, and at δ=1, with binomial expansion.

When the converter time constant is negligible ($T_c \cong 0$) the state equation in (3.2) becomes:

$$\begin{bmatrix} \dot{\omega} \\ \dot{i}_a \\ \dot{\theta} \end{bmatrix} = \begin{bmatrix} -B_m/J_m & K_b/J_m & 0 \\ -K_t/R_aT_a & -1/T_a & 0 \\ 1 & 0 & 0 \end{bmatrix} \begin{bmatrix} \omega \\ i_a \\ \theta \end{bmatrix} + \begin{bmatrix} 0 \\ K_c/R_aT_a \\ 0 \end{bmatrix} u(t) + \begin{bmatrix} -1/J_m \\ 0 \\ 0 \end{bmatrix} T_L(t), \quad (3.44)$$

and the design equations can be found from the dominant root assignment and the complete damping condition of the speed loop [70]:

$$\begin{aligned} K_I &= \left[2\Omega_0 T_a(1+2\delta)-1\right] R_a/K_c \\ K_V &= \left[\Omega_0^2 T_a T_m (1+2\delta)^2 - 1\right] K_b/K_c \\ K_P &= 2\Omega_0^3 T_a T_m (1+\delta) K_b/K_c. \end{aligned} \quad (3.45)$$

The desired characteristic equation in this case is

$$\Delta_c(s) = (s^2 + 2\delta\Omega_0 s + \Omega_0^2)(s + 2(1+\delta)\Omega_0) = 0. \quad (3.46)$$

A comparison of the proposed method with state feedback control using other criteria such as binomial expansion, Butterworth, or magnitude optimum (see Appendix A) indicates that modal control gives smaller steady-state errors with a ramp reference input or a step load torque (Alferov & Ha [75]).

Example 3.1: Consider the system of Figure 3.1 with the plant specifications: $R_a = 0.524 ohm$, $T_a = 0.143 \text{sec}$, $T_m = 0.8 \text{sec}$, $K_b = 23.5 V \text{sec}/rad$, $J_m = 843 kgm^2$, $K_t = 23.5 Nm/A$, $K_c = 29$, and $T_c = 0.01 \text{sec}$.

The base frequency is chosen at $\Omega_0 = 10 s^{-1}$ for a modal controller with different criteria of pole assignment. With the desired dominant roots chosen at $-7 \pm j7$, the feedback gain obtained from (3.45) is $K_I = 0.106 V/A$, $K_V = 52.6 Vs/rad$, and $K_P = 315 V/rad$.

The step response with a constant load torque exerted at $t = 1 \text{sec}$ is shown in Figure 3.2. It is observed that the response using a dominant root-based modal controller (Figure 3.2(a)) gives better steady-state performance in comparison with the other criteria such as binomial expansion (Figure 3.2(b)), Butterworth (Figure 3.2(c)), or ITAE (Figure 3.2(d)).

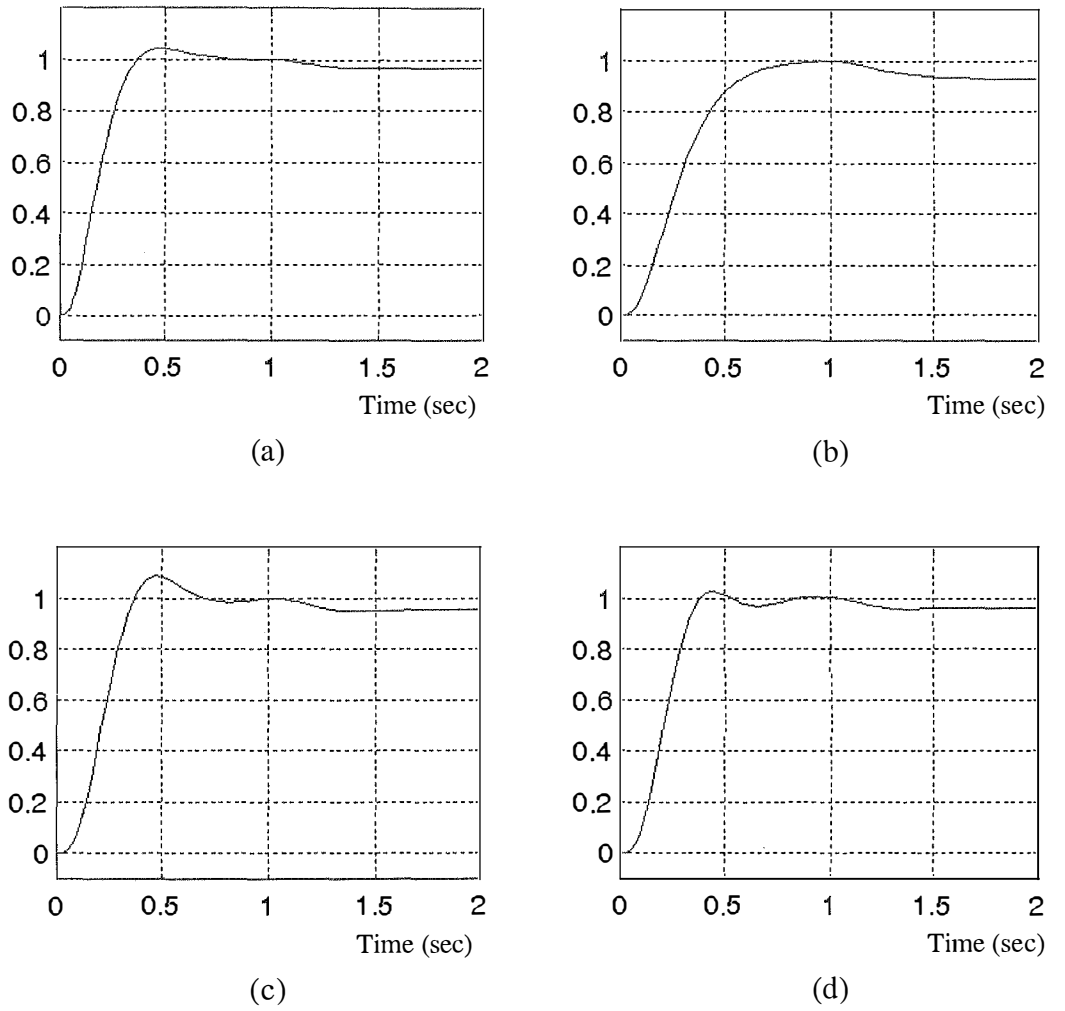

Figure 3.2. Step response of an one-mass system with a load torque at $t = 1$ sec using modal control with: (a) dominant pole-based, (b) binomial expansion, (c) Butterworth, and (d) ITAE polynomial.

A modal controller for speed control of two-mass flexible systems is shown in Figure 3.3, where the plant has the block diagram of Figure 2.18(b) with the feedback vector $\mathbf{k}^T = \left[K_T \;\; K_{\omega_1} \;\; K_{T_{12}} \;\; K_{\omega_2}\right]$. The closed-loop characteristic equation is

$$\Delta(s) = \left|s\mathbf{I}_4 - \mathbf{A} + \mathbf{b}\mathbf{k}^T\right| = s^4 + \frac{1+\beta K_T}{T_e}s^3 + \left(\frac{\gamma}{T_e T_m}(1+K_{\omega_1}) + \Omega_N^2\right)s^2 + \\ + \frac{\Omega_N^2}{T_e}(1+\beta K_T + \frac{\gamma-1}{\gamma}\beta K_{T_{12}})s + \frac{\Omega_N^2}{T_e T_m}(1+K_{\omega_1}+K_{\omega_2}) = 0, \tag{3.47}$$

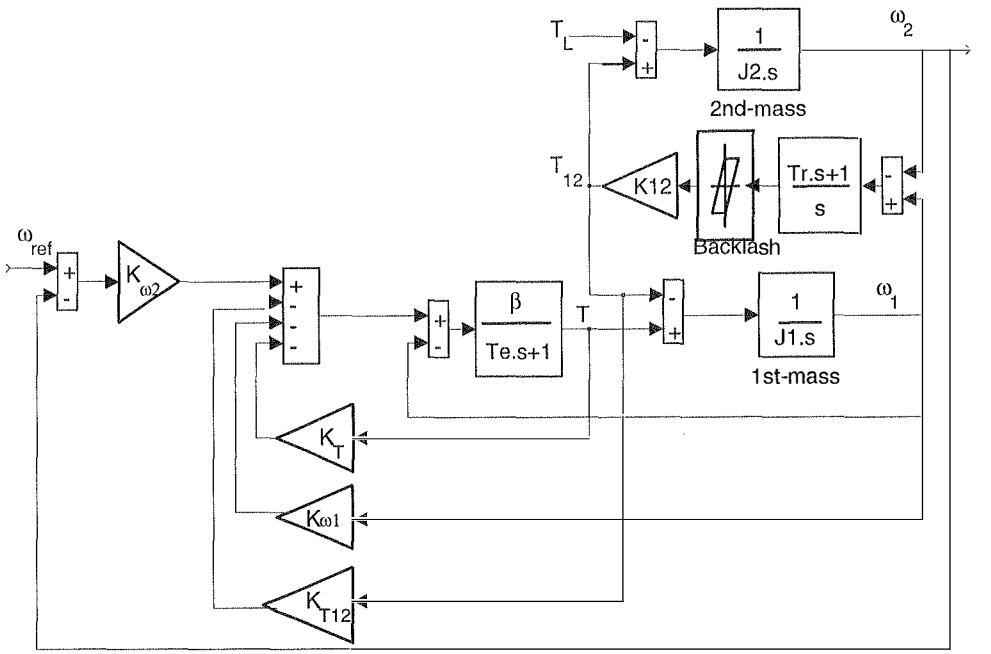

Figure 3.3. Modal control of a two-mass system.

where the plant resonant frequency Ω_N, mass ratio γ, and electromechanical time constant T_m are given in (2.6a), (2.6b) and (2.8), respectively. The design also starts with choosing the dominant roots $-\delta\Omega_0 \pm j\Omega_0\sqrt{1-\delta^2}$ according to the required transient performance. In two-mass systems, since the problem of vibration suppression is important, it is of interest to choose the second term of (3.41) for improving damping capability of the system. Equating the coefficients of (3.47) and (3.41) at maximal damping (see Section 2.4) yields:

$$K_T = \frac{4\delta\rho\tau_e - 1}{\beta}, \tag{3.48}$$

$$K_{\omega_1} = \frac{\tau_e\tau_m}{\gamma}\left[\rho^2(2+4\delta^2)-1\right]-1,$$

$$K_{T_{12}} = \frac{4\delta\gamma\rho\tau_e}{(\gamma-1)\beta}(\rho^2-1),$$

$$K_{\omega_2} = \frac{\tau_e\tau_m}{\gamma}\left[\gamma\rho^4-(2+4\delta^2)\rho^2+1\right],$$

where the dimensionless time-constants τ_e and τ_m are given in (2.37) and the frequency ratio is defined as $\rho = \frac{\Omega_0}{\Omega_N}$. The design equations for complete damping of the closed loop system can be obtained by substituting $\delta=1$ in equations (3.37) (binomial expansion) while an assignment with the magnitude optimum criterion requires $\delta=0.707$. Backlash nonlinearity (see, e.g., Kuo [60] for the backlash describing function) combined in the coupling shaft gear is taken into account in the following example.

Example 3.2: For an illustration, the system of Figure 3.3 is used with the following specifications (see Section 2.7): T_e=0.03sec, T_m=0.116sec, J_1=0.814kgm^2, J_2=0.012kgm^2, γ=1.015, $\beta = 7.12 Nm.s/rad$, Ω_N=4.21$rad/\sec$, $T_r \cong 0$, and K_{12}=0.21Nm/rad. The frequency ratio $\rho = \Omega_0/\Omega_N$ is chosen equal to 2.5. The dominant root-based design equation (3.48) for complete damping ($\delta = 1$) gives $K_T = 0.0371 rad/Nm.s$, $K_{\omega_1} = 1.2187$, $K_{T_{12}} = 63.96 rad/Nm.s$, and $K_{\omega_2} = 0.1863$. The influence of backlash nonlinearity is considered to evaluate vibration suppression capability of modal control with different pole-placement criteria.

Figures 3.4 and 3.5 plot the step response with a backlash deadband width of $2D = 0.02$. As it can be expected, the response using the design equations (3.48) at complete damping condition ($\delta = 1$) give a well-damped response (Figure 3.4(a)) while oscillations are observed in the response using the magnitude optimum (Figure 3.4(b)), Butterworth (Figure 3.5(a)), or ITAE criterion (Figure 3.5(b)).

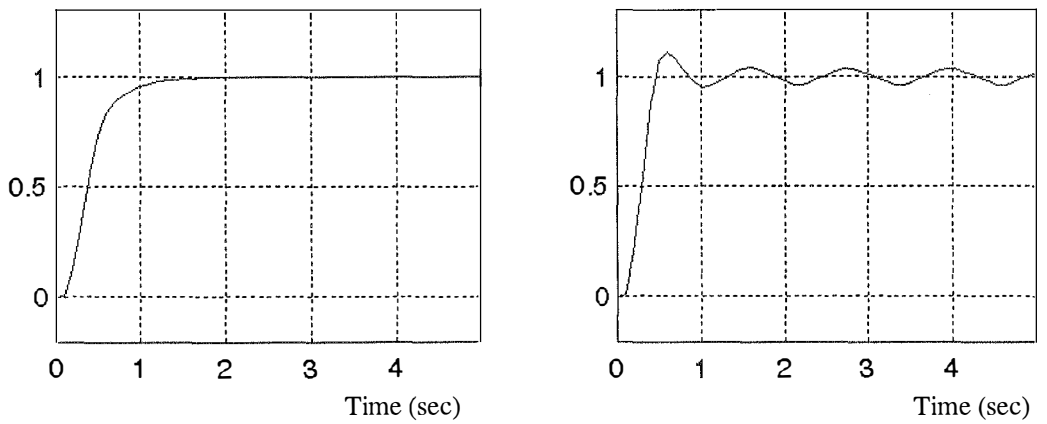

Figure 3.4. Step response of a two-mass system with backlash using modal control using: (a) dominant root-based, complete damping, (b) magnitude optimum.

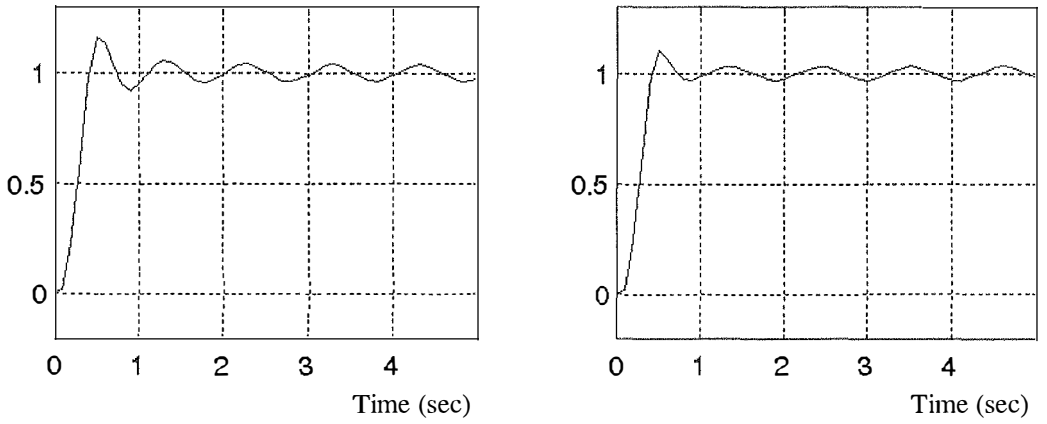

Figure 3.5. Step response of a two-mass system with backlash using modal control using: (a) Butterworth, and (b) ITAE polynomial.

3.3.2 Sensitivity analysis

It is known that the dynamic behaviour of a closed-loop system is mainly determined by an eigenvalue assignment technique with modal control. Robustness of a modal control system is associated with the sensitivity of its eigenstructure with respect to system parameters. Thus, the insight into the behaviour of a drive system obtained from an eigenvalue sensitivity analysis can provide useful guidance in its analysis and design. One way to quantify how sensitive an eigenvalue λ_i to variations in a parameter χ is to take the limiting ratio of a relative perturbation in λ_i to a relative perturbation in χ (Doyle *et al.* [89]):

$$\lim_{\chi \to 0} \frac{\Delta\lambda_i / \lambda_i}{\Delta\chi / \chi} = \frac{\partial\lambda_i}{\partial\chi} \frac{\chi}{\lambda_i} = \frac{\partial \ln \lambda_i}{\partial \ln \chi}. \tag{3.49}$$

Two types of eigenvalue sensitivities can be distinguished, the real part of (3.49) or the attenuation sensitivity, and the imaginary part of (3.49) or the frequency sensitivity. In the following the modulus of (3.49) will be used for evaluating the eigenvalue sensitivity:

$$S_{\chi}^{\lambda_i} = \left| \frac{\partial \ln \lambda_i}{\partial \ln \chi} \right|. \tag{3.50}$$

Using the right and left eigenvectors defined in (3.12) the eigenvalue sensitivities of a high-order system can be evaluated by another way (Wu *et al.* [90]):

$$\frac{\partial \lambda_i}{\partial \chi} = \frac{\mathbf{v}_i^T (\partial \mathbf{A}/\partial \chi)\mathbf{u}_i}{\mathbf{v}_i^T \mathbf{u}_i}, \tag{3.51}$$

where $\mathbf{u}_i$ and $\mathbf{v}_i$ are the right eigenvectors of the system matrix $\mathbf{A}$, respectively.

Consider the position drive of Figure 3.1. The plant dominant roots are found from the characteristic equation (3.39) in a general one-mass drive system:

$$\lambda_{1,2} = -\frac{1}{2T_a}\left(1 \pm \sqrt{1 - 4\frac{T_a}{T_m}}\right), \tag{3.52}$$

or in the case of a DC drive:

$$\lambda_{1,2} = -\frac{R_a}{2L_a}\left(1 \pm \sqrt{1 - 4\frac{L_a K_b K_t}{J_m R_a^2}}\right), \tag{3.53}$$

where all the parameters are specified in Section 3.2.1. The sensitivity of the dominant roots with respect to variations of the total moment of inertia can be derived as following (Ha & Alferov [91]):

$$S_{J_m}^{\lambda} = \left|\frac{\partial \ln \lambda}{\partial \ln J_m}\right| = \left|\frac{J_m}{\lambda}\frac{\partial \lambda}{\partial J_m}\right| = \begin{cases} \dfrac{1}{2}\left[\left(\dfrac{J_m/J_{cr}}{J_m/J_{cr}-1}\right)^{1/2} \pm 1\right], & J_m > J_{cr} \\ \dfrac{1}{2}\left(1 - J_m/J_{cr}\right)^{-1/2}, & J_m < J_{cr} \end{cases} \tag{3.54}$$

where $J_{cr} = 4L_a K_b K_t / R_a^2$.

Figure 3.6 plots the relationship between $S_{J_m}^{\lambda}$ and J_{cr}/J_m. It is known that the system dominant roots are most sensitive to any variations of the moment of inertia around its critical value ($J_{cr}/J_m = 1$). In some electrical drives of manipulators, the plant moment of inertia J_m can be expressed as $J_m = J_o + \Delta J \sin \Psi(t)$. If the average value J_o lies in the interval $(0.9 - 1.3)J_{cr}$, corresponding to $S_{J_m}^{\lambda} \geq 1.5$, then the system dynamics is very sensitive to variations of load moment of inertia.

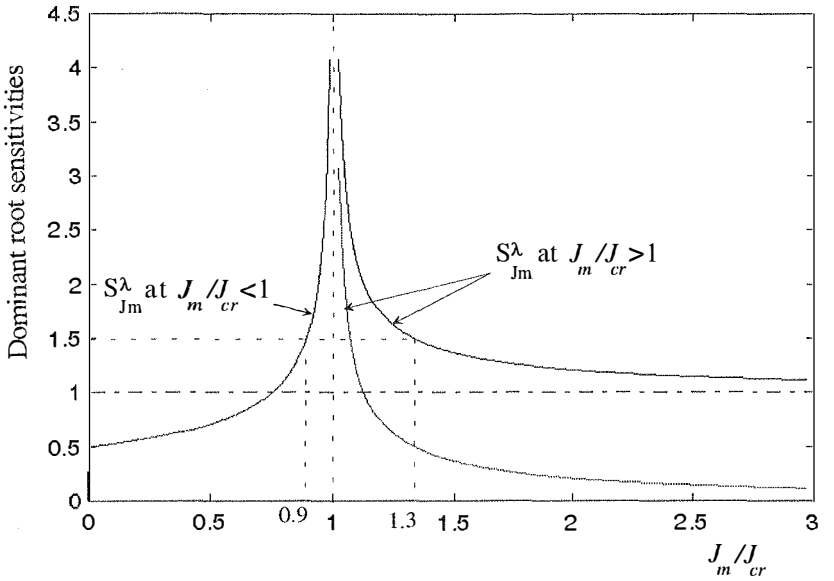

Figure 3.6. Dominant root sensitivities $S^{\lambda}_{J_m}$.

Similar remarks can be obtained with sensitivities $S^{\lambda}_{R_a}$ and $S^{\lambda}_{L_a}$:

$$S^{\lambda}_{R_a} = \frac{R_a/R_{cr}}{\sqrt{\left|(R_a/R_{cr})^2 - 1\right|}}, \tag{3.55}$$

$$S^{\lambda}_{L_a} = \begin{cases} \dfrac{1}{2}\left[\left(1 - L_a/L_{cr}\right)^{-1/2} \pm 1\right], & L_a < L_{cr} \\ \dfrac{1}{2}\left(\dfrac{L_a/L_{cr}}{L_a/L_{cr} - 1}\right)^{1/2}, & L_a > L_{cr} \end{cases} \tag{3.56}$$

where $R_{cr} = 2\sqrt{K_b K_t L_a / J_m}$ and $L_{cr} = J_m R_a^2 / 4K_b K_t$.

These sensitivities are shown in Figure 3.7 and 3.8. As it can be seen, within some vicinity of critical values the dominant root sensitivities increase significantly.

As in the closed-loop case, it is known that in modal control, the system states are fed back to the controller in order to assign the desired closed-loop eigenstructure and thus, reduce its sensitivities. This is illustrated by the following sensitivity analysis for the modal controller design using (3.45).

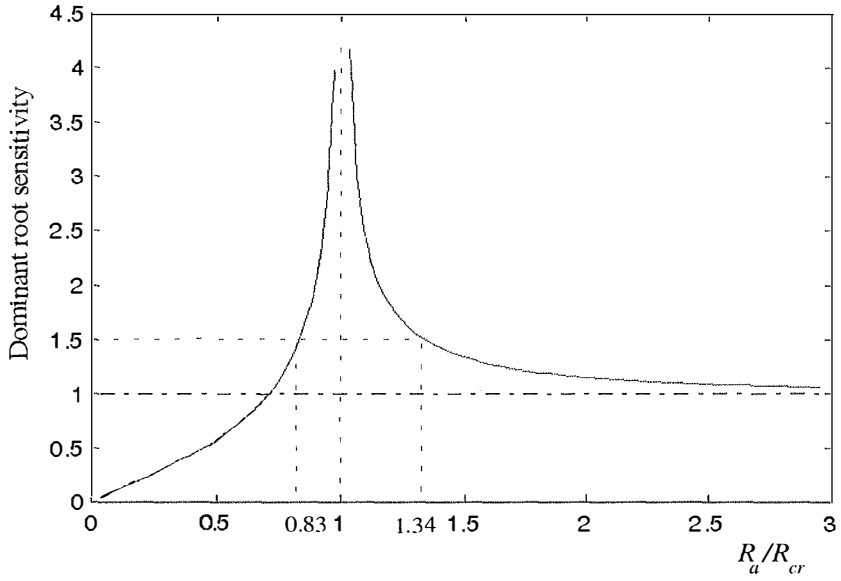

Figure 3.7. Dominant root sensitivity $S^{\lambda}_{R_a}$.

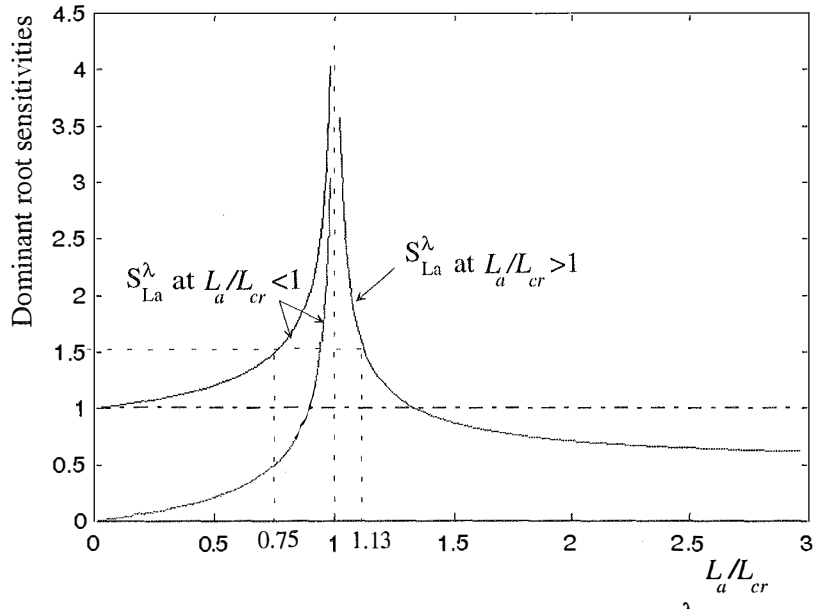

Figure 3.8. Dominant root sensitivities $S^{\lambda}_{L_a}$.

Equalising the coefficients α_i $(i=1,2,3)$ of the closed-loop characteristic polynomial (3.31) and of the desired one $(s^2+2\delta\Omega_0 s+\Omega_0^2)(s+\alpha_3-2\delta\Omega_0)$ gives:

$$\begin{aligned}\alpha_1 &= \Omega_0^2\alpha_3 - 2\delta\Omega_0^3 \\ \alpha_2 &= (1-4\delta^2)\Omega_0^2 + 2\delta\Omega_0\alpha_3\end{aligned}, \quad \alpha_3 > 2\delta\Omega_0, \tag{3.57}$$

where $\alpha_1 = K_t K_c K_P / J_m L_a$, $\alpha_2 = K_t(K_b + K_c K_V)/J_m L_a$, and $\alpha_3 = (R_a + K_c K_I)/L_a$, and Ω_0 and δ are the dominant root frequency and damping factor, respectively. The values of Ω_0 and δ, in practice, are affected by variations of plant parameters, e.g. moment of inertia J_m and total resistance R_a of the armature circuit.

The differentials $d\Omega_0$ and $d\delta$ can be obtained from (3.57)

$$d\delta = \frac{\partial \delta}{\partial R_a} dR_a + \frac{\partial \delta}{\partial J_m} dJ_m, \tag{3.58}$$

$$d\Omega_0 = \frac{\partial \Omega_0}{\partial R_a} dR_a + \frac{\partial \Omega_0}{\partial J_m} dJ_m$$

where $$\frac{\partial \delta}{\partial R_a} = \frac{1 + 2\delta^2 - \delta\alpha_3/\Omega_0}{\Omega_0 L_a \Delta}, \quad \frac{\partial \delta}{\partial J_m} = -\frac{[(\alpha_3/\Omega_0 - 2\delta)^2 - 1]\delta}{J_m \Delta},$$

$$\frac{\partial \Omega_0}{\partial R_a} = -\frac{(\alpha_3/\Omega_0 - 2\delta)}{L_a \Delta}, \quad \frac{\partial \Omega_0}{\partial J_m} = -\frac{[(\alpha_3/\Omega_0 - 2\delta)^2 + 1]\Omega_0}{J_m \Delta} dJ_m,$$

$$\Delta = 2[(\alpha_3/\Omega_0 - 3\delta)^2 + 1 - \delta^2].$$

The sensitivities of dominant roots of the closed-loop system are then determined as:

$$S_{R_a}^{\delta} = \left|\frac{R_a}{\delta}\frac{\partial \delta}{\partial R_a}\right| = \frac{1}{\Delta\Omega_0 T_a}\left|(2\delta + \frac{1}{\delta}) - \frac{\alpha_3}{\Omega_0}\right|, \quad S_{J_m}^{\delta} = \left|\frac{J_m}{\delta}\frac{\partial \delta}{\partial J_m}\right| = \frac{1}{\Delta}\left|(\frac{\alpha_3}{\Omega_0} - 2\delta)^2 - 1\right|, \tag{3.59}$$

$$S_{R_a}^{\Omega_0} = \left|\frac{R_a}{\Omega_0}\frac{\partial \Omega_0}{\partial R_a}\right| = \frac{1}{\Delta\Omega_0 T_a}\left|\frac{\alpha_3}{\Omega_0} - 2\delta\right|, \quad S_{J_m}^{\Omega_0} = \left|\frac{J_m}{\Omega_0}\frac{\partial \Omega_0}{\partial J_m}\right| = \frac{1}{\Delta}\left|(\frac{\alpha_3}{\Omega_0} - 2\delta)^2 + 1\right|.$$

It is inherent that infinitive sensitivities (3.59) correspond to a multiple root the characteristic equation with the binomial expansion criterion (α_3=3Ω_0, δ=1). Since $S_{R_a}^{\Omega_0} \neq 0$ and $S_{J_m}^{\Omega_0} \neq 0$, a design with low sensitivities can be based on the conditions:

$$S_{R_a}^{\delta} = 0 \Rightarrow \alpha_3 = (2\delta + 1)\Omega_0, \tag{3.60a}$$

$$S_{J_m}^{\Omega_0} = 0 \Rightarrow \alpha_3 = (2\delta + \frac{1}{\delta})\Omega_0, \tag{3.60b}$$

Note that the condition (3.60a) at δ=0.5 corresponds to the Butterworth (or magnitude optimum) criterion. Using the dominant root-based modal controller (3.45) the value of coefficient α_3 is determined from (3.46):

$$\alpha_3 = 2(1+2\delta)\Omega_0. \tag{3.61}$$

Substituting the values of α_3 given in (3.60a), (3.60b) and (3.61) in (3.59) indicates that the values of $S_{R_a}^{\Omega_0}$ and $S_{J_m}^{\Omega_0}$ at $0.43 < \delta < 1$ using the proposed dominant root-based modal control (3.61) are the least in comparison with the other techniques (3.60a) and (3.60b) (Ha & Alferov [91]).

3.4 Combined observer for state and disturbance estimation

Modal control is capable of assigning the closed-loop eigenstructure for desired transient performance. However, all states are assumed to be measured, whereas in practice not all of them are accessible. Another problem with modal control is that there is no guarantee for the control accuracy. Any external disturbance may result in a steady state error. Combining state feedback with integral control can be a solution to the problem, but it increases the degree of the system. An observer is required to estimate the states and disturbance and thus, enables accomplishing feedback from all the states and providing a feedforward compensation for the disturbance.

3.4.1 Combined observer

This section is devoted to the design of a combined observer or a subsystem that performs the observation of not only the state variables but also the external unknown inputs based on information received from the measurements of the input and output. The observer is implemented in a flexible system to estimate the elastic or reaction torque, load speed as well as a load torque disturbance.

Consider the linearised model (3.1). Assuming that the system can be written in a partitioned form as

$$\begin{pmatrix}\dot{\mathbf{x}}_1(t)\\ \dot{\mathbf{x}}_2(t)\end{pmatrix} = \begin{pmatrix}\mathbf{A}_{11} & \mathbf{A}_{12}\\ \mathbf{A}_{21} & \mathbf{A}_{22}\end{pmatrix}\begin{pmatrix}\mathbf{x}_1(t)\\ \mathbf{x}_2(t)\end{pmatrix} + \begin{pmatrix}\mathbf{B}_1\\ \mathbf{B}_2\end{pmatrix}\mathbf{u}(t) + \begin{pmatrix}\mathbf{D}_1\\ \mathbf{D}_2\end{pmatrix}\mathbf{v}(t) \tag{3.62}$$

$$\mathbf{y}(t) = \mathbf{C}\mathbf{x}(t) = (\mathbf{I}_m \;\; \mathbf{0})\mathbf{x}(t) = \mathbf{x}_1(t),$$

where $\mathbf{x}_1(t) \in R^m$ is the vector of measurable state variables, $\mathbf{x}_2(t) \in R^{n-m}$ is the vector of inaccessible state variables; $\mathbf{A}_{ij}$, $\mathbf{B}_i$, and $\mathbf{D}_i$, $i, j = 1,2$, are matrices of appropriate dimensions; and the pair ($\mathbf{C}$, $\mathbf{A}$) is observable. The problem is to construct an observer for estimating both the state $\mathbf{x}_2(t)$ and the disturbance $\mathbf{v}(t) \in R^q$.

Designing observers for recovering all the states of linear systems with unknown inputs has attracted much research in the last few decades. State variables in general can be estimated on the basis of a full-order or reduced-order Luenberger observer [92] with known inputs. For state estimation in the unknown input case, some *a priori* information about the inputs is assumed in Meditch & Hostetter [93]. An existence condition for a minimal-order observer, shown in Kudva *et al.* [94], is that

$$rank(\mathbf{CD}) = q \quad \text{with} \quad q \le m. \tag{3.63}$$

A necessary and sufficient condition for a full-order unknown input observer with a direct design procedure is provided in Yang & Wilde [95]. A simple approach for designing a reduced-order observer without any knowledge of the inputs is proposed in Guan & Saif [96]. Other attempts focus on the estimation of not only state variables but also unknown inputs. In Park & Stein [97], the state equation is transformed through some substitutions into a special system model for a reduced-order observer to simultaneously estimate states and unknown inputs. The problem of designing observers for systems with unknown inputs is shown equivalent to that for conventional unknown input free reduced-order systems, using a special descriptor form in Hou & Muller [98]. On a practical standpoint, the design procedure in Alferov & Ha [73] is straightforward with the introduction of a predictive coefficient to approximate the unknown input rate of change. The idea behind this approach is to augment the state equation of (3.38) with an equation approximately describing the dynamics of the external inputs (Kuzovkov [68], Meditch & Hostetter [88]):

$$\dot{\mathbf{v}}(t) = \Gamma \mathbf{v}(t), \tag{3.64}$$

where $\Gamma \in R^{q \times q}$. The state model (3.8) can be written as:

$$\begin{pmatrix} \dot{\mathbf{x}}_1 \\ \dot{\mathbf{w}} \end{pmatrix} = \overline{\mathbf{A}} \begin{pmatrix} \mathbf{x}_1 \\ \mathbf{w} \end{pmatrix} + \overline{\mathbf{B}}\mathbf{u}, \tag{3.65}$$

$$\mathbf{y} = \overline{\mathbf{C}}\begin{pmatrix}\mathbf{x}_1\\ \mathbf{w}\end{pmatrix} = \mathbf{x}_1$$

where $\mathbf{w} = (\mathbf{x}_2 \ \mathbf{v})^T$ is to be estimated, $\overline{\mathbf{A}} = \begin{pmatrix}\overline{\mathbf{A}}_{11} & \overline{\mathbf{A}}_{12}\\ \overline{\mathbf{A}}_{21} & \overline{\mathbf{A}}_{22}\end{pmatrix}$, $\overline{\mathbf{B}} = \begin{pmatrix}\overline{\mathbf{B}}_1\\ \overline{\mathbf{B}}_2\end{pmatrix}$, and $\overline{\mathbf{C}} = (\mathbf{I}_m \ \ \mathbf{0})$ with $\overline{\mathbf{A}}_{11} = \mathbf{A}_{11}$, $\overline{\mathbf{A}}_{12} = (\mathbf{A}_{12} \ \mathbf{D}_1)$, $\overline{\mathbf{B}}_1 = \mathbf{B}_1$, $\overline{\mathbf{A}}_{21} = \begin{pmatrix}\mathbf{A}_{21}\\ \mathbf{0}\end{pmatrix}$, $\overline{\mathbf{A}}_{22} = \begin{pmatrix}\mathbf{A}_{22} & \mathbf{D}_2\\ \mathbf{0} & \Gamma\end{pmatrix}$, and $\overline{\mathbf{B}}_2 = \begin{pmatrix}\mathbf{B}_2\\ \mathbf{0}\end{pmatrix}$. For the system (3.41) a Luenberger observer exists if the pair $(\overline{\mathbf{C}} \ \ \overline{\mathbf{A}})$ is observable, i.e. if

$$rank(\overline{\mathbf{C}}^T \ \overline{\mathbf{A}}^T\overline{\mathbf{C}}^T \ \overline{\mathbf{A}}^{T^2}\overline{\mathbf{C}}^T \ \ldots \ \overline{\mathbf{A}}^{T^{n-1}}\overline{\mathbf{C}}^T) = n + q. \tag{3.66}$$

The pair $(\overline{\mathbf{A}}_{12} \ \ \overline{\mathbf{A}}_{22})$ is then also observable and a reduced-order observer can be constructed (Luenberger [92]):

$$\begin{aligned}\dot{\mathbf{z}}(t) &= \mathbf{F}\mathbf{z}(t) + \mathbf{G}\mathbf{y}(t) + \mathbf{H}\mathbf{u}(t)\\ \hat{\mathbf{w}}(t) &= \mathbf{z}(t) + \mathbf{L}\mathbf{y}(t)\end{aligned}, \tag{3.67}$$

where $\mathbf{z}(t) \in R^{n-m+q}$ is the observer state, $\hat{\mathbf{w}}(t) = (\hat{\mathbf{x}}_2 \ \hat{\mathbf{v}})^T$ is the estimate of $\mathbf{w}(t)$. The observer matrices are determined as

$$\mathbf{F} = \overline{\mathbf{A}}_{22} - \mathbf{L}\overline{\mathbf{A}}_{12} = \begin{pmatrix}\mathbf{F}_{11} & \mathbf{F}_{12}\\ \mathbf{F}_{21} & \mathbf{F}_{22}\end{pmatrix} = \begin{pmatrix}\mathbf{A}_{22} - \mathbf{L}_1\mathbf{A}_{12} & \mathbf{D}_2 - \mathbf{L}_1\mathbf{D}_1\\ -\mathbf{L}_2\mathbf{A}_{12} & \mathbf{P} - \mathbf{L}_2\mathbf{D}_1\end{pmatrix}, \tag{3.68}$$

$$\mathbf{G} = \mathbf{F}\mathbf{L} + \overline{\mathbf{A}}_{21} - \mathbf{L}\overline{\mathbf{A}}_{11} = \begin{pmatrix}\mathbf{G}_1\\ \mathbf{G}_2\end{pmatrix} = \begin{pmatrix}\mathbf{F}_{11}\mathbf{L}_1 + \mathbf{F}_{12}\mathbf{L}_2 + \mathbf{A}_{21} - \mathbf{L}_1\mathbf{A}_{11}\\ \mathbf{F}_{21}\mathbf{L}_1 + \mathbf{F}_{22}\mathbf{L}_2 - \mathbf{L}_{21}\mathbf{A}_{11}\end{pmatrix},$$

$$\mathbf{H} = \overline{\mathbf{B}}_2 - \mathbf{L}\overline{\mathbf{B}}_1 = \begin{pmatrix}\mathbf{H}_1\\ \mathbf{H}_2\end{pmatrix} = \begin{pmatrix}\mathbf{B}_2 - \mathbf{L}_1\mathbf{B}_1\\ -\mathbf{L}_2\mathbf{B}_1\end{pmatrix},$$

where the observer matrix gain $\mathbf{L} = \begin{pmatrix}\mathbf{L}_1\\ \mathbf{L}_2\end{pmatrix}$, with $\mathbf{L}_1 \in R^{(n-m)\times m}$ and $\mathbf{L}_2 \in R^{q\times m}$, is chosen according to the eigenvalue assignment of the observer characteristic equation:

$$\left|s\mathbf{I}_{n-m+q} - \mathbf{F}\right| = 0. \tag{3.69}$$

The observer eigenvalues, which determine how fast the estimates converge to their actual, should be located in such a way that the observer responds at least four or five times faster than the closed loop system with a modal controller. If the external disturbances $\mathbf{v}(t)$ are slowly varying, the matrix Γ in (3.64) can be set equal to $\mathbf{0}$. However, in many cases, $\mathbf{v}(t)$ may be arbitrary functions of time. Taking account of time derivatives of disturbances till the $(N-1)$-*th* order, $\mathbf{v}(t)$ can be approximated by

$$\mathbf{v}(t) \cong \mathbf{v}_0 + \mathbf{v}_0^{(1)} t + \mathbf{v}_0^{(2)} \frac{t^2}{2} + \ldots + \mathbf{v}_0^{(N-1)} \frac{t^{N-1}}{(N-1)!}, \tag{3.70}$$

where $\mathbf{v}_0^{(i)}$ is the i-*th* time derivative of $\mathbf{v}(t)$ at some $t = t_0$, $i = 1, 2, \ldots, N-1$, and $\mathbf{v}^{(N)}(t) \cong 0$. An observer of the order $n - m + Nq$ can be constructed on the basis of the augmented state model (3.41) to estimate vector $\mathbf{w}(t) = \left(\mathbf{x}_2 \ \mathbf{v} \ \mathbf{v}^{(1)} \ \ldots \ \mathbf{v}^{(N-1)} \ \mathbf{v}^{(N)}\right)^T$ with (Ha [9]):

$$\overline{\mathbf{A}} = \begin{pmatrix} \mathbf{A}_{11} & \mathbf{A}_{12} & \mathbf{D}_1 & \mathbf{0} & \ldots & \mathbf{0} & \mathbf{0} \\ \mathbf{A}_{21} & \mathbf{A}_{22} & \mathbf{D}_2 & \mathbf{0} & \ldots & \mathbf{0} & \mathbf{0} \\ \mathbf{0} & \mathbf{0} & \mathbf{0} & \mathbf{I}_q & \ldots & \mathbf{0} & \mathbf{0} \\ \vdots & \vdots & \vdots & \vdots & \ddots & \vdots & \\ \mathbf{0} & \mathbf{0} & \mathbf{0} & \mathbf{0} & \ldots & \mathbf{0} & \mathbf{I}_q \\ \mathbf{0} & \mathbf{0} & \mathbf{0} & \mathbf{0} & \ldots & \mathbf{0} & \mathbf{0} \end{pmatrix}, \ \overline{\mathbf{B}} = \begin{pmatrix} \mathbf{B}_1 \\ \mathbf{B}_2 \\ \mathbf{0} \\ \vdots \\ \mathbf{0} \\ \mathbf{0} \end{pmatrix}, \text{ and } \overline{\mathbf{C}} = \begin{pmatrix} \mathbf{I}_m & \mathbf{0} & \mathbf{0} & \ldots & \mathbf{0} & \mathbf{0} \end{pmatrix}.$$

Such an observer can give better estimates of the unknown input dynamics, however an increase in the observer order causes an adverse effect of lower reliability and makes the system more sensitive to measurement noises. As an alternative to the problem, a digital predictive observer is described in the next section.

3.4.2 Digital predictive observer

Consider the linearised state model (3.28). The partitioned form as in (3.62) is written in the discrete-time form as:

$$\begin{pmatrix} \mathbf{x}_1(k+1) \\ \mathbf{x}_2(k+1) \end{pmatrix} = \begin{pmatrix} \mathbf{A}_{11} & \mathbf{A}_{12} \\ \mathbf{A}_{21} & \mathbf{A}_{22} \end{pmatrix} \begin{pmatrix} \mathbf{x}_1(k) \\ \mathbf{x}_2(k) \end{pmatrix} + \begin{pmatrix} \mathbf{B}_1 \\ \mathbf{B}_2 \end{pmatrix} \mathbf{u}(k) + \begin{pmatrix} \mathbf{D}_1 \\ \mathbf{D}_2 \end{pmatrix} \mathbf{v}(k) \tag{3.71}$$

$$\mathbf{y}(k) = \mathbf{C}\mathbf{x}(k) = (\mathbf{I}_m \ \mathbf{0})\mathbf{x}(k) = \mathbf{x}_1(k),$$

The idea of a combined observer can be implemented by augmenting the state equation with an equation modelling the disturbances $\mathbf{v}(k)$ by suitably chosen dynamics. By introducing the derivatives $\mathbf{v}^{(1)}(k)$, $\mathbf{v}^{(2)}(k)$, ..., $\mathbf{v}^{(N)}(k)$, the external disturbances at the $(k+1)$-th sampling point can be expressed as:

$$\mathbf{v}(k+1) \cong \mathbf{v}(k) + \mathbf{v}^{(1)}(k)T + \mathbf{v}^{(2)}(k)\frac{T^2}{2} + \ldots + \mathbf{v}^{(N)}(k)\frac{T^N}{N!}, \tag{3.72}$$

where T is the sampling period. The state equation of (3.71) is then written in the augmented form:

$$\begin{pmatrix} \mathbf{x}_1(k+1) \\ \mathbf{x}_2(k+1) \\ \mathbf{v}(k+1) \\ \mathbf{v}^{(1)}(k+1) \\ \vdots \\ \mathbf{v}^{(N)}(k+1) \end{pmatrix} = \begin{pmatrix} \mathbf{A}_{11} & \mathbf{A}_{12} & \mathbf{D}_1 & \mathbf{0} & \cdots & \mathbf{0} \\ \mathbf{A}_{21} & \mathbf{A}_{22} & \mathbf{D}_2 & \mathbf{0} & \cdots & \mathbf{0} \\ \mathbf{0} & \mathbf{0} & \mathbf{I}_q & \mathbf{I}_q T & \cdots & \mathbf{I}_q \frac{T^N}{N!} \\ \mathbf{0} & \mathbf{0} & \mathbf{0} & \mathbf{I}_q & \cdots & \mathbf{I}_q \frac{T^{(N-1)}}{(N-1)!} \\ \vdots & \vdots & \vdots & \vdots & & \vdots \\ \mathbf{0} & \mathbf{0} & \mathbf{0} & \mathbf{0} & \cdots & \mathbf{I}_q \end{pmatrix} \begin{pmatrix} \mathbf{x}_1(k) \\ \mathbf{x}_2(k) \\ \mathbf{v}(k) \\ \mathbf{v}^{(1)}(k) \\ \vdots \\ \mathbf{v}^{(N)}(k) \end{pmatrix} + \begin{pmatrix} \mathbf{B}_1 \\ \mathbf{B}_2 \\ \mathbf{0} \\ \mathbf{0} \\ \vdots \\ \mathbf{0} \end{pmatrix} \mathbf{u}(k). \tag{3.73}$$

In order to avoid a considerable increase in the observer dimension when using the augmented form (3.73), a predictive approximation for $\mathbf{v}(k+1)$ was proposed in Alferov & Ha [73]:

$$\mathbf{v}(k+1) \cong (\mathbf{I}_q + \Gamma)\mathbf{v}(k) - \Gamma\mathbf{v}(k-1), \tag{3.74}$$

where $\Gamma = diag(\gamma_{ii})$ is the diagonal matrix of predictive coefficients $\gamma_{ii} \in (-1,1)$, $i = 1, 2, \ldots, q$. The augmented form for the state model (3.28) using (3.74) is obtained as:

$$\begin{pmatrix} \mathbf{x}_1(k+1) \\ \mathbf{x}_2(k+1) \\ \mathbf{v}(k+1) \end{pmatrix} = \begin{pmatrix} \mathbf{A}_{11} & \mathbf{A}_{12} & \mathbf{D}_1 \\ \mathbf{A}_{21} & \mathbf{A}_{22} & \mathbf{D}_2 \\ \mathbf{0} & \mathbf{0} & \mathbf{I}_q + \Gamma \end{pmatrix} \begin{pmatrix} \mathbf{x}_1(k) \\ \mathbf{x}_2(k) \\ \mathbf{v}(k) \end{pmatrix} + \begin{pmatrix} \mathbf{B}_1 & \mathbf{0} \\ \mathbf{B}_2 & \mathbf{0} \\ \mathbf{0} & -\Gamma \end{pmatrix} \begin{pmatrix} \mathbf{u}(k) \\ \mathbf{v}(k-1) \end{pmatrix} \tag{3.75}$$

$$\mathbf{y}(k) = (\mathbf{I}_m \;\; \mathbf{0} \;\; \mathbf{0}) \begin{pmatrix} \mathbf{x}_1(k) \\ \mathbf{x}_2(k) \\ \mathbf{v}(k) \end{pmatrix} = \mathbf{x}_1(k),$$

If system (3.75) is observable, estimates for $\mathbf{v}(k)$ can be obtained from a reduced-order Luenberger on the basis of measurements $\mathbf{x}_1(k)$, the control signals $\mathbf{u}(k)$ and the previous estimates $\hat{\mathbf{v}}(k-1)$:

$$\begin{pmatrix} \mathbf{z}_1(k+1) \\ \mathbf{z}_2(k+1) \end{pmatrix} = \begin{pmatrix} \mathbf{F}_{11} & \mathbf{F}_{12} \\ \mathbf{F}_{21} & \mathbf{F}_{22} \end{pmatrix} \begin{pmatrix} \mathbf{z}_1(k) \\ \mathbf{z}_2(k) \end{pmatrix} + \begin{pmatrix} \mathbf{G}_1 \\ \mathbf{G}_2 \end{pmatrix} \mathbf{y}(k) + \begin{pmatrix} \mathbf{H}_1 & \mathbf{0} \\ \mathbf{H}_2 & -\Gamma \end{pmatrix} \begin{pmatrix} \mathbf{u}(k) \\ \hat{\mathbf{v}}(k-1) \end{pmatrix}, \quad (3.76a)$$

$$\begin{pmatrix} \hat{\mathbf{x}}_2(k) \\ \hat{\mathbf{v}}(k) \end{pmatrix} = \begin{pmatrix} \mathbf{z}_1(k) \\ \mathbf{z}_2(k) \end{pmatrix} + \begin{pmatrix} \mathbf{L}_1 \\ \mathbf{L}_2 \end{pmatrix} y(k),$$

where

$$\mathbf{F}_{11} = \mathbf{A}_{22} - \mathbf{L}_1\mathbf{A}_{12}, \;\; \mathbf{F}_{12} = \mathbf{D}_2 - \mathbf{L}_1\mathbf{D}_1, \;\; \mathbf{F}_{21} = -\mathbf{L}_2\mathbf{A}_{12}, \;\; \mathbf{F}_{22} = \mathbf{I}_q + \Gamma - \mathbf{L}_2\mathbf{D}_1;$$

$$\mathbf{G}_1 = \mathbf{F}_{11}\mathbf{L}_1 + \mathbf{F}_{12}\mathbf{L}_2 + \mathbf{A}_{21} - \mathbf{L}_1\mathbf{A}_{11}, \;\; \mathbf{G}_2 = \mathbf{F}_{21}\mathbf{L}_1 + \mathbf{F}_{22}\mathbf{L}_2 - \mathbf{L}_2\mathbf{A}_{11}; \quad (3.76b)$$

$$\mathbf{H}_1 = \mathbf{B}_2 - \mathbf{L}_1\mathbf{B}_1, \;\; \mathbf{H}_2 = -\mathbf{L}_2\mathbf{B}_1;$$

and where $\mathbf{z}_1(k) \in R^{n-m}$ and $\mathbf{z}_2(k) \in R^q$ are observer state variables, $\mathbf{L}_1 \in \mathcal{R}^{(n-m)\times m}$ and $\mathbf{L}_2 \in \mathcal{R}^{q\times m}$ are observer matrix gains, $\hat{\mathbf{x}}_2(k)$ gains, $\hat{\mathbf{x}}_2$ and $\hat{\mathbf{v}}$ are the estimates of $\mathbf{x}_2$ and $\mathbf{v}$. By denoting the estimation error vectors $\mathbf{e}_x(k) = \mathbf{x}_2(k) - \hat{\mathbf{x}}_2(k)$, $\mathbf{e}_v(k) = \mathbf{v}(k) - \hat{\mathbf{v}}(k)$, $\mathbf{e} = (\mathbf{e}_x \;\; \mathbf{e}_v)^T$ and using (3.76), we obtain the following error dynamics

$$\mathbf{e}(k+1) = \mathbf{F}\mathbf{e}(k) + \mathbf{F}_1\mathbf{e}(k-1) = \begin{pmatrix} \mathbf{F}_{11} & \mathbf{F}_{12} \\ \mathbf{F}_{21} & \mathbf{F}_{22} \end{pmatrix} \mathbf{e}(k) + \begin{pmatrix} \mathbf{0} & \mathbf{0} \\ \mathbf{0} & -\Gamma \end{pmatrix} \mathbf{e}(k-1). \quad (3.77)$$

The entries l_{ij} and γ_{ii} of matrices $\mathbf{L}_1$, $\mathbf{L}_2$ and Γ, in general, are chosen by the desired dynamic conditions of the observer according to the root assignment of the characteristic equation

$$\left| z^2\mathbf{I}_{n-m+q} - z\mathbf{F} - \mathbf{F}_1 \right| = 0. \quad (3.78)$$

The number $(n-m)\times m + (q\times m) + m$ of chosen elements l_{ij}, γ_{ii} is always greater than the degree $(q+m)$ of (3.78). Therefore, for given coefficients $\gamma_{ii} = \gamma_{ii0}$, there

usually exists a proper choice of the matrix gain $\mathbf{L}_1$, $\mathbf{L}_2$ such that asymptotic stability of the observer as well as desirable rate of convergence can be achieved.

Example 3.3: Consider a DC motor two-mass electromechanical system of Figure 3.3. The block diagram with specifications is given in Figure 3.9. The motor is supplied by a thyristor converter. The state vector is chosen as $\mathbf{x} = (e_{sp}\ \ i_a\ \ \omega_1\ \ \omega_2\ \ T_{12})^T$, where e_{sp}, i_a, ω_1, ω_2 and T_{12} is the supply voltage, armature current, motor speed, load speed and elastic torque, respectively. The control voltage u is known input and load torque T_L is unknown input. The sampling time is $T = 0.05$ sec. The state equation with plant nominal parameters in the discrete-time form is found as:

$$\mathbf{x}(k+1) = \begin{pmatrix} 0.0067 & 0 & 0 & 0 & 0 \\ 0.2156 & 0.1028 & -3.4909 & -0.0005 & 0.1326 \\ 0.0366 & 0.0403 & 0.8008 & 0.0003 & -0.0532 \\ 0.0003 & 0.0005 & 0.0207 & 0.9782 & 4.1304 \\ 0.0002 & 0.0003 & 0.0095 & -0.0104 & 0.9753 \end{pmatrix} \mathbf{x}(k) + \begin{pmatrix} 24.8316 \\ 52.8009 \\ 2.4009 \\ 0.0100 \\ 0.0096 \end{pmatrix} u(k) + \begin{pmatrix} 0 \\ 0.0007 \\ -0.0005 \\ -4.1309 \\ 0.0244 \end{pmatrix} T_L(k)$$

$$\mathbf{y}(k) = \begin{pmatrix} 1 & 0 & 0 & 0 & 0 \\ 0 & 1 & 0 & 0 & 0 \\ 0 & 0 & 1 & 0 & 0 \end{pmatrix} \mathbf{x}(k), \tag{3.79}$$

- With load speed measurement (Alferov, Ha & Khusainov [74]):

The elastic torque T_{12} and load torque T_L (n=5, m=4, r=1, q=1) are to be estimated. First, by augmenting T_L in the state vector and partitioning the corresponding state matrices, we obtain the corresponding matrix blocks $\mathbf{A}_{ij}$, $\mathbf{B}_i$, $\mathbf{D}_i$ $(i, j = 1,2)$ of the form (3.75). Then, by choosing the observer matrix gain $\mathbf{L}_1 = [0\ \ l_1\ \ l_2\ \ 0]$ and $\mathbf{L}_2 = [0\ \ 0\ \ l_3\ \ 0]$ the observer equation is written as follows:

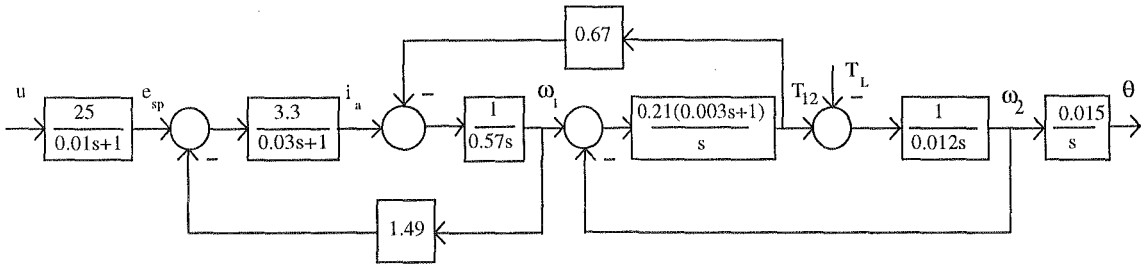

Figure 3.9. Block diagram of a two-mass position drive system.

$$
\begin{aligned}
z_1(k+1) &= f_{11}z_1(k) + f_{12}z_2(k) + g_{11}e_{sp}(k) + g_{12}i_a(k) \\
&\quad + g_{13}\omega_1(k) + g_{14}\omega_2(k) + h_1u(k), \\
z_2(k+1) &= f_{21}z_1(k) + f_{22}z_2(k) + g_{21}e_{sp}(k) + g_{22}i_a(k) \\
&\quad + g_{23}\omega_1(k) + g_{24}\omega_2(k) + h_2u(k) - \gamma\hat{T}_L(k-1), \\
\hat{T}_{12}(k) &= z_1(k) + l_1i_a(k) + l_2\omega_1(k), \quad \hat{T}_L(k) = z_2(k) + l_3\omega_1(k),
\end{aligned}
$$

where $z_1(k)$, $z_2(k)$ are the observer state variables, and the coefficients f_{ij}, g_{il}, h_i $(i,j=1,2,\ l=1,2,3,4)$ are calculated from (3.76b). The observer characteristic equation is found to be:

$$
z^3 + (f_{11} + f_{22})z^2 + (\gamma + f_{11}f_{22} - f_{12}f_{21})z - \gamma f_{11} = 0.
$$

For a given predictive coefficient $\gamma = \gamma_0$, the elements l_1, l_2, l_3 can be determined from the desired observer pole assignment. For example, the deadbeat condition gives:

$$
l_1 = \frac{\gamma_0 d_3 + (1+\gamma_0)(a_{35}d_5 - a_{55}d_3)}{(1+\gamma_0)(a_{35}d_2 - a_{25}d_3)}, \quad l_2 = \frac{a_{55} - l_1a_{25}}{a_{35}}, \quad l_3 = \frac{1+\gamma_0}{d_3},
$$

where a_{ij}, d_i $(i,j=1,2,\ldots,5)$ are the matrix entries of the discrete-time state model (3.79) at nominal parameters of the system.

- Without load speed measurement (Ha [39]):

The load speed ω_2, elastic torque T_{12} and load torque T_L will be estimated (n=5, m=3, r=1, q=1). By partitioning the state matrices into the form (3.76a) and choosing the observer gain $\mathbf{L}_1 = \begin{bmatrix} 0 & l_1 & l_2 \\ 0 & l_3 & l_4 \end{bmatrix}$ and $\mathbf{L}_2 = [0 \ \ l_5 \ \ l_6]$, the observer equation can be written as follows:

$$
\begin{aligned}
z_1(k+1) &= f_{11}z_1(k) + f_{12}z_2(k) + f_{13}z_3(k) + g_{11}e_{sp}(k) \\
&\quad + g_{12}i_a(k) + g_{13}\omega_1(k) + h_1u(k) \\
z_2(k+1) &= f_{21}z_1(k) + f_{22}z_2(k) + f_{23}z_3(k) + g_{21}e_{sp}(k) \\
&\quad + g_{22}i_a(k) + g_{23}\omega_1(k) + h_2u(k) \\
z_3(k+1) &= f_{31}z_1(k) + f_{32}z_2(k) + f_{33}z_3(k) + g_{31}e_{sp}(k) \\
&\quad + g_{32}i_a(k) + g_{33}\omega_1(k) + h_3u(k) - \gamma\hat{T}_L(k-1)
\end{aligned}
$$

$$\hat{\omega}_2(k) = z_1(k) + l_1 i_a(k) + l_2 \omega_1(k)$$
$$\hat{T}_{12}(k) = z_2(k) + l_3 i_a(k) + l_4 \omega_1(k)$$
$$\hat{T}_L(k) = w(k) + l_5 i_a(k) + l_6 \omega_1(k),$$

where $z_1(k)$, $z_2(k)$ and $z_3(k)$ are the observer state, f_{ij} , g_{ij}, and h_i $(i, j = 1,2,3)$ are coefficients calculated from (3.76b). The observer characteristic equation is found to be $z^4 + \alpha_4 z^3 + \alpha_3 z^2 + \alpha_2 z + \alpha_1 = 0$, where

$$\alpha_1 = \gamma(f_{11}f_{22} - f_{12}f_{21}),$$
$$\alpha_2 = f_{11}f_{23}f_{32} + f_{22}f_{13}f_{31} + f_{33}f_{12}f_{21} - f_{13}f_{32}f_{21} - f_{12}f_{23}f_{31} - f_{11}f_{22}f_{33} - \gamma(f_{11} + f_{22}),$$
$$\alpha_3 = f_{11}f_{22} + f_{22}f_{33} + f_{33}f_{11} - f_{12}f_{21} - f_{13}f_{31} - f_{23}f_{32} + \gamma,$$
$$\alpha_4 = -(f_{11} + f_{22} + f_{33}).$$

For a given coefficient $\gamma = \gamma_0$, a solution for the observer deadbeat condition can be obtained as follows:

$$l_1 = (a_{44}a_{35} - a_{45}a_{34}) / \Delta_1, \quad l_2 = (a_{24}a_{45} - a_{25}a_{44}) / \Delta_1,$$
$$l_3 = (a_{54}a_{35} - a_{55}a_{34}) / \Delta_1, \quad l_4 = (a_{24}a_{55} - a_{25}a_{54}) / \Delta_1,$$
$$l_5 = -(\gamma_0 d_3 + (1+\gamma_0)(f_{13}a_{34} + f_{23}a_{35})) / \Delta_2,$$
$$l_6 = (\gamma_0 d_2 + (1+\gamma_0)(f_{13}a_{24} + f_{23}a_{25})) / \Delta_2$$

with

$$f_{13} = d_4 - l_1 d_2 - l_2 d_3, \; f_{23} = d_5 - l_3 d_2 - l_4 d_3,$$
$$\Delta_1 = a_{24}a_{35} - a_{25}a_{34}, \; \Delta_2 = (f_{13}a_{24} + f_{23}a_{25})d_3 - (f_{13}a_{34} + f_{23}a_{35})d_2,$$

where the matrix elements a_{ij}, d_i $(i, j = 1, 2, \ldots, 5)$ found in the discrete-time state equation (3.79).

With the predictive coefficient chosen at γ_0=0.5 and the observer gains are chosen to meet the deadbeat condition, the actual and estimated load torque responses when T_L varies stepwise and sinusoidally are shown in Figure 3.10. Note that for the sake of simulation, the observer initial state variables are set at (1, 1). The result indicates that the proposed digital predictive observer with a well-chosen predictive coefficient can provide correct estimates of not only plant's inaccessible state variables but also an unknown load torque.

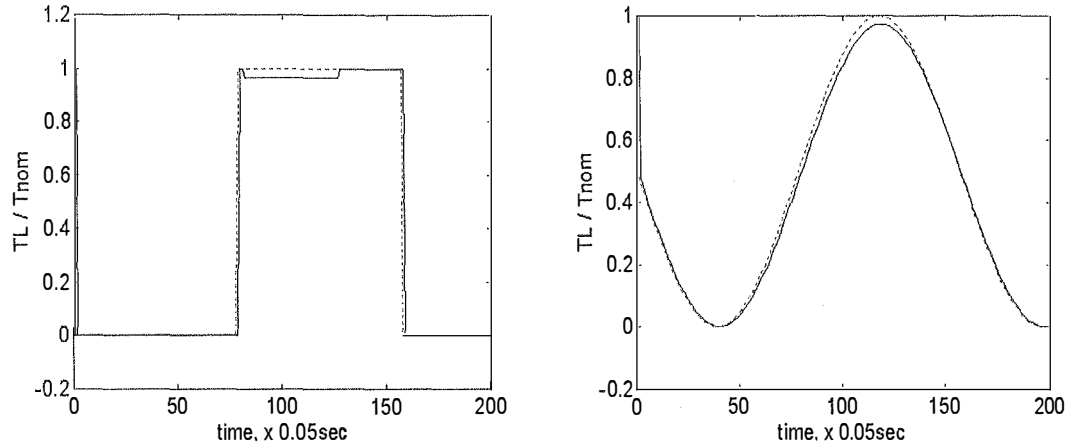

Figure 3.10. Actual and estimated load torque: (a) stepwise, and (b) sinusoidal.

3.5 Observer-based feedforward compensation

In high performance servo drive applications, control accuracy, fast response and insensitivity to any perturbations are increasingly important requirements. Load torque changes, parameter variation and nonlinear friction in servo systems are the main cause of speed fluctuation and may result in unacceptable motion error. Any variation in the motor generating torque, moment of inertia, or friction can be considered as equivalent to an uncertain load torque change (Dote [65]). Estimating load torque as an unknown input to a drive system becomes of interest for its monitoring and control. Load rejection for improving accuracy and system robustness can then be accomplished by feedforward compensation from the estimated load torque (Ohishi *et al.* [99], Ko *et al.* [78], Ha & Alferov [19]), where the feedforward gain is chosen from the zero steady-state error condition. In Schmidt & Lorenz [100], load induced motion error is reduced by acceleration feedback with the acceleration signal derived from a position signal via an observer. The acceleration signal can be evaluated by using knowledge of the estimated load torque (Hori *et al.* [64]). In this section, the feedforward control principles are introduced to compensate for the load torque influence using a disturbance observer.

Consider a linearised system with a continuous-time state model (3.1) or a discrete-time one (3.28). The key idea behind feedforward control here is to provide in addition to the modal control signal $\mathbf{u}_m$ (3.15b) or (3.29) a compensation signal $\mathbf{u}_f$, which depends on the estimated disturbance obtained from an observer:

$$\mathbf{u}_f = \mathbf{K}_f \hat{\mathbf{v}}, \tag{3.80}$$

where $\mathbf{K}_f \in R^{r\times q}$ is the matrix of feedforward coefficients. Since modal control, in general, does not guarantee steady-state performance, the entries of $\mathbf{K}_f$ can be chosen based on zero steady-state error conditions. In the following, we assume that $q = 1$ and a load torque T_L is considered as disturbance in drive systems with linearised models (3.2)-(3.5).

The schematic of a typical modal controller with feedforward compensation for a DC motor drive of Figure 3.1 is shown in Figure 3.11, where LTO is a load torque observer. When the load torque T_L is constant or slowly time-varying, the feedforward gain K_f determined from the condition of zero steady-state error (the motor speed ω=0, current $i_a = T_L/K_t$, supply voltage $e_{sp} = T_L R_a/K_t$, control voltage $u = T_L R_a/K_t K_{sp}$, and error $e_{ss} = 0$) is

$$K_f = R_a/K_t K_{sp} + (K_{es}R_a + K_I)/K_t, \tag{3.81}$$

where R_a and K_t are the motor armature resistance and torque constant, K_{sp} is the supply amplifier gain, K_{es} and K_{ia} are the supply voltage and current feedback gains.

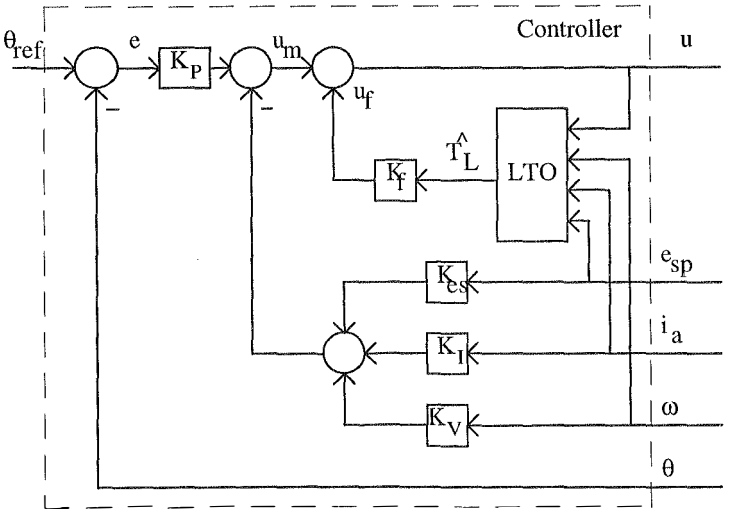

Figure 3.11. State feedback and feedforward controller.

For the case of a two-mass servo drive (Figure 3.2) using a DC motor, the controller block diagram has the form of Figure 3.12. The zero steady-state condition requires the motor and load speed $\omega_1 = \omega_2 = 0$, elastic torque $T_e = T_L$, current $i_a = T_L/K_t$, supply voltage $e_{sp} = T_L R_a/K_t$, control voltage $u = T_L R_a/K_t K_{sp}$, and error $e_{ss} = 0$. The feedforward coefficient is found in the same way:

$$K_f = R_a/K_t K_c + K_{es} R_a/K_t + K_{ia}/K_t + K_{T12}, \tag{3.82}$$

where K_{T12} is the elastic torque feedback gain.

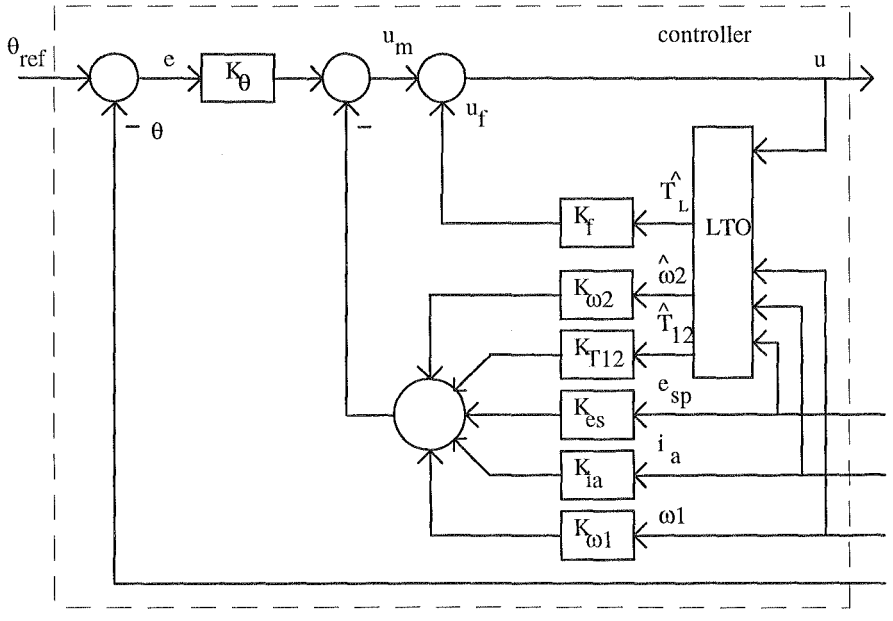

Figure 3.12. Feedforward controller block diagram for a two-mass position drive.

Example 3.4 (Alferov & Ha [75]): Consider the one-mass system of Example 3.1. Obviously, a steady-state error due to a load torque disturbance still exists even with the use of a dominant root-based modal controller, as shown in Figure 3.2. With the feedforward gain obtained from (3.81), load torque influence can be completely rejected as shown in Figure 3.13 for the one-mass system case.

Example 3.5: Consider the two-mass system of Example 3.2. Figure 3.14 plots the dominant root-based modal control step response with a load torque disturbance exerted on a two-mass system at $t = 3\,\text{sec}$ with and without feedforward compensation. As it can be seen in Figure 3.14(b), the influence of a load torque is quickly alleviated.

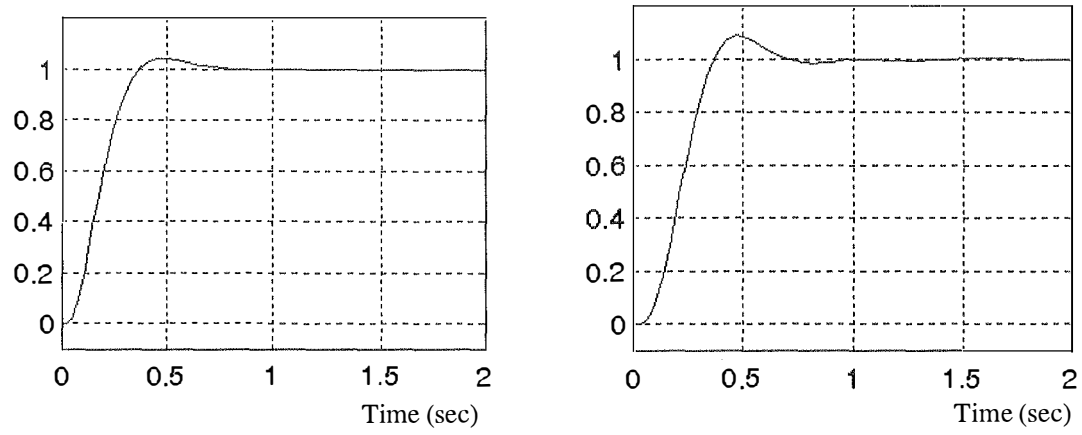

Figure 3.13. Step response of an one-mass system with a load torque at $t = 1\,\text{sec}$ using feedforward signal in: (a) dominant root-based, and (b) Butterworth pole placement.

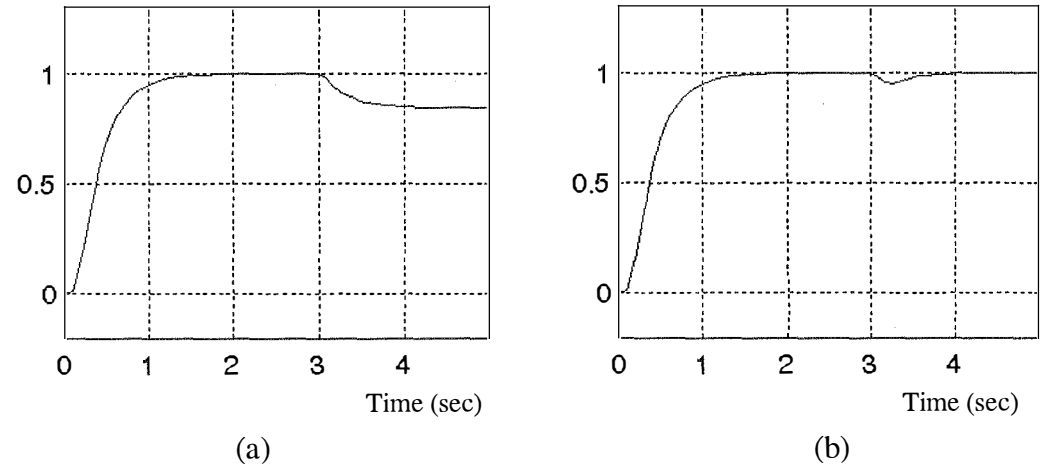

Figure 3.14. Step response of an two-mass system with a load torque at $t = 3\,\text{sec}$, using dominant root-based modal control: (a) without compensation, and (b) with feedforward compensation.

The results obtained indicate that observer-based feedforward compensation is a good approach to the problem of load rejection in electromechanical systems. A main disadvantage of the observer-based modal control is that the feedback and feedforward controllers require correct knowledge of the plant parameters. Thus, parameter sensitivity is a problem of this technique. Issues about robustness against parameter variations will be discussed in the next section and in Chapters 5, 6, and 7.

3.6 Robust modal control

For improving robustness in servo drives, several control techniques are evolving such as the sliding mode in variable structure systems (Chang *et al.* [101]), self-tuning and model reference adaptive controls (Bortsov *et al.* [87], Egami *et al.* [102]). Sliding mode control is efficient dealing with structured uncertainty such as changing parameters and load. However, the observation noise and the chattering phenomena due to large control gains are challenging issues and there is a trade-off between robustness and chattering. Conventional adaptive control adaptive control algorithms are usually complicated and thus, need excessive computation effort for real-time implementation. Modal controllers, in general, are designed depending on an accurate linearised model of the controlled system. In electromechanical systems, design equations of modal control (3.43), (3.45) or (3.48), and of feedforward control (3.81) or (3.82) indicate explicitly the relationship between the controller's and plant's parameters. In order to obtain satisfactory control performance, the dynamics of controlled systems are assumed to be known so that any control strategy can be successfully applied. However, when the structure of the plant is unknown and the parameter variation is excessive, the effectiveness of modal control diminishes. Here, in order to obtain parameter-insensitivity a robust control signal is added to the modal control signal. Thus, the control signal consists of three components: the modal control signal $u_m(t)$, the feedforward control signal $u_f(t)$, and the robust feedback signal $u_r(t)$. Such a controller is called a *robust modal controller* in Ha [9]. Design procedures for continuous-time and discrete-time robust modal controllers are given in this section. The asymptotic stability of the overall system is guaranteed by using the second method of Lyapunov. Simulation results for one-mass and two-mass servo systems are given to verify the validity of the proposed method.

3.6.1. Continuous-time robust modal controller

The design procedure starts with the assumption that the influence of external disturbances $\mathbf{v}(t)$ has been alleviated by the compensation signal $u_f(t)$ and then, the single input ($r = 1$) linearised model (3.1) with structured uncertainty can be brought into the form:

$$\dot{\mathbf{x}}(t) = (\mathbf{A}_0 + \Delta\mathbf{A})\mathbf{x}(t) + (\mathbf{b}_0 + \Delta\mathbf{b})(u_m(t) + u_r(t)), \tag{3.83}$$

$$\mathbf{y}(t) = \mathbf{C}_0\mathbf{x}(t),$$

where $\mathbf{A}_0$, $\mathbf{b}_0$, and $\mathbf{C}_0$ are the nominal system matrices, and $\Delta\mathbf{A}$ and $\Delta\mathbf{b}$ are the system uncertainties. The triple $(\mathbf{A}_0, \mathbf{b}_0, \mathbf{C}_0)$ is assumed controllable and observable. The principles of robust modal control are illustrated by a block diagram shown in Figure 3.15. A combined state-disturbance observer (SDO) as described in Section 3.4 is used for evaluating the physically inaccessible state $\mathbf{x}_2(t)$ and the unknown disturbances $\mathbf{v}(t)$. The modal controller (MC) then accomplishes feedback from the output $\mathbf{y}(t) = \mathbf{x}_1(t)$ and the estimated state $\hat{\mathbf{x}}_2(t)$:

$$u_m(t) = U_{ref} - \mathbf{k}^T[\mathbf{x}_1(t) \;\; \hat{\mathbf{x}}_2(t)]^T, \tag{3.84}$$

where U_{ref} is the reference input, defining the steady state component. Considering the transient response, the reference U_{ref} is set equal to 0. Neglecting the observer error, the modal signal (3.84) has the form of (3.15b). In order to deal with uncertainties, the robust controller (RC) employs an additional robust feedback signal $u_r(t)$ which will be determined in the following discussion. The feedforward controller (FC) provides the compensation signal $u_f(t)$ (3.80) for eliminating the external disturbance influence, hence $\mathbf{v}(t)$ can be omitted in the state equation (3.83). Substituting (3.15b) and the robust feedback signal $u_r(t)$ into (3.83) gives:

$$\dot{\mathbf{x}}(t) = (\mathbf{A}_0 - \mathbf{b}_0\mathbf{k}^T)\mathbf{x}(t) + (\Delta\mathbf{A} - \Delta\mathbf{b}\mathbf{k}^T)\mathbf{x}(t) + (\mathbf{b}_0 + \Delta\mathbf{b})u_r(t) + \varepsilon(t), \tag{3.85}$$

where $\varepsilon(t) \in R^n$ is an infinitesimal vector due to the observer error and incomplete compensation. Denoting $\mathbf{A}_m = \mathbf{A}_0 - \mathbf{b}_0\mathbf{k}^T$ and $\Delta\mathbf{A}_m = \Delta\mathbf{A} - \Delta\mathbf{b}\mathbf{k}^T$, and neglecting $\varepsilon(t)$, (3.85) becomes:

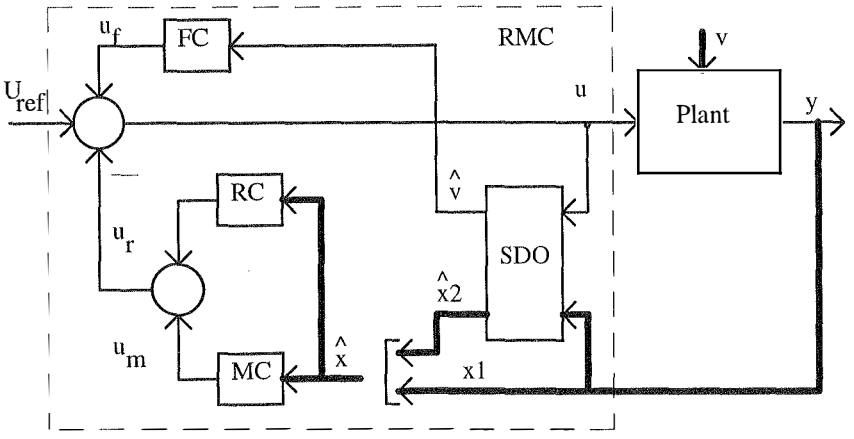

Figure 3.15. Robust modal control block diagram.

$$\dot{\mathbf{x}}(t) = (\mathbf{A}_m + \Delta\mathbf{A}_m)\mathbf{x}(t) + (\mathbf{b}_0 + \Delta\mathbf{b})\mathbf{u}_r(t). \tag{3.86}$$

The following assumptions are made (Jabbari & Schmitendorf [103]):

A1. The uncertainties are continuous matrix functions of the vector of varying system parameters $\mathbf{p} \in \mathcal{P} \subset R^p$, where $\mathcal{P}$ is a compact set:

$$\Delta\mathbf{A}_m = \Delta\mathbf{A}_m(\mathbf{p}), \quad \Delta\mathbf{b} = \Delta\mathbf{b}(\mathbf{p}). \tag{3.87}$$

A2. There exist a vector $\mathbf{r}(\mathbf{p}) \in R^n$ and a scalar $s(\mathbf{p})$ such that (matching conditions):

$$\Delta\mathbf{A}_m = \mathbf{b}_0\mathbf{r}^T(\mathbf{p}) \text{ and } \|\mathbf{r}(\mathbf{p})\| \le \rho, \ \forall\mathbf{p} \in \mathcal{P}, \tag{3.88}$$

$$\Delta\mathbf{b} = \mathbf{b}_0 h(\mathbf{p}) \text{ and } |h(\mathbf{p})| \le \sigma < 1, \ \forall\mathbf{p} \in \mathcal{P},$$

where $\| \cdot \|$ denotes the Euclidean norm.

Theorem 3.2 (Ha [9])
Consider the continuous-time system (3.86) satisfying the assumptions A1 and A2, given in (3.87) and (3.88). For any positive-definite matrix $\mathbf{Q}$ and positive scalar γ_r satisfying:

$$\lambda_{\min}(\mathbf{Q}) > \rho^2 \text{ and } \gamma_r > \frac{1}{1-\sigma}, \tag{3.89}$$

where $\lambda_{\min}(\mathbf{Q})$ is the minimum eigenvalue of $\mathbf{Q}$, the control law

$$u_r = -\mathbf{k}_r^T\mathbf{x}(t) = -\gamma_r\mathbf{b}_0^T\mathbf{P}\mathbf{x}(t) \tag{3.90}$$

is a robust stabilising control with the robust feedback gain $\mathbf{k}_r = \gamma_r\mathbf{P}\mathbf{b}_0$, where $\mathbf{P}$ is the solution of the Lyapunov equation:

$$\mathbf{A}_m^T\mathbf{P} + \mathbf{P}\mathbf{A}_m + \mathbf{Q} = \mathbf{0}, \ \mathbf{Q} > \mathbf{0}. \tag{3.91}$$

Proof: Choose a Lyapunov function candidature of the form $V(\mathbf{x}) = \mathbf{x}^T(t)\mathbf{P}\mathbf{x}(t)$, where $\mathbf{P}$ is a unique positive-definite solution of (3.91). The trajectory time derivative is obtained using (3.86) and (3.90):

$$\dot{V}(\mathbf{x}) = \dot{\mathbf{x}}^T\mathbf{P}\mathbf{x} + \mathbf{x}^T\mathbf{P}\dot{\mathbf{x}} =$$
$$= [\mathbf{x}^T(\mathbf{A}_m + \Delta\mathbf{A}_m)^T + u_r(\mathbf{b}_0 + \Delta\mathbf{b})^T]\mathbf{P}\mathbf{x} + \mathbf{x}^T\mathbf{P}[(\mathbf{A}_m + \Delta\mathbf{A}_m)\mathbf{x} + (\mathbf{b}_0 + \Delta\mathbf{b})u_r] =$$
$$\dot{V}(\mathbf{x}) = \mathbf{x}^T[\mathbf{A}_m^T\mathbf{P} + \mathbf{P}\mathbf{A}_m + \Delta\mathbf{A}_m^T\mathbf{P} + \mathbf{P}\Delta\mathbf{A}_m - 2\gamma_r\mathbf{P}\mathbf{b}_0\mathbf{b}_0^T\mathbf{P} - 2\gamma_r h(\mathbf{p})\mathbf{P}\mathbf{b}_0\mathbf{b}_0^T\mathbf{P}]\mathbf{x}$$
$$= \mathbf{x}^T\mathbf{L}(\mathbf{p})\mathbf{x},$$

where $\mathbf{L}(\mathbf{p}) = -\mathbf{Q} + \mathbf{r}(\mathbf{p})\mathbf{b}_0^T\mathbf{P} + \mathbf{P}\mathbf{b}_0\mathbf{r}^T(\mathbf{p}) - 2\gamma_r(1 + h(\mathbf{p}))\mathbf{P}\mathbf{b}_0\mathbf{b}_0^T\mathbf{P}$.

Applying to the above equation the following identity $\mathbf{X}\mathbf{X}^T + \mathbf{Y}\mathbf{Y}^T \geq \mathbf{X}\mathbf{Y}^T + \mathbf{Y}\mathbf{X}^T$ for $n \times m$-matrices $\mathbf{X}$ and $\mathbf{Y}$ gives:

$$\mathbf{L}(\mathbf{p}) \leq -\mathbf{Q} + \mathbf{r}\mathbf{r}^T - \gamma_r(2 + 2h(\mathbf{p}) - \frac{1}{\gamma_r})\mathbf{P}\mathbf{b}_0\mathbf{b}_0^T\mathbf{P}.$$

If the coefficient γ_r is chosen such that $\gamma_r \geq \dfrac{1}{2(1+h(\mathbf{p}))}$, then

$$\dot{V} \leq -\mathbf{x}^T(\mathbf{Q} - \mathbf{r}\mathbf{r}^T)\mathbf{x} \leq -(\lambda_{\min}(\mathbf{Q}) - \|\mathbf{r}\|^2)\|\mathbf{x}(t)\|^2.$$

Since $\sup\limits_{\mathbf{p}\in\mathcal{P}} \dfrac{1}{1+h(\mathbf{p})} = \dfrac{1}{1-\sigma}$ and $\sup\limits_{\mathbf{p}\in\mathcal{P}}\|\mathbf{r}(\mathbf{p})\| = \rho$, the derivative of the Lyapunov function is negative definite if $\mathbf{Q}$ and γ_r are chosen satisfying (3.89). This concludes the proof.

Example 3.6: Consider Example 3.2 with the two-mass system of Figure 3.3. Assume that the dynamic stiffness of the drive speed-torque characteristics is an uncertain parameter with a variation of 50% of its nominal value. The state model (3.5) can be obtained as

$$\begin{bmatrix} T_m \\ \omega_1 \\ T_{12} \\ \omega_2 \end{bmatrix} = \begin{bmatrix} -33.3 & -\alpha & 0 & 0 \\ 1.23 & 0 & 1.23 & 0 \\ 0 & 0.21 & 0 & -0.21 \\ 0 & 0 & 83.3 & 0 \end{bmatrix} \begin{bmatrix} T_m \\ \omega_1 \\ T_{12} \\ \omega_2 \end{bmatrix} + \begin{bmatrix} \alpha \\ 0 \\ 0 \\ 0 \end{bmatrix} \omega_{ref} + \begin{bmatrix} 0 \\ 0 \\ 0 \\ -83.3 \end{bmatrix} T_L$$

where $\alpha = 237.3 \pm 118.7$. The dominant root-based method gives the state feedback gain $\mathbf{k}^T = [0.0371 \quad 1.2187 \quad 63.96 \quad 0.1863]$. With $(\Delta A)_{1,2} = (\Delta B)_1 = 118.7$ and $(\Delta A)_{i,j\neq 1,2} = (\Delta B)_{i\neq 1} = 0$, the rows of $\Delta\mathbf{A}_m$ are found to be $(\Delta A_m)_{i\neq 1} = [0 \; 0 \; 0 \; 0]$ and $(\Delta A_m)_1 = -10^{-2}[0.02 \quad 0.11 \quad 31.98 \quad 0.09]$. Thus, the bounds ρ and σ are determined as 0.32 and 0.5, respectively. From the solution of the Lyapunov equation (3.91), the

robust feedback gain according to (3.90) is calculated as $\mathbf{k}_r^T = [-0.1 \quad 0.0004 \quad 0.03 \quad 0.002]$. The step response of the load speed with a 50% reduction in the dynamic stiffness ($\alpha = 118.7$) without robust feedback is shown in Figure 3.16(a), and with robust feedback in Figure 3.16(b) where an improvement of transient performance is observed. The influence of backlash nonlinearity with a deadband width of $2D = 0.02$ in the coupling shaft gear is considered in Figure 3.17. It is indicated that an additional robust feedback (Figure 3.17(b)) helps increasing robustness against unstructured uncertainty such as backlash nonlinearity.

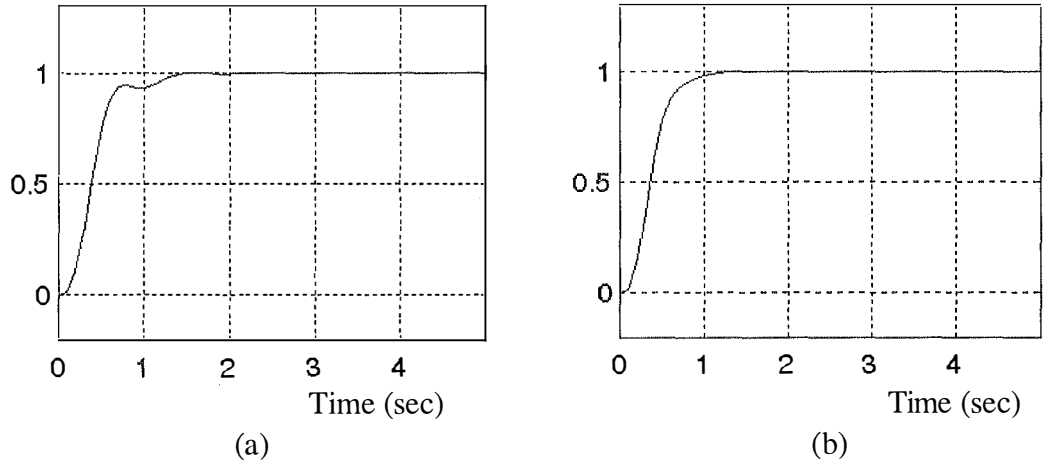

Figure 3.12. Step response of the load speed with a 50% reduction in the dynamic stiffness: (a) without robust feedback, and (b) with robust feedback.

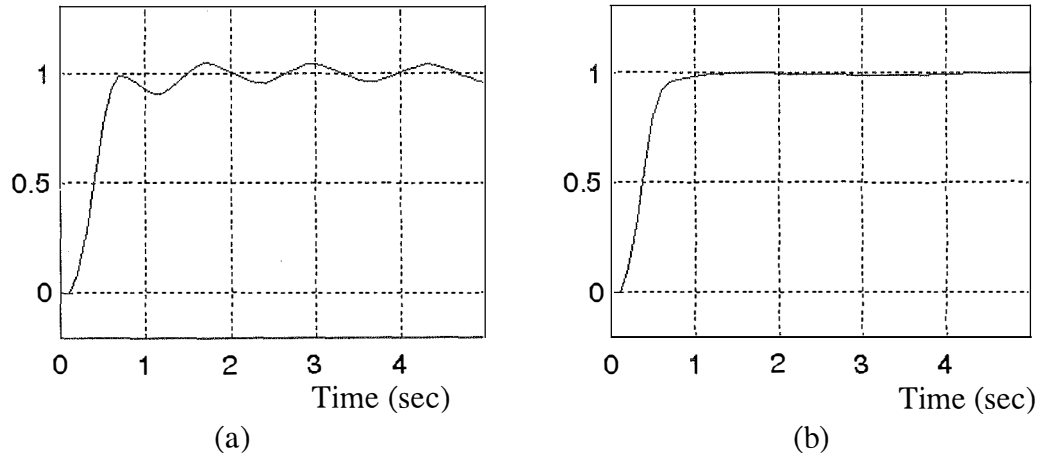

Figure 3.17. Step response of the load speed with backlash $2D = 0.02$: (a) without robust feedback, and (b) with robust feedback.

3.6.2. Discrete-time robust modal controller

Now consider the discrete-time case when the state model can be written as:

$$\mathbf{x}(k+1) = (\mathbf{A}_0 + \Delta\mathbf{A})\mathbf{x}(k) + (\mathbf{b}_0 + \Delta\mathbf{b})(u_m(k) + u_r(k)), \tag{3.92}$$

$$\mathbf{y}(k) = \mathbf{C}_0\mathbf{x}(k),$$

where $\mathbf{A}_0$, $\mathbf{b}_0$, and $\mathbf{C}_0$ are the nominal system matrices, and $\Delta\mathbf{A}$ and $\Delta\mathbf{b}$ are the system uncertainties for the model written in the discrete-time form. The triple ($\mathbf{A}_0$, $\mathbf{b}_0$, $\mathbf{C}_0$) is assumed controllable and observable. It is also assumed that the influence of external disturbances $\mathbf{v}(k)$ in the state model (3.28) has been compensated for with the use of a feedforward signal $u_f(k)$. Following the schematic shown in Figure 3.11, and again assuming a complete rejection of $\mathbf{v}(k)$, the closed-loop dynamics with discrete-time robust modal control can be described by:

$$\mathbf{x}(k+1) = (\mathbf{A}_m + \Delta\mathbf{A}_m)\mathbf{x}(k) + (\mathbf{b}_0 + \Delta\mathbf{b})u_r(k), \tag{3.93}$$

where $\mathbf{A}_m = \mathbf{A}_0 - \mathbf{b}_0\mathbf{k}^T$, $\Delta\mathbf{A}_m = \Delta\mathbf{A} - \Delta\mathbf{b}\mathbf{k}^T$, and $\mathbf{k}^T$ is the feedback gain of the modal controller (MC). The determination of the robust controller (RC) is given in the following theorem:

Theorem 3.3 (Alferov & Ha [36])
Consider the discrete-time system (3.93) satisfying the assumptions A1 and A2, given in (3.87) and (3.88). For any positive-definite matrix $\mathbf{Q}$ satisfying:

$$\lambda_{\min}(\mathbf{Q}) > \mathbf{b}_0^T\mathbf{P}\mathbf{b}_0\left(\frac{\rho}{1-\sigma}\right)^2 = \lambda_{cr}, \tag{3.94}$$

where $\lambda_{\min}(\mathbf{Q})$ is the minimum eigenvalue of matrix $\mathbf{Q}$, and $\mathbf{P}$ is the solution of the discrete-time Lyapunov equation:

$$\mathbf{A}_m^T\mathbf{P}\mathbf{A}_m - \mathbf{P} + \mathbf{Q} = \mathbf{0}, \quad \mathbf{Q} > \mathbf{0}, \tag{3.95}$$

the control law:

$$u_r(k) = -\mathbf{k}_r^T \mathbf{x}(k) = -\frac{\mathbf{b}_0^T \mathbf{P} \mathbf{A}_m}{\mathbf{b}_0^T \mathbf{P} \mathbf{b}_0} \mathbf{x}(k) \tag{3.96}$$

is a robust stabilising control.

Proof: Define the scalar function $h(k) = \mathbf{r}^T(\mathbf{p})\mathbf{x}(k) + (1 + s(\mathbf{p}))u_r(k)$, the above state equation (3.93) can be rewritten as

$$\mathbf{x}(k+1) = \mathbf{A}_m \mathbf{x}(k) + \mathbf{b}_0 h(k).$$

Since $\mathbf{A}_m$ is stable, there exists a symmetric positive definite matrix $\mathbf{P}$ satisfying the Lyapunov function (3.95) for any given symmetric positive definite matrix $\mathbf{Q}$. Choose a Lyapunov function candidature of the form $V(\mathbf{x}) = \mathbf{x}^T(k)\mathbf{P}\mathbf{x}(k)$. The differential change

$$\Delta V(k) = V(k+1) - V(k) = \mathbf{x}^T(k+1)\mathbf{P}\mathbf{x}(k+1) - \mathbf{x}^T(k)\mathbf{P}\mathbf{x}(k),$$

can be expressed as

$$\begin{aligned}\Delta V(k) &= [\mathbf{A}_m \mathbf{x}(k) + \mathbf{b}_0 h(k)]^T \mathbf{P}[\mathbf{A}_m \mathbf{x}(k) + \mathbf{b}_0 h(k)] - \mathbf{x}^T(k)\mathbf{P}(k)\mathbf{x}(k) \\ &= \mathbf{x}^T(k)[\mathbf{A}_m^T \mathbf{P} \mathbf{A}_m - \mathbf{P}]\mathbf{x}(k) + h(k)[\mathbf{b}_0^T \mathbf{P} \mathbf{b}_0 h(k) + 2\mathbf{b}_0^T \mathbf{P} \mathbf{A}_m \mathbf{x}(k)]\end{aligned}$$

$$\Delta V(k) = -\mathbf{x}^T(k)\mathbf{Q}\mathbf{x}(k) + h(k)[\gamma_0 h(k) + 2\varphi(k)],$$

where $\gamma_0 = \mathbf{b}_0^T \mathbf{P} \mathbf{b}_0$ is a positive constant, and $\varphi(k) = \mathbf{b}_0^T \mathbf{P} \mathbf{A}_m \mathbf{x}(k)$ is a scalar function. The quadratic form $h(k)[\gamma_0 h(k) + 2\varphi(k)]$ will be non-positive if $h(k)$ lies in the interval between 0 and $-2\varphi(k)/\sigma$. Under the control law:

$$\frac{-\frac{2\varphi(k)}{\gamma_0} + \rho\|\mathbf{x}(k)\|}{1+\sigma} \le u_r(k) \le \frac{-\rho\|\mathbf{x}(k)\|}{1-\sigma}, \quad \text{when} \quad \varphi(k) \ge \frac{\gamma_0 \rho}{1-\sigma}\|\mathbf{x}(k)\|$$

$$u_r(k) = 0, \qquad \text{when} \qquad \varphi(k) = 0$$

$$\frac{\rho\|\mathbf{x}(k)\|}{1-\sigma} \le u_r(k) \le \frac{-\frac{2\varphi(k)}{\gamma_0} + \rho\|\mathbf{x}(k)\|}{1+\sigma}, \quad \text{when} \quad \varphi(k) \le -\frac{\gamma_0 \rho}{1-\sigma}\|\mathbf{x}(k)\|.$$

the differential change $\Delta V(k)$ has an upper bound given by (Yang & Tomizuka [104]):

$$\Delta V(k) \le -\left(\lambda_{\min}(\mathbf{Q}) - \mathbf{b}_0^T \mathbf{P} \mathbf{b}_0 \left(\frac{\rho}{1-\sigma} \right)^2 \right) \|\mathbf{x}(k)\|^2 .$$

Thus, if the condition (3.94) is satisfied then the system will be asymptotical stable under the control law above. By this control law, the robust feedback signal $u_r(k)$ should lie in the interval between

$$\frac{-2\varphi(k)/\gamma_0 + \rho\|\mathbf{x}(k)\| sgn(\varphi(k))}{1-\sigma} \quad \text{and} \quad \frac{-\rho\|\mathbf{x}(k)\| sgn(\varphi(k))}{1-\sigma}.$$

The problem is to determine two positive real numbers κ_1 and κ_2 satisfying $\kappa_1 + \kappa_2 = 1$ such that the resulting robust feedback signal

$$u_r(k) = \kappa_1 \frac{-2\varphi(k)/\gamma_0 + \rho\|\mathbf{x}(k)\| sgn(\varphi(k))}{1-\sigma} + \kappa_2 \frac{-\rho\|\mathbf{x}(k)\| sgn(\varphi(k))}{1-\sigma}$$

can tolerate the largest uncertainty range, or have the simplest form. The latter leads to the choice

$$\kappa_1 = \frac{1+\sigma}{2} \quad \text{and} \quad \kappa_2 = \frac{1-\sigma}{2}$$

by which the nonlinear term $\rho\|\mathbf{x}(k)\| sgn(\varphi(k))$ can be omitted from the control signal $u_r(k)$. In that case, the robust feedback signal $u_r(k)$ is then obtained

$$u_r(k) = \frac{-\varphi(k)}{\gamma_0} = -\frac{\mathbf{b}_0^T \mathbf{P} \mathbf{A}_m}{\mathbf{b}_0^T \mathbf{P} \mathbf{b}_0} \mathbf{x}(k) = -\mathbf{k}_r^T \mathbf{x}(k).$$

This concludes the proof.

Example 3.7 (Alferov & Ha [19, 36]): Consider the system of Figure 3.1 using the DC motor of the type PGT-2 with the following specifications: $K_c = 12$, $T_c = 0.007\text{sec}$, $R_a = 0.785ohm$, $L_a = 3.92mH$, $B_m = 0$, $J_m = 0.002kgm^2$, $K_b = 0.297Vs\ /\ rad$ and $K_t = 0.297V\ /\ A$. The sampling time is $T = 0.003\text{sec}$.

The state feedback gain $\mathbf{k}^T = [K_E \; K_V \; K_I \; K_P]$ computed using the magnitude optimum criterion is $\mathbf{k}^T = [0.133 \; 0.025 \; 0.005 \; 4.362]$. Assume that the total inertia and armature resistance vary in the intervals $J_m \in [1,\ 2]J_{m,nom}$ and $R_a \in [1,\ 1.2]R_{a,nom}$. From the uncertainty matrices $\Delta\mathbf{A}_m$ and $\Delta\mathbf{b}$ of the form (3.93), the values of ρ, σ, and λ_{cr} is found to be 0.115, 0.17, and 0.92, respectively. Choosing $\mathbf{Q} = \mathbf{I}$, the robust feedback gain $\mathbf{k}_r^T = [\Delta K_E \; \Delta K_V \; \Delta K_I \; \Delta K_P]$ is obtained from (3.95) to be $\mathbf{k}_r^T = -[0.06 \; 0.059 \; 0.11 \; 0]$.

The position step response with $J_m = 2J_{m,nom}$ and $R_a = 1.2R_{a,nom}$ is plotted in Figure 3.18. It is observed in Figure 3.18(b) that robustness of the system is significantly improved with the use of an additional robust feedback gain transient.

Further comparison between the methods of assigning the closed-loop poles, the influence of parameter and load variations, and simulation and experimental results were reported in Ha [9] and Ha & Alferov [75, 19, 36, 91]. The results verify that robust modal control can be an efficient technique for vibration suppression, load rejection with high robustness in electromechanical systems, especially systems with flexible structures.

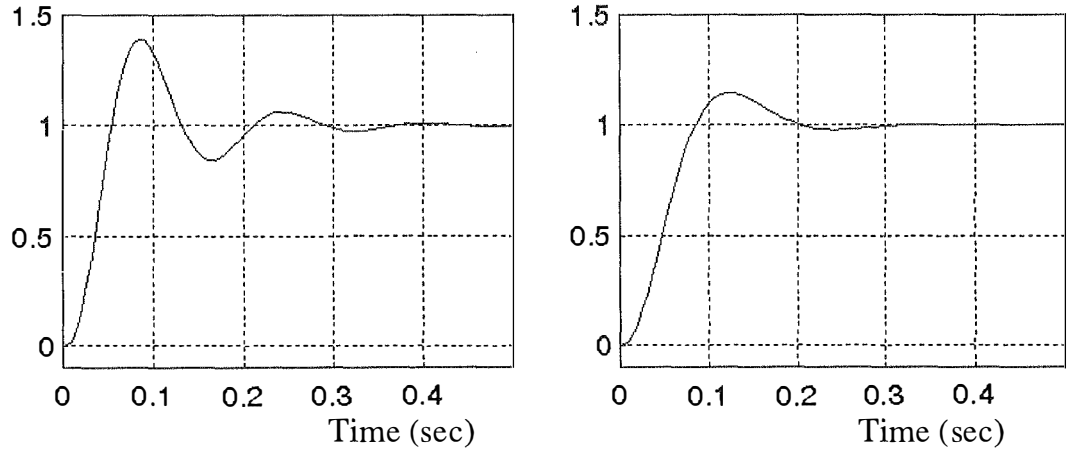

(a) (b)

Figure 3.18. Position step response with $J_m = 2J_{m,nom}$ and $R_a = 1.2R_{a,nom}$: (a) without robust feedback, and (b) with robust feedback.

3.7 Summary

An overview of the robust modal control technique has been comprehensively outlined in this chapter. It started with the mathematical description of linearised models for some position drives and focused on the servo drives with flexible structures. The methodology to construct a modal controller for these systems is addressed, considering both continuous-time and discrete-time cases.

The first contribution of this chapter is the proposed dominant root-based technique applied for one-mass and two-mass servo systems. The key idea here is that the closed-loop system dynamics is decided mainly by the location of the dominant root pair. Thus, when choosing the desired poles for determining the state feedback gain, additional conditions relating to accuracy or damping capability can be taken into consideration. This may remove the drawback that modal control cannot affect the steady-state control performance, and relax the conservatism of Kukharenko's method combining the equalising equations in modal control with control accuracy requirements. Design equations for servo systems with maximum damping are provided. Vibration suppression capability when the system is subject to backlash nonlinearity is verified. Insight into robustness of servo systems with modal control is provided by an eigenvalue sensitivity analysis. It is shown that in the vicinity of some critical values of the drive parameters, the dominant root sensitivities increase significantly. With the damping ratio lying between 0.43 and 1, the dominant root-based technique provides some advantage over other standard assignment criteria in terms of sensitivities.

As a matter of fact, not all the system state variables are physically available to be fed back in modal control, hence, they need to be estimated. Moreover, unknown inputs to the system also need to be evaluated for the compensation purpose. An interesting part of this chapter is devoted to the design of a combined observer for simultaneously estimating the system states and external disturbances, based on measurements of the system input and output and some *a priori* information of the unknown inputs. Such an observer can take into consideration the disturbance rate of change. A digital predictive observer is constructed on the basis of an augmented form of the state equation with an additional equation approximating the disturbance dynamics. The proposed observer can be applied to estimate the torsional torque and load speed, and load torque in a multi-mass servo system. Based on load torque

estimates, feedforward compensation principles can be applied to reject the disturbance influence. It is shown that with a properly chosen feedforward gain, any deteriorations in servo performance due to load changes can be completely compensated for.

Considering the parameter variation problem, a robust feedback signal is added to the modal signal. The control signal then consists of three components: modal control signal, feedforward compensation signal, and robust feedback signal. When the matching conditions are satisfied, given the bounds of uncertain matrices of the state model, the asymptotic stability condition can be determined via the second method of Lyapunov. Design procedures for the continuous-time and discrete-time robust modal controllers are illustrated in servo drive systems. Simulation results demonstrate the system parameter- and load-insensitivity, and also robustness against nonlinear phenomenon such as backlash in the coupling shaft gear of a two-mass servo system.

Although robust modal control is efficient for systems with flexible structures, the observer and feedforward compensator are designed based on system nominal parameters, and thus parametric robustness of the whole system has not completely achieved. The following chapters will address this problem using artificial intelligent tools such as fuzzy logic and neural network approaches.

Chapter 4

Fuzzy Logic and Fuzzy Logic Control

Fuzzy logic has been explored for over three decades and is currently the focus of popular and technical press. The area of process and control engineering has attracted much attention in fuzzy logic. This is explained by the salient advantage of fuzzy logic as a valuable tool in the design of embedded machine intelligence. Yet control systems exploit only a fraction of its representational power. Oriented toward applications, it is believed that the tolerance for imprecision of fuzzy logic makes it suitable to address the problems of robustness. As an introduction to the use of fuzzy logic schemes to enhance robust performance of motion control systems, this chapter briefly describes basic concepts about fuzzy logic and fuzzy logic control, and outlines some current research to fuzzy control systems.

4.1 Introduction

Fuzzy logic is a method for representing information in a way that resembles natural human communication, and for manipulating that information in a way that resembles how humans reason with it. In the early 1960s, Prof. Lotfi A. Zadeh, the inventor of Fuzzy, began to feel that traditional systems analysis techniques were too precise for real-world problems and a new technique, a "fuzzy" kind of mathematics, was needed (Perry [105]). That idea came to Zadeh in July 1964 and he published the first paper on fuzzy sets in 1965 [12]. Through over a decade after that seminal paper, fuzzy set theory was raising controversial debates within academic community. Eventually, fuzzy theory was taken seriously by the Japanese electronics companies with its implementations in numerous of consumer products (dishwashers, washing machines, air conditioners, cameras, microwave ovens, camcorders, and so on). Since successful applications of fuzzy logic ranging from consumer products to industrial process control, medical instrumentation, decision-support system and portfolio selection (Zadeh [106]), fuzzy logic has not only won a wide acceptance but also become hot

topic with an explosion of literature on it: hundreds of books, thousands of technical papers have been written on this subject.

Among diverse areas of fuzzy logic applications, control is the area to which fuzzy systems are most widely applied today. The genesis of fuzzy logic control was a 1972 paper by Chang and Zadeh [13] outlining the basic approach. An important landmark in this development was the introduction of the linguistic variables whose values are linguistic terms rather than numbers (Zadeh [107]). Fuzzy technology, Zadeh explained, is a means of computing with words for which the role model is the human ability to reason and make decisions without the use of numbers [108]. The first implementation of these ideas was described in a paper by Mamdani in 1974 [109]. The key principle underlying fuzzy logic control is based on a logical model which represents the thinking process that an operator might go through to control the system manually. The viability of fuzzy logic control has been demonstrated through wide-spread applications (Schwartz *et al.* [14]). Fuzzy logic control can be considered as one of intelligent control techniques where engineering knowledge is reflected in the controllers. It has been found that such controllers have definite advantage over the traditional PID controllers in that they are more robust with respect to structured and unstructured uncertainties. The linguistic characteristics of fuzzy control provide a very good approach in order to account for the sensor noise, unmodelled dynamics, parameter variation, disturbance influence and nonlinearities (Lee [110]).

It is known that classical PID controllers do not work well for the case of nonlinear control and, even for linear control they typically have to be redesigned according to a new set of the basic system parameters. Adaptive controllers have been proposed for these systems. By means of some tuning schemes, the controller parameters can be continuously adjusted to improve robustness against any changing environment. Auto-tuning (Astrom *et al.* [16]) or auto-calibration (Voda & Landau [17]) of controllers for plants with uncertainties is useful although some knowledge of the process is needed. Tuning the controller parameters to achieve better performance can be accomplished by means of fuzzy logic (Tseng & Hwang [20], Ha & Negnevitsky [21]). In Truong & Hofmann [111], conventional controller parameters are modified during operation by incorporated fuzzy tuners. Fuzzy tuning with explicit schemes has been proven to be capable of enhancing robustness without increasing computational burden to the controller (Ha [112], Ha & Negnevitsky [35]).

Despite a large number of technical publications focusing on fuzzy systems, there exists some doubtful opinion on fuzzy controllers mainly because of some misunderstanding about fuzzy control. Attempts have been made to clear up this misunderstanding, e.g. Jager [113]. It is, therefore, of interest to start the notable part of this thesis, using fuzzy tool in combination with other techniques, with a short primer on fuzzy set theory, fuzzy reasoning, and fuzzy logic control.

4.2 Fuzzy set theory

There is a vast amount of literature on fuzzy logic. This literature is growing rapidly in recent years, making it difficult to present a comprehensive survey of its wide applications. A lot of it is too theoretical to be applied to engineering problems. The purpose of this section is to briefly summarise the basic concepts that are necessary in order to understand fuzzy logic and fuzzy inference from a practical viewpoint.

4.2.1. Fuzzy sets (Mendel [114])

A *universe of discourse* U is the set of allowable values for a variable, denoted generically by $\{x\}$ which could be discrete or continuous, where x represents the *generic element* of U.

A *crisp set* A in a universe of discourse U can be defined as $A = \{x | \mu_A(x)\}$, where $\mu_A(x)$ is, in general, a condition by which $x \in A$. If we introduce a zero-one characteristic function such that $A \Rightarrow (\mu_A(x) = 1 \text{ if } x \in A \text{ and } \mu_A(x) = 0 \text{ if } x \notin A)$ then $\mu_A(x)$ is called a *membership function* for A.

A *fuzzy set* F in a universe of discourse U is characterised by a membership function $\mu_F(x)$ which takes on values in the interval [0, 1]. A fuzzy set is a generalisation of an ordinary (i.e. crisp) set whose membership function only takes on two values $\{0, 1\}$. A membership function for a fuzzy set F provides a *measure of the degree of similarity* of an element in U to F. A fuzzy set F in U may be represented as a set of ordered pairs of a generic element x and its grade of membership function: $F = \{(x, \mu_X(x)) | x \in U\}$. When U is continuous, F can be written concisely as $F = \int_U \mu_F(x)/x$, where the integral sign denotes the collection of all points $x \in U$ with associated membership function $\mu_F(x)$. When U is discrete, F is represented as $F = \sum_U \mu_F(x)/x$, where the summation sign denotes the set theoretic operation union. The slash in these expressions associates the elements in U with their

membership grades, where $\mu_F(x) > 0$. Note that in fuzzy sets, an element can reside in more than one set to different degrees of similarity. This cannot occur in a crisp set theory.

The *support* of a fuzzy set F is the crisp set of all points $x \in U$ such that $\mu_F(x) > 0$. The element $x \in U$ at which $\mu_F(x) = 0.5$ is called the *crossover point.* For example, the formal domain for normal weight might be 40 to 100 *kg*. However, the fuzzy sets HEAVY and LIGHT can have non-zero membership grade at 50 to 90 *kg* with a crossover point at 70 *kg*, as shown in Figure 4.1. A fuzzy set whose support is a single point x in U with $\mu_F(x) = 1$ is called a *singleton.* In a singleton output space, fuzzy set membership functions are represented as single vertical points. Figure 4.2 illustrates how a variable SPEED can be composed on individual single points.

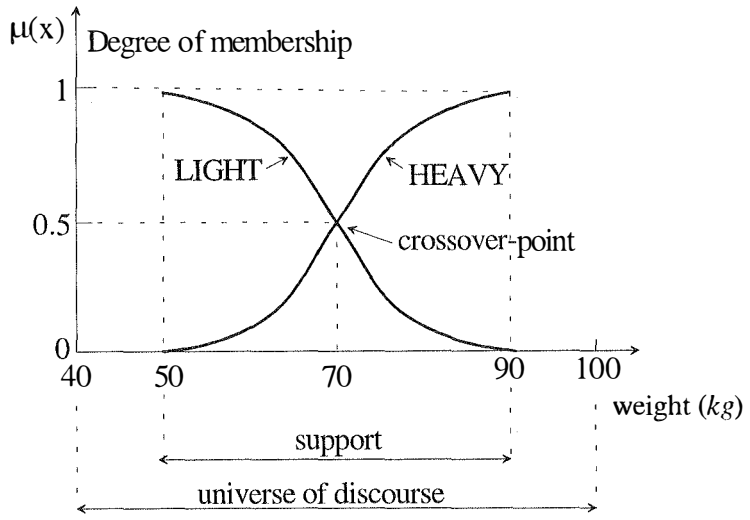

Figure 4.1. Fuzzy variable "weight".

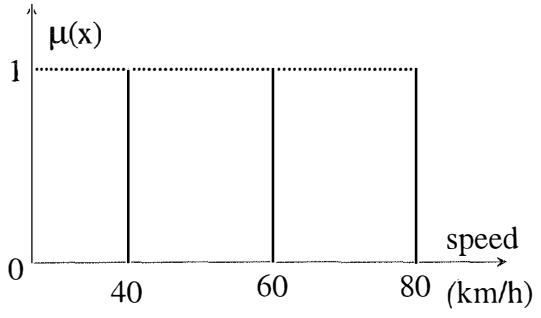

Figure 4.2. Singleton representation.

A technical concept closely related to the support set is the alpha-level set or the $\alpha-cut$. An alpha level is a threshold restriction on the domain based on the membership grade of each domain value. An $\alpha-$cut contains all the domain values that are part of the support at a minimum membership grade of α. There are two types of $\alpha-$cuts: *weak* and *strong*. The strong $\alpha-$cut is defined as $\mu_F(x) \geq 0.5$, and the weak $\alpha-$cut is indicated by $\mu_F(x) > 0.5$. Thus, the strong $0-$cut defines the support of a fuzzy set. Figure 4.3 depicts an $0.2-$cut on the domain of fuzzy set HEAVY.

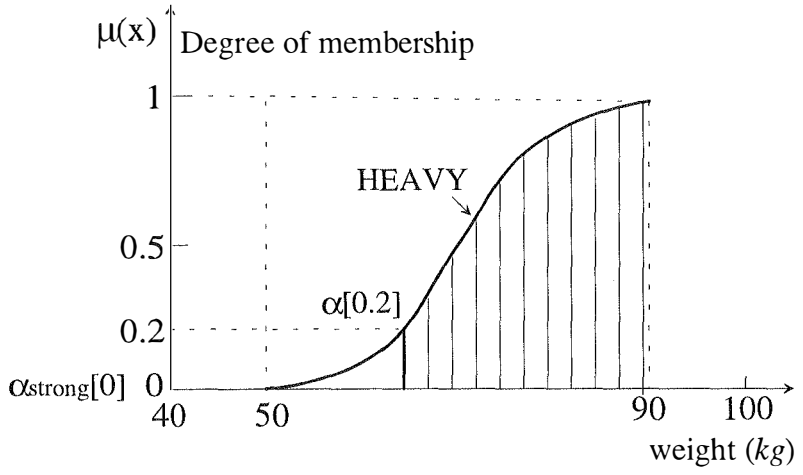

Figure 4.3. An $\alpha-$cut for the fuzzy set HEAVY.

4.2.2 Set theoretic operations (Lee [110])

Let fuzzy sets A and B in U be described by their membership functions $\mu_A(x)$ and $\mu_B(x)$. The set theoretic operations of union, intersection, and complement for fuzzy sets are defined as following:

Union: The membership function of the union $A \cup B$ is pointwise defined for all $x \in U$ by

$$\mu_{A \cup B}(x) = \max\{\mu_A(x), \mu_B(x)\}. \tag{4.1}$$

Intersection: The membership function of the intersection $A \cap B$ is pointwise defined for all $x \in U$ by

$$\mu_{A \cap B}(x) = \min\{\mu_A(x), \mu_B(x)\}. \tag{4.2}$$

Complement: The membership function of the complement of A is pointwise defined for all $x \in U$ by

$$\mu_{\bar{A}} = 1 - \mu_A(x). \tag{4.3}$$

In order to model fuzzy union and fuzzy intersection other operators can be chosen. In his pioneering first paper [12], Zadeh defined maximum (4.1) and algebraic sum

$$\mu_{A \cup B}(x) = \mu_A(x) + \mu_B(x) - \mu_A(x)\mu_B(x) \tag{4.4}$$

for fuzzy union, and minimum (4.2) and algebraic product

$$\mu_{A \cap B}(x) = \mu_A(x)\mu_B(x) \tag{4.5}$$

for fuzzy intersection. Later, based on axiomatic definitions (see, e.g. Yager & Filev [115]), general triangular conorm ($t-$conorm or $s-$norm, denoted $\oplus$) operators were introduced for fuzzy union, and general triangular norm ($t-$norm, denoted $*$) operators for fuzzy intersection. Some other examples of $t-$conorms are *bounded sum:*

$$x \oplus y = \min(1, x + y), \tag{4.6}$$

and *drastic sum*:

$$x \oplus y = \begin{cases} x & \text{if } y = 0, \\ y & \text{if } x = 0, \\ 1 & \text{if } x, y > 0. \end{cases} \tag{4.7}$$

Some other examples of $t-$norms are *bounded product:*

$$x * y = \max(0, x + y - 1), \tag{4.8}$$

and *drastic product*:

$$x * y = \begin{cases} x & \text{if } y = 1, \\ y & \text{if } x = 1, \\ 0 & \text{if } x, y < 1. \end{cases} \tag{4.9}$$

Although there are different operators, most engineering applications of fuzzy sets use the minimum or algebraic product $t-$norm for fuzzy intersection, the max $t-$conorm for fuzzy union and (4.3) for the membership function of fuzzy complement (Mendel [114]).

Hint: Unlike crisp sets, the *Law of Contradiction*, $A \cup \overline{A} = U$, and the *Law of Excluded Middle*, $A \cap \overline{A} = \varnothing$, do not hold in fuzzy set theory, i.e. for fuzzy sets: $A \cup \overline{A} \neq U$ and $A \cap \overline{A} \neq \varnothing$.

Cartesian product: If $A_1,...,A_n$ are fuzzy sets in $U_1,...,U_n$, respectively, the Cartesian product of $A_1,...,A_n$ is a fuzzy set in the product space $U_1 \times ... \times U_n$ with the membership function

$$\mu_{A_1 \times ... \times A_n}(x_1,...,x_n) = \min\left\{\mu_{A_1}(x_1),...,\mu_{A_n}(x_n)\right\} \tag{4.10a}$$

or

$$\mu_{A_1 \times ... \times A_n}(x_1,...,x_n) = \mu_{A_1}(x_1)...\mu_{A_n}(x_n). \tag{4.10a}$$

Fuzzy relations: Fuzzy relations represent a degree of presence or absence of association, interaction, or interconnection between the elements of two or more fuzzy sets. An $n-$ary fuzzy relation is a fuzzy set in $U_1 \times ... \times U_n$ and is expressed as

$$R_{U_1 \times ... \times U_n} = \left\{((x_1,...,x_n),\ \mu_R(x_1,...,x_n)) |\ (x_1,...,x_n) \in U_1 \times ... \times U_n\right\}. \tag{4.11}$$

Compositions: Because fuzzy relations are fuzzy sets in the product space, set theoretic and algebraic operations can be defined using operators for fuzzy union, intersection and complement. Let R and S be fuzzy relations in $U \times V$. The intersection and union of R and S, which are *compositions* of the two relations, are defined as

$$\mu_{R \cap S}(x,y) = \mu_R(x,y) * \mu_S(x,y) \tag{4.12a}$$

and

$$\mu_{R \cup S}(x,y) = \mu_R(x,y) \oplus \mu_S(x,y), \tag{4.12b}$$

respectively, where $*$ is any $t-$norm, and $\oplus$ is any $t-$conorm.

Next, consider the composition of fuzzy relations from different products spaces that share a common set. If R and S are two fuzzy relations in $U \times V$ and $V \times W$,

respectively, the *sup-star composition* of $R(U \times V)$ and $S(V \times W)$ is a fuzzy relation denoted by $R \circ S(U \times W)$ and is defined by

$$R \circ S = \left\{ (x,z),\ \sup_{y \in V} [\mu_R(x,y) * \mu_S(y,z)],\ x \in U, y \in V, z \in W \right\}, \tag{4.13}$$

where $*$ could be any operator in the class of $t-$norm (the sup-min and sup-product is most commonly used). When U, V and W are discrete universe of discourse, the sup operation is the maximum. Figure 4.4 depicts a block diagram for the sup-star composition.

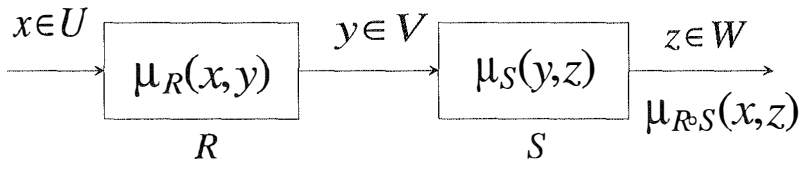

Figure 4.4. Block diagram interpretation for the sup-star composition.

Suppose fuzzy relation R is just a fuzzy set, then $\mu_R(x,y)$ becomes $\mu_R(x)$ and $V = U$, consequently, $\sup_{y \in V}[\mu_R(x,y) * \mu_S(y,z)] = \sup_{x \in U}[\mu_R(x) * \mu_S(x,z)]$. Thus, when R is just a fuzzy set, the membership function for $R \circ S$ is

$$\mu_{R \circ S}(z) = \sup_{x \in U}[\mu_R(x) * \mu_S(x,z)]. \tag{4.14}$$

Figure 4.5 represents the block diagram interpretation for the sup-star composition when the first relation is just a fuzzy set.

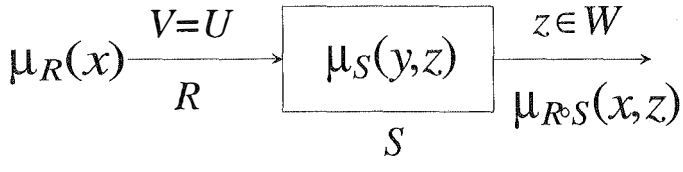

Figure 4.5. Sup-star composition when $V = U$.

4.2.3 Linguistic representation

A. Linguistic variables

The use of fuzzy sets provides a basis for a systematic way of for the management of vague and imprecise concepts. According to Zadeh [116], in retreating from precision in the face of overpowering complexity, it is natural to explore the use of what might be called *linguistic variable*, i.e., variables whose values are not numbers but words or sentences in a natural or artificial language. Fuzzy sets can be employed to represent linguistic variable. Consider a real line as a continuous universe of discourse U. A *fuzzy number* F in U is a fuzzy set which is normal and convex, i.e.,

$$\max_{x \in U} \mu_F(x) = 1, \tag{4.15a}$$

$$\mu_F(\lambda x_1 + (1-\lambda)x_2) \geq \min(\mu_F(x_1), \mu_F(x_2)),\ x_1, x_2 \in U,\ \lambda \in [0,1]. \tag{4.15b}$$

A linguistic variable can be regarded as a variable whose value is a fuzzy number or whose values are defined in linguistic terms or *labels*. A linguistic variable is characterised by its name u; the term set of u, i.e., the set of terms $T(u)$ of linguistic values of u with each value being a fuzzy number defined on U; a syntactic rule for generating the names of values of u; and a semantic rule for associating with each value its meaning.

As an example, let SPEED (u) of a car be a linguistic variable. It can be decomposed into the following set of terms $T(u)$={slow, medium, fast}, where each term is characterised by a fuzzy set in the universe of discourse U= [0 km/h, 100 km/h]. "Slow" speed might be interpreted as "a speed below about 40 km/h", "medium" as "a speed close to 60 km/h", and "fast" as "a speed above about 80 km/h". These terms can be characterised as fuzzy sets whose membership functions are shown in Figure 4.6. A vertical line from any measured value of speed intersects at most two membership functions. So, for example, a speed of 45 km/h resides in the fuzzy sets slow and medium to a similarity degree of 0.75 and 0.25, respectively.

B. Hedges: linguistic modifiers

A *linguistic hedge* or modifier is an operation that modifies the meaning of a fuzzy set or a term. Hedges can be viewed as operators that act upon a fuzzy's set membership

function to modify it. Hedges play the same role in fuzzy modelling system as adverbs and adjectives do in a natural language. Accordingly, the number and order of hedges are significant, e.g. *not very large* and *very not large* relates to two different interpretations. A representative collection of commonly-used hedges with their effects is contained in Table 4.1 (Cox [117]).

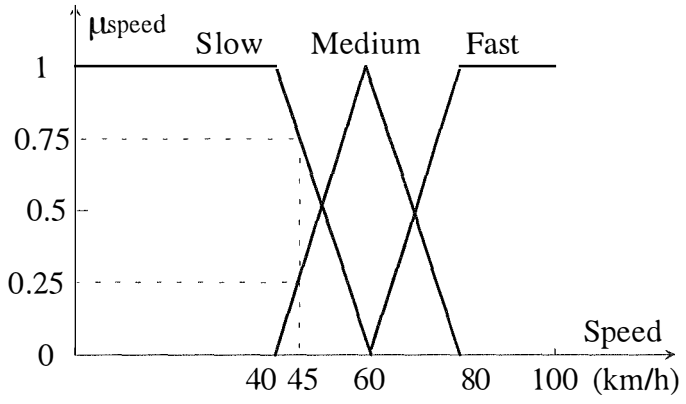

Figure 4.6. Linguistic variable "speed" with three labels "slow", "medium", and "fast".

Hedge	Meaning
about, around, near, roughly	Approximate a scalar
above, more than	Restrict a fuzzy region
almost, definitely, positively	Contrast intensification
below, less than	Restrict a fuzzy region
vicinity of	Approximate broadly
generally, usually, normally	Contrast diffusion
neighbouring, close to	Approximate narrowly
not, not-so, not really	Negation or complement
quite, rather, somewhat, more-or-less	Dilute a fuzzy region
very, extremely	Intensify a fuzzy region

Table 4.1. Fuzzy linguistic hedge and their approximate meanings.

Power hedges (Zimmermann, [118]): The power hedges operate on grades of membership and are represented by the general operator:

$$\mu_{pow(U)}(x) \equiv [\mu_U(x)]^p, \tag{4.16}$$

where p is a parameter specific to a certain linguistic modifier. The exponent p used in the hedge membership function is quite arbitrary, it can be changed depending on our interpretation of the hedge. If $p = 1$, fuzzy set is not modified. Two cases are distinguished:

1) *Concentration*: $p > 1$, fuzzy set is concentrated. Because membership functions are assumed to be normalised, the operation of *concentration* leads to a membership function that lies within the membership function of the original fuzzy set; both have the same support, and the same membership values where the value of the original membership function equals unity or zero.

The modifier *very* corresponds to $p = 2$. For example, if *slow speed* is a fuzzy set with membership function $\mu_S(x)$, then *very slow speed* and *very very slow speed* are fuzzy sets with membership function $[\mu_S(x)]^2$, $[\mu_S(x)]^4$, respectively. An *artificial hedge* providing milder degree of concentration is the *plus*, whose membership function is $\mu_{plus(U)}(x) \equiv [\mu_U(x)]^{1.25}$.

2) *Dilation*: $p < 1$, fuzzy set is dilated. The operation of *dilation* leads to a membership function that lies outside of the membership function of the original fuzzy set; both have the same support, and the same membership values where the value of the original membership function equals unity or zero.

The modifier *more or less* corresponds to $p = 1/2$. For example, *more or less slow speed* is a fuzzy set with membership function $[\mu_S(x)]^{1/2}$. Another hedge quite useful is the *minus*, whose membership function is $\mu_{minus(U)}(x) \equiv [\mu_U(x)]^{0.75}$.

4.3 Fuzzy logic and fuzzy reasoning

Fuzzy logic is a logical system that is much closer in spirit to human thinking and natural language than traditional logic systems. As a calculus of compatibility, fuzzy logic is quite different from probability which is based on frequency distributions in a random population. Fuzzy logic describes the characteristic properties of continuously varying values by associating partitions of these values with a semantic label (Cox [117]). Fuzziness is different from probability. The laws of contradiction and

excluded middle are broken in fuzzy logic but are not broken in probability. Conditional probability, which must be defined in probability theory, can be derived from first principles using fuzzy logic (Kosko [119]). Much of the description power of fuzzy logic comes from the fact that these semantic partitions can overlap (see Figure 4.6) corresponding to the transition from one term to the next.

Fuzzy set theory serves as the basis for fuzzy logic. Fuzzy set theory starts with some basic concepts coming from crisp set theory, fuzzy logic also begins by borrowing some crisp logic notions. In crisp logic, a *proposition* is an ordinary statement involving terms already defined, and must be meaningful to call it "true" or "false". A *tautology* is a proposition formed by combining other propositions p, q, r,... , which is true regardless of the truth or falsehood of p, q, r,... .

Let us start with the basic primitives of fuzzy logic: fuzzy propositions. A fuzzy proposition represents a statement like "speed (u) is SLOW", where SLOW is a linguistic label, defined by a fuzzy set on the universe of discourse of speed. Fuzzy propositions connect variables with linguistic labels defined for those variables. As in classical logic, fuzzy propositions can be combined by using logical connectives *and* and *or*, which are implemented by $t-$norms and $t-$conorms, respectively.

Fuzzy logic provides a means of modelling human decision making within the conceptual framework of fuzzy logic and approximate reasoning (or fuzzy reasoning). In fact, reasoning with fuzzy logic is based on fuzzy rules which are expressed as logical implications, i.e. in the forms of IF-THEN statements. In fuzzy logic, the definition of a fuzzy implication may be expressed as a fuzzy implication function. Various implication functions can be classified into three main categories: *fuzzy conjunction*, *fuzzy disjunction*, and *fuzzy implication*. A fuzzy rule "IF u is A, THEN v is B", is represented by a fuzzy implication and is denoted by $A \rightarrow B$, where A and B are fuzzy sets in the universes U and V with membership functions μ_A and μ_B, respectively. Membership function of the fuzzy implication, denoted by $\mu_{A\rightarrow B}(x,y)$, measures the degree of truth of the implication between $x \in U$ and $y \in V$.

Fuzzy conjunction: The fuzzy conjunction is defined for all $x \in U$ and $y \in V$ by

$$A \rightarrow B = A*B, \tag{4.17}$$

where $*$ is an operator representing a $t-$norm.

Fuzzy disjunction: The fuzzy disjunction is defined for all $x \in U$ and $y \in V$ by

$$A \rightarrow B = A \oplus B, \tag{4.18}$$

where $\oplus$ is an operator representing a $t-$conorm.

Fuzzy implication: An extension is made by determining the fuzzy versions of some tautologies of $p \rightarrow q$ in crisp logic, e.g. $\sim p \vee q$, $\sim p \vee pq$, and $(\sim p \wedge \sim q) \vee q$. Thus, the fuzzy implication is associated with the corresponding families of fuzzy implication functions:

(i) Material implication:

$$A \rightarrow B = \text{not } A \oplus B \tag{4.19}$$

(ii) Propositional calculus:

$$A \rightarrow B = \text{not } A \oplus (A * B) \tag{4.20}$$

(iii) Extended propositional calculus:

$$A \rightarrow B = (\text{not } A * \text{not } B) \oplus B \tag{4.21}$$

In traditional propositional logic there are two very important inference rules, *Modus Ponens* (MP) and *Modus Tollens* (MT). Modus ponens is associated with the implication $[A \rightarrow B]$:

Premises	Consequence
Premise 1: x is A	y is B
Premise 2: IF x is A THEN y is B	

In terms of propositions p and q, modus ponens is expressed as $(p \wedge (p \rightarrow q)) \rightarrow q$. Modus tollens is associated with the implication [not $B \rightarrow$ not A]:

Premises	Consequence
Premise 1: y is not B	x is not A
Premise 2: IF x is A THEN y is B	

In terms of propositions p and q, modus tollens is expressed as $(\sim q \wedge (p \rightarrow q)) \rightarrow \sim p$. In fuzzy logic, modus ponens is extended to *Generalised Modus Ponens* (GMP):

Premises	Consequence
Premise 1: x is A^*	y is B^*
Premise 2: IF x is A THEN y is B	

and modus tollens to *Generalised Modus Tollens* (GMT):

Premises	Consequence
Premise 1: y is B^*	x is A^*
Premise 2: IF x is A THEN y is B	

where A, A^*, B, B^* are fuzzy sets introduced via linguistic variables x, y (Dubois and Prade [120]). Two more families of fuzzy implication function obtained from GMP and GMT are:

(iv) Generalisation of modus ponens:

$$A \rightarrow B = \sup\{c \in [0, 1], A * c \leq B\} \tag{4.22}$$

(v) Generalisation of modus tollens:

$$A \rightarrow B = \inf\{t \in [0, 1], B \oplus t \leq A\} \tag{4.23}$$

Based on the definitions (4.17-4.23), many membership functions for fuzzy implication may be generated by employing appropriate triangular norms and conorms. For example, $\mu_{A \rightarrow B}(x, y)$ can be found from (4.19) as

$$\mu_{A \rightarrow B}(x, y) = \max[1 - \mu_A(x), \mu_B(y)], \tag{4.24a}$$

$$\mu_{A \rightarrow B}(x, y) = 1 - \min[\mu_A(x), 1 - \mu_B(y)], \tag{4.24b}$$

or

$$\mu_{A \rightarrow B}(x, y) = 1 - \mu_A(x)(1 - \mu_B(y)), \tag{4.24c}$$

with appropriate operators for the $t-$norm $*$ and $t-$conorm $\oplus$. From the fuzzy conjunction (4.17), membership functions for *minimum implication*, proposed by Mamdani [109]:

$$\mu_{A\to B}(x,y) \equiv \min[\mu_A(x),\mu_B(y)], \tag{4.25}$$

and *product implication*, introduced by Larsen [121]:

$$\mu_{A\to B}(x,y) \equiv \mu_A(x)\mu_B(y) \tag{4.26}$$

can be obtained using minimum and algebraic product, respectively. It can be shown that membership functions (4.24a-c) agree with the accepted propositional logic definition of implication, demonstrated in Table 4.2, while neither Mamdani membership function (4.25) nor Larsen one (4.26) does. As shown in Table 4.2, minimum and product inferences preserve *cause and effect*, i.e. these implications are fired only when the antecedent and the consequent are both true.

$\mu_p(x)$	$\mu_q(x)$	$\mu_{p\to q}(x,y)$	$\min[\mu_A(x),\mu_B(y)]$	$\mu_A(x)\mu_B(y)$
1	1	1	1	1
1	0	1	0	0
0	1	0	0	0
0	0	1	0	0

Table 4.2. Implication with propositional logic, and min and product inference.

This is why minimum and product inferences are the most widely used inferences in engineering applications of fuzzy logic, and referred to as *engineering implications* (Mendel [114]).

A comprehensive comparison between the available fuzzy implication rules is given in Lee [110], based on some intuitive criteria for choosing a fuzzy implication that is as close as possible to the input truth value function value. Although the minimum operation rule (4.25) and the product operation rule (4.26) of fuzzy implication do not have a well-defined logical structure, it is shown [110] that they are well suited for approximate reasoning, especially for the generalised modus ponens. The GMP,

reducing to modus ponens when $A^* = A$, $B^* = B$, is closely related to the forward data-driven inference, particularly useful in control systems. The GMT, reducing to modus tollens when $A^* = \text{not } A$, $B^* = \text{not } B$, is closely related to the backward goal-driven inference, commonly used in expert systems.

Figure 4.7 illustratively interprets that GMP is a fuzzy composition where the first fuzzy relation is merely a fuzzy set, A^* (see Figure 4.5). Consequently, $\mu_{B^*}(y)$ can be obtained from the sup-star composition (4.14):

$$\mu_{B^*}(y) = \sup_{x \in A^*} [\mu_{A^*}(x) * \mu_{A \to B}(x, y)], \tag{4.26}$$

where max-min or max-product formula can be stated for modus ponens. Note that in crisp logic, a rule is fired only if the first premise is exactly the same as the antecedent of the rule, and the result of such rule-firing is the rule's actual consequent. On the other hand, a fuzzy rule is fired so long as there is a non zero degree of similarity between the first premise and the antecedent of the rule, and, the result of such rule-firing is a consequent that has a non zero degree of similarity to the rule's consequent.

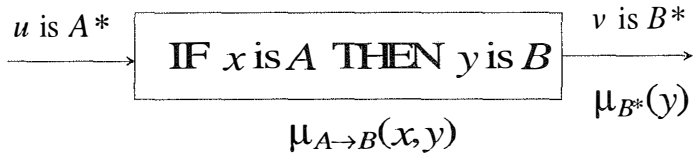

Figure 4.7. Sup-star composition when $V = U$.

4.4 Fuzzy logic control

During the past several years, fuzzy logic control, first appeared in Chang and Zadeh's 1972 paper [13], has emerged as one of the most active and impressive areas for research in the applications of fuzzy set theory. Using fuzzy logic as an effective means of capturing approximate, inexact nature of the real world, a fuzzy logic controller provides an algorithm which can convert the linguistic control strategy based on expert knowledge into an automatic control strategy. In particular, the methodology of fuzzy logic control has been proven through recent successful applications (Schwartz *et al.* [14]) to be superior to conventional control when the processes are too complex, or when the available sources of information are

interpreted imprecisely, or uncertainly. In this sense, fuzzy logic control may be viewed as a rapprochement between conventional control and human-like decision making techniques for improving robustness of control systems. This section gives a brief summary of the prolific literature on fuzzy logic control and illustrates the design procedure of a fuzzy logic controller for an overhead crane model.

4.4.1 Fuzzy logic controllers

Fuzzy inference is the actual process of mapping from a given input to an output using fuzzy logic. A fuzzy logic controller (FLC) is a fuzzy inference system which maps an input data vector into a scalar control output. Figure 4.8 depicts a fuzzy control system, where the elements of the fuzzy logic controller are rules, fuzzifier, inference engine, and defuzzifier.

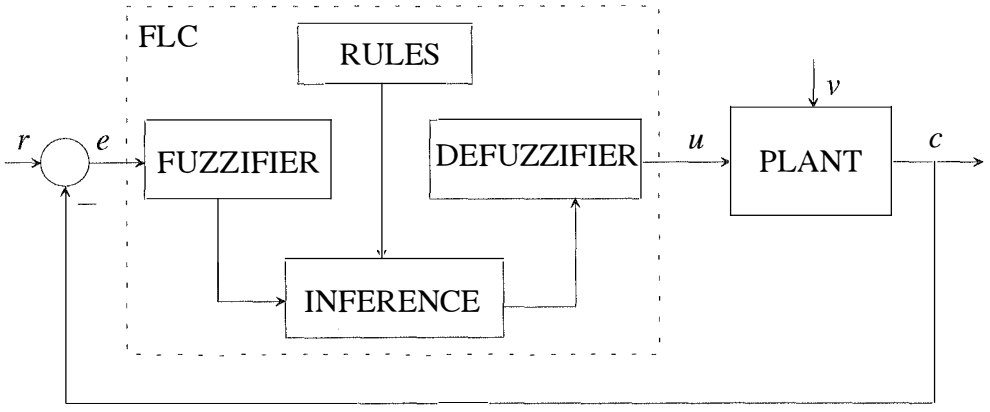

Figure 4.8. Block diagram of a fuzzy logic control system.

Once the fuzzy rules have been chosen, an FLC can be considered as a nonlinear mapping from inputs (error e, change of error Δe) to outputs (control signal u). This mapping can be expressed quantitatively as $u = f(e, \Delta e)$. The design of an FLC is how to obtain explicitly this relation so that the control requirements are satisfied.

Rules may be provided by experts or can be extracted from numerical data. In either cases, engineering heuristic rules are expressed as a collection of IF-THEN statements. Each rule consists of linguistic variables, linguistic terms, logical connections, and implications. Each linguistic term is a fuzzy set associated with its fuzzy membership function.

The *fuzzifier* maps crisp number into fuzzy sets of a linguistic variable. The *inference engine* of an FLC maps fuzzy sets into fuzzy sets in the way fuzzy rules are combined. There are many different fuzzy logic inference procedures but only a few of them are commonly used in engineering applications of fuzzy logic. The *defuzzifier* maps output sets into crisp numbers corresponding to the control action u.

A fuzzy logic controller can be viewed as a system employing a fuzzy inference process to produce crisp control output from fuzzy rules for given input values. The inference process is the internal mechanism involving three steps: fuzzification, rule evaluation, and defuzzification, as shown in Figure 4.9.

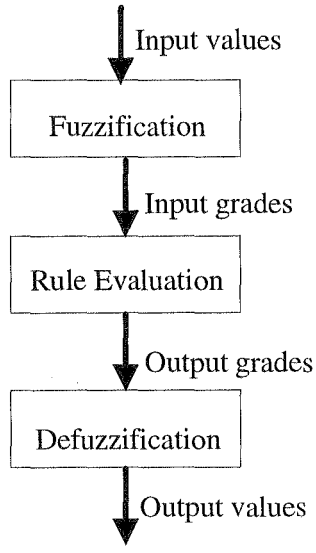

Figure 4.9. Inference process.

A. Fuzzification

In general, fuzzification is the process of translating real world values of an input variable (input values) to the grades of its input labels (input grades). Fuzzification involves measuring the values of input variables, performing a scale mapping to transfer the range of values of input variables into corresponding universes of discourse, and converting input data into suitable linguistic values by means of labels (terms of a linguistic variable) of fuzzy sets. The input variables of an FLC, which can be a voltage, current, speed, or position in motion control systems, are usually the control error, e, or its change, Δe. Symbolically, the process of transforming crisp data into fuzzy sets can be represented by

$$x = fuzzifier(x_0), \tag{4.27}$$

where x_0 is a crisp input value (e or Δe), x is a fuzzy set, and *fuzzifier* is a fuzzification operator. In order to develop useful rules, appropriate membership functions associated with each label should be well chosen. Therefore, it is necessary to have a good intuitive feel for the nature of the variables. The defining membership functions for all variables would be based on designer's intuitive assumptions, just as the rules themselves are. The fuzzification process also provides necessary conditions for defining linguistic control rules and fuzzy data manipulation in an FLC, including the discretisation/normalisation of the universes of discourse, fuzzy partition of the input and output spaces, and choice of the appropriate membership function of a primary fuzzy set.

Discretisation of a universe of discourse is the process of quantising it into a certain number of segments (quantisation levels) with corresponding labels and thus, forming a discrete universe. A fuzzy set is then defined by assigning grade of membership values to each label. A scale mapping is needed to transform measured variables into values in the discretised universe. The choice of quantisation levels determines how fine a control can be obtained. Normalisation of a universe requires discretising it into a finite number of segments. Each segment is mapped into a suitable segment of the normalised universe which normally is the closed interval [0, 1] or [−1, 1].

In general, a linguistic variable is associated with a term set. Each term in the term set is defined on the same universe of discourse. A fuzzy partition, then, determines the number of terms in a term set. This number affects the granularity of the fuzzy control. Figure 4.10 shows a fuzzy partition in the normalised universe [−1, 1] with seven terms: NB, NM, NS, ZE, PS, PM, and PB, which mean negative big, negative medium, negative small, zero, positive small, positive medium, and positive big, respectively.

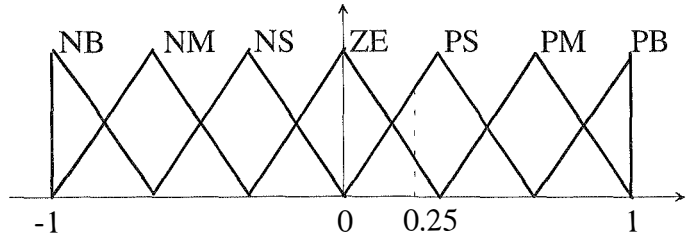

Figure 4.10. A fuzzy partition representation.

A membership function (MF), which defines how each point in the input space of a label is mapped to a degree of membership between 0 and 1, can principally take any nonlinear or piece-wise linear form. The latter is either a triangular or trapezoidal functions as shown, for example, in Figures 4.6 and 4.10. They are the simplest and most commonly-used in engineering applications. The vertex of a triangular fuzzy label usually corresponds to the mean value of a data set, while the base is twice the standard deviation of the data set.

Crisp value can be converted into a fuzzy singleton (see Figure 4.2) within a certain universe of discourse. This kind of membership function is widely used in fuzzy control applications because it is natural and easy to implement. The other commonly-used membership functions, with universes of discourse scaled to [0, 1], are described below. The Gaussian MF, determined by

$$\mu(x,\sigma,c) = \exp\left(-\frac{(x-c)^2}{2\sigma^2}\right), \tag{4.28}$$

where σ and c are two positive parameters, has the forms of Figure 4.11(a). A combination of two Gaussian membership functions gives the two-sided form of Figure 4.11(b).

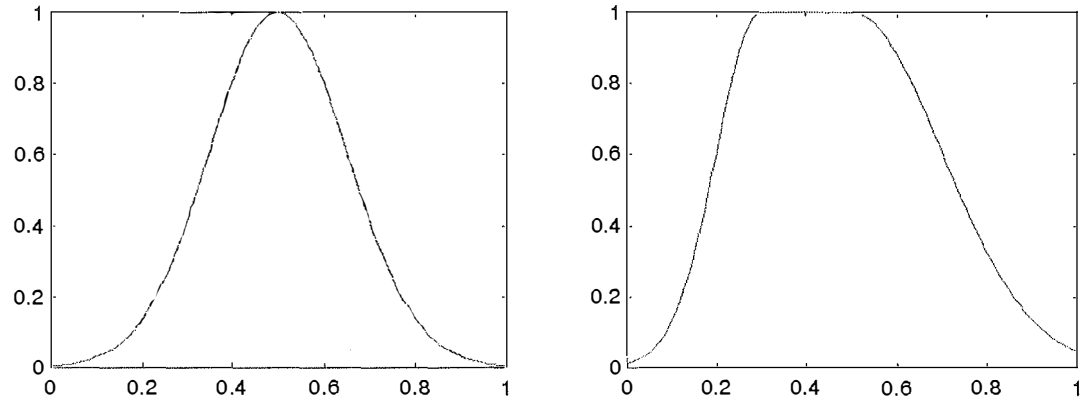

Figure 4.11. Gaussian membership functions:
(a) $\sigma = 0.15$, $c = 0.5$, and (b) $\sigma_1 = 0.1$, $c_1 = 0.3$, $\sigma_2 = 0.2$, $c_2 = 0.5$.

The generalised bell-shape MF with the form of Figure 4.12 is described by

$$\mu(x,a,b,c) = \frac{1}{1+\left|\frac{x-c}{a}\right|^{2b}}, \tag{4.29}$$

where $a > 0$, $b > 0$, and $c > 0$. Both Gaussian and bell-shape membership functions have the advantage of being smooth and nonzero at all points, however they cannot specify asymmetry. Open (left or right) forms can be synthetised using exponential membership functions. Figure 4.13 shows an open right MF

$$\mu(x,\sigma) = 1 - \exp(-\frac{x}{\sigma}), \tag{4.30}$$

where $\sigma > 0$.

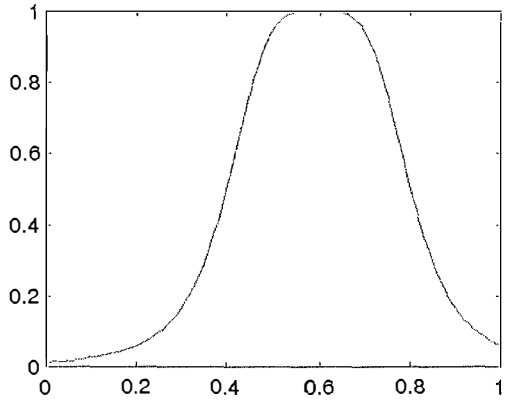

Fig. 4.12. Bell MF, $a = 0.2$, $b = 2$, $c = 0.6$.

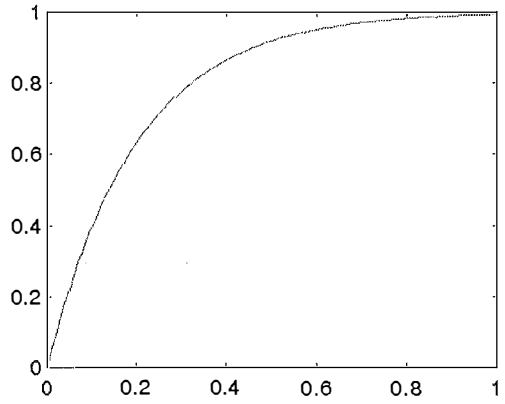

Fig. 4.13. Exponential MF, $\sigma = 0.2$.

The sigmoid can also be used to specify asymmetric membership functions, which are important in certain applications. Figure 4.14(a) plots the form of an open right sigmoidal MF defined by

$$\mu(x,a,c) = \frac{2}{1+\exp(-a(x-c))}, \tag{4.30}$$

where $a > 0$ and $c > 0$. An asymmetric and closed (i.e. not open to the left or right) M can be synthetised by the difference of two sigmoidal functions as represented in

Figure 4.14(b). The smoothness of the curves in Figures 4.11 to 4.14 accounts for the use of the corresponding membership functions in fuzzy tuning, which will be addressed in the next chapter.

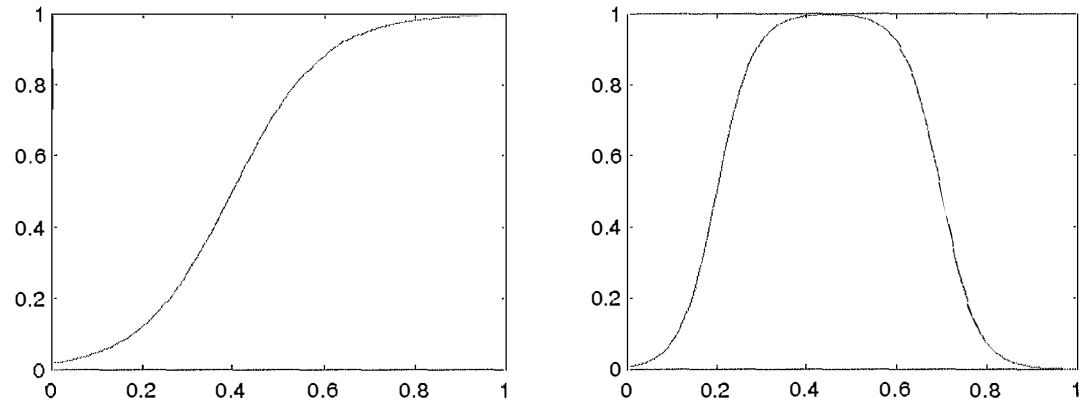

(a) (b)

Figure 4.14. Sigmoidal MFs: (a) sigmoid ($a = 10,\ c = 0.4$), and (b) difference of two sigmoids ($a_1 = 25,\ c_1 = 0.2,\ a_2 = 25,\ c_2 = 0.7$).

For fuzzy control applications, triangular and trapezoidal functions seem to perform as well in practice as those based on some other forms of membership functions, and, in many cases, are simpler to implement. It would be an interesting psychological problem to investigate whether or not triangular membership functions are as accurate as some other forms in expressing intuitive concepts of fuzzy numbers (Schwartz *et al.* [14]).

B. Rule evaluation

Rule evaluation is the process of obtaining the grades of output labels (output grades) from input grades. The rule evaluation process is mainly important in the design of an FLC. It involves a fuzzy rule base and an inference unit. The rule base characterises the control goals and control strategy of the domain experts by means of a set of linguistic control rules. As the kernel of an FLC, the inference unit is capable of simulating human decision making based on fuzzy concepts and of inferring fuzzy control actions employing fuzzy implication and the rules of inference in fuzzy logic.

Based on expert knowledge and fuzzy reasoning, the rule base of an FLC can be formatted in *fuzzy conditional statements* as follows:

$$R_i: \text{ IF (set of conditions) THEN (set of consequences), } (i = 1,2,..,n) \quad (4.31)$$

where the antecedents and the consequents of these rules are associated with linguistic values (labels). A *fuzzy control rule* is a fuzzy conditional statement in which the antecedent is a condition determined in an application domain and the consequent is a control action for the plant. A rule base is normally formed by a set of fuzzy control rules combined by using the sentence connectives *and* and *also*. In most FLCs, the sentence connective *and* is usually implemented as a fuzzy conjunction in a Cartesian product space, in which the underlying variables take values in different universes of discourse. When the ordering of the fuzzy rules are immaterial, the sentence connective *also* is used with the associated properties of commutativity and associativity. From a practical point of view, the union operator is normally used for the connective *also* for constructing fuzzy models (Lee [110]). The overall system behaviour can then be characterised by a single fuzzy relation R which is the combination of the fuzzy relations R_i. Symbolically,

$$R = also(R_1, R_2, \ldots, R_i, \ldots, R_n), \quad (4.32)$$

where *also* represents a sentence connective.

In general, there are four modes of deriving fuzzy control rules: from expert experience and control engineering knowledge, from human operator's control actions, from the fuzzy model of a process, and from learning. A fuzzy control rule normally has the form of a fuzzy conditional statement relating the state variables in the antecedent and the control action in the consequent. Most FLCs employ engineering knowledge and experience which are expressed in the language of fuzzy IF-THEN rules based on an introspective verbalisation of human expertise or an interrogation of experienced experts or operators. Many industrial control systems can be empirically controlled by skilled human operators without any quantitative models in mind. As pointed out by Sugeno [123] in order to automate such processes, it is expedient to express the operator's control rules as fuzzy IF-THEN rules using linguistic variables. Fuzzy control rules can also be generated based on the linguistic description of the dynamic characteristics of the plant known as fuzzy model. Although this approach is somewhat more complicated, it yields better performance

and reliability, and provides a more attractable structure for dealing theoretical with the FLC (see, e.g., Cao *et al.* [124]). Focusing on the ability to create fuzzy control rules and to modify them based on experience (learning), Procyk & Mamdani [125] described the first self-organising controller with a hierarchical structure of two rule bases: the general rule base and the "meta-rules". The latter exhibit human-like learning ability to create and modify the general rule base according to the desired overall performance of the system. Self-organising control (Shao [126]) or fuzzy learning systems with model reference (Kwong *et al.* [127]) and neuro-fuzzy approach (Jang & Sun [128]) have become increasingly interesting subjects for fuzzy control studies.

In a typical fuzzy system, the FLC rule base describes the relationship between the change of the control $\Delta u(k) = u(k) - u(k-1)$ on one hand, and the error $e(k)$ and its change $\Delta e(k) = e(k) - e(k-1)$ on the other hand, where k is discretised time. The actual controller output $u(k)$, first proposed by Mamdani & Assilian [129],

$$u(k) = u(k-1) + \Delta u(k), \tag{4.33}$$

is called the *Mamdani-type* FLC. The similarity between the Mamdani-type FLC and the conventional propotional-integral (PI) controller is that the change of the control $\Delta u(k)$ is calculated depending on the error $e(k)$ and its change $\Delta e(k)$:

$$\Delta u(k) = f(e(k) + \Delta e(k)) = K_P \Delta e(k) + K_I e(k), \tag{4.44}$$

where K_P and K_I are the parameters of the proportional-integral (PI) controller. If the output variable is not the change of the control action $\Delta u(k)$, but the control value $u(k)$ itself, we obtain a control law

$$u(k) = f(e(k),\ \Delta e(k)), \tag{4.45}$$

which is similar to the known proportional-derivative (PD) control law. An example of a PD-like FLC rule base is presented as follows:

IF the error $e(k)$ is *Positive* AND the change of error $\Delta e(k)$ is *Positive* THEN the control $u(k)$ is *Positive*,

IF the error $e(k)$ is *Positive* AND the change of error $\Delta e(k)$ is *Approximately zero* THEN the control $u(k)$ is *Positive*,

IF the error $e(k)$ is *Positive* AND the change of error $\Delta e(k)$ is *Negative* THEN the control $u(k)$ is *Approximately zero*,

IF the error $e(k)$ is *Approximately zero* AND the change of error $\Delta e(k)$ is *Approximately zero* THEN the control $u(k)$ is *Approximately zero*,

IF the error $e(k)$ is *Approximately zero* AND the change of error $\Delta e(k)$ is *Positive* THEN the control $u(k)$ is *Positive*,

IF the error $e(k)$ is *Approximately zero* AND the change of error $\Delta e(k)$ is *Negative* THEN the control $u(k)$ is *Negative.*

IF the error $e(k)$ is *Negative* AND the change of error $\Delta e(k)$ is *Positive* THEN the control $u(k)$ is *Approximately zero*,

IF the error $e(k)$ is *Negative* AND the change of error $\Delta e(k)$ is *Approximately zero* THEN the control $u(k)$ is *Negative*,

IF the error $e(k)$ is *Negative* AND the change of error $\Delta e(k)$ is *Negative* THEN the control $u(k)$ is *Negative*,

The fuzzy control rules may be formulated into a *look-up table* as shown in Table 4.3, where the linguistic labels N, Z, and P mean negative, positive, and approximately zero. The look-up table can be a significant tool for simplification of the internal representation of an FLC.

$e(k)$ / $\Delta e(k)$	N	Z	P
N	N	N	Z
Z	N	Z	P
P	Z	P	P

Table 4.3. Fuzzy rules for the control action $u(k)$ of a PD-like FLC.

The PD-like FLC can be extended by including in (4.45) the sum of the errors $\sum e(k) = \sum_{l=0}^{k-1} e(l)$ with the fuzzy mapping :

$$u(k) = f(e(k), \sum e(k), \Delta e(k)), \tag{4.46}$$

which is similar to the proportional-integral-derivative (PID) control algorithm. The difference between conventional controllers and FLCs is that the fuzzy control relationship is nonlinear, in general. Naturally, it is rather unrealistic to expect that an operator or expert can determine reasonable control rules, considering higher differences of the control error. This is why the most common FLCs are the PI-like or PD-like controllers (Yager & Filev [130]).

Completeness of an FLC is its capability of inferring a proper control action for every state of process (Lee [110]). The union of the supports on which primary fuzzy sets are defined should cover the related universe of discourse of a fuzzy partition in relation to some level set ε. This property is called ε*−completeness.* Usually, the level ε is chosen at the crosspoints as shown in Figure 4.10 so that it always exists a dominant rule associated with the grade of membership greater than 0.5 at any scaled input value (e.g. at 0.25 in Figure 4.10, the rule associated with the label PS will be dominant). Completeness can also be incorporated into fuzzy control rules depending on design experience and engineering knowledge. An additional rule can be added whenever a fuzzy condition is not included in the rule base to show that no control action will result. Or whenever the degree of partial match between some inputs and the predefined fuzzy conditions is lower than some level ε, the additional rule then indicates that no dominant rule will be fired.

C. Defuzzification

The defuzzification process is the final stage in a fuzzy reasoning system involving the selection of a representative element based on the output fuzzy subset. Defuzzification is a mapping from a space of fuzzy control actions defined over an output universe of discourse into a space of real world (crisp) control actions. A defuzzification strategy is aimed at producing a non-fuzzy control action that represents the possibility distribution of an inferred fuzzy control action. Many strategies have been proposed in the literature; however their scientific bases are so inadequate that defuzzification is considered as an art rather than a science (Mendel [114]). For the purpose of computational simplicity, the maximum criterion, mean of maxima and the centre of area used as defuzzification methods.

The *maximum criterion method* examines the fuzzy set B and selects as its output the value y^* the possibility distribution, obtained by an aggregation operator using fuzzy reasoning, $\mu_B(y)$, is a maximum. Figure 4.15 depicts two undesirable cases of this

defuzzification strategy. The first case can lead to a hang-up because the maximum of $\mu_B(y)$ occurs for a range of y (Figure 4.15(a)). Peculiar values can be resulted when using maximum defuzzifier (Figure 4.15(b)).

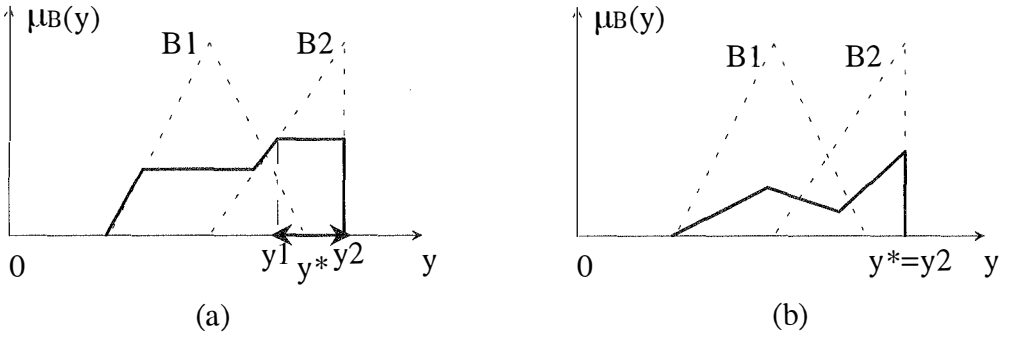

Figure 4.15. Undesirable cases of defuzzification with the maximum method.

The *Mean of Maxima method* (MOM) determines a control action which represents the mean value of all local control actions having maximal membership grades. More specifically, in the case of a discrete universe, the MOM strategy gives:

$$y^* = \frac{1}{q}\sum_{j=1}^{q} y_j, \tag{4.47}$$

where y_j is the support value at which the membership function reaches the maximum value $\mu_B(y_j)$, and q is the number of such support values. If the maximum value of the possibility distribution $\mu_B(y)$ occurs at a single point, the MOM defuzzifier reduces to the maximum defuzzifier and the crisp value obtained by the MOM strategy in some cases does not make sense as illustrated in Figure 4.16.

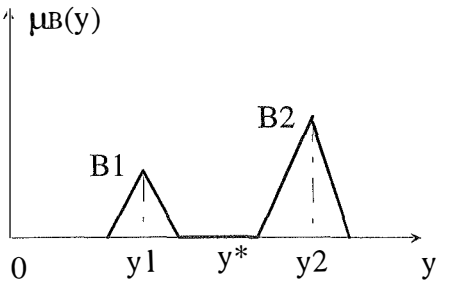

Figure 4.16. Case showing the MOM defuzzification makes no sense.

The widely-used *Centre of Area method* (COA) determines the crisp value of the control action as the centre of gravity (centroid) of its possibility distribution:

$$y^* = \frac{\int_S y\mu_B(y)dy}{\int_S \mu_B(y)dy}, \tag{4.48a}$$

where S denotes the support of $\mu_B(y)$. For a discretised universe, summations replace integrations in (4.48a):

$$y^* = \frac{\sum_{j=1}^{n} \mu_B(y_j)y_j}{\sum_{j=1}^{n} \mu_B(y_j)}, \tag{4.48b}$$

where n is the number of quantisation levels of the output. Figure 4.17 illustrates a centroid of a resultant fuzzy set.

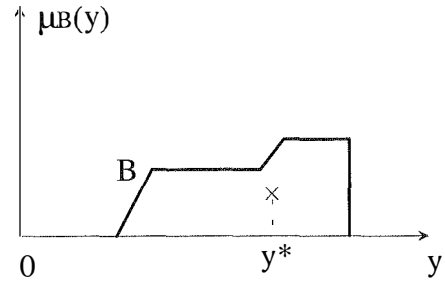

Figure 4.17. Centroid of resultant fuzzy set.

Among the defuzzification strategies, the MOM and COA are the most commonly-used for defuzzification. Larkin [131] compared the two defuzzification methods through a fuzzy control application and concluded that the COA yields superior results. The centroid technique is unique; however, it is not computationally simple. Pacini & Kosko [119] prove that for product inference and additive combining of rules, y^* can be computed using centroid information about the individual fuzzy rules. While this result does not extend to other $t-$norms and $t-$conorms, it justifies the use of *height defuzzification* (Mendel [114]) and *modified height defuzzification* (Hellendoorn & Thomas [132]). Cox in [117] noted that unless we have reason to

suspect that our model will behave better under other defuzzification techniques, the centroid method appears to provide a consistent and well-balanced approach. Although by nature, the centroid method is sensitive to the height and width of the total fuzzy region, it is well suited to handling solution regions that are maintained as sparse singletons. The method using singletons (single vertical points) instead of fuzzy set membership functions to describe output labels is referred to as *Sugeno-style* fuzzy inference method while the inference method discussed thus far using fuzzy sets to describe the output labels is called *Mamdani's method.* In Sugeno's method, the aggregation step is no longer necessary and the COA defuzzification method is slightly simplified. The centroid is calculated without a numerical integration of the entire fuzzy set surface as in (4.48a). Instead, the domain value at each singleton is multiplied by the height (truth membership value) of the singleton. This technique, in general, provides an equivalent centroid as to the centroid found by taking the area across an entire fuzzy set. Because it is more compact and computationally efficient representation than the Mamdani system, the Sugeno-style inference method lends itself to adaptive techniques (Jang & Gulley [133]).

4.4.2. An example of fuzzy logic control

Over the last five or ten years, fuzzy models have supplanted more conventional technologies in many scientific applications and engineering systems, especially in control systems and pattern recognition. This wide and diverse range of successful applications of fuzzy technology is, in the main, responsible for the increasing interest in the subject area (Schwartz *et al.* [14]). Among new trends in control theory, fuzzy logic issues have been introduced to electrical engineering curriculums in tertiary institutions (Ha & Negnevitsky [16]).

In this section, the design and implementation of a fuzzy logic controller for an overhead crane model, reported in Negnevitsky, Ha *et al.* [134] is described as an illustrative example. Here the problem is how to move a load from an initial position to a specified final one with minimal pendulum-like swing of a load. The crane system is subject to uncertainty in mass and chain length. Crane operations have been successfully performed in traditional installations which are totally reliant on the skill of human operators without having any quantitative knowledge of the underlying dynamics. The model is thus an example when fuzzy control may be applied to obtain a controller which can demonstrate robustness against external disturbances and parameter variations, and nonlinearity.

A. Plant description

A simple two-degree-of-freedom controlled model of the overhead crane system is used. It consists of a trolley, which can be moved along tracks carved out from the wooden base of the model. The trolley position is controlled using a dc motor, connected to a pulley system. A pendulum in the form of a metal rod is suspended from the centre of the trolley and imitates the cable and load of an actual crane as shown in Figure 4.18. The control goal is to move the trolley and the mass underneath from an initial horizontal position to a final one as fast as possible while suppressing the load swinging. This model is well known and used in many laboratories. The second equation of Lagrange is applied to find the crane dynamics. The horizontal position of the trolley, the velocity of the trolley, the angle of the chain, the angular velocity of the chain, and the force exerted by the drive onto the trolley are denoted by x_1, x_2, x_3, x_4 and f, respectively. The plant state equation obtained is a nonlinear one which can then be written as:

$$\dot{x}_1 = x_2, \quad \dot{x}_2 = -\Phi\frac{L}{\cos x_3} - g\tan x_3, \quad \dot{x}_3 = x_4, \quad \dot{x}_4 = \Phi, \tag{4.49}$$

with

$$\Phi = -\frac{g(M+m)\sin x_3 + (f + Lmx_4^2 \sin x_3)\cos x_3}{L(M + m\sin^2 x_3)} \quad \text{and} \quad f = K_t\frac{u - K_b x_2/\rho}{R\rho},$$

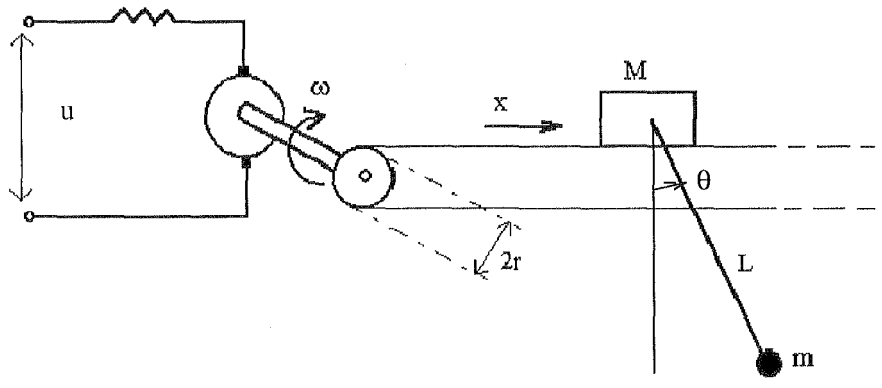

Figure 4.18. Schematic of an overhead crane model.

where g is the gravitational acceleration, M is the trolley mass, ρ is the trolley motor drum radius, and K_t, K_b and R are the motor torque constant, back emf constant and armature resistance, respectively. The load mass m and the chain length L are the changing parameters of the crane system. The motor voltage u is used to control both the trolley position and the load mass. In order to demonstrate the capability of the fuzzy control system to suppress the load swinging due to any disturbance deviations of the swing angle, the nonlinear state equations are used to describe the crane system dynamics instead of the linearised ones.

B. Fuzzy logic controller design

The control goal can be achieved by conventional methods (cascade control, pole placement, optimal control, etc.). However, a skilful operator is also perfectly capable of accomplishing the task. The problem is how to adapt the human experience to design the controller using fuzzy logic. Dealing with some uncertainty about the load mass or the chain length, an operator should control the motor voltage coarsely to move the trolley to a specified position and finely to reduce the load swing. In other words, because the swing of the load is to be kept minimal throughout the motion of the trolley, i.e. the swing should be minimal irrespective of the trolley position, the position of the trolley and the swing of the load are controlled using two separate fuzzy control units. The position fuzzy controller (XFC), consequently, depends on the position error e and the past value u_1 of the controller output u. Then, the output v of the XFC and the swing angle θ are used to adjust the controller output through the swing fuzzy controller (SFC). Figure 4.19 shows the overall structure used for the control of the overhead crane. These fuzzy controllers are cascaded with the output the XFC fed into the SFC. As the swing of the load is dependent on the acceleration of the trolley, the output of the SFC gives the change δu of the control voltage u to the system. The control signal u to the system is obtained as by a Mamdani-type (PI-type) fuzzy logic controller (4.33):

$$u(k) = u(k-1) + \delta u. \tag{4.50}$$

A delay voltage $u_1 = u(k-1)$ is used as the input to the XFC instead of the current system control value to reduce the acceleration of the trolley and thus, to minimise the load swing. The first step for designing a fuzzy controller is to fuzzify the controller inputs and outputs. These variables are described by linguistic labels NB, NM, NS, ZE, PS, PM and PB which mean negative big, negative medium, negative small, zero,

positive small, positive medium and positive big, respectively. The problem is how to choose the corresponding membership functions for each label of the inputs (position error e, delay voltage u_1, SFC input v, and swing angle θ) and outputs (XFC output v and control voltage change δu).

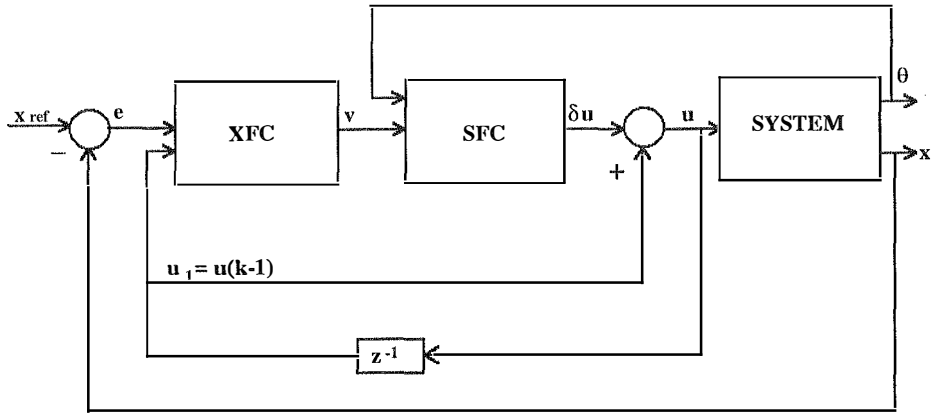

Figure 4.19. Fuzzy logic controller for the crane system.

The proposed membership functions for XFC is shown in Figure 4.20. Triangular membership functions are used for the input labels of position error e and delay voltage u_1 (Figure 4.20a-b), and singletons for the output membership functions (Figure 4.20c). Figure 4.21 shows the membership functions for SFC labels of the swing angle θ, the voltage input, and the control voltage change δu (SFC output). The fuzzy rules are written as a representation of human operations to control the trolley and the load underneath. Following typical instructions of an operator for the control task, a fuzzy rule can be expressed like

- "If the position error is positive big and the delay voltage is negative big then the position controller output is positive big", or
- "If the swing angle is positive medium and the position controller output is positive small then the control voltage change is positive medium", etc.

A proposed set of fuzzy rules for the XFC and SFC is presented in Tables 4.4 and 4.5. They are developed in the Fuzzy Inference Units (FIU) using the Fuzzy Inference Development Environment (FIDE') software package (Aptronix [135]).

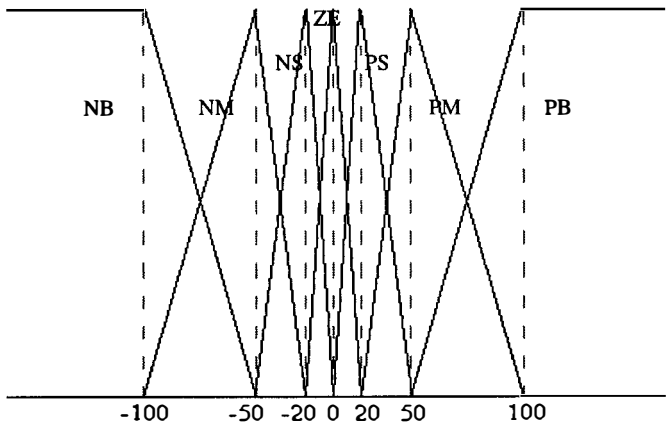

(a)

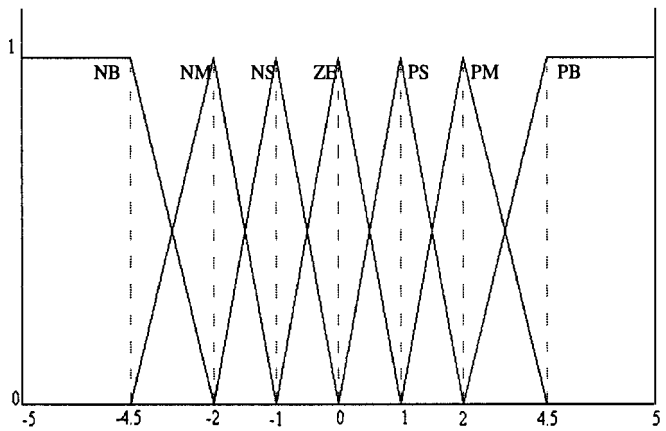

(b)

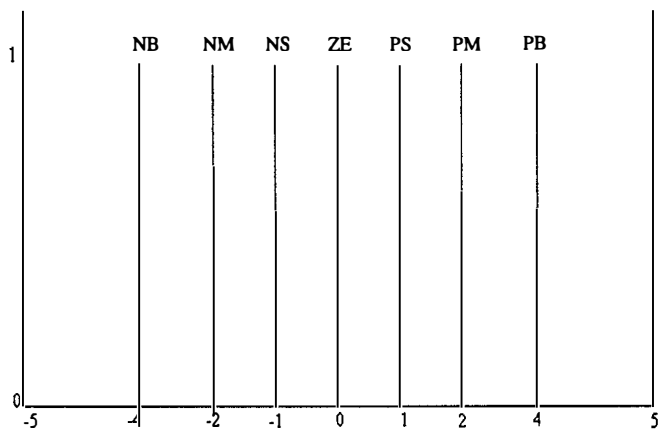

(c)

Figure 4.20. Membership functions for: (a) error, (b) delay voltage, (c) XFC output.

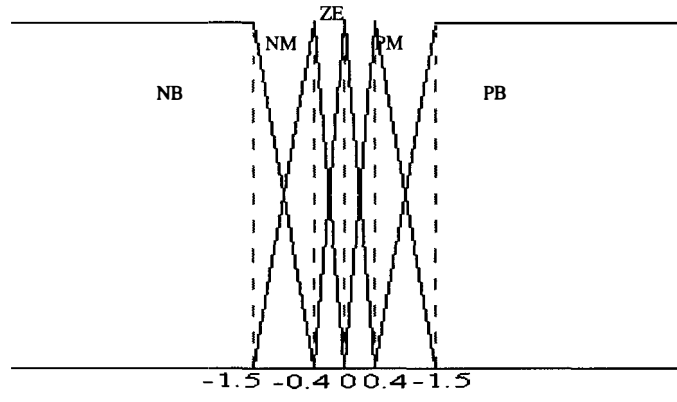

(a)

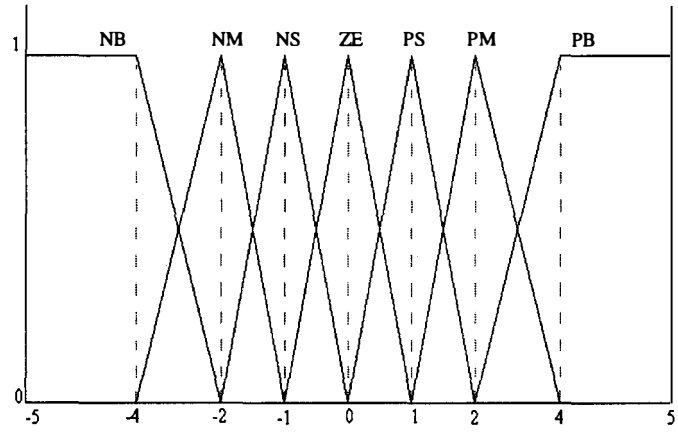

(b)

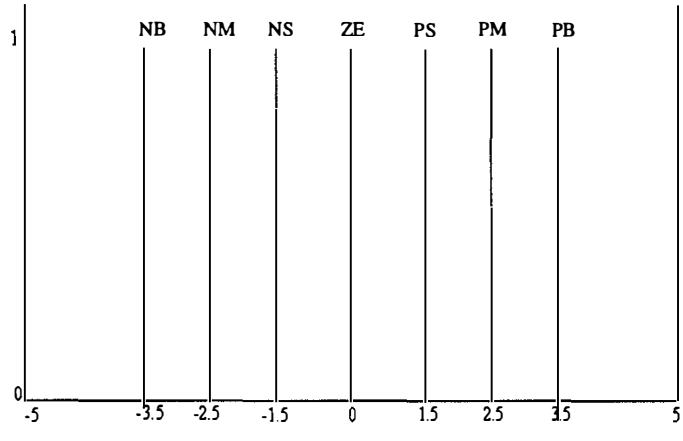

(c)

Figure 4.21. Membership functions for: (a) angle, (b) voltage input (c) SFC output.

XFC e u_1 v	NB	NM	NS	ZE	PS	PM	PB
NB	ZE	PS	PM	PB	PB	PB	PB
NM	NS	ZE	PS	PM	PM	PM	PB
NS	NM	NS	ZE	PS	PS	PM	PB
ZE	NB	NM	NS	ZE	PS	PB	PB
PS	NB	NM	NS	NS	ZE	PS	PM
PM	NB	NM	NM	NM	NS	ZE	PS
PB	NB	NB	NB	NB	NM	NS	ZE

Table 4.4. Fuzzy rules of XFC.

SFC θ v δu	NB	NM	ZE	PM	PB
NB	NB	NB	NB	NM	NS
NM	NB	NM	NM	NS	ZE
NS	NB	NM	NS	ZE	PS
ZE	NM	NS	ZE	PS	PM
PS	NS	ZE	PS	PM	PB
PM	ZE	PS	PM	PM	PB
PB	PS	PM	PB	PB	PB

Table 4.5. Fuzzy rules of SFC.

Surface views for the two control units are shown in Figure 4.22 and 4.23. A Fuzzy Inference System is created by the composer tool to configure the whole system, as presented in Figure 4.24.

Simple arithmetic calculations in the system are performed by the Fuzzy Operation Units (FOU). The crane dynamics is represented by the Fuzzy Execution Unit (FEU) with the fourth order Runge-Kutta integration algorithm for the non-linear state equations (4.49). This unit links executable 'C' code developed outside of FIDE' to the integrated system. Debugging options are utilised to analyse and fine-tune the final design. The FIU files can also be translated to assembly code which is used for real time control of the crane model.

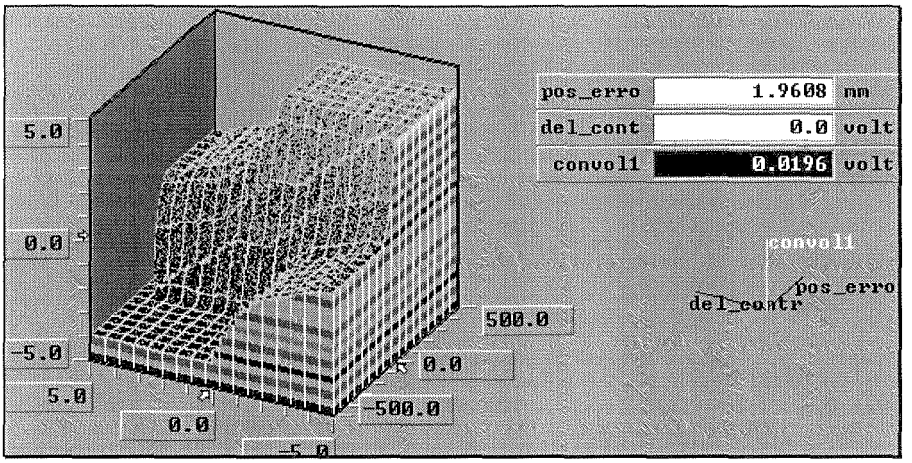

Figure 4.22. Surface view of the position fuzzy controller XFC.

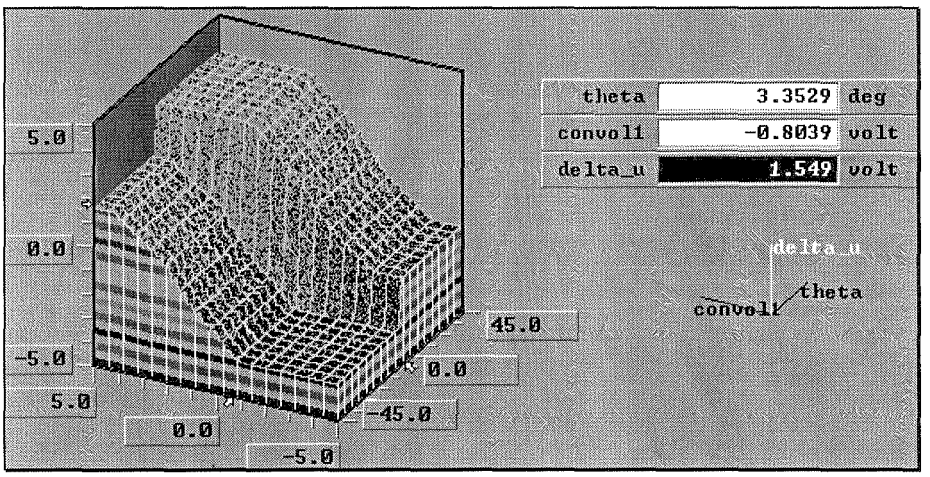

Figure 4.23. Surface view of the swing fuzzy controller SFC.

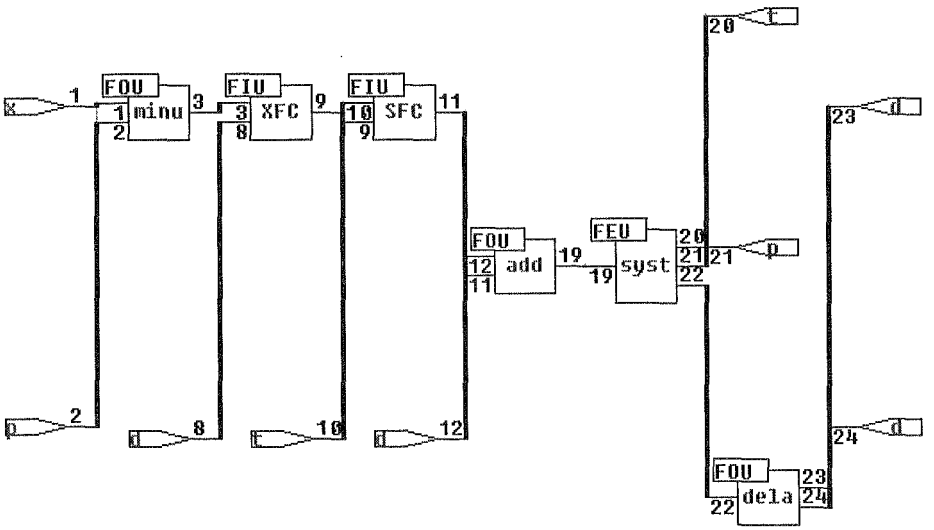

Figure 4.24. Composer/Graphics of the control system.

C. Simulation and experimental results

The numerical parameters of this overhead crane model are given in the Table 4.6. The FIDE' software package provides facilities for debugging, analysing, and fine tuning the membership functions and fuzzy rules to improve control quality. The position and swing responses obtained by simulation are shown in Figure 4.25 (dotted lines). A reference position for the trolley is achieved after a settling time of about 3 seconds with a maximal swing less than 5 degrees.

Parameter	Value
Chain length, *m*	0.5
Trolley mass, *kg*	1
Load mass, *kg*	0.25
Motor torque constant, *Nm/A*	0.0066
Motor back emf constant, *V/rad/s*	0.0066
Motor armature resistance, *ohm*	0.67
Trolley motor drum radius, *m*	0.01
Gravitational acceleration, m/s^2	9.81

Table 4.6. Crane system parameters.

A photograph of the laboratory set-up is displayed in Figure 4.26. The crane model is driven by a 57W DC-motor of the type UGTMEM-03MB2, supplied with a Pulse-Width Modulation (PWM) bridge. A rotary potentiometer connected to a shaft to which the pendulum rod is connected, is used to obtain a measurement of the pendulum swing angle. The trolley position is measured by using another rotary potentiometer, mounted on the motor shaft. The analog readings are converted to digital values with an ADC. The membership functions and fuzzy-rule-base for the XFC and SFC are realised using 'C' code generated from the FIDE' package. The host computer, a 486 PC/AT, performs on-line processing of the appropriate crisp output control voltage. This voltage is fed to the PWM circuit for the dc motor through a DAC.

The experimental position and swing responses are as shown in Figure 4.25 (solid lines) to compare with the simulation results (dotted lines). The results obtained coincide well with those obtained from simulation.

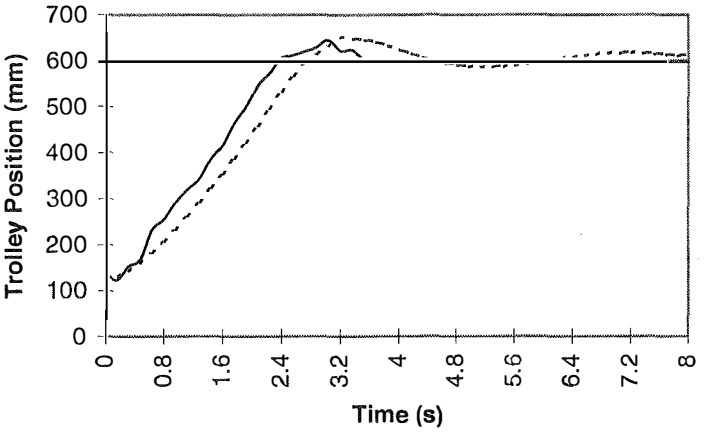

(a)

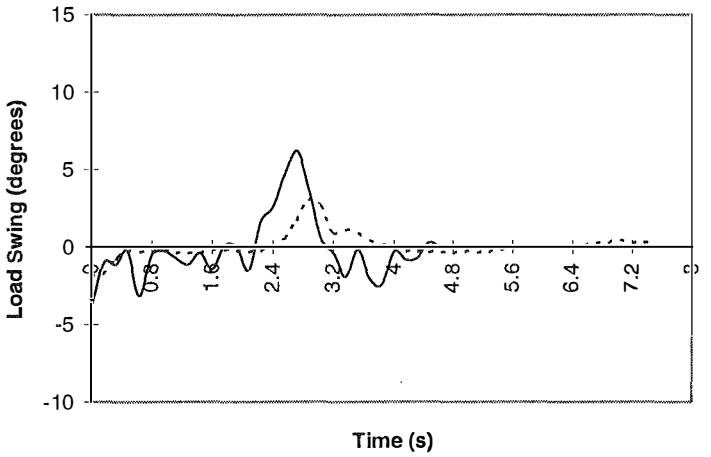

(b)

Figure 4.25. Simulation (dotted lines) and experimental (solid lines) (a) position, and (b) swing responses.

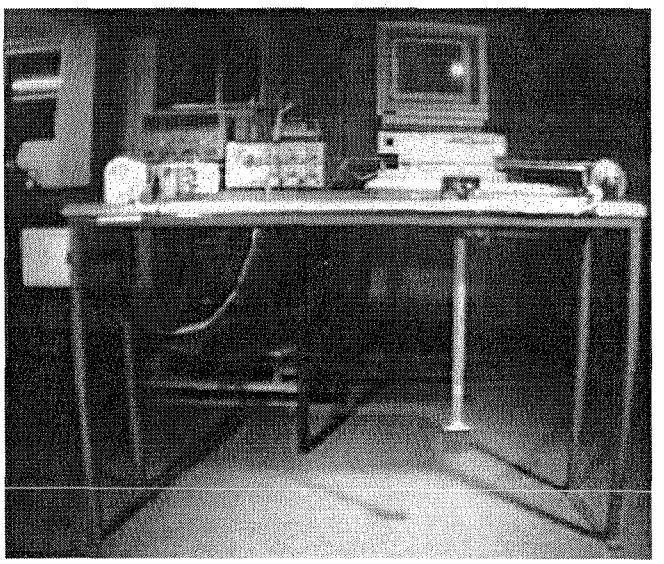

Figure 4.26. A photograph of the model.

The experimental responses with proportional (P) and proportional-integral (PI) controllers are shown in Figure 4.27 to confirm the fuzzy logic controller advantage in reducing load swing. The influences of external disturbances on the load swing and variations of the load mass and chain length are investigated. Figure 4.28 depicts the swing responses of the crane system with an initial swing angle of 36 degrees and different load masses. The swing responses with varying pendulum length are shown in Figure 4.29. The results obtained demonstrate the system insensitivity with respect to any variations.

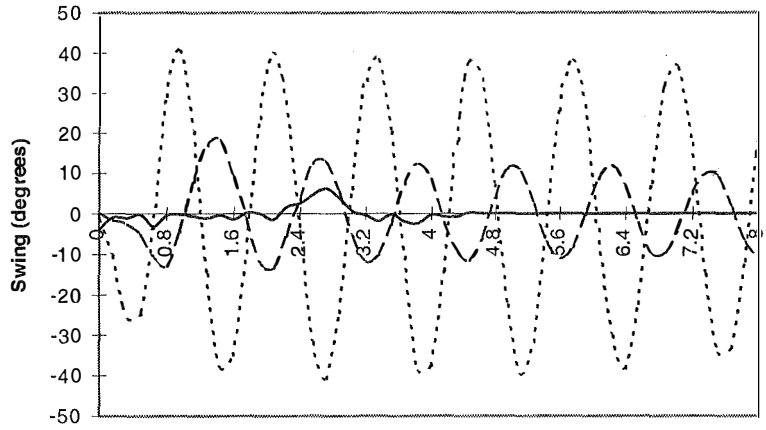

Figure 4.27. Swing responses with FLC (solid line), P (dotted line), and PI (dashed line) controllers.

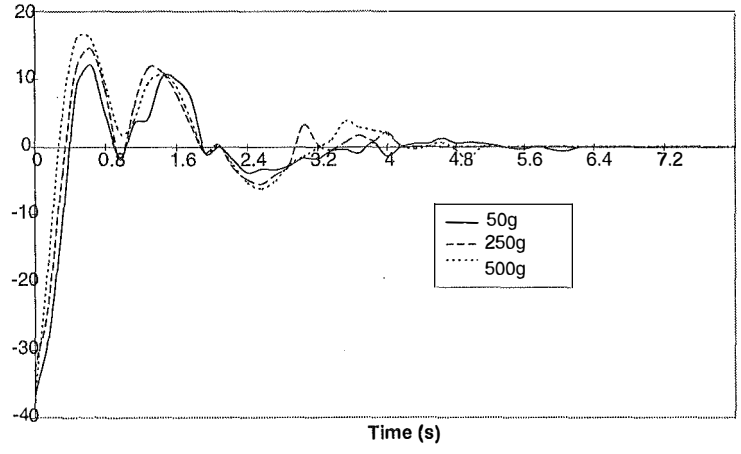

Figure 4.28. Swing responses with an initial angle deviation and different masses (50, 250, 500 *g*).

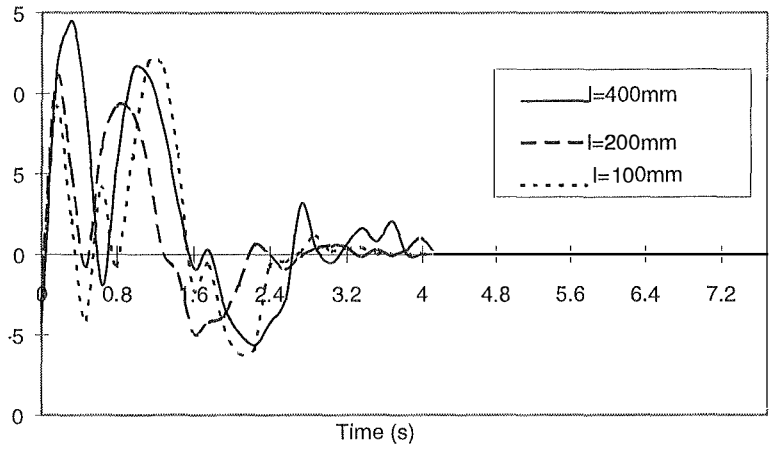

Figure 4.29. Swing responses with chain length variations (100, 200, 400 *mm*).

In the example described above as in many of its applications, an FLC is either designed by a domain expert or in close collaboration with domain experts. Knowledge acquisition in FLC applications plays an important role in determining the control performance. However, domain experts and skilled operators do not structure their decision making by any formal way. Although fuzzy logic provides an effective tool for linguistic knowledge representation and Zadeh's compositional rule of inference serves as a useful guideline, more efficient and more systematic methods for knowledge acquisition are still needed as discussed in the next section.

4.5 Fuzzy control: pros, cons, and perspective

Classical control theory has been well-developed and provides an effective toll for mathematical system analysis and design when a precise model of a system is available. In a complementary way, fuzzy controllers have found many of practical applications as a means of replacing a skilled operators. Fuzzy control has emerged as a practical alternative to several conventional control schemes and, in general, can be applied in a broad class of systems where successful applications have been shown (Schwartz *et al.* [14]). Moreover, their superiority is found in many nontraditionally modelled industrial processes such as linguistically controlled devices and systems with unmodelled effects and uncertainties that cannot be precisely described by mathematical formulations. While fuzzy logic control is attractive for dealing with uncertainty, non-linearity, and complexity in systems, it is lacking in documented theory to direct the design process and is reliant on common sense engineering

heuristics. Indeed, the design of fuzzy controllers is usually performed in an *ad hoc* manner where it is often difficult to choose the controller parameters (e.g., the membership functions). Considerable effort is required in choosing the most adequate membership functions, their form, fuzzy rule base, and inference methods, or a well-founded procedure for system design. In response to this requirement, a theory of *fuzzy dynamic systems* has been under investigation (Kiszka *et al.* [136], Cao *et al.* [124]). For the practical viewpoint, a disadvantage of fuzzy control might be the computational burden while implementing the controllers. Fuzzy tuning which results in explicit expressions for continuously changing the controller parameters can be a compromise alternative (Ha [112, 39, 40], Ha & Negnevitsky [21, 37, 41, 42]). The proposed technique combining the salient features of conventional and fuzzy control techniques will be discussed in the following chapters of this thesis. Another drawback is that the fuzzy controller constructed for the nominal plant may later perform inadequately if significant and unpredictable plant parameter variations occur. Furthermore, fuzzy control normally depends on the rule base representing the experience and intuition of human experts, thus an efficient control cannot be expected as long as the rule base of human experts is not available. Addressing this problem, *fuzzy model reference* learning control is proposed, e.g. in Moudgal *et al.* [137], Kwong *et al.* [127], with the capability of automatically synthetising a rule-base and of automatically tuning the fuzzy controller to achieve robustness. A *self-organising* FLC (Shao [126], Park et al. [138]) needs no expert in rule making; instead, rules are generated using the history of input/output pairs, stored in a fuzzy rule space and updated on-line by replacing the stored rule with a new one using a performance index. The problems of determination of the linguistic space, definition of the membership functions of each term and the derivation of the control rules can be solved by application of machine learning. One of the new learning algorithms modelled on natural and biological systems is the *genetic algorithm* based on the processes of natural evolution (Linkens & Nyongesa [139]). Genetic algorithms are able to automate and provide objective criteria in defining fuzzy controller parameters.

Another direction of recent exploration is the conception and design of fuzzy systems that have the capability of learning from experience. In this area, a combination of techniques drawn from both fuzzy logic and neural network theory may provide a powerful tool for the design of systems which can emulate the remarkable human ability to learn and adapt to changes in environment. The recent resurgence of interest in the field of artificial neural networks has injected a new driving force into studies on fuzzy systems. Applying neural techniques, fuzzy control systems are able not only

to take linguistic information from human experts but also to adapt itself using input/output data to improve system performance. The essential part of neuro-fuzzy approaches comes from a common framework called adaptive networks, which combines both neural networks and fuzzy models. It should capture concise and interpretable knowledge automatically from numerical data. Once a fuzzy controller is transformed into an adaptive network-based fuzzy inference system, it can take advantage of all the neural network design techniques (Jang & Sun [128]). Some neuro-fuzzy applications for improving robustness of motion control systems (Palis, Ha *et al.* [33, 140], Ha & Negnevitsky [44]) are introduced in Chapter 7. New ways of employing fuzzy logic in control applications and new forms of fuzzy control are continually being investigated.

4.6 Summary

Fuzzy thinking has originated from a philosophical basis on indeterminism (McNeil & Freiberger [141]). An inherent uncertainty and unpredictability, spontaneity and freedom, integrity and openness characterise the stunning complexity of our world and life. That is why the way fuzzy thinking has emerged in order to grasp real world complexity. The following chapters will employ fuzzy thinking to enhance robust performance of motion control systems. As an introduction, this chapter provides an overview of fuzzy logic and fuzzy logic control. Fuzzy sets, fuzzy set operations, and fuzzy linguistic representation such as linguistic variables and linguistic modifiers (hedges) have been briefly outlined. Fuzzy reasoning or approximate reasoning is considered from the engineering viewpoint with IF-THEN fuzzy implications using Mamdani's minimum inference and Larsen's product inference. A fuzzy logic controller, mapping an input data vector into a scalar control output, normally comprises a rule base, fuzzifier, and defuzzifier. Commonly-used kinds of membership functions are described, focusing on control applications. Based on expert knowledge and fuzzy reasoning, fuzzy conditional statements are formulated typically similar to conventional PI or PD controllers. The centre of area method with Sugeno's fuzzy inference provides the simplest strategy for defuzzification. The FLC design procedure was illustrated through the control of a crane model with two main objectives, load minimal swing and robustness. Discussions about advantages and disadvantages of fuzzy control with some perspective tendencies of its development are provided to conclude this primer chapter on fuzzy logic and fuzzy logic controllers.

Chapter 5

Robustness Enhancement with Fuzzy Tuning

The proportional-integral (PI) controllers are still the majority of the controllers used in industrial control systems. In the field of electrical drives, PI controllers have been widely used in current and speed loops where the plant model is assumed to be known. However, servomechanism may be affected when the plant is subject to uncertainties or nonlinearities. Sliding mode controllers are robust but chattering is the main drawback. In PI control, a skilful operator can tune the controller parameters to achieve robustness against environment changes. Moreover, in sliding mode control, the tuning action can be obtained by some heuristic schemes to accelerate the reaching phase and reduce chattering. It is, therefore, worth developing an appropriate methodology for the automatic adjustment of the controller parameters or the control action in order to enhance robustness. These problems are addressed in this chapter with the use of fuzzy logic in tuning schemes.

5.1 Introduction

Standard conventional proportional-integral controllers, while simple to implement and commonly used in motion control systems, suffer from poor performance when applied to systems containing structured uncertainties, such as parameter and load variations, and unstructured uncertainties, such as unmodelled dynamics, and unknown and time varying nonlinearities. In order to design a controller which is capable of employing expert knowledge, it is desirable to develop a mechanism to adjust the controller parameters so that the following requirements could be fulfilled:

- Simple computation of the controller parameters.
- Easy interpretation and implementation of the tuning process.
- Large field of application (guaranteed performance).
- High robustness in the field of application.
- Acceptable performances beyond the field of application.

- No *a priori* knowledge required.

The auto-calibration method, proposed by Voda & Landau [18], is based on the computation of the controller parameters from the knowledge of one point of the plant characteristics inspired by Kessler's symmetrical optimum [142]. The key idea behind this method is identifying the plant model parameters and then calculating the PI controller parameters. The identification process is accomplished by making feedback experiment with a relay with hysteresis in the loop to obtain oscillations at a certain frequency, e.g. $\omega = \omega_{135}$, where the phase lag of the plant is $\angle\Phi = -135^0$. The controller parameters are determined by tuning formulae given in a table. Originated by Ziegler & Nichols [143] and the modified Ziegler-Nichols rules in Hang *et al.* [144], the identification of the critical point $\omega = \omega_{180}$ on the frequency characteristics of the plant (gain and phase) enables autotuning of the controller parameters depending on the updated plant parameters. It is the opinion of Voda & Landau [18] that there is a lack of an analytical approach taking into account both robustness and closed-loop performance. Moreover, both of the autotuning and indirect autotuning (auto-calibration) techniques are useful but require some knowledge about the process, obtained either by a relay feedback in the loop (Astrom & Hagglund [145]) in the former or by a plant experiment in the latter. Truly effective adaptive autotuning, in general, is restricted to a linear process within the presumed range of operation. In order to cope with sensor noise, modelled or unmodelled uncertainties, and shifts in operating point in linearised systems, the linguistic characteristics of fuzzy control can provide a very attractive approach to the uncertainty problem. The idea of using fuzzy logic to modify the rate of change of the integrator state based on the control error has been described in Dote [146]. The controller structure is changed continuously by fuzzy logic such that if the error is large or its rate of change is large, then the controller makes the system respond quickly and vice versa in order to achieve robust performance. Such a fuzzy-tuned controller was applied to the control of a servo drive system by Suyitno *et al.* [147].

This chapter, based mainly on the works of Ha [112], Ha & Negnevitsky [21, 37], and Ha *et al.* [38], is devoted to the application of fuzzy tuning schemes used in cascade PI controllers. The idea of fuzzy tuning can be extended to sliding mode control. In Ha [148] and Ha *et al.* [22], a fuzzy tuned component is added to the control signal to accelerate the reaching phase and reduce the influence of unmodelled dynamics and chattering. By using some engineering heuristics and expert knowledge to tune the control action, robust performance is demonstrated even in the presence of modelled

and unmodelled uncertainties. The interesting features of fuzzy tuning approach is that all the tuning schemes result in explicit expressions, and only input and output data are required. Thus, the tuning process is easily accomplished, and the computational cost for implementation is low. Although the controlled objects used in this chapter are electrical drive systems, it is believed that the proposed method can, in general, be applied to a variety of dynamic systems suffering from severe uncertainties.

5.2 Fuzzy tuning in PI controllers

In motion or process control systems, the plant transfer function usually has the following form:

$$H_p(s) = \frac{K_0}{(1+T_m s)\prod_{j=1}^{n-1}(1+\tau_j s)e^{s\tau_n}} \cong \frac{K_0}{(1+T_m s)(1+T_\mu s)}, \tag{5.1}$$

where T_m is large time constant with respect to the uncompensatable time constant T_μ, which is the sum of parasitic time constants τ_j and time delay τ_n, i.e.

$$T_m >> \sum_{j=1}^{n} \tau_j = T_\mu . \tag{5.2}$$

In the field of electrical drives, proportional-integral (PI) controllers are widely used because of their design simplicity. A typical speed control system is shown in Figure 5.1, where n_{ref} is the reference speed, T_L is the disturbance torque, e is the error, u is the control signal and n_m is the output speed. K_P, T_I, T_μ, T_f, K_0, and T_m are the PI controller gain, time-constant, current loop equivalent time-constant which is the smallest uncompensatable time-constant, prefilter time-constant, plant overall gain and mechanical time-constant, respectively. In order to reduce overshoot of the system's input response an input filter is used to cancel the zero of the controller. This filter is placed outside the loop, so as not to affect the load response. It is assumed that $T_\mu \le T_m/4$ so that $1+T_m s \cong T_m s$ for high frequencies, $\omega \ge 1/4T_\mu$. The values of K_P and T_I can be obtained, for example, by the symmetric optimum method (Kessler [142], Voda & Landau [18]), dependent on T_μ, K_0, and T_m. Other design equations for K_P and T_I using the magnitude optimum criteria, or the Graham-Lathrop minimisation of the integral of time absolute error (ITAE) [150] are given in Table 5.1.

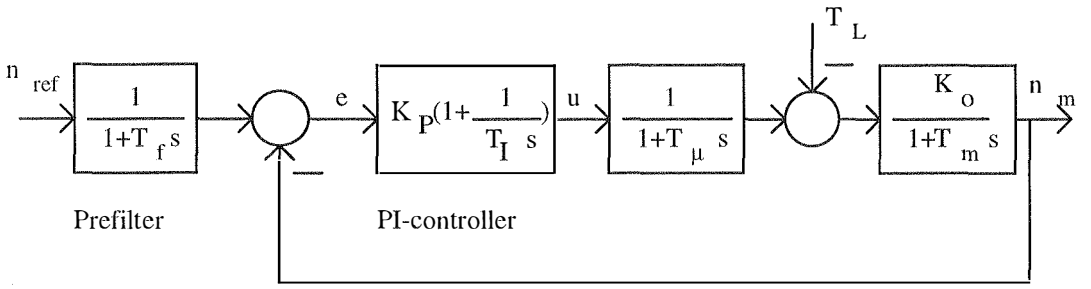

Figure 5.1: Conventional speed control.

Criteria	Controller parameters		Reference response	
	gain, K_P	time-constant, T_I	steady-state time, t_s	overshoot, %OS
Symmetric	$T_m/(2T_\mu K_0)$	$4T_\mu$	$16.5T_\mu$	4.3
Magnitude	$T_m/(2T_\mu K_0)$	T_m	$8.4T_\mu$	4.3
ITAE	$0.7T_m/(T_\mu K_0)$	$3.76T_\mu$	$3.6T_\mu$	3

Table 5.1. PI controller parameters with different criteria.

A comprehensive comparison of these methods can be found in Umland & Safiuddin [82]. With conventional PI controllers, it is difficult to achieve a high tracking performance with respect to both parameter insensitivity and disturbance rejection. An approach to the problem can be application of the fuzzy proportional-integral controller where the change of the control output depends on the error and its change as in (4.44). It has demonstrated in Ying *et al.* [151] that better performance than conventional controllers can be obtained with fuzzy proportional-integral controllers.

In order to improve the system robustness, the usual engineering practice is to tune the controller parameters. It is believed that by changing the gains automatically and continuously with the error and its change, the controller becomes self-tuning and capable of handling uncertainties and nonlinearities. In addition, it has been argued in Ying [152] that the simplest fuzzy controllers that use different inference methods are the fuzzy PID controllers with variable gains. The price to this achievement is in computation: The fuzzy PI controller is driven by a set of control rules rather than by two constant proportional and integral gains. In Ha [112], fuzzy tuning schemes result in simple explicit formulas for continuously changing the coefficients K_P and T_I in

depending of the error control and its rate of change. Tuning a coefficient, K, is a continuously smooth process of adjusting its value. Recently, Truong & Hofmann [111] proposed a two-degree-of-freedom fuzzy tuners with two input labels and two singleton output labels. The idea of using fuzzy logic to make the PI controller structure continuously changed was introduced by Dote [146] and applied to the control of servomotors in Suyitno *et al.* [147]. A technical parameter, X, can be described in a simple way as either large (XL) or small (XS) with the corresponding exponential membership functions:

$$\mu_{XS}(X) = \exp(-|X|/\sigma_X), \quad \mu_{XL}(X) = 1 - \exp(-|X|/\sigma_X), \tag{5.3}$$

where σ_X is some positive constant. Figure 5.2 shows the membership functions μ_{XS} and μ_{XL}. The following singletons are used for the output labels KL (K is large) and KS (K is small):

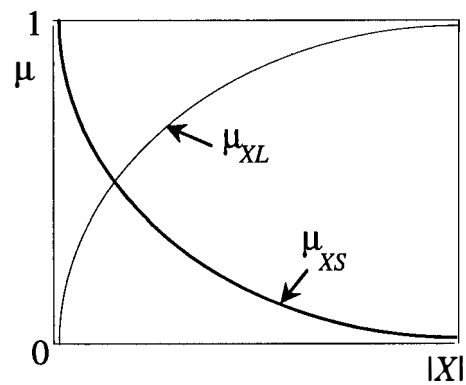

Figure 5.2. Membership functions μ_{XS} and μ_{XL}

$$\mu_{KL}(K) = \begin{cases} 1, & K = K_{\max} \\ 0, & K \neq K_{\max} \end{cases}, \quad \mu_{KS}(K) = \begin{cases} 1, & K = K_{\min} \\ 0, & K \neq K_{\min} \end{cases}, \tag{5.4}$$

where $K_{\max}$ and $K_{\min}$ are the maximum and minimum values of K. Engineering heuristics from an operator for tuning K with respect to X can be stated as:

(i) *If XS then KS*, *If XL then KL*,

or

(ii) *If XS then KL*, *If XL then KS*.

Using the max-min inference method and centroid technique for defuzzification, the nonlinear relationship of K with respect to X can be found as follows

$$K(X) = \begin{cases} \dfrac{\mu_{XS}K_{\min} + \mu_{XL}K_{\max}}{\mu_{XS} + \mu_{XL}}, & \text{for scheme (i),} \\ \dfrac{\mu_{XS}K_{\max} + \mu_{XL}K_{\min}}{\mu_{XS} + \mu_{XL}}, & \text{for scheme (ii).} \end{cases} \tag{5.5}$$

By analysing the frequency characteristics of the open loop plant including the controller

$$H_p(s) = \frac{K_0 K_P (1 + T_I s)}{T_m T_I s^2 (1 + T_\mu s)}, \tag{5.6}$$

in order to reduce the control error and the system rise time, it is required to increase the gain K_P and to decrease the time-constant T_I. In other words, the rules for tuning K_P and T_I can be expressed as:

If the error e is large, then the gain K_P is large,
If the error e is small, then the gain K_P is small,
If the error e is large, then the time-constant T_I is small,
If the error e is small, then the time-constant T_I is large.

Therefore, the scheme (i) is proposed for tuning K_P, and (ii) for tuning T_I with respect to the control error e. Taking the time rate of change of error into account, the tuning process has a scaling factor, w_c. When the change of the error is large, the scaling factor should be large and vice versa. Thus, the fuzzy rules for w_c are stated as

If the change of the error e is large, then the scaling factor w_c is large,
If the change of the error e is small, then the scaling factor w_c is small.

The value of w_c is continuously changed by scheme (i) according to $de(k) = e(k) - e(k-1)$, where k is discretised time. The following scaled error, ε, and change of error, $\partial\varepsilon$, are introduced:

$$\varepsilon = sat(\frac{e}{e^{sat}}) \quad \text{and} \quad \partial\varepsilon = \begin{cases} sign(-e(k-1)), & \text{if } e(k) = 0, \\ sat(\dfrac{de(k)}{e(k)}), & \text{if } e(k) \neq 0, \end{cases} \tag{5.7}$$

where

$$sat(x) = \begin{cases} 1, & x \geq 1 \\ x, & -1 \leq x \leq 1 \\ -1, & x \leq -1 \end{cases}$$

and e^{sat} is the maximum magnitude of the error corresponding to saturation. By choosing the maximum and minimum values of K_P, T_I and w_c, the tuning expressions for K_P and T_I are found as follows (Ha [112]):

$$K_P = w_c K_{P,tun}(\varepsilon) = w_c[K_{P,\max} - (K_{P,\max} - K_{P,\min})\exp(-|\varepsilon|/\sigma_\varepsilon)], \quad (5.8)$$

and

$$T_I = w_c T_{I,tun}(\varepsilon) = w_c[T_{I,\min} + (T_{I,\max} - T_{I,\min})\exp(-|\varepsilon|/\sigma_\varepsilon)], \quad (5.9)$$

where

$$w_c(\partial\varepsilon) = [w_{c,\max} - (w_{c,\max} - w_{c,\min})\exp(-|\partial\varepsilon|/\sigma_{\partial\varepsilon})], \quad (5.10)$$

and σ_ε and $\sigma_{\partial\varepsilon}$ are some positive constants. The values of $T_{I,nom}$ and $K_{P,nom}$ are calculated from the nominal values $K_{0,nom}$, $T_{m,nom}$, and $T_{\mu,nom}$ using one of the symmetrical or magnitude optimum, or other criteria. The prefilter time constant T_f is set at $T_{I,nom}$.

The simulation parameters of the system K_0, T_m and T_μ in Figure 5.1 are given in Table 5.2. The values of $T_{I,nom}$ and K_P are calculated from the values $K_{0,nom}$, $T_{m,nom}$ and $T_{\mu,nom}$ using the symmetrical optimum given in Table 5.1. The prefilter time constant T_f is set at $T_{I,nom}$. Choosing the minimum and maximum values for K_P, T_I and w_c as shown in Table 5.2, and the coefficients σ_ε=$\sigma_{\partial\varepsilon}$= 0.01, the controller parameters are on-line tuned by the following forms

$$K_P = [2 - 1.5\exp(-100|\partial\varepsilon|)][8 - 6\exp(-100|\varepsilon|)],$$

$$T_I = [2 - 1.5\exp(-100|\partial\varepsilon|)][0.1 + 0.3\exp(-100|\varepsilon|)].$$

$K_{0,nom}$	$T_{m,nom}$	$T_{\mu,nom}$	$K_{P,nom}$	$T_{I,nom}$	$w_{c,nom}$
1	0.4	0.05	4	0.2	1

Table 5.2. Simulation parameters for tuning PI controller parameters.

The unit step reference response is shown in Figure 5.3 for the nominal case (solid lines) ($K_0 = K_{0,nom}$, $T_m = T_{m,nom}$, and $T_\mu = T_{\mu,nom}$) and for a critical case of changing parameters (dash-dotted lines) ($K_0 = 0.5K_{0,nom}$, $T_m = 2T_{m,nom}$, and $T_\mu = 2T_{\mu,nom}$), with fuzzy tuning (curves 1) and without fuzzy tuning (curves 2).

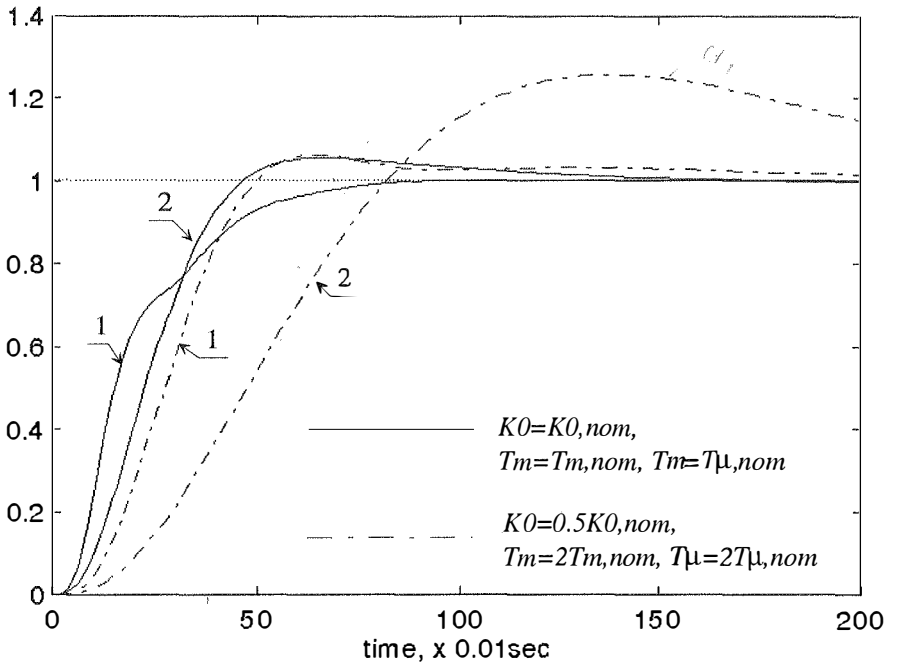

Figure 5.3. Unit step reference response with fuzzy tuning (curves 1) and without fuzzy tuning (curves 2).

The unit step disturbance response is shown in Figure 5.4 under the same conditions. As it can be seen, a well-damped response with adequately fast dynamics is observed even in the cases of parameter variation. With fuzzy tuning the disturbance response exhibits a reduction of approximately 50% in the maximum deviation.

Simulation results indicate that transient performance and disturbance rejection capability are significantly improved with any set of parameters K_0, T_m, and T_μ given in the range between half and twice of the nominal values. It should be noted that fuzzy tuning schemes with different membership functions, such as Gaussian or sigmoidal, for μ_{XS} and μ_{XL} can be incorporated in (5.5) instead of exponential functions. For example, the tuning formulas (5.7-5.9) using Gaussian membership functions (4.28) can be written as

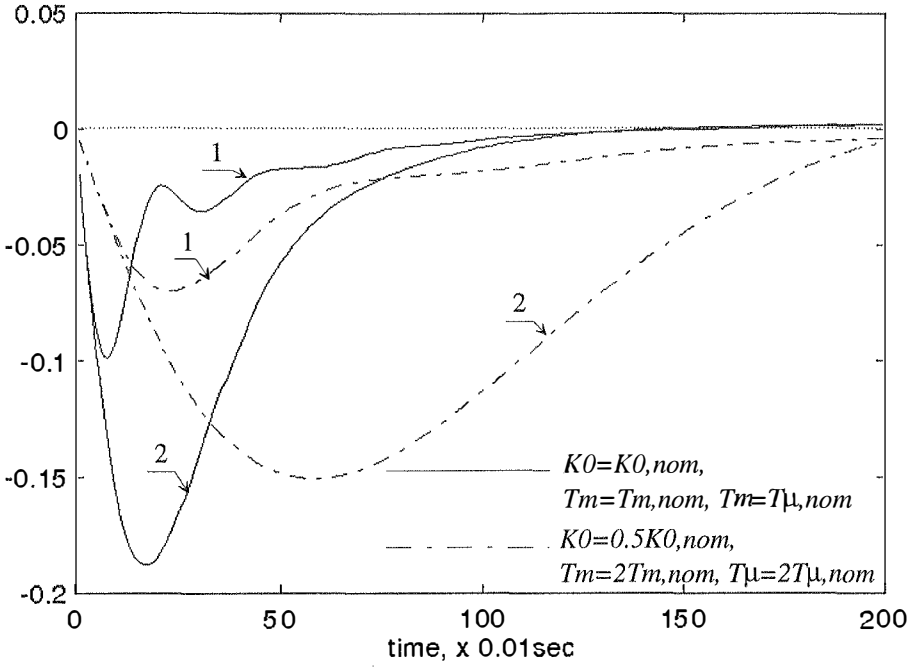

Figure 5.4. Unit step disturbance response with fuzzy tuning (curves 1) and without fuzzy tuning (curves 2).

$$K_P = w_c K_{P,tun}(\varepsilon) = w_c[K_{P,\max} - (K_{P,\max} - K_{P,\min})\exp(-|\varepsilon|^2/2\sigma_\varepsilon^2)], \quad (5.11)$$

and

$$T_I = w_c T_{I,tun}(\varepsilon) = w_c[T_{I,\min} + (T_{I,\max} - T_{I,\min})\exp(-|\varepsilon|^2/2\sigma_\varepsilon^2)], \quad (5.12)$$

where

$$w_c(\partial\varepsilon) = [w_{c,\max} - (w_{c,\max} - w_{c,\min})\exp(-|\partial\varepsilon|^2/2\sigma_{\partial\varepsilon}^2)]. \quad (5.13)$$

When using sigmoidal membership functions (4.30), the tuning formulas for the controller parameters are written as:

$$K_P = w_c K_{P,tun}(\varepsilon) = w_c[K_{P,\max} - 2(K_{P,\max} - K_{P,\min})/(1+\exp(-|\varepsilon|/2\sigma_\varepsilon))], \quad (5.14)$$

and

$$T_I = w_c T_{I,tun}(\varepsilon) = w_c[T_{I,\min} + 2(T_{I,\max} - T_{I,\min})/(1+\exp(-|\varepsilon|/2\sigma_\varepsilon))], \quad (5.15)$$

where

$$w_c(\partial\varepsilon) = [w_{c,\max} - 2(w_{c,\max} - w_{c,\min})/(1+\exp(-|\varepsilon|/2\sigma_\varepsilon))]. \quad (5.16)$$

PI controllers with fuzzy tuning can be implemented in cascaded controllers for current, speed, and position loops of drive systems where the problem of changing parameters and load is serious. Taking into consideration not only the control error but also the control signal saturation, the problem of anti-windup (De Vegte [67]) can also be considered with some fuzzy tuning schemes.

At large values of T_m, we have $1+T_m s \cong T_m s$. The closed loop characteristic equation for the system of Figure 5.1 can then be written as follows:

$$T_m T_I T_\mu s^3 + T_m T_I s^2 + K_0 K_P T_I s + K_0 K_P = 0. \tag{5.17}$$

The stability condition for the system of Figure 5.1 is found as $T_I > T_\mu$. Thus, with fuzzy tuning the overall system is stable if

$$T_{I,\min} > T_{\mu,\max}. \tag{5.18}$$

5.3 Cascade PI controllers with fuzzy tuning

In this section, the proposed PI controllers with fuzzy tuning are applied to flexible electromechanical structures using cascade control principles. Simulation results indicate that, with fuzzy tuning, the reference response is well-damped with adequately fast dynamics and the maximum deviation of the disturbance response is reduced even in the case of changing plant parameters. The use of cascade PI controllers with fuzzy tuning increases the capability of vibration suppression in a multi-mass system, dealing with parameter changes, load disturbance, and backlash nonlinearity.

5.3.1 Overview of cascade control

The principles of cascade control, which is quite popular in the field of electrical drives, is illustrated in Figure 5.5, where X_{1ref}, X_{2ref}, and X_{3ref} are reference inputs to the first, second, and third loop of the system, respectively. The outputs X_1, X_2, and X_3 can be the current, speed, and position in a drive system. If the plant structure is known and its parameters are invariant, the parameters of the PI- (or P-) controllers PI_1, PI_2, and PI_3 are determined by bringing the open-loop transfer functions into the approximated form (5.1), and then shaping the open-loop frequency characteristics

according to Kessler's symmetric optimum [142] or assigning the closed-loop characteristic polynomials according to a pole-placement criterion, e.g. magnitude optimum, Butterworth, or ITAE.

Consider first the symmetric optimum method. Figure 5.6 shows the desirable Bode magnitude diagram of the open-loop transfer function after shaping. The 0-*dB* crossover frequency for such a system is $\omega_c = 1/2T_\mu$, and as can be seen, two-fold symmetry about the $(1/2T_\mu,\ 0\ dB)$ point is observed, thus explaining the symmetric optimum designation. As remarked by Voda & Landau [18], the symmetric optimum also has an $H\infty$ interpretation.

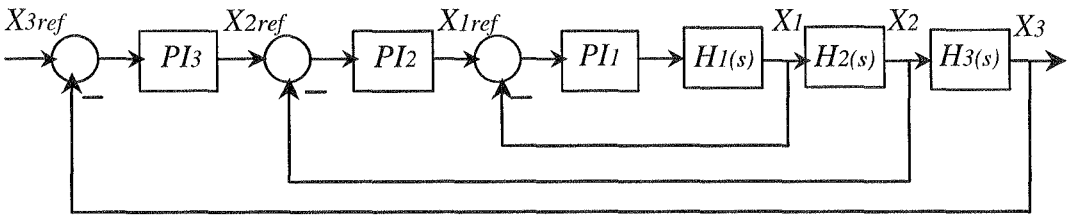

Figure 5.5. Multi-loop cascade control.

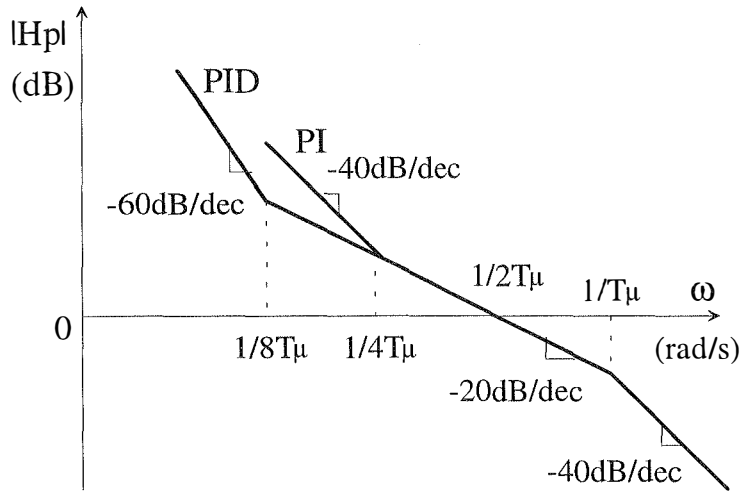

Figure 5.6. Bode plot of the open loop transfer function using symmetric optimum.

In the magnitude optimum method, the design objective is to maintain the magnitude response curve as flat as close to unity for a large bandwidth as possible (maximally

flat response), for a given plant and cascade controller combination. This is analytically interpreted as follows:

$$|M(j\omega)|^2_{\omega=0} = 1, \quad \frac{d^k}{d\omega^k}\left(|M(j\omega)|^2\right)_{\omega=0} = 0, \; k = 1,2,... \tag{5.19}$$

where $|M(j\omega)|$ is the magnitude closed-loop frequency response. Therefore, the magnitude optimum technique seeks to eliminate the sensitivity of the magnitude response to low frequencies. The final closed-loop system characteristic polynomial results in a practical form:

$$2^l T_\mu s\{...2^2 T_\mu s[2T_\mu s(T_\mu s+1)+1]+1+...\}+1, \tag{5.20}$$

where $l = 1,2,3,...$. The magnitude optimum technique only optimises the closed-loop transfer function between the reference input and the variable to be controlled, thus the system's response due to any disturbance, applied at locations other than at the reference input, is not optimal.

Two other techniques for determining the controller coefficients are the Butterworth pole assignment and ITAE methods. The Butterworth pattern is a simple-pole configuration where the n poles, s_i, $(i = 1,2,..,n)$ of the closed-loop system are equally spaced on a circle of radius ω_0 (the system bandwidth) in the left-half plane:

$$\frac{(\mathrm{Re}\, s_i)^2 + (\mathrm{Im}\, s_i)^2}{{\omega_0}^2} = 1. \tag{5.21}$$

In the ITAE method, the controller coefficients are obtained from the minimisation of

$$ITAE = \min \int_0^\infty t|e(t)|dt, \tag{5.22}$$

where $e(t) = 1 - x(t)$ is the control error, and $x(t)$ is the control output. Appendix A provides a summary of the normalised characteristic polynomials corresponding to these methods.

The design with cascade control is quite simple but it has the drawback that the possibility of any disturbances to the system such as a load torque is ignored and the approximation (5.1) is not applicable in the presence of uncertainties such as

parameter variations or nonlinearities. It is believed that using the proposed PI-controllers with fuzzy tuning can improve robustness of cascade control systems. In the following section, a flexible structure system with backlash nonlinearity combined with the gear torsion is used for simulation.

5.3.2 Application to a two-mass servo drive

Consider the speed control of a two-mass servo system of Figure 3.3, reported in Ha *et al.* [38]. In order to suppress vibration and reject load disturbance in flexible structure systems, observer-based state feedback techniques with feedforward compensation have been demonstrated to have significant advantages in comparison with the conventional PI controllers (Hori *et al.* [64] or Ha & Negnevitsky [43]. This problem is addressed here by using the proposed PI-controllers with fuzzy tuning designed with the principles of magnitude optimum cascade control. Figure 5.7 shows the system block diagram with a PI-controller in the current loop and a P-controller in the speed loop.

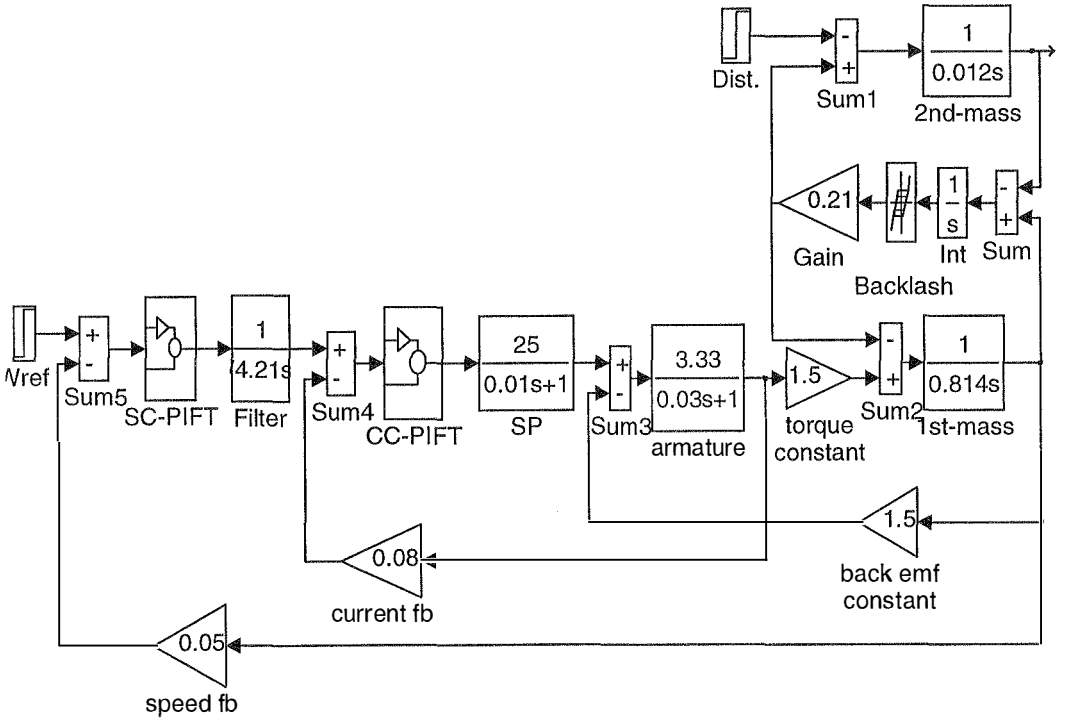

Figure 5.7. Two-mass servo system with fuzzy-tuned PI controllers.

Figure 5.8 shows the unit step response of the system without tuning (Figure 5.8(a)) and with fuzzy tuning (Figure 5.8(b)) when the load inertia increases to 500% ($J_2 = 5J_{2,nom}$).

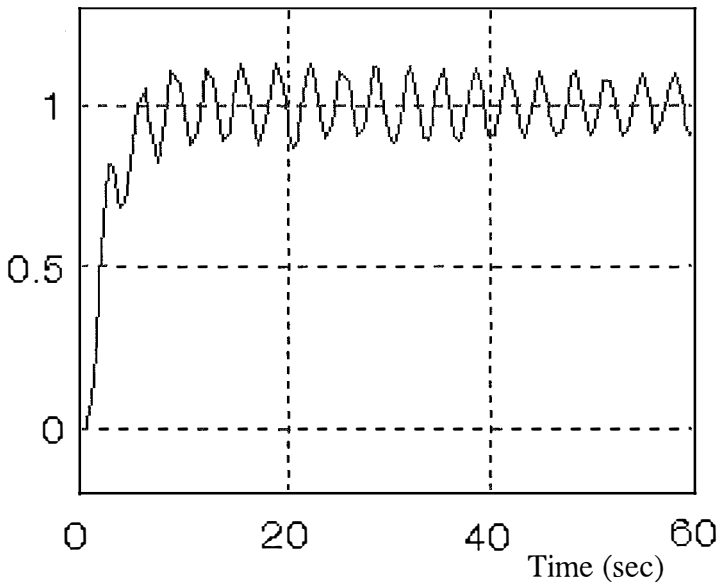

(a)

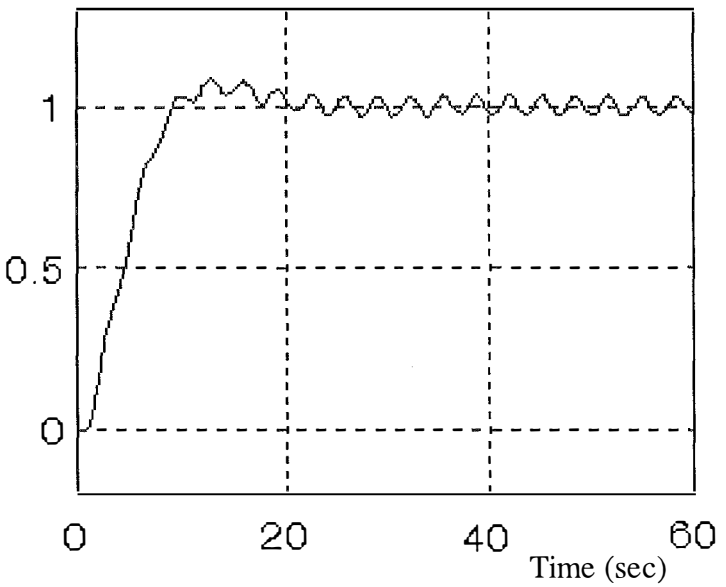

(b)

Figure 5.6. Step response $J_2 = 5J_{2,nom}$:
(a) without tuning, (b) with fuzzy tuning.

The influence of a load disturbance $T_L = T_{L,nom}$ exerted at $t = 20\,\text{sec}$ is considered in Figure 5.9.

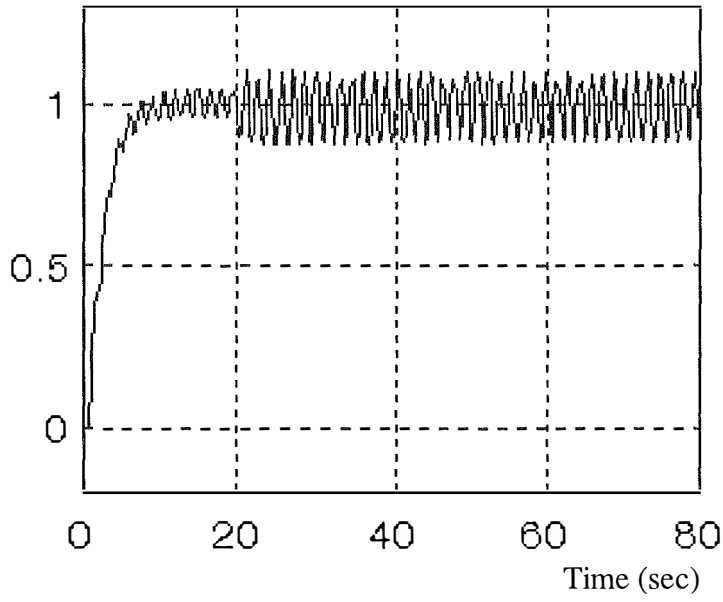

(a)

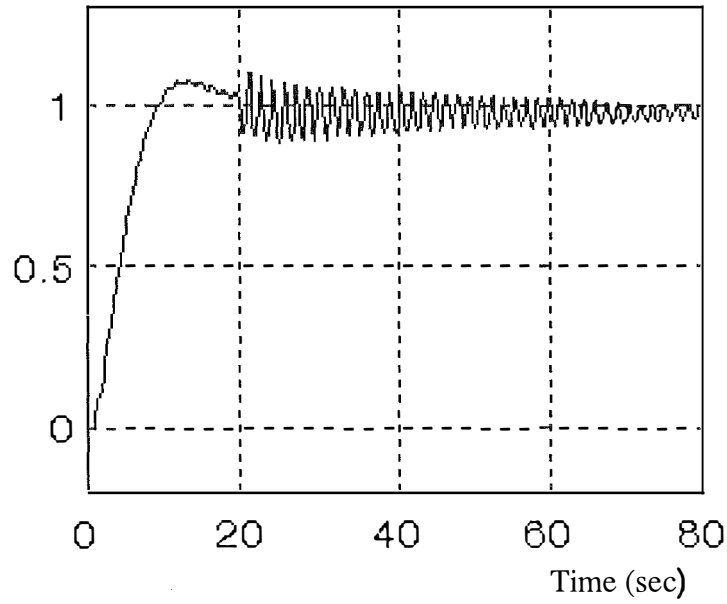

(b)

Figure 5.9. Step response $T_L = T_{L,nom}$ at $t = 20\,\text{sec}$:
(a) without tuning, (b) with fuzzy tuning.

The response with backlash of a dead-band width $2D = 0.002$ is shown in Figure 5.10.

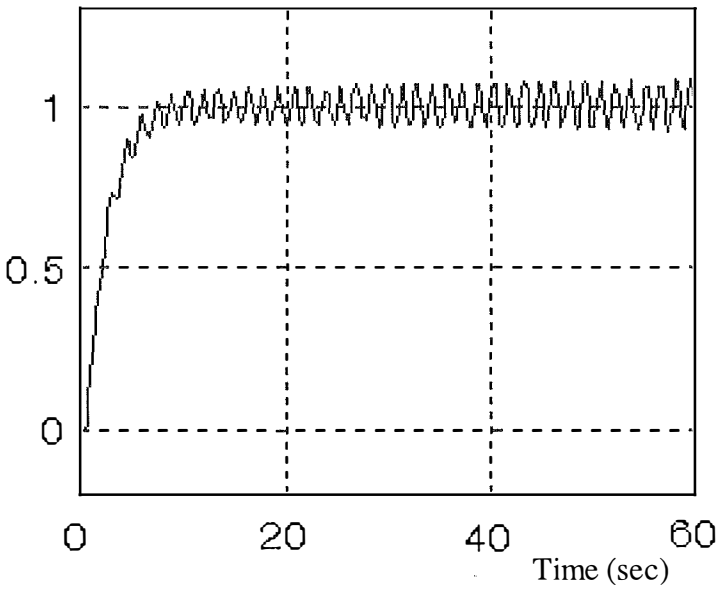

(a)

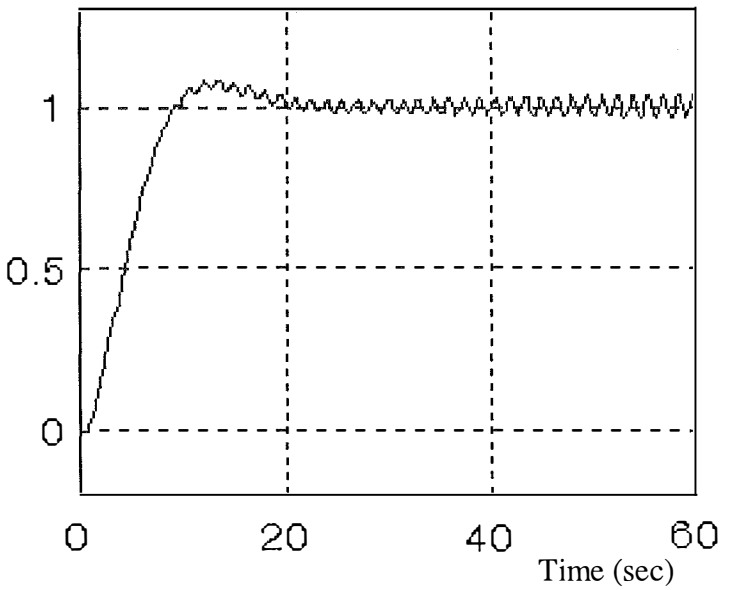

(b)

Figure 5.10. Step response with backlash $2D = 0.002$:
(a) without tuning, (b) with fuzzy tuning.

Comparing the responses in Figures 5.8, 5.9, and 5.10 demonstrates fuzzy tuning can be applied to cascade controllers in flexible electromechanical systems to increase robustness to some extent for parameter and load variations, and nonlinearities.

5.4 Sliding mode control with fuzzy tuning

Sliding mode control, based on the theory of variable structure systems, first proposed by Emelyanov [7] in 1967, has attracted a lot of research on control systems for the last two decades. The salient advantage of sliding mode control, developed by Utkin [8], is the robust property against structured and unstructured uncertainties. The main drawback of sliding mode control is the associated undesirable chattering problem which can excite high frequency unmodelled dynamics. Several methods to reduce this chattering have been reported, e.g. using a boundary layer in the sliding mode as in Stoline & Sastry [152] and Spurgeon [153], or a continuous sliding mode control strategy as in Zhou & Fisher [154] and Nguyen & Nguyen [155]. The first approach provides no guarantee for the exact convergence to the sliding mode while the second tends to produce conservative designs and there is a trade-off between chattering and robustness. Another method for reducing chattering phenomenon without the sacrifice of robust performance is to combine the attractive features of sliding mode control and fuzzy control (Lu & Cheng [156] and Wang *et al.* [157]).

Fuzzy logic has been proven to be a vigorous tool in ill-defined or parameter-variant plants. Employing expert's engineering heuristics, a fuzzy logic controller can cope well with severe uncertainties, however it may suffer from a heavy computational burden when implemented. Fuzzy tuning with explicit tuners for the controller parameters can avoid this problem as shown above.

In this section a new technique is presented for linearised systems with uncertainties using sliding mode control with an additional fuzzy-tuned component to the control action. The reaching condition in the vicinity of the hyperplane is guaranteed by the Lyapunov stability method. For accelerating the state trajectories to reach the sliding hyperplane and compensating for the influence of unmodelled dynamics and chattering, fuzzy tuning schemes are introduced to continuously change the control action. Simulation results for a two-mass servo drive demonstrate robust performance in the presence of parameter and load variations, and backlash nonlinearity.

The linearised model of a dynamic system can be written as:

$$\dot{\mathbf{x}} = (\mathbf{A} + \Delta\mathbf{A})\mathbf{x} + (\mathbf{b} + \Delta\mathbf{b})u, \tag{5.23}$$

where $\mathbf{x} \in R^n$ is the state vector, $u \in R$ is the control signal, $\mathbf{A} \in R^{n\times n}$ and $\mathbf{b} \in R^n$ are the nominal system matrices, and $\Delta\mathbf{A}$ and $\Delta\mathbf{b}$ are uncertainties. The following assumptions are made (Ha *et al.* [22]):

A1. The uncertainties are continuous matrix functions of the vector of varying system parameters, $\mathbf{p} \in \mathcal{P} \subset R^p$, where $\mathcal{P}$ is a compact set:

$$\Delta\mathbf{A} = \Delta\mathbf{A}(\mathbf{p}), \quad \Delta\mathbf{b} = \Delta\mathbf{b}(\mathbf{p}). \tag{5.24}$$

A2. There exist a vector $\mathbf{r}(\mathbf{p}) \in R^n$ and a scalar $h(\mathbf{p})$ such that the following matching conditions are satisfied:

$$\begin{aligned} \Delta\mathbf{A} = \mathbf{b}\mathbf{r}^T(\mathbf{p}) \ \text{ and } \ \max\{|r_i(\mathbf{p})|\} \le \rho, \ \forall \mathbf{p} \in \mathcal{P}, \\ \Delta\mathbf{b} = \mathbf{b}h(\mathbf{p}) \ \text{ and } \ |h(\mathbf{p})| \le \sigma < 1, \ \forall \mathbf{p} \in \mathcal{P}. \end{aligned} \tag{5.25}$$

The objective is to design a controller that provides robust performance in the presence of uncertainties (5.24) given their bounds ρ and σ. In this approach, the control law is written as:

$$u = u_{eq} + u_r + u_{ft} = -(\mathbf{k}_e^T + \mathbf{k}_r^T)\mathbf{x} + u_{ft}, \tag{5.26}$$

where u_{eq}, u_r, and u_{ft} are the control signals for the equivalent motion, reaching phase with respect to uncertainties (5.24), and fuzzy tuning to improve control performance, respectively. The control gains $\mathbf{k}_e^T$ and $\mathbf{k}_r^T$, and the fuzzy control signal u_{ft} will be determined in the following.

5.4.1. Robust controller with sliding mode

A sliding-mode controller normally consists of two distinct operating modes: reaching and sliding. Let us define a switching hyperplane variable:

$$S(\mathbf{x}) = \mathbf{c}^T\mathbf{x} = \sum_{i=1}^{n} c_i x_i, \quad (c_n = 1), \tag{5.27}$$

and the sliding mode

$$S(\mathbf{x}) = 0 \text{ or } \mathbf{c}^T\mathbf{x} = 0. \tag{5.28}$$

By properly choosing the parameters c_i $(i = 1,2,...,n)$, the desired dynamics of the closed-loop system can be described by the sliding equation (5.28). Generally, a sliding mode controller is designed in the sense that, for any initial state $\mathbf{x}_0 = \mathbf{x}(t_0)$ in S, the system state $\mathbf{x}(t)$ can remain in S for all $t > t_0$. If $\mathbf{x}_0$ is not in S, the controller can drive the system state $\mathbf{x}(t)$ to the sliding mode $S(\mathbf{x}) = 0$.

A. The equivalent gain and sliding surface

In the sliding mode $S(\mathbf{x}) = 0$, a necessary condition for the state trajectory to stay on this hyperplane is $\dot{S}(\mathbf{x}) = 0$ or:

$$\mathbf{c}^T\dot{\mathbf{x}} = \mathbf{c}^T(\mathbf{A}\mathbf{x} + \mathbf{b}u_{eq}) = (\mathbf{c}^T\mathbf{A} - \mathbf{c}^T\mathbf{b}\mathbf{k}_e^T)\mathbf{x} = 0. \tag{5.29}$$

The equivalent feedback gain, $\mathbf{k}_e^T$, can then be expressed as:

$$\mathbf{k}_e^T = (\mathbf{c}^T\mathbf{b})^{-1}\mathbf{c}^T\mathbf{A}, \tag{5.30}$$

where the existence of the inverse of $\mathbf{c}^T\mathbf{b}$ is a necessary condition. Note that the closed-loop system eigenstructure includes $(n-1)$ sliding eigenvalues λ_i $(i = 1,2,...,n-1)$, and an eigenvalue at the origin of the complex plane $\lambda_n = 0$ generated from the condition $S(\mathbf{x}) = 0$. Thus, the equivalent feedback gain $\mathbf{k}_e^T$ can be determined by a pole placement technique to assign the desired roots λ_i $(i = 1,2,...,n)$ to the characteristic equation:

$$\left|\lambda\mathbf{I} - \mathbf{A} + \mathbf{b}\mathbf{k}_e^T\right| = 0. \tag{5.31}$$

Vector $\mathbf{c}$ in the sliding surface definition (5.28) can then be derived from (5.30):

$$(\mathbf{A} - \mathbf{b}\mathbf{k}_e^T)^T\mathbf{c} = \mathbf{0}, \tag{5.32}$$

where the condition $(c_n = 1)$ in (5.27) is applied to obtain a possible solution for the singular equation (5.32).

B. The switching gain in reaching mode

Any variations from the nominal system may result in a deviation of the representative point from the sliding surface. A robust feedback with the switching gain, $\mathbf{k}_r^T$, is developed to meet the reaching condition under which the system state is driven to reach the sliding surface.

Theorem 5.1: (Ha [148]) Consider the linearised system with uncertainties (5.23) satisfying the assumptions A1 and A2. If the robust sliding-mode controller is designed such that

$$u = u_{eq} + u_r = -(\mathbf{k}_e^T + \mathbf{k}_r^T)\mathbf{x}, \tag{5.33}$$

where $\mathbf{k}_e^T$ is the equivalent gain given in (5.30), and $\mathbf{k}_r^T$ is the robust gain to deal with the system uncertainties, whose i -th element is given by:

$$k_{r,i} = \frac{\rho + |k_{e,i}|\sigma}{1-\sigma} sgn(\mathbf{c}^T\mathbf{b}x_i S), \ (i = 1,2,...,n), \tag{5.34}$$

then the state vector $\mathbf{x}(t)$ asymptotically converges to zero.

Proof: Let us define a positive definite Lyapunov function $V = \frac{1}{2}S^2$. For the occurrence of sliding motion, the trajectories in the neighbourhood of $S = 0$ must be directed towards the mode of

$$\lim_{S \to 0} \dot{V} \le 0.$$

From (5.23), (5.28), (5.29) and (5.33), we have

$$\begin{aligned}
\dot{S} &= \mathbf{c}^T\dot{\mathbf{x}} = \mathbf{c}^T[(\mathbf{A} + \Delta\mathbf{A})\mathbf{x} + (\mathbf{b} + \Delta\mathbf{b})(-\mathbf{k}_e^T\mathbf{x} - \mathbf{k}_r^T\mathbf{x})] \\
&= \mathbf{c}^T\Delta\mathbf{A}\mathbf{x} - \mathbf{c}^T\mathbf{b}\mathbf{k}_r^T\mathbf{x} - \mathbf{c}^T\Delta\mathbf{b}\mathbf{k}_r^T\mathbf{x} - \mathbf{c}^T\Delta\mathbf{b}\mathbf{k}_e^T\mathbf{x} \\
&= \mathbf{c}^T\mathbf{b}[\mathbf{r}^T(\mathbf{p}) - (1 + h(\mathbf{p}))\mathbf{k}_r^T - h(\mathbf{p})\mathbf{k}_e^T]\mathbf{x}
\end{aligned}$$

Thus, the first order derivative of the Lyapunov function can be expressed as:

$$\dot{V} = \dot{S}S = \mathbf{c}^T\mathbf{b}[\mathbf{r}^T(\mathbf{p}) - (1 + h(\mathbf{p}))\mathbf{k}_r^T - h(\mathbf{p})\mathbf{k}_e^T]\mathbf{x}S$$

or

$$\dot{V} = \sum_{i=1}^{n} [r_i - (1+h)k_{r,i} - hk_{e,i}](\mathbf{c}^T\mathbf{b})x_i S.$$

The condition $\lim_{S\to 0} \dot{V} \le 0$ will hold if each term of the sum above is non-positive. Consider first the case $(\mathbf{c}^T\mathbf{b})x_i S > 0$. From (5.25) we have:

$$r_i - (1+h)k_{r,i} - hk_{e,i} \le 0, \ \forall \mathbf{p} \in \mathcal{P} \ \text{ if}$$

$$k_{r,i} \ge \frac{r_i - hk_{e,i}}{1+h}, \ \forall \mathbf{p} \in \mathcal{P}, \text{ or } k_{r,i} \ge \frac{\rho + \sigma|k_{e,i}|}{1-\sigma}.$$

Similarly, when $(\mathbf{c}^T\mathbf{b})x_i S < 0$, we obtain:

$$r_i - (1+h)k_{r,i} - hk_{e,i} \ge 0, \ \forall \mathbf{p} \in \mathcal{P} \ \text{ if}$$

$$k_{r,i} \le \frac{r_i - hk_{e,i}}{1+h}, \ \forall \mathbf{p} \in \mathcal{P}, \text{ or } k_{r,i} \le \frac{-\rho - \sigma|k_{e,i}|}{1-\sigma}.$$

In the case $(\mathbf{c}^T\mathbf{b})x_i S = 0$, the value of $k_{r,i}$ can be chosen to be 0.

In summary, the switching gain can be written as

$$k_{r,i} = \frac{\rho + |k_{e,i}|\sigma}{1-\sigma} sgn(\mathbf{c}^T\mathbf{b}x_i S) \quad (i = 1,2,\ldots,n),$$

where $sgn(x) = \begin{cases} 1, & x > 0 \\ 0, & x = 0 \\ -1, & x < 0 \end{cases}$. This concludes the proof.

Hence, based on the bounds of uncertain plant parameters, the existence and hitting conditions of a robust sliding regime are derived and the switching gain is determined as in (5.34).

5.4.2. Performance enhancement with fuzzy tuning

In order to accelerate the reaching phase and reduce chattering while maintaining sliding behaviour, an additional control signal, u_{ft}, is introduced:

$$u = u_{eq} + u_r + u_{ft}. \tag{5.35}$$

This signal is continuously adjusted by the use of fuzzy logic, depending on S defined in (5.26) and $\dot{S}$ (Hwang & Lin [158]). From empirical knowledge in the design of sliding mode controllers, a large switching gain will force the state trajectories to approach the sliding surface rapidly, but at the same time, tend to excite chattering. Thus, when the state trajectories are far from the sliding hyperplane, i.e. when the value of $|S|$ is large, the switching gain should be correspondingly increased and vice versa. Furthermore, when the state trajectories are deviating from the sliding surface ($\dot{S}S > 0$), if $|\dot{S}|$ is large the switching gain should be increased to force the trajectories back, and vice versa. When the state trajectories are approaching the sliding surface ($\dot{S}S < 0$), if $|\dot{S}|$ is large the switching gain should be decreased in order to reduce chattering, and vice versa. Using simple fuzzy labels *large* and *small* for the scaled modulus of S and $\dot{S}$:

$$S_* = \frac{|S|}{\sum_{i=1}^{n} |c_i x_i|}, \quad \dot{S}_* = \begin{cases} sgn(-S^{k-1}), \text{ if } S^k = 0 \\ sat(\dfrac{S^k - S^{k-1}}{S^k}), \text{ if } S^k \neq 0 \end{cases}, \tag{5.36}$$

where $sat(x) = \begin{cases} sgn(x), & |x| > 1 \\ x, & |x| < 1 \end{cases}$, S^k is the value of S at $t = kT$, T is the sampling period, the following exponential membership functions are defined (Ha [148]):

$$\begin{aligned} \mu_{S\_large} &= 1 - \exp(-\frac{S_*}{\sigma_S}), \ \mu_{S\_small} = \exp(-\frac{S_*}{\sigma_S}), \\ \mu_{\dot{S}\_large} &= 1 - \exp(-\frac{\dot{S}_*}{\sigma_{\dot{S}}}), \ \mu_{\dot{S}\_small} = \exp(-\frac{\dot{S}_*}{\sigma_{\dot{S}}}), \end{aligned} \tag{5.37}$$

where σ_S and $\sigma_{\dot{S}}$ are some positive constants. Based on the above discussed heuristics, the following fuzzy rules are proposed:

(i) *If* S_* *is large, then* w_S *is large,*
(ii) *If* S_* *is small, then* w_S *is small,*
(iii) *If* $\dot{S}S > 0$ *and* $\dot{S}_*$ *is large, then* u_{ft} *is large,*
(iv) *If* $\dot{S}S > 0$ *and* $\dot{S}_*$ *is small, then* u_{ft} *is small,*
(v) *If* $\dot{S}S < 0$ *and* $\dot{S}_*$ *is large, then* u_{ft} *is small,*
(vi) *If* $\dot{S}S < 0$ *and* $\dot{S}_*$ *is small, then* u_{ft} *is large,*

where w_S is a weighting factor depending on S. Singletons are defined as membership functions for u_{ft} and w_S:

$$\mu_{u\_large} = \begin{cases} 1, & u_{ft} = w_s \\ 0, & u_{ft} \neq w_s \end{cases}, \mu_{u\_small} = \begin{cases} 1, & u_{ft} = 0 \\ 0, & u_{ft} \neq 0 \end{cases},$$
$$\mu_{w_s\_large} = \begin{cases} 1, & w_s = w_0 \\ 0, & w_s \neq w_0 \end{cases}, \mu_{w_s\_small} = \begin{cases} 1, & w_s = 0 \\ 0, & w_s \neq 0 \end{cases}, \tag{5.38}$$

where w_0 is some scaling factor. Using the centroid defuzzification method for fuzzy schemes (iii)-(vi) we obtain:

$$u_{ft} = \frac{\mu_{\dot{S}\_large} w_s + \mu_{\dot{S}\_small} 0}{\mu_{\dot{S}\_large} + \mu_{\dot{S}\_small}} = w_s (1 - \exp(-\frac{\dot{S}_*}{\sigma_{\dot{S}}})), \quad \dot{S}S > 0$$
$$u_{ft} = \frac{\mu_{\dot{S}\_large} 0 + \mu_{\dot{S}\_small} w_s}{\mu_{\dot{S}\_large} + \mu_{\dot{S}\_small}} = w_s \exp(-\frac{\dot{S}_*}{\sigma_{\dot{S}}})), \quad \dot{S}S < 0 \tag{5.39}$$

where the weighting factor w_S can be obtained by defuzzifying the schemes (i)-(ii) as follows:

$$w_S = \frac{\mu_{S\_large} w_0 + \mu_{S\_small} 0}{\mu_{S\_large} + \mu_{S\_small}} = w_0 (1 - \exp(-\frac{S_*}{\sigma_S})). \tag{5.40}$$

From (39) and (40) the fuzzy control signal u_{ft} can be written as:

$$u_{ft} = \begin{cases} w_0 (1 - \exp(-\frac{S_*}{\sigma_S}))(1 - \exp(-\frac{\dot{S}_*}{\sigma_{\dot{S}}})), & \dot{S}S > 0 \\ w_0 (1 - \exp(-\frac{S_*}{\sigma_S})) \exp(-\frac{\dot{S}_*}{\sigma_{\dot{S}}}), & \dot{S}S < 0 \end{cases} \tag{5.41}$$

where w_0, σ_S and $\sigma_{\dot{S}}$ are three parameters of the tuner.

As an illustrative example, the proposed technique is applied to the design of a robust controller for a two-mass servo drive system with backlash nonlinearity in the

coupling shaft gear (Ha *et al.* [22]). The plant model and specifications were given in Figure 5.7. The linearised state model of the plant can be written as:

$$\begin{bmatrix} T_m \\ \omega_1 \\ T_{12} \\ \omega_2 \end{bmatrix} = \begin{bmatrix} -33.3 & -\alpha & 0 & 0 \\ 1.23 & 0 & 1.23 & 0 \\ 0 & 0.21 & 0 & -0.21 \\ 0 & 0 & 83.3 & 0 \end{bmatrix} \begin{bmatrix} T_m \\ \omega_1 \\ T_{12} \\ \omega_2 \end{bmatrix} + \begin{bmatrix} \alpha \\ 0 \\ 0 \\ 0 \end{bmatrix} \omega_{ref} + \begin{bmatrix} 0 \\ 0 \\ 0 \\ -83.3 \end{bmatrix} T_L$$

where T_m, ω_1, T_{12} and ω_2 are the motor torque, motor speed, elastic torque and load speed, respectively, ω_{ref} and T_L are the reference input and external load torque, $\alpha = 237.3 \pm 118.7$ is an uncertain element depending on the stiffness of the drive speed-torque characteristics. The hyperplane eigenvalues are chosen to be $\lambda_{1,2,3} = [-11 \ -11 \ -11]$. The equivalent feedback gain obtained by a pole placement technique is found to be $\mathbf{k}_{eq}^T = [-0.0074 \ \ 0.0789 \ \ 9.8844 \ \ -1.0789]$. The parameters for the sliding surface are obtained from (5.32) as $\mathbf{c}^T = [0.035 \ \ 0.924 \ \ 44.843 \ \ 1]$. The switching gain $\mathbf{k}_r^T$ is calculated from (5.34) and the tuner parameters are chosen to be $w_0 = 6$, $\sigma_S = 0.5$, and $\sigma_{\dot{S}} = 0.01$. The step response of the load speed as the system output is shown in Figures 5.11, 5.12, and 5.13 for the cases of a constant load torque T_L exerted at $t = 5\,\text{sec}$, backlash with a deadband width of $2D = 0.03$, and a 50% reduction of the drive stiffness with $2D = 0.01$ and a load torque, respectively. It is observed that sliding mode control can cope well with nonlinearity and parameter variation, but cannot achieve load-insensitivity.

Comparing with the responses obtained by pole placement (Figures 5.13(a)), sliding mode control without tuning (Figure 5.13(b)) indicates that an additional fuzzy tuner inherently improves system robustness against load torque disturbance (Figures 5.13(c)) without the sacrifice of good sliding behaviour.

5.5 Summary and further discussion

In this chapter, simple fuzzy tuning schemes are introduced to continuously change the controller parameters or the control action in order to enhance robustness. The gain and time constant of a conventional PI controller are made continuously changed by some exponential functions, resulting from some engineering heuristics with the use of fuzzy logic. System robustness is verified through high performance of transient responses in changing environment conditions. Explicit expressions for the controller parameters facilitate the tuning process at a low computational cost.

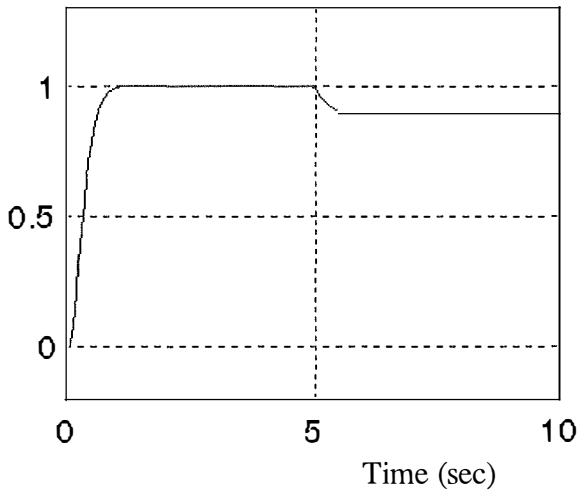

(a)

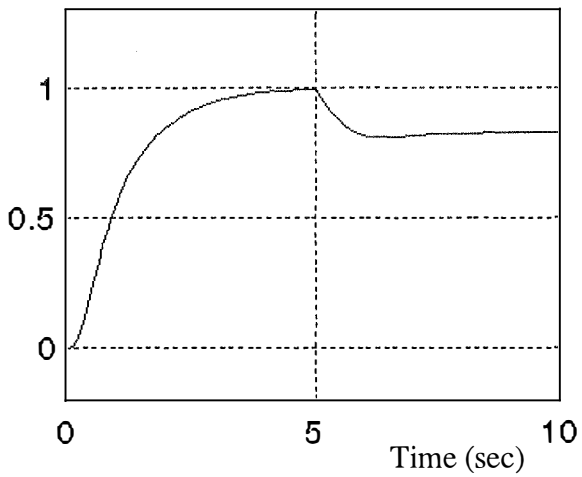

(b)

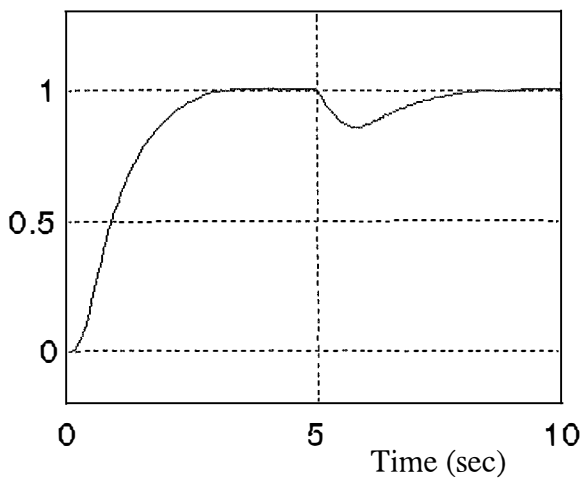

(c)

Figure 5.11. Step response with a load torque exerted at $t = 5\,\text{sec}$.

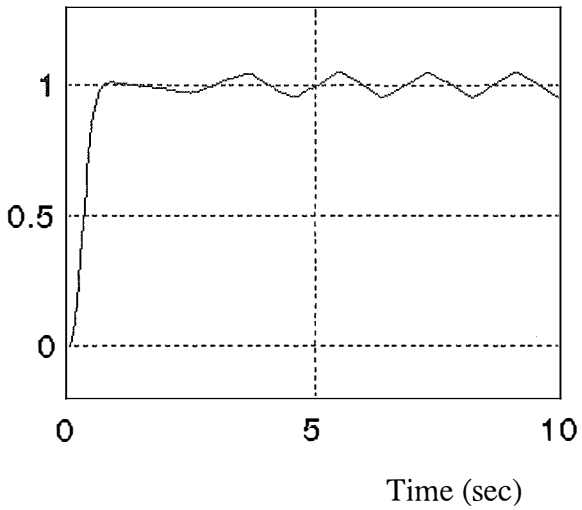

(a)

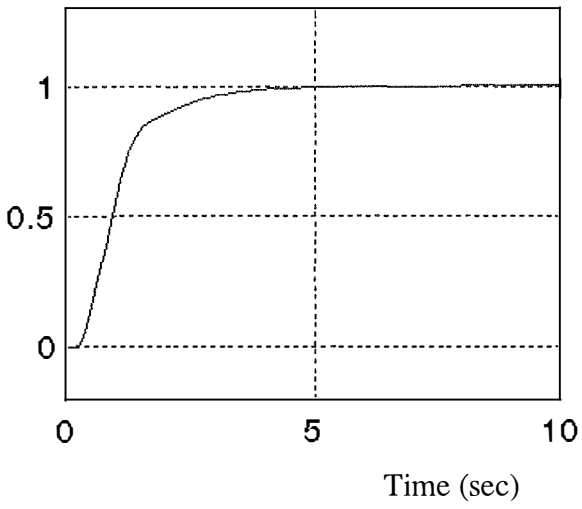

(b)

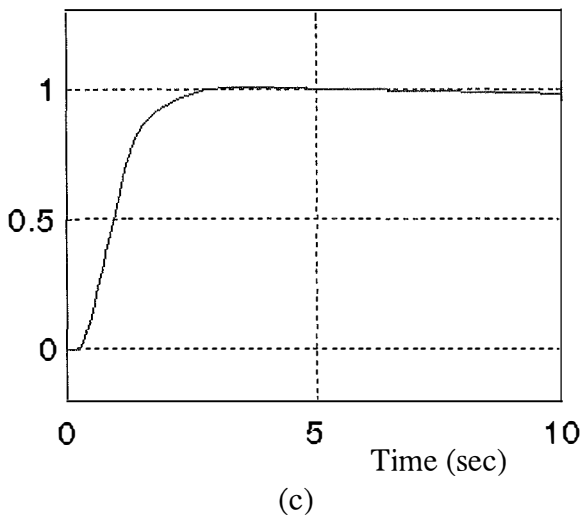

(c)

Figure 5.12. Step response with backlash $2D = 0.03$.

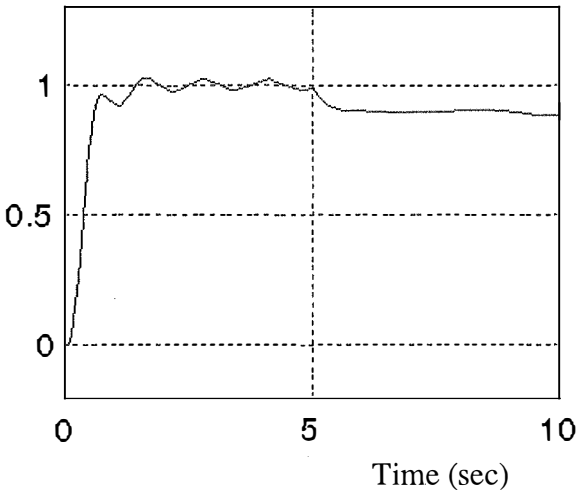

(a)

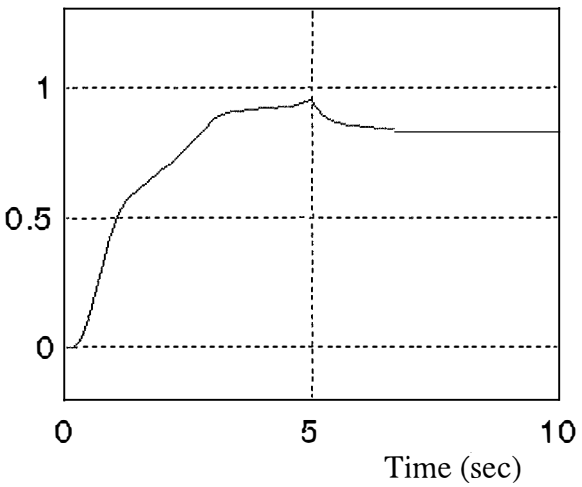

(b)

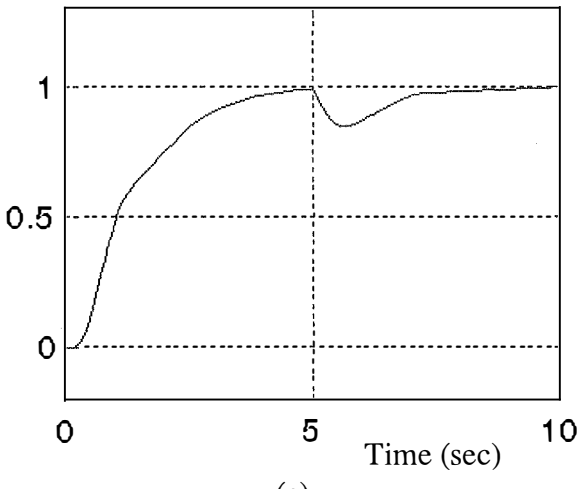

(c)

Figure 5.13. Step response with a 50% reduction of the drive stiffness with $2D = 0.01$ and a load torque.

The results can be extended to multi-loop cascade control. In each loop, a PI controller with fuzzy tuning is used instead of a conventional one. Simulation results in a two-mass system indicate that fuzzy tuning can be applied to cascade controllers in flexible electromechanical systems to increase robustness to some extent for parameter and load variations, and nonlinearities.

In Section 5.4, fuzzy schemes are applied to tune not the controller parameters but the control action itself to deal with unmodelled dynamics in sliding mode control. This technique combines the features of sliding mode control and fuzzy control. First, the equivalent motion is determined from the desired sliding eigenstructure. The reaching condition in the neighbourhood of the sliding surface is satisfied by the use of a switching gain based on the Lyapunov stability theory. Fuzzy tuning schemes are then employed to accelerate the reaching phase, reduce chattering, and hence, improve robust performance. The proposed technique can be applied to the control of a elastic drive system. Simulation results in a servo two-mass drive demonstrate its validity. Again, the explicit expressions for fuzzy schemes facilitate the computational implementation of the proposed controller.

Fuzzy tuning of the PI controller parameters has demonstrated the capability of improving system robustness to parameter and load variations, and nonlinearities in motion control systems. Moreover, windup is an inherent problem that should be taken into account due to integrator saturation, especially in process control. In order to cope with these types of nonlinearites the design method should be adjusted with some ad hoc fix anti-windup. This anti-windup is normally designed to prevent the integrator state in the controller to become too large. The idea is to decrease the rate of change of the integrator state when the control error is large for a longer period of time. Utilising not only the control error but also the control signal saturation, Hansson *et al.* [160] proposed anti-windup schemes with fuzzy tuning for controllers applied in the control of a double tank. Fuzzy tuning may also be implemented in other control strategies with the purpose of robustness enhancement. In particular, proportional-derivative (PD) controllers provide high sensitivity and tend to increase the stability of overall feedback control system. In addition, PD controllers can reduce overshoot and increase damping capability of the system. It has been proven that a PD controller can show its effectiveness in low-order systems, but usually can hardly be suitable for higher-order and nonlinear systems. Malki *et al.* [159] demonstrate that fuzzy PD controllers, where the control output depends on the error and its derivative

as in (4.45), have some remarkable advantages over conventional one. It is worth to elaborate on some fuzzy tuning schemes to extend the application of PD controllers to high order systems and improve robust performance in the comparison with conventional PD controllers.

While sliding mode control guarantees system invariance under parameter variations, it has one major disadvantage - unmodelled dynamics or chattering. In most industrial applications, the ideal sliding mode is smoothed by introducing a bounder layer containing the sliding hyperplane. Thus, "soft" sliding control with a boundary layer (Stoline & Li [161]) leads to the possibility of selecting the layer thickness which can be tuned experimentally, based on engineering experience and judgment. This justifies the use of an additional component in the control law (5.35). Further research in sliding mode control with fuzzy tuning may result in a simpler control law consisting of two signals or even one signal because, essentially, fuzzy logic control is also a variable structure system (Yager & Filev [130]).

Conventional proportional-integral-derivative (PID) controllers in various combinations have been widely used for industrial processes due to their simplicity and effectiveness for linear systems. Thus it is of importance to have good tuning algorithms for these controllers. Scaling factors for the controller parameters can be introduced and rules can be derived to update these factors, in dependence on the performance of the closed loop system, and utilising the known strategies for tuning PID controller parameters. In general, the criteria for tuning are based on the values of the transient response overshoot, settling time, and amplitude of oscillation. For example, a prototype rule set for tuning PI controller parameters are given in Section 5.2. It is straightforward to extend the approach to other conventional controllers. In the following chapter it is applied to robust modal control described in Chapter 3.

Chapter 6

Robust Modal Control with Fuzzy Tuning

In Chapter 3, robust modal control has demonstrated the capability of providing high performance response for electromechanical systems with flexible structures. However, the observer and feedforward compensator are designed on the basis of system nominal parameters. Consequently, parametric robustness of the whole system has not completely achieved. This chapter employs tuning schemes, heuristically inferred with fuzzy logic, to improve invariant performance of robust modal controllers.

6.1 Introduction

In high performance position drive applications, it is required to develop a controller that can provide high positioning accuracy, fast dynamic response and insensitivity to any perturbations, such as load torque disturbance, parameter variations, nonlinear friction, etc. A great majority of position drives in industry utilise DC-motors with a cascade controller consisting of a PI-current controller loop, a PID-velocity controller loop and a P- (or PI-) position controller loop. Although cascade control design is simple and straightforward, there are trade-offs in achieving all the performance requirements. The adaptive controller is effective in drive systems with an uncertain parameter model but it gives undesirable responses (Dote [65]). The variable structure system control is insensitive to variations of the drive system but chattering phenomenon is a problem and in some cases the sliding mode does not exist (Furuta [71]). There have been many formalised approaches to improve robustness of position drive system [162, 78, 64, 19]. The robust model matching principle in Eisaka *et al.* [162] is based on zeroing the transfer function from the equivalent disturbances to the controlled output. The feedforward compensation is used in Ko *et al.* [78] and Hori *et al.* [64] to provide quick and effective results for reduction of motor speed fluctuation

due to load variations. However, the parameter-insensitivity of the overall drive system has not been considered.

Robust modal control has been elaborated (Chapter 3) to improve the performance of the system subject to both load and parameter variations. The modal controller applies full state feedback from the drive state variables. A predictive observer (Alferov & Ha [73]) is used to estimate simultaneously the external disturbance and the states not directly measurable. To obtain load-insensitivity, the modal control signal is feedforward compensated from the estimated disturbance. To deal with the problem of parameter variation, a robust control signal is added to the modal control signal. The asymptotic stability of the overall system with parameter uncertainty is guaranteed by the second method of Lyapunov. While robust modal control can give desirable dynamic and static performance of the drive system in the presence of load disturbance, the observer is still sensitive to parameter variation and the step response rise time at nominal parameters is slightly slower than the rise time in standard modal control. This can be explained by the fact that all the controller coefficients were set constant (see, e.g. Ha & Alferov [19]). This chapter focuses on using fuzzy logic schemes to tune the observer predictive coefficients, the feedforward gain and the robust feedback gain. As described in Chapter 4, fuzzy logic control has recently arisen as a powerful approach to deal with uncertainty. Tuning the controller coefficients to achieve robust tracking is non-trivial. The simulation results indicate that by fuzzy tuning the controller coefficients, the drive system is made more robust to load and parameter variations without loss of performance at the system's nominal parameters. Exponential, sigmoidal, and Gaussian can be used for membership functions in fuzzy rule set. The material of this chapter is based mainly on the studies by Ha [39, 40], Ha & Negnevitsky [21, 37, 41, 42, 43], and Ha & Palis [163].

6.2 Digital predictive observer with fuzzy tuning

In robust modal control, it is required to estimate the state variables that are not directly measurable for state feedback, as well as the unknown inputs for their compensation. such as load torque also needs to be estimated for rejection purposes in order to increase the system robustness. Designing observers that are capable of simultaneously estimating state variables and unknown inputs becomes of interest. In Park & Stein [97], the state equation is transformed into a special system model for a reduced-order observer. The design procedure in Alferov & Ha [73] is straightforward

with the introduction of a predictive coefficient to approximate the unknown input. However, the predictive coefficient was set to be constant.

In this section, the proposed approach is generalised and the observer robustness is improved by tuning the predictive coefficients, taking into account the disturbance rate of change. The observer performance is verified through an illustrative example of a two-mass position drive (Ha [39]). Not restricted to motion control, the proposed observer can be applied, in terms of the estimated states, to obtain the parameter trajectories in order to detect incipient faults, as described in Ha & Negnevitsky [43].

Consider a linear time invariant dynamic system described by the following discrete-time state equation:

$$\begin{aligned} \mathbf{x}(k+1) &= \mathbf{A}\mathbf{x}(k) + \mathbf{B}\mathbf{u}(k) + \mathbf{D}\mathbf{v}(k) \\ \mathbf{y}(k) &= \mathbf{C}\mathbf{x}(k) \end{aligned}, \tag{6.1}$$

where $\mathbf{x}(k) \in R^n$ is the state vector, $\mathbf{u}(k) \in R^r$ is the control vector, $\mathbf{v}(k) \in R^q$ is the disturbance vector, and $\mathbf{y}(k) \in R^m$ is the output vector the system, respectively. The matrices $\mathbf{A} \in R^{n \times n}$, $\mathbf{B} \in R^{n \times r}$, $\mathbf{C} \in R^{m \times n}$, and $\mathbf{D} \in R^{n \times q}$ are constant matrices subject to parametric uncertainties.

Following the design approach described in Section 3.4.2, we obtain a combined observer for state and disturbance estimation with the state equation given in (3.76). The observer response depends the choice of matrix $\Gamma = diag(\gamma_{ii})$ of predictive coefficients γ_{ii}, $i = 1, 2, \ldots, q$. For given predictive coefficients $\gamma_{ii} = \gamma_{ii0}$, there usually exists a proper choice of the matrix gain $\mathbf{L}_1$, $\mathbf{L}_2$ such that desirable observer dynamics can be obtained. If the unknown inputs vary slowly with time and there is no deviation in system parameters from their nominal values, γ_{ii0} can be set equal 0. In practice, the rate of change of unknown inputs is uncertain and the system is subject to parameter variations.

Inspired by fuzzy tuning schemes discussed in Chapter 5, it is worth improving robustness the proposed observer by continuously changing the predictive coefficients. In Ha [39], γ_{ii} is made continuously changed by the use of fuzzy logic so that the approximation in Equation (6) is tuned with respect to the rate of change of v_i. Note that if modulus of the change of the estimated unknown input $\hat{v}_i$ is large, then the corresponding predictive coefficients γ_{ii} should be kept small in order to guarantee smoothness and thus, robustness. By defining

$$r_i(k) = \begin{cases} sign(-\hat{v}_i(k-1)) \text{ if } \hat{v}_i(k) = 0 \\ sat\left(\dfrac{\hat{v}_i(k) - \hat{v}_i(k-1)}{|\hat{v}_i(k)|} \right) \text{ if } \hat{v}_i(k) \neq 0 \end{cases} \tag{6.2}$$

where

$$sign(x) = \begin{cases} 1, & x > 0 \\ 0, & x = 0 \\ -1, & x < 0 \end{cases}, \text{ and } sat(x) = \begin{cases} 1, & x \geq 1 \\ x, & -1 < x < 1, \\ -1, & x \leq -1 \end{cases}$$

the following simple rules are then introduced:

if r_i is *large*, then γ_{ii} is *small.*
if r_i is *small*, then γ_{ii} is *large.*

The typical membership functions for r_i and γ_{ii} can be shown in Figure 6.1. A given value of r_i can be fuzzified as having μ_1 grade *small* and μ_2 grade *large*. The predictive coefficient γ_{ii} at the *k-th* sampling is then inferred by the well-known max-min rule and the centroid method, described in Chapter 4:

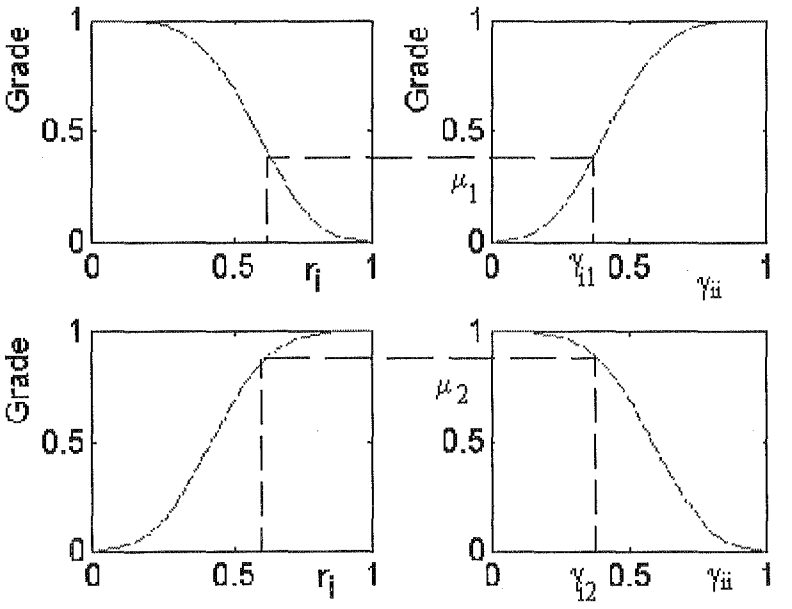

Figure 6.1. Membership functions for r_i and γ_{ii}.

$$\gamma_{ii} = \frac{\mu_1 \gamma_{i1} + \mu_2 \gamma_{i2}}{\mu_1 + \mu_2}, \tag{6.3}$$

where μ_1 and γ_{i1} (μ_2 and γ_{i2}) are the membership grade and crisp value of γ_{ii} corresponding to the fuzzy set r_i *is small* (*large*).

As scheme (ii) (see Section 5.2) is used for inferring the predictive coefficients γ_{ii}, when using exponential membership function for r_i and singleton for γ_{ii} as in (5.3) and (5.4):

$$\mu_1(r_i) = \exp(-|r_i|/\sigma_{r_i}), \quad \mu_2(X) = 1 - \exp(-|r_i|/\sigma_{r_i}), \tag{6.4a}$$

and

$$\mu_{large}(\gamma_{ii}) = \begin{cases} 1, & \gamma_{ii} = \gamma_{ii,m} \\ 0, & \gamma_{ii} \neq \gamma_{ii,m} \end{cases}, \quad \mu_{small}(\gamma_{ii}) = \begin{cases} 1, & \gamma_{ii} = 0 \\ 0, & \gamma_{ii} \neq 0 \end{cases}, \tag{6.4b}$$

the value of γ_{ii} can be obtained from (5.5) or (6.3) as in Ha & Negnevitsky [37]:

$$\gamma_{ii} = \gamma_{ii,m} \exp(-|r_i|/\sigma_{r_i}), \tag{6.5}$$

where $\gamma_{ii,m}$ and σ_{r_i} are some positive constants.

The design procedure can be included in the following steps:

Step1: Find the discrete-time state equation (6.1) describing the system with unknown inputs. Obtain the matrix blocks of the augmented form (3.75).

Step2: Choose the observer matrix gain $\mathbf{L}_1$, $\mathbf{L}_2$. For given matrix of predictive coefficients Γ_0, determine the elements l_{ij} for the observer desired dynamics.

Step3: Define membership functions for the rate of change r_i and coefficient γ_{ii}. Tune γ_{ii} in the approximation (3.74) by the defuzzification formula (6.3) of by fuzzy tuning expression (6.5).

Example 6.1: Consider again Example 3.3 of a DC motor two-mass electromechanical system of Figure 3.3. The block diagram with specifications is also in Figure 3.5. The elaboration of *Step 1* and *Step 2* is described in Example 3.3. In *Step3*, the predictive coefficient γ in the approximation

$$T_L(k+1) = (1+\gamma)T_L(k) - \gamma T_L(k-1)$$

is made changing in dependence of the normalised rate of change of estimated load torque $r(k)$ defined in (6.2). Exponential and singleton membership functions (6.4) are assigned to the rate of change $r(k)$ and γ, respectively. Thus, tuning expression for the predictive coefficient γ can be obtained from (6.5) as $\gamma = \gamma_m e^{-\sigma|r|}$, where γ_m is some constant and σ is positive. The nonlinear relationship between γ and r can be represented in Figure 6.2. The realisation schematic diagram of the proposed digital predictive observer (DPO) is presented in Figure 6.3.

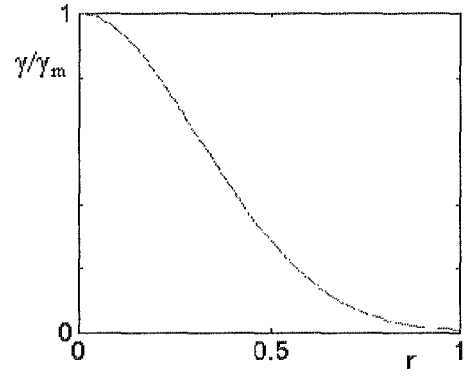

Figure 6.2. Nonlinear γ with respect to r.

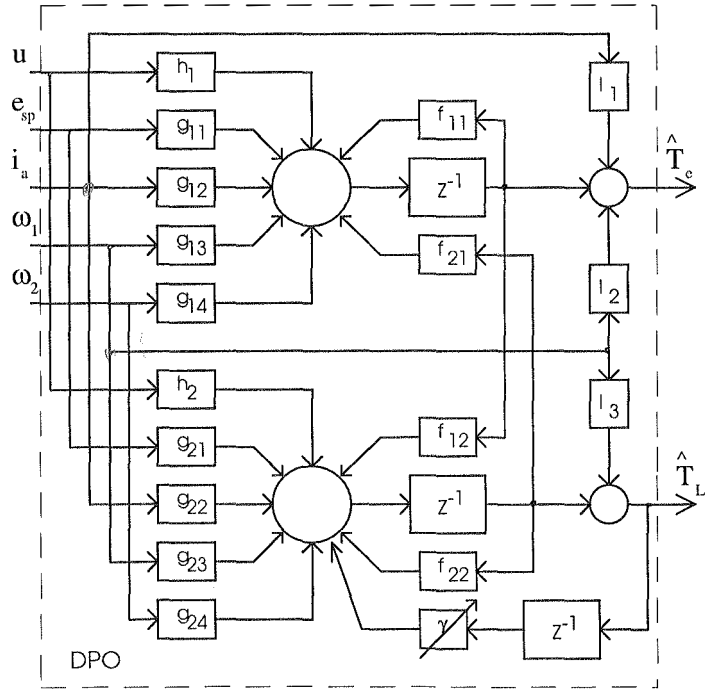

Figure 6.3. DPO schematic diagram.

To suppress elastic mechanical vibration and achieve load- and parameter-insensitivity in this system (Figure 3.5), a robust controller described in Example 3.7 is used with feedback from the measurable and estimated state variables and feedforward from the estimated load torque. With tuned predictive coefficient $\gamma = 0.5e^{-0.1r}$ (γ_m= 0.5 and σ= 0.1), Figures 6.4(a) and 6.4(b) show the actual (dotted line) and estimated (solid line) load torque when the unknown input varies stepwise and sinusoidally at nominal values of the plant parameters. The actual and estimated elastic torque are shown in Figure 6.5 when T_L varies stepwise. Note that in the simulation, the observer initial state variables are set at (1, 1) as in Example 3.3. The results indicate that the proposed digital predictive observer with fuzzy tuning is capable of producing correct estimates when the unknown input is time-varying.

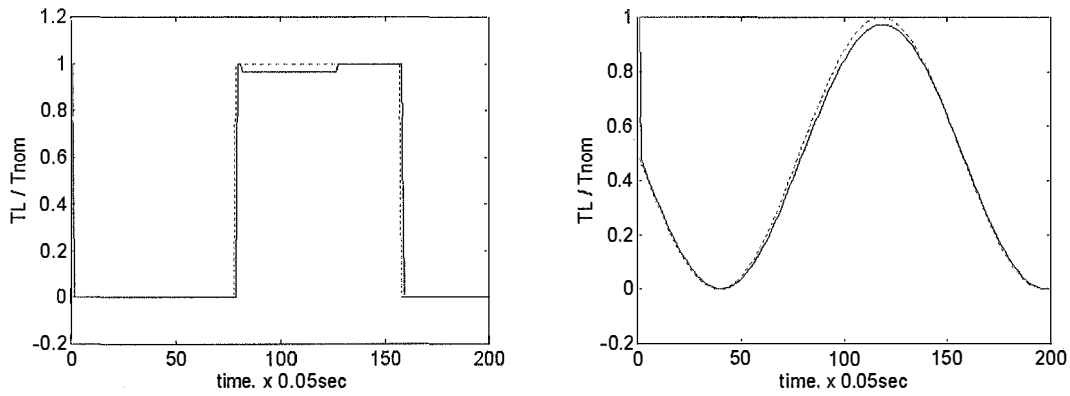

(a) (b)

Figure 6.4. Actual and estimated load torque: (a) stepwise, and (b) sinusoidal.

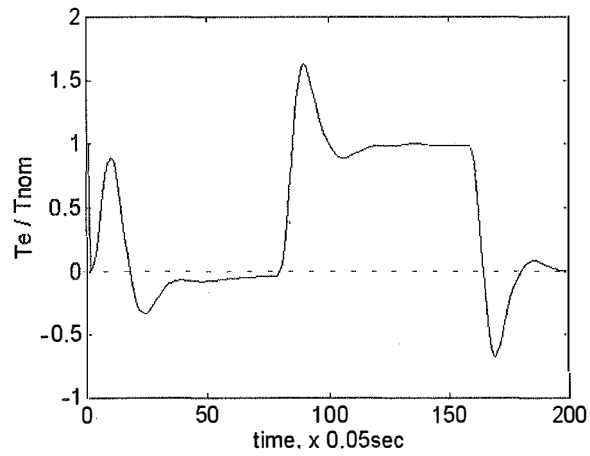

Figure 6.5. Actual and estimated elastic torque when T_L varies stepwise.

To demonstrate the observer robustness, Figure 6.6 depicts the actual and estimated load torque when the load moment of inertia J_2 increases to $J_2 = 5J_{2,nom}$ ($J_{2,nom} = 0.012\ kgm^2$) without tuning γ (Figure 6.6(a)) and with tuned γ (Figure 6.6(b)). Step response of the closed-loop system with robust modal control using the proposed observer is shown in Figure 6.7 when T_L varies stepwise and $J_2 = 5J_{2,nom}$. Comparing Figures 6.6(a) and 6.6(b), and Figures 3.6 and 6.4 shows that fuzzy tuning makes the observer less sensitive to system parameter variations without affecting observer performance at nominal parameters. Similar conclusions can be derived when using fuzzy tuning in the case of unavailable load speed measurement (see Example 3.3) (Ha [39]).

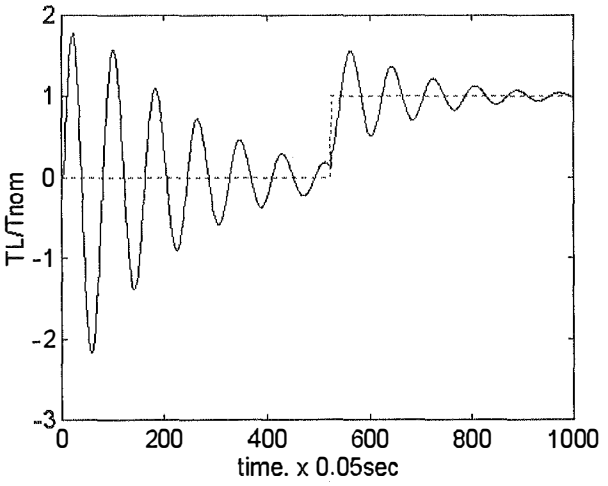

(a)

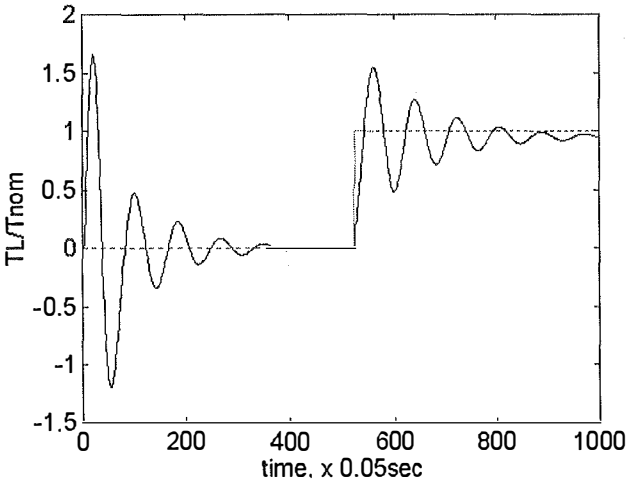

(b)

Figure 6.6. Actual and estimated load torque at $J_2 = 5J_{2,nom}$:
(a) without tuning, and (b) with fuzzy tuning.

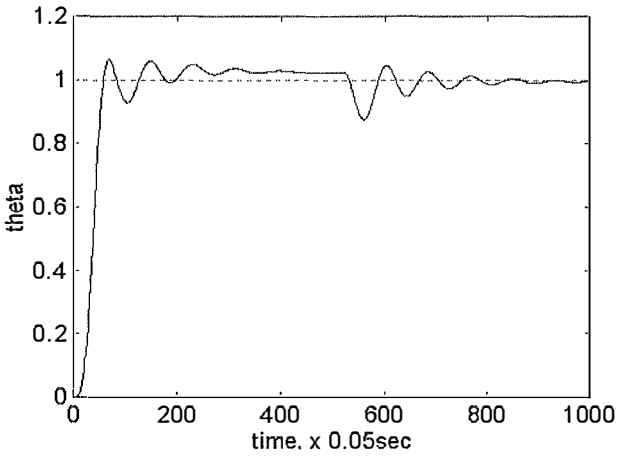

Figure 6.7. Position output step response when T_L varies stepwise and $J_2 = 5J_{2,nom}$.

A simple and straightforward approach for designing digital predictive observers (DPO) with fuzzy tuning has been presented. This observer is used for simultaneously estimating the unmeasurable state variables and unknown inputs. The observer is capable of providing correct estimates when the unknown inputs are time-varying. The rate of change of disturbances is taken into account by changing the predictive coefficient with the use of an explicit fuzzy scheme. Thus, the observer is made more robust to system parameter variations and the tuning is easy. The simulation demonstrates that the proposed observer can be used with a robust modal controller to suppress vibration and reject load disturbance influences in multi-mass electromechanical systems. Its application can also be found in incipient fault detection in power systems as given in Ha & Negnevitsky [43] (see Appendix B).

6.3 Feedforward controller with fuzzy tuning

In the observer-based controllers discussed in Section 3.5, the load torque T_L was assumed to be constant. However, an equivalent unknown load torque to servo systems can be time-varying and thus, a dynamic compensation for its influence is required. In this section the time rate of change of T_L is also considered taking into account the uncertainty in variations of friction, load, and parameters. Dynamic feedforward controller is introduced to compensate for the load torque and its rate of change, which can be estimated using a digital predictive observer described above. Here, the feedforward gain is continuously changed by fuzzy logic, dependent on the magnitude and rate of change of motion error. Thus, the drive system is made more

robust to any perturbations. Simulation results are provided for the cases of one-mass and two-mass position drives.

The basic equation for electric drives is given by

$$T_m = J\frac{d\omega}{dt} + B\omega + T_L, \tag{6.6}$$

where T_m, ω, J, B, and T_L are the motor electromagnetic torque, speed, moment of inertia, viscous friction coefficient and load torque, respectively. Variations in generating torque ΔT_m, moment of inertia ΔJ, friction ΔB can be equivalently referred to as an uncertain load torque change ΔT_L:

$$\Delta T_L = \Delta J\frac{d\omega}{dt} + \Delta B\omega - \Delta T_m. \tag{6.7}$$

Servo drives with several types of motors can then be modelled in the discrete-time state space under linearised conditions by the following equation (Ha & Alferov [19]):

$$\begin{aligned} \mathbf{x}(k+1) &= \mathbf{A}\mathbf{x}(k) + \mathbf{B}u(k) + \mathbf{D}T_L(k) \\ \mathbf{y}(k) &= (\mathbf{I}_m \quad \mathbf{0})\mathbf{x}(k), \end{aligned} \tag{6.8}$$

where $\mathbf{x}(k) \in R^n$ is the drive state vector (position, velocity, current, supply voltage, etc.), $u(k) \in R$ is the control signal, $T_L(k) \in R$ is the external disturbance to the drive system, $\mathbf{y}(k) \in R^m$ is the output vector, $\mathbf{I}_m$ is the $m \times m$ identity matrix, and $\mathbf{A}$, $\mathbf{B}$, $\mathbf{D}$ are constant matrices with dimensions $n \times n$, $n \times 1$, $n \times 1$, respectively. The proposed dynamic feedforward controller will be constructed on the basis of a disturbance observer. A digital predictive observer (DPO) is proposed in Section 3.3 for simultaneous estimation of the unknown inputs and state variables which are not directly measurable. To improve observer robustness a fuzzy logic scheme is introduced to tune the predictive coefficients as described in the section above.

The discrete-time control signal $u(k)$ with full state feedback and observer-based feedforward compensation (Ohishi *et al.* [99], Ko *et al.* [78], Ha & Alferov [19], Yori *et al.* [64]) can then be written as

$$u(k) = U_{ref} + u_m(k) + u_f(k), \tag{6.9}$$

where U_{ref} is the reference input which is a step value as in a tracking servo problem, $u_m(k) = -\mathbf{K}_m\mathbf{x}(k)$ is the feedback signal from the drive state $\mathbf{x}(k)$, and $u_f(k)$ is the feedforward compensation signal. An unknown load torque $T_L(k)$, in general, can be considered as a combination a slowly time-varying component T_{L0} and a perturbation component $\dot{T}_L kT$ dependent on its time derivative $\dot{T}_L$ (T is the sampling period). The feedforward signal will then consist of a static signal u_{fs} and dynamic signal u_{fd}:

$$u_f(k) = u_{fs}(k) + u_{fd}(k) = K_{fs}\hat{T}_L(k) + K_{fd}(\hat{T}_L(k) - \hat{T}_L(k-1)), \qquad (6.10)$$

where K_{fs} and K_{fd} are found from the condition of zero steady state error with respect to a constant and ramp disturbance input, and $\hat{T}_L(k)$ is the estimate of the load torque obtained from a disturbance observer.

6.3.1 One-mass servo drive

The block diagram of the observer-based feedforward controller for an one-mass servo drive is shown in Figure 6.8 (Ha [40]). The unknown input $T_L(k)$ is estimated by the observer DPO. When the load torque is constant, the static feedforward gain K_{fs} is determined from the condition of zero steady-state error (the motor speed $\omega = 0$, current $i_a = T_L/K_t$, supply voltage $e_{sp} = T_L R_a/K_t$, control voltage $u = T_L R_a/(K_t K_{sp})$, and error $e_{ss} = 0$):

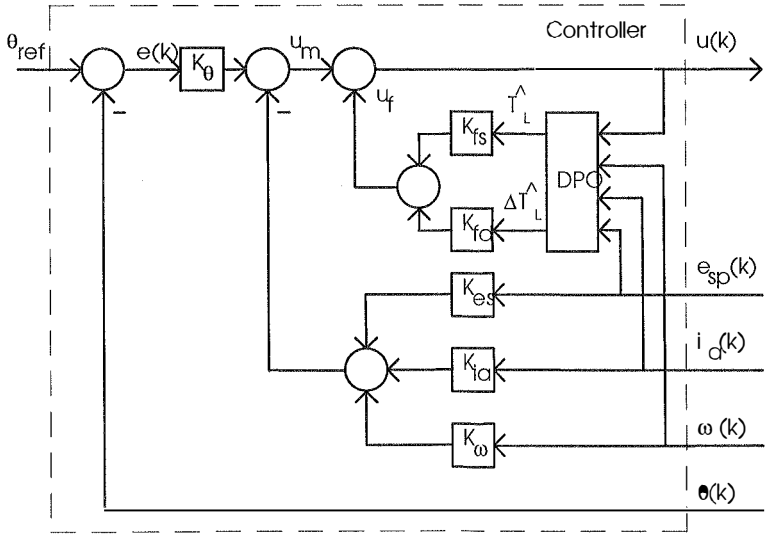

Figure 6.8. Feedforward controller block diagram for one-mass position drives.

$$K_{fs} = R_a / K_t K_{sp} + (K_{es} R_a + K_{ia}) / K_t , \tag{6.11}$$

where R_a and K_t are the motor armature resistance and torque constant, K_{sp} is the supply amplifier gain, K_{es} and K_{ia} are the supply voltage and current feedback gain. The dynamic feedforward gain is found in the same way with a ramp load torque $T_L(t) = \dot{T}_L t$.

In the steady-state tracking regime, the motor speed $\omega = 0$, current $i_a = \dot{T}_L t / K_t$, supply voltage $e_{sp} = R_a \dot{T}_L (T_a + t) / K_t$, and control voltage $u = R_a \dot{T}_L (T_a + T_{sp} + t) / K_t K_{sp}$. Thus, the condition $e_{ss} = 0$ with $t = kT$ and $\dot{T}_L \cong (\hat{T}_L(k) - \hat{T}_L(k-1)) / T$ gives

$$K_{fd} = K_{d0} + K_{fs} k, \quad K_{d0} = (K_{es} T_a / K_t + (T_a + T_{sp}) / K_{sp} K_t) R_a / T , \tag{6.12}$$

where T_a and T_{sp} are the motor armature and supply amplifier time-constants.

6.3.2 Two-mass servo drive

The block diagram of the observer-based feedforward controller for two-mass servo drives (Hori *et al.* [64]) is shown in Figure 6.9. Here the load torque $T_L(k)$ as an unknown input, and the load speed $\omega_2(k)$ and elastic torque $T_e(k)$ as the states, which are not directly measurable, will be estimated. For the case of a two-mass servo drive, the static feedforward coefficient is found as in the former case (the motor and load speed $\omega_1 = \omega_2 = 0$, elastic torque $T_e = T_L$, current $i_a = T_L / K_t$, supply voltage $e_{sp} = T_L R_a / K_t$, control voltage $e_{sp} = T_L R_a / K_t K_{sp}$, and error $e_{ss} = 0$):

$$K_{fs} = R_a / K_t K_{sp} + (K_{es} R_a + K_i) / K_t + K_{Te}, \tag{6.13}$$

where K_{Te} is the elastic torque feedback gain. With $T_L(t) = \dot{T}_L t$ as a ramp input, the zero steady-state tracking error requires the load speed $\omega_2 = 0$, motor speed $\omega_1 = \dot{T}_L / K_{12}$, elastic torque $T_e = \dot{T}_L t$, current $i_a = \dot{T}_L t / K_t$, supply voltage $e_{sp} = (K_b / K_{12} + R_a (T_a + t) / K_t) \dot{T}_L$, and control voltage $u = e_{sp} / K_{sp}$. The dynamic feedforward gain in this case is found to be

$$\begin{aligned} K_{fd} &= K_{d0} + K_{fs} k, \\ K_{d0} &= (K_{es} R_a T_a / K_t + R_a (T_a + T_{sp}) / K_{sp} K_t + K_b / K_{sp} K_{12} + (K_{es} K_b + K_{\omega 1}) / K_{12}) / T \end{aligned} \tag{6.14}$$

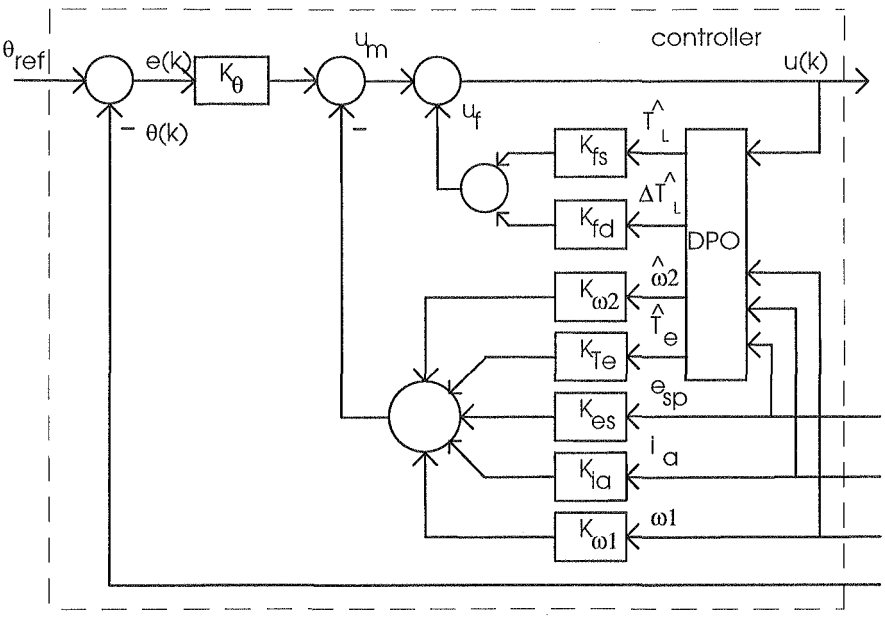

Figure 6.9. Feedforward controller block diagram for two-mass position drives.

where $K_{\omega 1}$ is the motor speed feedback gain, K_b is the motor back emf constant, and K_{12} is the coupling rigidity modulus.

6.3.3 Fuzzy logic tuning

While feedforward gains in Equations (6.11)-(6.14) are defined at the system nominal parameters the compensation in Equation (6.10) is still sensitive to parameter variations. To improve the robustness of the servo accuracy, a fuzzy tuning scheme is proposed. Fuzzy logic has been proposed to tune the coefficients of PI-controllers in the previous chapter. It is believed that the idea of fuzzy logic tuning can be extended to more complex controllers, benefiting directly from human engineering experience. Here the dynamic feedforward coefficients will be tuned according to knowledge of the control error and the estimated load torque. By denoting $e = \theta_{ref} - \theta$, where θ_{ref} and θ are the reference and actual output of the position drive, the error modulus is reflected by

$$\varepsilon(k) = \begin{cases} \left| \dfrac{e(k)}{e^{sat}} \right| & if \ |e(k)| \le |e^{sat}| \\ 1, \ otherwise, \end{cases} \tag{6.15}$$

where e^{sat} is the maximal magnitude of the control error corresponding to saturation of the servo power amplifier. The following conditional scheme is provided for continuously changing the dynamic feedforward gain, dependent on the signs of $e(k)$ and $d\hat{T}_L(k) = \hat{T}_L(k) - \hat{T}_L(k-1)$:

If SDTESE and EL then KDL, If SDTESE and ES then KDS,
If SDTNESE and ES then KDZ, If SDTNESE and EL then KDN,

where the labels EL, ES, KDL, KDS, KDZ, KDN, SDTESE, and SDTNESE mean $\varepsilon(k)$ is large, $\varepsilon(k)$ is small, K_{fd} is large, K_{fd} is small, K_{fd} is zero, K_{fd} is negative, $sign(d\hat{T}_L) = sign(e)$, and $sign(d\hat{T}_L) \neq sign(e)$, respectively. By defining the corresponding membership functions as

$$\mu_{SDTESE} = \begin{cases} 1, & sign(d\hat{T}_L) = sign(e) \\ 0, & sign(d\hat{T}_L) \neq sign(e) \end{cases}, \quad \mu_{SDTNESE} = \begin{cases} 1, & sign(d\hat{T}_L) \neq sign(e) \\ 0, & sign(d\hat{T}_L) = sign(e) \end{cases},$$

$$\mu_{EL} = 1 - e^{-\sigma_\varepsilon \varepsilon}, \quad \mu_{ES} = e^{-\sigma_\varepsilon \varepsilon} \tag{6.16}$$

$$\mu_{KDL} = \begin{cases} 1, & K_{fd} = 2K_{d0} \\ 0, & K_{fd} \neq 2K_{d0} \end{cases}, \quad \mu_{KDS} = \begin{cases} 1, & K_{fd} = K_{d0} \\ 0, & K_{fd} \neq K_{d0} \end{cases},$$

$$\mu_{KDZ} = \begin{cases} 1, & K_{fd} = 0 \\ 0, & K_{fd} \neq 0 \end{cases}, \quad \mu_{KDN} = \begin{cases} 1, & K_{fd} = -K_{d0} \\ 0, & K_{fd} \neq K_{d0} \end{cases},$$

the value of K_{fd} is found by the max-min inference and centroid method (Ha [40]):

$$K_{fd} = \begin{cases} K_{do}(2 - e^{-\sigma_\varepsilon \varepsilon}), & sign(d\hat{T}_L) = sign(e) \\ -K_{do}(1 - e^{-\sigma_\varepsilon \varepsilon}), & sign(d\hat{T}_L) \neq sign(e). \end{cases} \tag{6.17}$$

The explicit form of the above equation provides an easy tuning for the controller coefficient and thus results in a cheap computational implementation.

Example 6.2 (Ha [40]) Consider first the one-mass servo system of the radial arm motion of an ABB robot using a DC motor F12M4 (43V, 240W, 3000 r/min) supplied by a PWM transistor chopper. The block diagram of the servo system with cascade controllers (PI-current regulator, PID-speed regulator and P-position regulator) is shown in Figure 6.10.

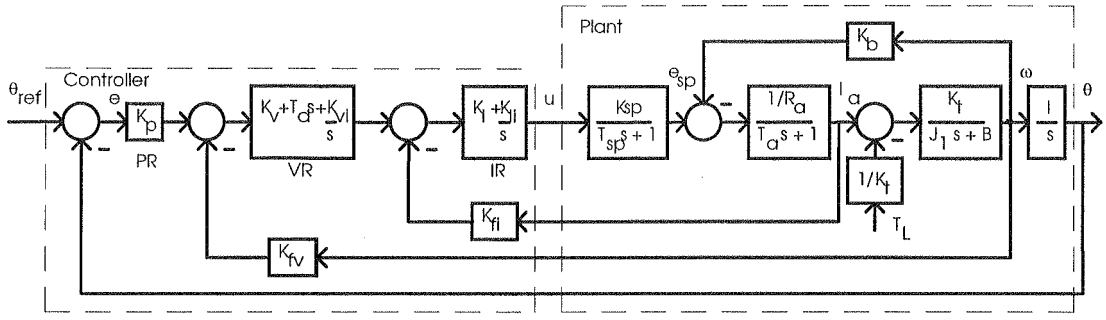

Figure 6.10. Block diagram of a one-mass system with a cascade controller.

The parameter nomenclature and nominal specifications are listed in Table 6.1. The controller parameters are given in Table 6.2. Experiments and simulations indicate that with cascade control, the third pattern motion (to and fro along x-axis) of the robot is sensitive to load and inertia variations. Figure 6.11 depicts the voltage waveform corresponding to the x-axis position of the robot when moment of inertia $J \cong 2J_{nom}$.

An observer-based feedforward controller described above is proposed. The sampling period is $T = 1ms$. The ITAE criteria is used for pole placement with base frequency chosen as $\omega_n = 47$ *rad/sec* (steady-state time 0.1 *sec*, overshoot 10%). The feedback gain obtained, $\mathbf{k}^T = (K_\theta \;\; K_{es} \;\; K_{ia} \;\; K_\omega)$ together with the values of feedforward coefficients K_{fs} and K_{d0} according to Equations (5,6) are given in Table 6.3.

Parameter	Value
Supply amplifier gain, K_{sp}	10
Supply amplifier time constant, T_{sp}	0.01 *(ms)*
Armature resistance, R_a	0.93 (*ohm*)
Electromagnetic time constant, T_a	0.03 (*sec*)
Back-EMF constant, K_b	0.11 (V/sec^{-1})
Torque constant, K_t	0.11 (*Nm/A*)
Motor moment of inertia, J	0.00034 (kgm^2)
Electromechanical time constant, T_m	0.025 (*sec*)
Speed reduction ratio, i	1:100

Table 6.1. Nominal parameters of a robot arm one-mass position drive

Parameter	Value
PI current regulator (IR):	
proportional coefficient, K_I	2
integral coefficient, K_{Ii}	18600 (sec^{-1})
feedback coefficient, k_{fI}	0.633 (*V/A*)
PID velocity regulator (VR):	
proportional coefficient, K_V	11
integral coefficient, K_{Vi}	100 (sec^{-1})
derivative coefficient, T_d	0.1 (*sec*)
feedback coefficient, k_{fV}	0.016 (*Vsec/rad*)
P position regulator (PR):	
proportional coefficient, K_P	25

Table 6.2. Cascade controller parameters

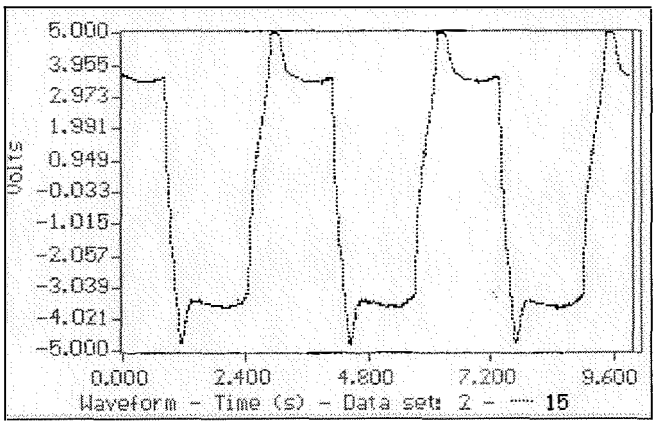

Figure 6.11. The robot third pattern motion when moment of inertia $J \cong 2J_{nom}$.

Coefficient	Value
Position feedback coefficient, K_θ	0.13 (*V/rad*)
Voltage feedback coefficient, K_{es}	-140.69
Current feedback coefficient, K_{ia}	130.12 (*V/A*)
Speed feedback coefficient, K_ω	17.33 (*Vsec/rad*)
Static compensation coefficient, K_f	-5.55 (*V/Nm*)
Dynamic compensation coefficient, K_{d0}	-107.97 (*V/Nm*)
Tuning coefficient, σ_ε	2

Table 6.3. Feedforward controller coefficients

The dynamic feedforward gain K_{fd} is inferred by Equation (11) with $e^{sat} = u^{sat}/K_\theta$ (the saturation control voltage u^{sat} = 15V) where the value of σ_ε is also given in Table 6.3. Figures 6.12, 6.13, and 6.14 show the step response of the x-axis motion with a cascade controller, an observer-based state feedback with static feedforward, and with fuzzy tuned dynamic feedforward, respectively, when the robot arm moment of inertia varies by $J = J_{nom}(1 + 0.8\sin 100t)$ at $T_L = T_{L,nom}$.

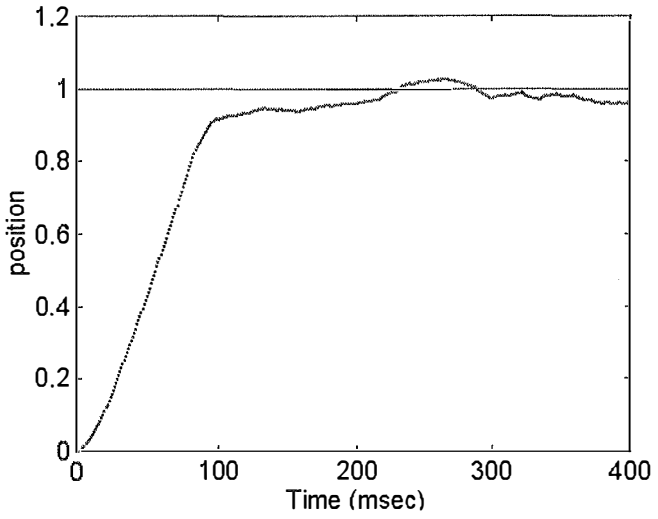

Figure 6.12. Step response with a cascade controller under the conditions $J = J_{nom}(1 + 0.8\sin 100t)$ and $T_L = T_{L,nom}$.

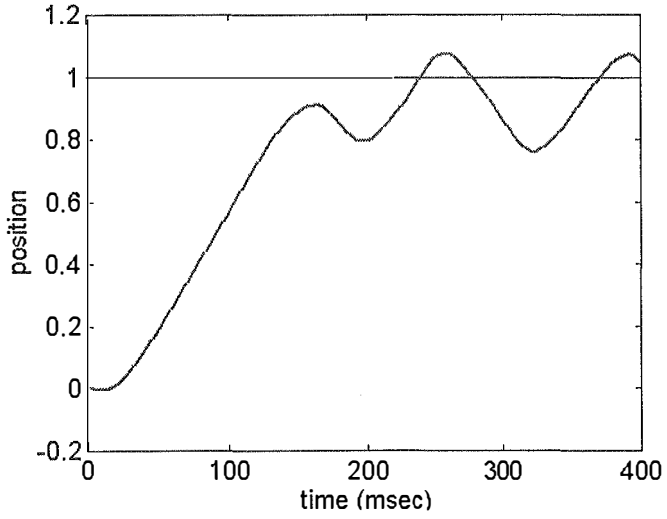

Figure 6.13. Step response with a static feedforward controller under the conditions $J = J_{nom}(1 + 0.8\sin 100t)$ and $T_L = T_{L,nom}$.

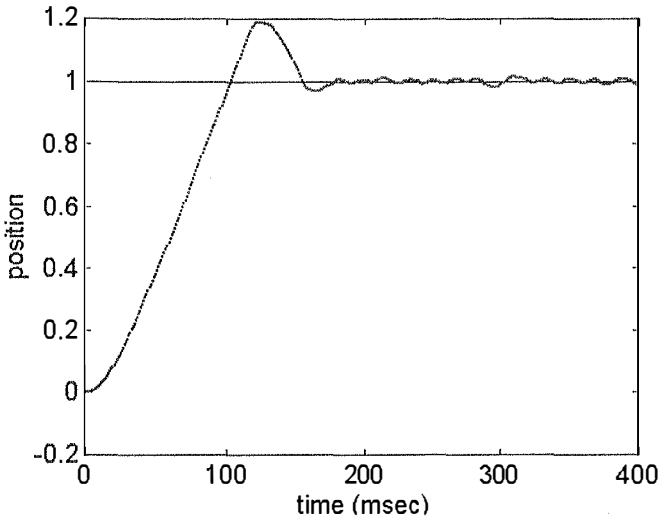

Figure 6.14. Step response with a fuzzy-tuned dynamic feedforward controller under the conditions $J = J_{nom}(1+0.8\sin 100t)$ and $T_L = T_{L,nom}$.

A comparison of these responses confirms the superiority in servo performance of the proposed method in terms of robustness enhancement.

Example 6.3 A servo drive of an antenna illustrates the case of two-mass systems. The drives consists of two DC motors DPM31 (110V, 12kW, 1400r/min) in series, supplied by a reversible thyristor converter. The system's nominal parameters are given in Table 6.4.

With a very small damping factor $\zeta = 0.003$ vibration suppression is a serious problem in this system (see Example 2.2). A feedforward controller with fuzzy tuning is proposed in this case. The sampling period is $T = 0.05sec$.

A digital predictive observer can be designed to estimate the load speed ω_2, elastic torque T_e and load torque T_L (see Examples 3.3 and 6.1). By the ITAE pole placement with base frequency ω_n = 4.5 *rad/sec*, the feedback coefficients obtained $\mathbf{k}^T = (K_\theta \; K_{es} \; K_{ia} \; K_{\omega 1} \; K_{\omega 2} \; K_{Te})$ are given in Table 6.5. The feedforward gains K_{fs} and K_{d0} according to Equations (6.13) and (6.14), and the tuning constant σ_ε are also given in Table 6.5.

Parameter	Value
Supply amplifier gain, K_{sp}	25
Supply amplifier time constant, T_{sp}	0.01 (*sec*)
Armature resistance, R_a	0.3 (*ohm*)
Electromagnetic time constant, T_a	0.03 (*sec*)
Back-EMF constant, K_b	1.5 (V/sec^{-1})
Torque constant, K_t	1.5 (*Nm/A*)
Motor moment of inertia, J_1	0.814 (kgm^2)
Electromechanical time constant, T_{m1}	0.116 (*sec*)
Coupling rigidity modulus, K_{12}	0.21 (*Nm/rad*)
Coupling viscous friction, B_{12}	$6.3.10^{-5}$ (Nm/sec^{-1})
Load moment of inertia, J_2	0.012 (kgm^2)
Speed reduction ratio, i	1:66

Table 6.4. Nominal parameters of a two-mass position drive

Coefficient	Value
Position feedback coefficient, K_θ	0.52 (*V/rad*)
Voltage feedback coefficient, K_{es}	-0.08
Current feedback coefficient, K_{ia}	0.008 (*V/A*)
Motor speed feedback coefficient, $K_{\omega 1}$	0.07 (*Vsec/rad*)
Load speed feedback coefficient, $K_{\omega 2}$	-0.002
Elastic torque feedback coefficient, K_{Te}	0.08
Static compensation coefficient, K_f	0.08 (*V/Nm*)
Dynamic compensation coefficient, K_{d0}	0.82 (*V/Nm*)
Tuning coefficient, σ_ε	1

Table 6.5. Controller coefficients

Figures 6.15, 6.16, and 6.17 show the step response of the position output with a cascade controller, an observer-based state feedback and feedforward compensation without tuning, and with fuzzy tuned dynamic feedforward, respectively, when the load torque varies sinusoidally $T_L = 0.5T_{L,nom}(1+\sin t)$ at $J_2 = 1.33J_{2,nom}$. Comparing these responses confirms the advantage of fuzzy tuning in terms of

robustness amelioration. The simulation results indicate that dynamic feedforward compensation with fuzzy tuning is capable of suppressing mechanical vibrations and improving the system robustness to load and parameter variations. The explicit form of the dynamic feedforward coefficient enables its simple implementation and easy tuning.

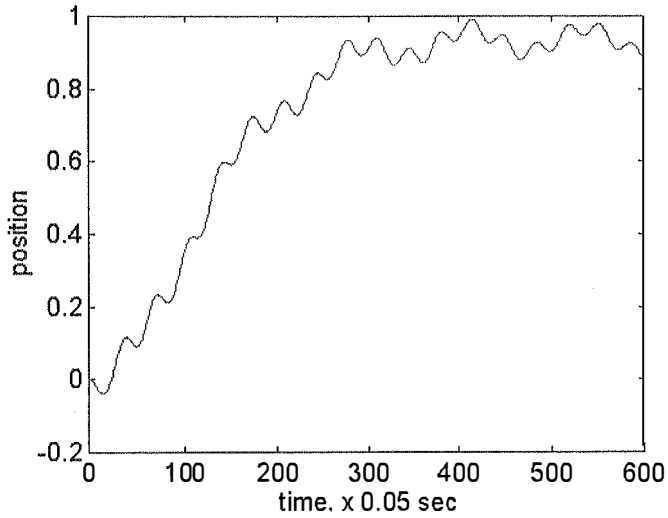

Figure 6.15. Step response with a cascade controller under the conditions $J_2 = 1.33J_{2,nom}$ and $T_L = 0.5T_{L,nom}(1+\sin t)$.

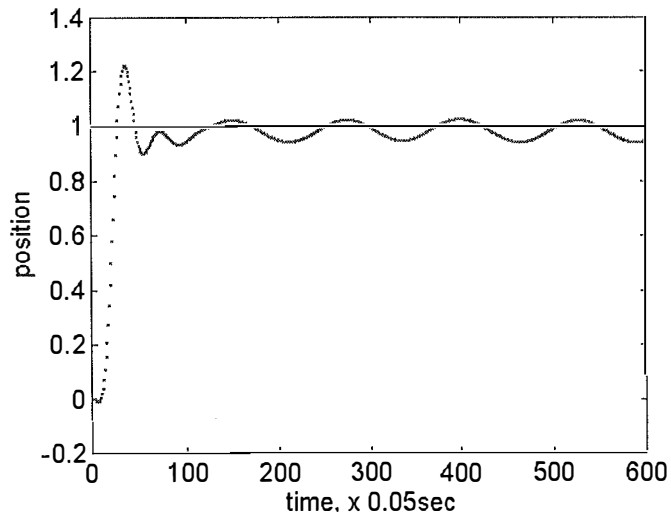

Figure 6.16. Step response with a static feedforward controller under the conditions $J_2 = 1.33J_{2,nom}$ and $T_L = 0.5T_{L,nom}(1+\sin t)$.

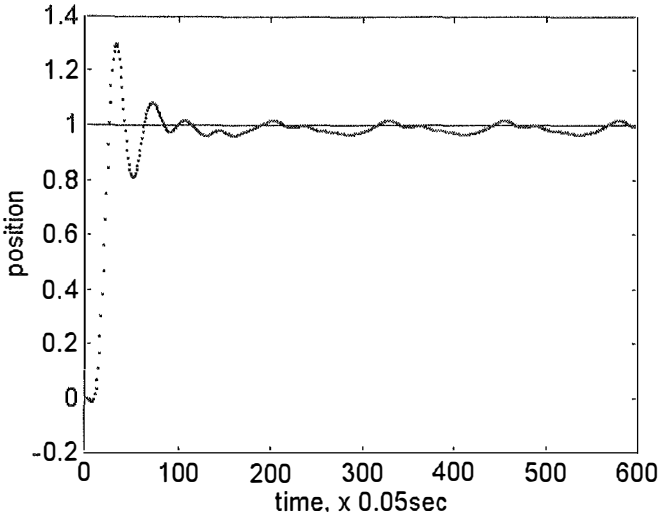

Figure 6.17. Step response with a fuzzy-tuned dynamic feedforward controller under the conditions $J_2 = 1.33J_{2,nom}$ and $T_L = 0.5T_{L,nom}(1+\sin t)$.

In this section a dynamic feedforward controller with fuzzy tuning has been proposed for electromechanical systems to improve robustness of servo performance dealing with any cause of motion error such as load torque or parameter variations. The controller design is based on a digital predictive observer to simultaneously estimate the disturbance and the unmeasurable state. Full state feedback is used to assign the desirable closed-loop poles. A compensation signal taking into account the load torque rate of change is then fed forward to alleviate the influences of any variations. The dynamic feedforward gain is made continuously changing by a conditional fuzzy logic scheme, benefiting directly designers' engineering knowledge. The simulation results provided for one-mass and two-mass position drives verify the validity of the proposed method.

6.4 Modal controller with fuzzy tuning

Consider a single input, single output system with the discrete-time state equation (3.92) with the system uncertainties $\Delta\mathbf{A}$ and $\Delta\mathbf{b}$. Under matching conditions given in Section 3.6, theorem 3.3 gives the robust feedback gain $\mathbf{k}_r^T$ in (3.96).

$$\mathbf{k}_r^T = \frac{\mathbf{b}_0^T\mathbf{P}\mathbf{A}_m}{\mathbf{b}_0^T\mathbf{P}\mathbf{b}_0}, \tag{6.18}$$

where $\mathbf{b}_0$ and $\mathbf{A}_m$ are defined in (3.92) and (3.93), and $\mathbf{P}$ is the solution of the discrete-time Lyapunov equation (3.95). Such a constant robust feedback gain can improve dynamic performance of the drive system in the presence of parameter variations. However, the closed-loop poles at nominal parameters are slightly deviated from the desirable pole-assignment by modal control. This is taken into account by using a fuzzy tuning scheme for $\mathbf{k}_r^T$. Any deviation from the desired modal response due to parameter variations will result in the increase of the control error modulus $\varepsilon(k)$. For improving robustness to time-varying parameters, a weighting factor w_r, $0 \le w_r \le 1$, is introduced to tune the gain $\mathbf{k}_r^T$ defined in (6.18). The robust control signal then becomes

$$u_r(k) = \Delta\mathbf{k}_r^T\mathbf{x}(k) = w_r\mathbf{k}_r^T\mathbf{x}(k), \tag{6.19}$$

where $\Delta\mathbf{k}_r^T = w_r\mathbf{k}_r^T$ is the robust feedback gain. Control engineering knowledge indicates that in the case of large overshoot or undershoot, it is required to increase feedback gain or, in this case, weighting factor w_r. This implies that w_r depends not only on the error $\varepsilon(k)$ but also on $sign(e)$ and $sign(de)$, where $de = e(k) - e(k-1)$ is the control error difference. The following fuzzy scheme is proposed (Ha & Negnevitsky [41]):

If EL or SEESDE then WL,
If ES or SENESDE then WS

where EL, ES, and WL, WS mean that e is large, e is small, and w_r is large, w_r is small. Its physical meaning can be explained as follows. If error is large or the signs of error and its change are different, feedback signal should be increased. Also, if error is small or error and its change have the same signs, feedback signal should be decreased. Note that the membership functions of EL and ES are given in (6.16) and singletons:

$$\mu_{WL} = \begin{cases} 1, & w_r = w_{r0} \\ 0, & w_r \neq w_{r0} \end{cases} \text{ and } \mu_{WS} = \begin{cases} 1, & w_r = 0 \\ 0, & w_r \neq 0 \end{cases}, \tag{6.20}$$

are used for WL and WS, where w_{r0} is the maximal value of the weighting factor, w_r. The labels SEESDE and SENEDE mean $sign(e)=sign(de)$ and $sign(de)\neq sign(de)$ with the following membership functions:

$$\mu_{SEESDE} = \begin{cases} 1, & sign(e) = sign(de) \\ 0, & sign(e) \neq sign(de) \end{cases} \quad \mu_{SENESDE} = \begin{cases} 1, & sign(e) \neq sign(de) \\ 0, & sign(e) = sign(de) \end{cases}. \tag{6.21}$$

Using the max-min inference rule, the value of w_r is derived as follows. When $sign(e) = sign(de)$:

$$w_r = \frac{\mu_{SEESDE} \cdot w_{r0} + \mu_{ES} \cdot 0}{\mu_{SEESDE} + \mu_{ES}} = \frac{w_{r0}}{1 + \exp(-\frac{\varepsilon}{\sigma_\varepsilon})}, \tag{6.22a}$$

and when $sign(e) \neq sign(de)$:

$$w_r = \frac{\mu_{EL} \cdot w_{r0} + \mu_{SENESDE} \cdot 0}{\mu_{EL} + \mu_{SENESDE}} = \frac{1 - \exp(-\frac{\varepsilon}{\sigma_\varepsilon})}{2 - \exp(-\frac{\varepsilon}{\sigma_\varepsilon})} w_{r0}. \tag{6.22b}$$

Example 6.4. (Ha & Negnevitsky [41]) In this example, the proposed robust modal controller with fuzzy tuning is applied to control a two-mass position drive system of Examples 3.3, 6.1, and 6.3. The parameter nomenclature and nominal specifications are listed in Table 6.4. Choosing the state vector $\mathbf{x} = \left(\theta \;\; e_{sp} \;\; i_a \;\; \omega_1 \;\; \omega_2 \;\; T_e\right)^T$, the state equation is written

$$\frac{d\mathbf{x}(t)}{dt} = \begin{bmatrix} 0 & 0 & 0 & 0 & i & 0 \\ 0 & -1/T_{sp} & 0 & 0 & 0 & 0 \\ 0 & 1/R_aT_a & -1/T_a & -K_b/R_aT_a & 0 & 0 \\ 0 & 0 & K_t/J_1 & 0 & 0 & -1/J_1 \\ 0 & 0 & 0 & 0 & 0 & 1/J_2 \\ 0 & 0 & B_{12}K_t/J_1 & K_{12} & -K_{12} & -B_{12}(1/J_1 + 1/J_2) \end{bmatrix} \mathbf{x}(t) + \begin{bmatrix} 0 \\ K_{sp}/T_{sp} \\ 0 \\ 0 \\ 0 \\ 0 \end{bmatrix} u(t) + \begin{bmatrix} 0 \\ 0 \\ 0 \\ 0 \\ -1/J_2 \\ B_{12}/J_2 \end{bmatrix} T_L(t)$$

where θ is the angular position of the antenna, e_{sp} is the motor supply voltage, i_a is the armature current, ω_1 is the motor shaft speed, ω_2 is the load shaft speed, T_e is the elastic torque, u is the control voltage, T_L is the load torque.

A. Design of RMC

1) Digital Predictive Observer: The unknown input T_L, state variables ω_2 and T_e, not directly measured, will be estimated via a digital predictive observer using measurements of e_{sp}, i_a, and ω_1. The design and results were described in Example 3.3.

2) Modal Controller: The resonant frequency of the drive system is $\Omega_0 = 4.21$ *rad/sec.* To suppress mechanical vibrations, the binomial expansion was proposed in Hori *et al.* [64] for assigning the closed loop poles. However, a multiple root will cause high sensitivity to any variations. Here we use the ITAE pole placement with base frequency ω_n=4.5 *rad/sec*, (steady-state time 1.5 *sec*, overshoot 3%), the obtained feedback gain $\mathbf{k}^T = (K_\theta \;\; K_{es} \;\; K_{ia} \;\; K_{\omega 1} \;\; K_{\omega 2} \;\; K_{Te})$ is given in Table 6.6.

3) Feedforward controller: The feedforward gain when K_{fs} is defined from the zero steady-state error condition when load torque is constant as in (6.13). The dynamic feedforward can be obtained from (6.14). The values of K_f and K_{d0} are given in Table 6.7.

4) Robust controller: Assume that the matching conditions (3.88) are satisfied for given intervals of parameter variations, defined from operating conditions of the system in practice. Here, for the sake of simulation the load moment of inertia varies from $[1, 2]J_{2,nom}$. Choose $\mathbf{Q} = \mathbf{I}_6$, the elements of vector $\mathbf{k}_r^T$ calculated from Equations (6.18) and (3.95) are given in Table 6.6.

	K_θ	K_{es}	K_{ia}	$K_{\omega 1}$	$K_{\omega 2}$	K_{Te}
$\mathbf{k}^T$	0.52	-0.08	0.008	0.07	-0.002	0.08
$\mathbf{k}_r^T$	-0.104	0.02	-0.001	-0.02	0.001	-0.01

Table 6.6. Modal controller coefficients

B. Tuning the RMC coefficients

The predictive coefficient γ of the observer is tuned by $\gamma_m e^{-\sigma_r r}$ as described in Example 6.1. The values of γ_m and σ_r chosen for simulation are given in Table 6.7. With the control error $e=\theta_{ref} - \theta$ and $e^{sat} = u^{sat}/K_\theta$ (the saturation control voltage u^{sat}=10*V*), the feedforward gains K_{fs} and K_{do}, and the value of σ_ε are given in Table 6.6. The weighting factor w_r for the robust feedback gain is continuously changed by using (6.22) with w_{r0} given in Table 6.7. All the fuzzy schemes are in an explicit form which will result in simple implementation.

K_{fs}	K_{do}	σ_ε	w_{ro}	γ_m	σ_r
0.08	0.82	1	0.2	0.5	0.5

Table 6.7. Coefficients for tuning schemes

C. Simulation results

The modal control step response at the nominal parameters of the system and without load torque ($T_L = 0$) is shown in Figure 6.18 where Figure 6.18(a) is the desirable transient process for the closed loop system.

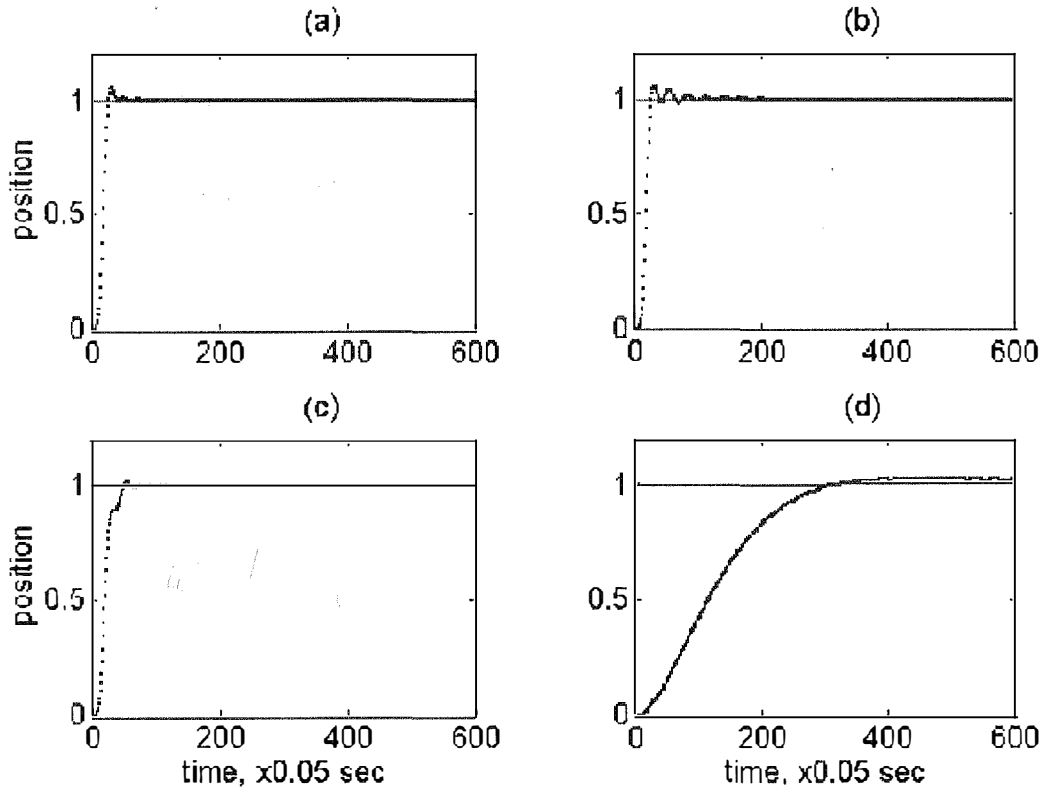

Figure 6.18. Step response at nominal parameters, $T_L = 0$.

The robust modal control step response without tuning is represented in Figure 6.18(b) and with fuzzy tuning in Figure 6.18(c). Note that with very small damping factor ζ=0.003, the system becomes almost unstable due to any perturbations. Hence, the design of a cascade controller becomes very difficult, especially to guarantee both fast response and stability. Figure 6.18(d) shows the step response with a cascade

controller consisting of the current loop (with PI-controller $G_I(s) = 0.15(s+33)/s$ and current feedback coefficient $k_{fI} = 0.08$), velocity loop (with P-controller $G_V(s)=0.5$, $k_{fV}=0.05$), and position loop (with PI-controller $G_P(s) = 0.52s + 0.002/s$, $k_{fP}=1$), designed by the conventional magnitude optimum principle (Kljuchev [54]). Robust modal control with fuzzy logic tuning (Figure 6.18(c)) can provide fast response without oscillation.

Consider next the case when load torque varies sinusoidally $T_L=0.5T_{L,nom}(1+sin0.3t)$ and moment of inertia increases twice $J_2 = 2J_{2,nom}$. The step response with modal controller shown in Figure 6.19(a) indicates that without feedforward compensation the system is load sensitive. If fast response is required, the controller without tuning coefficients (Figure 6.19(b)) still cannot completely suppress vibrations in the system. The position response with conventional cascade controller in Figure 6.19(d) shows that the system is sensitive to both load and parameter variations. With fuzzy tuning, robust modal control (Figure 6.19(c)) can provide the closest response to the benchmark curve in Figure 6.18(a). Such a controller achieves better behaviour thanks to its ability to benefit directly from the designer's engineering knowledge.

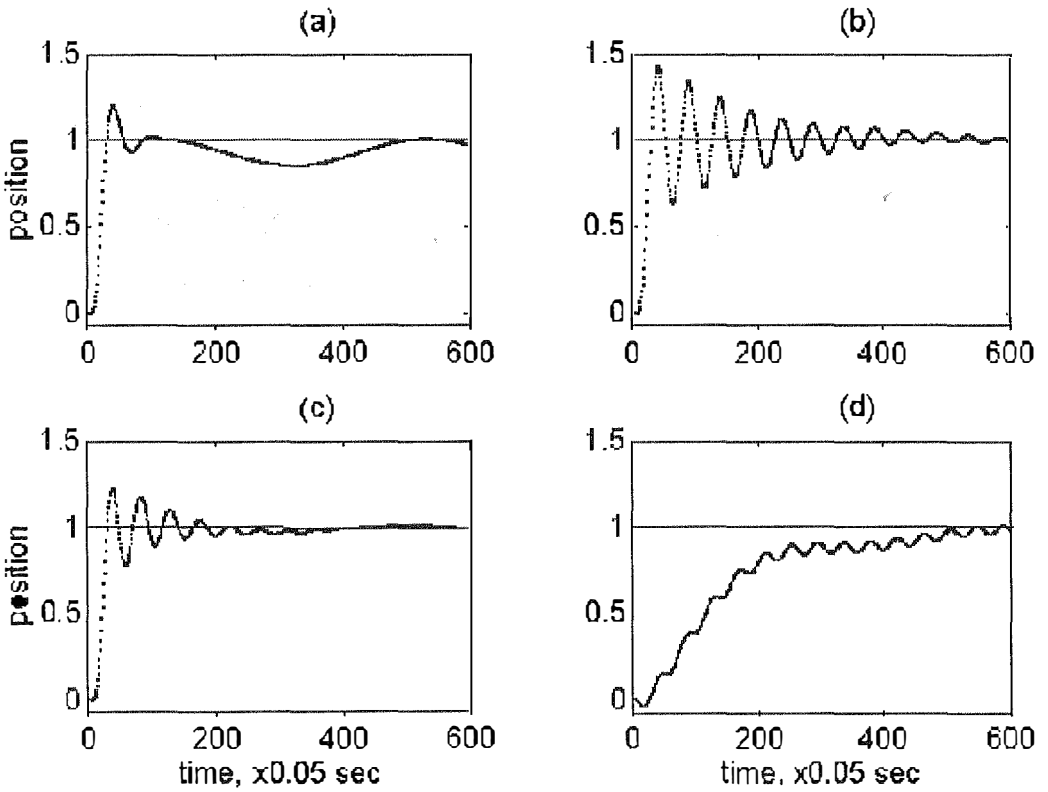

Figure 6.19. Step response at $J_2 = 2J_{2,nom}$, $T_L=0.5T_{L,nom}(1+sin0.3t)$.

Example 6.5. (Ha & Palis [163]) Consider again the servo system of the radial arm motion of an ABB robot of Example 6.3. The system nominal parameters are listed in Table 6.1. The cascade controller parameters are given in Table 6.2. As shown in Figure 6.11 and 6.12, with cascade control, the third pattern motion (to and fro along x-axis) of the robot (ABB [164]) is sensitive to load and inertia variations. A robust modal controller is proposed as shown in Figure 6.8, where the modal signal is augmented with a fuzzy tuned component. The design procedure is illustrated as follows:

Step 1: Design of Digital Predictive Observer (DPO)
The sampling period is chosen as T=1*msec*. The load torque T_L is to be estimated from the measurements of the motor supply voltage, speed, and current. The discrete-time state equation is augmented by the following approximation

$$T_L(k+1) = (1+\gamma)T_L(k) - \gamma T_L(k-1).$$

The following observer equation is then obtained

$$w(k+1) = fw(k) + g_1 e_{sp}(k) + g_2\omega(k) + g_3 i_a(k) + hu(k) - \gamma\hat{T}_L(k-1)$$
$$\hat{T}_L(k) = w(k) + l\omega(k)$$

where $w(k)$is the observer state; f, g_1, g_2, g_3, h, and l are constants, dependent on the choice of the observer dynamics. The predictive coefficient γ will be tuned by using (6.5), $\gamma = \gamma_m e^{-\sigma_r r}$, where r is defined as in (6.2) and the values of γ_m and σ_r are given in Table 6.8.

Step 2: Design of Modal Controller (MC)
The ITAE criteria is used for pole placement with base frequency chosen as ω_n= 47 *rad/sec* (steady-state time 0.1*sec*, overshoot 10%). The feedback gain obtained, $\mathbf{k}^T = \begin{pmatrix} K_\theta & K_{es} & K_{ia} & K_\omega \end{pmatrix}$ is given in Table 6.8.

Step 3: Design of Feedforward Controller (FC)
The feedforward gains K_{fs} and K_{d0}, defined from (6.11) and (6.12) are given in Table 6.8. With the control error e=$\theta_{ref} - \theta$ and $e^{sat} = u^{sat}/K_\theta$ (the saturation control voltage u^{sat}=15V), the dynamic feedforward gain K_d is tuned by (6.17) where the the value of σ_ε given in Table 6.8.

Coefficient	Value
Digital Predictive Observer (DPO)	
tuning coefficients, γ_m	0.5
σ_r	2
Modal Controller (MC):	
position feedback coefficient, K_θ	0.13 (*V/rad*)
voltage feedback coefficient, K_{es}	-140.69
current feedback coefficient, K_{ia}	130.12 (*V/A*)
speed feedback coefficient, K_ω	17.33 (*Vsec/rad*)
Feedforward Controller (FC):	
static compensation coefficient, K_f	-5.55 (*V/Nm*)
dynamic compensation coefficient, K_{f0}	-107.97 (*V/Nm*)
tuning coefficient, σ_ε	2
Robust Controller (RC):	
position feedback coefficient, $w_{ro}K_\theta$	-0.0001 (*V/rad*)
voltage feedback coefficient, $w_{ro}K_{es}$	0.141
current feedback coefficient, $w_{ro}K_{ia}$	-0.13 (*V/A*)
speed feedback coefficient, $w_{ro}K_\omega$	-0.017 (*Vsec/rad*)
tuning coefficient, σ_r	2

Table 6.8. Fuzzy-tuned robust modal controller coefficients

Step 4: Design of Robust Controller (RC)

Choosing $\mathbf{Q} = \mathbf{I}_6$, the robust feedback gain $\mathbf{k}_r^T$ is calculated from (6.18) and the Lyapunov solution of (3.95). The weighting factor w_r for the robust feedback gain $\mathbf{k}_r^T$ is continuously changed by using fuzzy tuned expression (6.22). The coefficients of vector $w_{r0}\mathbf{k}_r^T$ with the constant for tuning σ_r are given in Table 6.8.

Figure 6.20 represents the position step response with the fuzzy-tuned robust modal controller. The simulation was performed under the same conditions applied to the cascade controller of Example 6.3. In comparison to the conventional cascade controllers (Figure 6.12), the RMC with fuzzy tuning is more robust to parameter and load variations (Figure 6.20(b)). Such a controller achieves better behaviour thanks to its ability to benefit directly from the designer's engineering knowledge using fuzzy schemes.

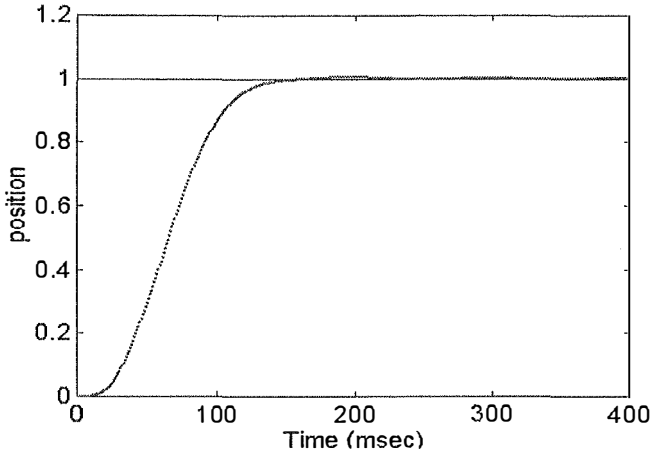

(a)

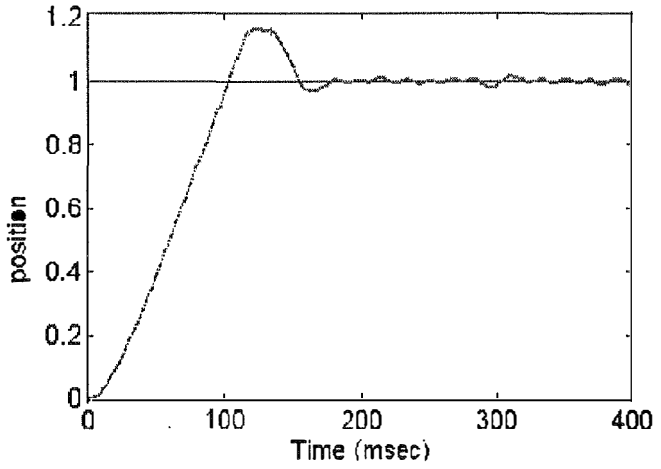

(b)

Figure 6.20. Step response with RMC with fuzzy tuning at (a) nominal parameters, and (b) $J = J_{nom}(1+0.8\sin 100t)$ at $T_L = T_{L,nom}$.

Robust modal control with fuzzy tuning for linear servo systems has been introduced in this section. The fuzzy schemes can utilise human experience and result in an explicit form for continuously changing the controller coefficients. Thus the cost of a computational implementation is reduced and the tuning made easier. The simulation results demonstrate that the proposed approach can be applied in such a way as to achieve robustness to load and parameter variations in the servo system of an ABB robot radial arm in motion. The proposed approach can be applied to suppress vibration and achieve robustness to load and parameter variations in multi-mass electro-mechanical systems.

6.5 Fuzzy tuning with different membership functions

Tuning a parameter is practically a continuously smooth process of adjusting its value. This explains why exponential, Gaussian, or sigmoidal membership functions of input labels are usually suggested for fuzzy tuning. Fuzzy tuning with exponential membership functions have been employed so far in this chapter. In this section, Gaussian and sigmoidal membership functions are used in fuzzy logic schemes to tune robust modal controller coefficients (Ha & Negnevitsky [42]). For example, for the fuzzy sets XL (X is *large*) and XS (X is *small*), instead of the exponential membership functions (5.2), the following Gaussian and sigmoidal membership functions can be used:

$$\mu_{XS}(X) = \exp(-\frac{X^2}{2\sigma_X{}^2}), \quad \mu_{XL}(X) = 1 - \exp(-\frac{X^2}{2\sigma_X{}^2}), \tag{6.23}$$

and

$$\mu_{XS}(X) = 2\exp(-\frac{|X|}{\sigma_X}) / (1 + \exp(-\frac{|X|}{\sigma_X})),$$

$$\mu_{XL}(X) = (1 - \exp(-\frac{|X|}{\sigma_X})) / (1 + \exp(-\frac{|X|}{\sigma_X})), \tag{6.24}$$

Thus, the alternatives for the observer predictive coefficients using the membership functions (6.23) and (6.24) can be obtained from (6.3) as

$$\gamma_{ii} = \gamma_{m,i} \exp(-\frac{r_i^2}{2\sigma_{r_i}{}^2}), \tag{6.25}$$

and

$$\gamma_{ii} = 2\gamma_{m,i} \exp(-\frac{r_i}{\sigma_{r_i}}) / (1 + \exp(-\frac{r_i}{\sigma_{r_i}})), \tag{6.26}$$

respectively, where $\gamma_{m,i}$ and σ_{r_i} are some constants, i=1,2,...,q.

Using the same rule set for the dynamic feedforward controllers of Section 6.3, and the Gaussian and sigmoidal exponential membership functions for the error modulus $\varepsilon(k)$ defined in (6.16), the dynamic feedforward gain K_{fd} has the following expressions:

$$K_{fd} = \begin{cases} K_{d0}(2 - \exp(-\dfrac{\varepsilon^2}{2\sigma_\varepsilon{}^2})), & sign(d\hat{T}_L) = sign(e) \\ -K_{d0}(1 - \exp(-\dfrac{\varepsilon^2}{2\sigma_\varepsilon{}^2})), & sign(d\hat{T}_L) \neq sign(e) \end{cases} \tag{6.27}$$

and

$$K_{fd} = \begin{cases} 2K_{d0} / (1 + \exp(-\dfrac{\varepsilon}{\sigma_\varepsilon})), & sign(d\hat{T}_L) = sign(e) \\ -K_{d0}(1 - \exp(-\dfrac{\varepsilon}{\sigma_\varepsilon})) / (1 + \exp(-\dfrac{\varepsilon}{\sigma_\varepsilon})), & sign(d\hat{T}_L) \neq sign(e) \end{cases} \tag{6.28}$$

respectively, where σ_ε and K_{d0} are some constants.

Similarly, the defuzzified value of the weighting factor, w_r, in the robust feedback (6.19) can be found as

$$w_r = \begin{cases} w_{r0} / (1 + \exp(-\dfrac{\varepsilon^2}{2\sigma_\varepsilon{}^2})), & sign(e) = sign(de) \\ w_{r0}(1 - \exp(-\dfrac{\varepsilon^2}{2\sigma_\varepsilon{}^2})) / (2 - \exp(-\dfrac{\varepsilon^2}{2\sigma_\varepsilon{}^2})), & sign(e) \neq sign(de), \end{cases} \tag{6.29}$$

when using Gaussian functions (6.23), or

$$w_r = \begin{cases} w_{r0}(1 + \exp(-\dfrac{\varepsilon}{\sigma_\varepsilon})) / (1 + 3\exp(-\dfrac{\varepsilon}{\sigma_\varepsilon})), & sign(e) = sign(de) \\ w_{r0}(1 - \exp(-\dfrac{\varepsilon}{\sigma_\varepsilon})) / 2, & sign(e) \neq sign(de), \end{cases} \tag{6.30}$$

when using sigmoidal membership functions (6.24), where w_{r0} is the maximal value of the weighting factor.

The possibility of using other membership functions such as sigmoidal or Gaussian instead of the above exponential membership functions in tuning expressions is demonstrated in the following example.

Example 6.6 (Ha & Negnevitsky [42]) Consider the control of an overhead crane model described in Section 4.4.2. The linearised state equation is obtained as

$$\begin{bmatrix}\dot{x}_1\\ \dot{x}_2\\ \dot{x}_3\\ \dot{x}_4\end{bmatrix}=\begin{bmatrix}0 & 1 & 0 & 0\\ 0 & -0.1625 & 9.81m & 0\\ 0 & 0 & 0 & 1\\ 0 & -0.1625/l & -9.81(1+m)/l & 0\end{bmatrix}\begin{bmatrix}x_1\\ x_2\\ x_3\\ x_4\end{bmatrix}+\begin{bmatrix}0\\ 0.985\\ 0\\ -0.985/l\end{bmatrix}u+\begin{bmatrix}0\\ -50\\ 0\\ -50/l\end{bmatrix}T_L$$

where x_1 is the trolley position, $x_2 = \dot{x}_1$, x_3 is the swing angle, u is the control voltage applied to the servo motor, and T_L is the unknown load torque due to any nonlinearities or external disturbances; m is the load mass, and l is the rope length. The sampling period is chosen as T=0.02 sec. The robust modal controller is designed at $m = m_0$= 0.25kg and $l = l_0$= 0.4m.

The closed-loop poles are assigned by the ITAE criteria. The feedback gain in (4) is calculated by Ackermann's formula $\mathbf{k}^T$=(43.0 19.5 -15.1 3.2). Choosing $\mathbf{L}$ = (1 0 0 0), the predictive observer is designed to estimate the unknown input T_L using the measured reading of the trolley position. The static feedforward gain is determined as in (6.11), K_{fs}= 50.8. Since the motor electromagnetic and power amplifier time-constants are negligible, the dynamic compensation is not necessary (K_{fd}=0). Choosing $\mathbf{Q} = \mathbf{I}_4$ the robust feedback gain, defined in (6.18) is found to be $\mathbf{k}_r^T$=(-43. -15.6 27.1 -21.6). The exponential, Gaussian, and sigmoidal membership functions are used for fuzzy tuning. Table 6.9 gives the values of tuner parameters, γ_m=0.5, σ_r=1, w_{r0}= 0.2, and σ_ε=0.2, when tuning with different membership functions.

Membership function	γ_m	σ_r	w_{r0}	σ_ε
exponential	0.5	1	0.2	0.2
Gaussian	0.5	0.1	0.2	0.07
sigmoidal	0.5	0.5	0.2	0.2

Table 6.19. Tuner parameters

The trapezoidal law is applied for the optimal speed reference of the trolley motion. Figure 6.21 shows the reference (dotted lines) and actual (solid lines) responses of the trolley position (a) and swing angle (b) with a conventional pole-placement controller. With $m = 2m_0$, $l = 0.5l_0$ and T_L=0 oscillations due to parameter sensitivity are observed.

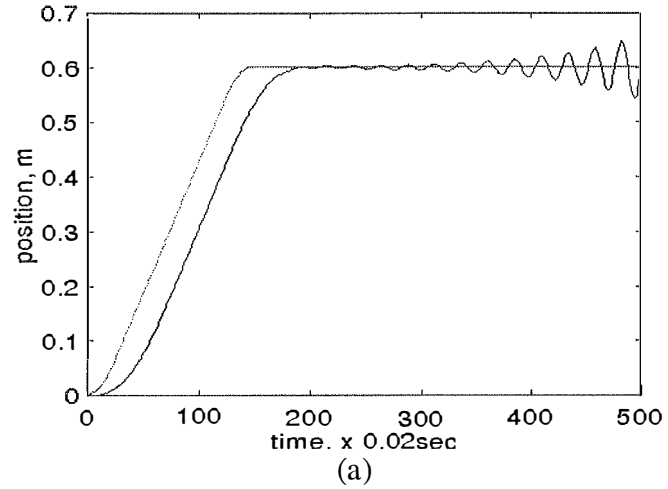

(a)

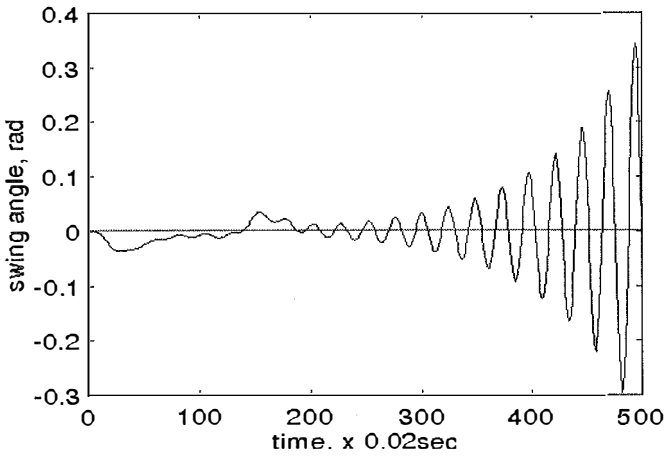

(b)

Figure 6.21. Position (a) and swing (b) responses with pole placement controller, $m = 2m_0$, $l = 0.5l_0$, T_L=0.

These responses with a fuzzy logic controller (Negnevitsky, Ha *et al.* [134]) are shown in Figure 6.22. While fuzzy logic controller is robust to parameter variations, its performance is affected by an external load torque, T_L. Figure 6.23 depicts the responses with the proposed controller under the same conditions and $T_L = 0.5T_{nom}(1+\sin t)$, where T_{nom}= 0.037Nm. It is observed that the responses in Figure 6.23 are more robust to both parameter variations and disturbances. Note that fuzzy tuning with sigmoidal or Gaussian membership functions also provides similar results.

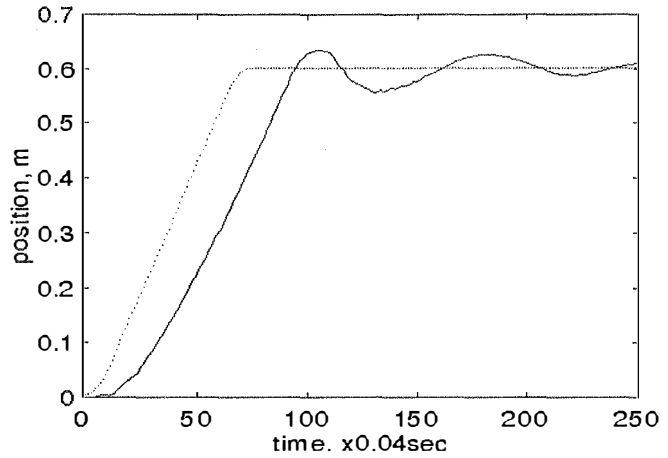

(a)

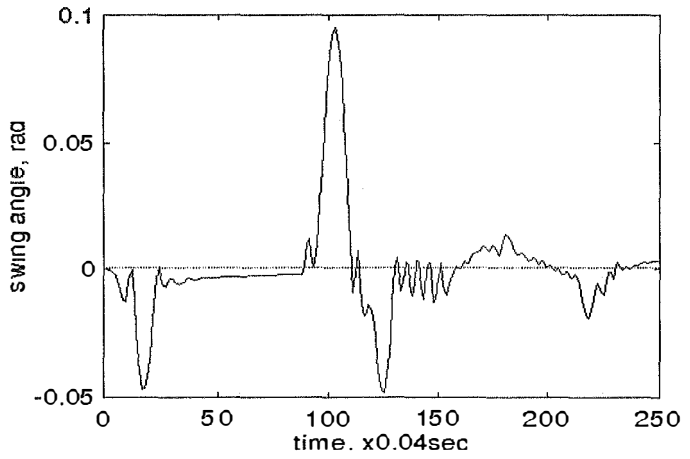

(b)

Figure 6.22. Position (a) and swing (b) responses with fuzzy logic controller, $m = 2m_0$, $l = 0.5l_0$, T_L=0.

The application of fuzzy logic in tuning the coefficients of a robust modal controller has been verified through the control of an overhead crane model. The fuzzy schemes adopt human experience for continuously changing the coefficients of a robust modal controller. Exponential, Gaussian, and sigmoidal membership functions can be employed to input labels to result in explicit expressions for tuning. It is observed that robust modal control with fuzzy tuning can result in strong robustness of the system against parameter variations and external disturbances.

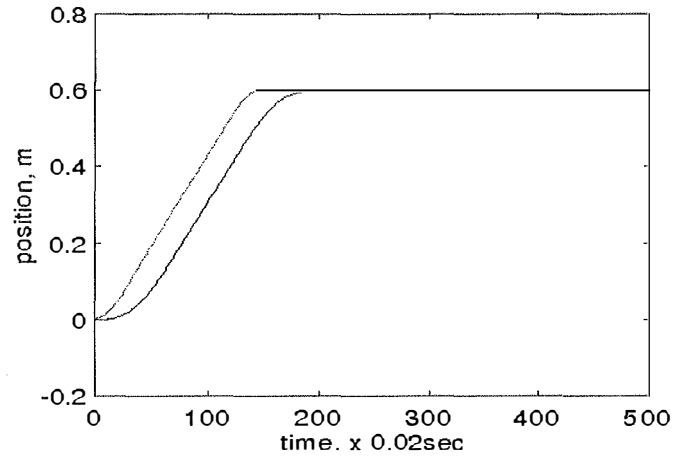

(a)

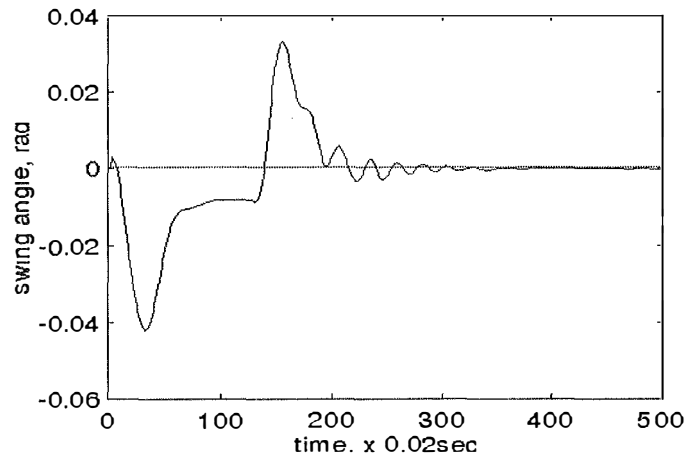

(b)

Figure 6.23. Position (a) and swing (b) responses with fuzzy tuned robust modal controller, $m = 2m_0$, $l = 0.5l_0$, $T_L = 0.5T_{nom}(1+\sin t)$.

6.6 Summary

This chapter has presented a methodology using fuzzy logic and some engineering heuristics to tune the parameters of robust modal controllers for improving robustness. Simple tuning schemes are applied for continuously changing the predictive observer coefficients, the feedforward controller coefficients, and the robust feedback coefficients.

The predictive coefficients of an unknown input observer are tuned taking into account the change of estimated disturbances. As illustrated in estimating the load torque of a two-mass servo system, observer robustness is improved with fuzzy

tuning. Conditional schemes are given for tuning the dynamic feedforward coefficient in relation to the signs of the error and the change of the estimated load torque disturbance. Robustness achieved by the fuzzy-tuned feedforward compensation is verified through the control of a robot arm motion, and a two-mass position drive. Other fuzzy schemes are also proposed to tune the robust feedback gain according to the signs of the error and the change of error. Simulation results obtained through the position control of a two-mass resonant system indicate that the observer-based controllers with fuzzy tuning can be applied to make the system more robust to parameter and load variations. Thus, it can be feasible in flexible structures where the problem of vibration suppression and load rejection is challenging.

Using singletons and the centroid technique for defuzzification, all the fuzzy schemes result in explicit expressions, thus the tuning process is easy and the computational cost is low. The membership functions for input labels can be exponential as well as Gaussian or sigmoidal. Servo drives are chosen here as controlled objects, however, the proposed method can be applied to other linearised dynamic systems suffering from severe uncertainties.

Chapter 7

Neural Network Application to Motion Control

Artificial neural network for control and systems has developed as an interesting topic over the last few years, not only in terms of the research being carried out, but also in terms of the potential range of applications. This chapter provides a brief overview of recent developments of neural network-based controllers in motion control systems and some neural network-based approaches to the control of electrical drives and manipulators with changing parameters and load, and with nonlinearities.

7.1 Introduction

Artificial intelligence (AI), systematically used since the late 1950's, is a machine emulation of the human thinking processes. Artificial intelligence tools, such as expert system, fuzzy logic, and neural network are believed to usher a new area in motion control in the coming decades (Bose [11]).

Expert systems, flourishing since 1960's, are computer programs that emulate the reasoning process of a human expert in certain domain. The core of the expert system is the representation of knowledge transferred from human domain expertise. Knowledge can be shown in two types: the expert knowledge embedded in the knowledge base, and the data, facts, and statements that are normally embedded in the database for supporting the expert knowledge. Expert system techniques have the potential for practical applications in some aspects of power electronics and motion control. In fault diagnosis and monitoring for AC drives, the expert system can identify the fault by embedding the expertise of a diagnostic technician. With easily modified and updated database, the expert system can help in drive product selection. In real-time expert system-based control, the input parameters are accessed from the sensors. The expert system is used to process these signals and generate the appropriate control action. Since its genesis in the mid 1960's, fuzzy logic gradually

helped to supplement the expert system and a more general methodology of reasoning called fuzzy expert system was born. In general, fuzzy expert system which is applicable wherever the knowledge base of an expert system contains fuzziness, can provide an enhancement for reasoning with uncertainty and imprecision (Hall and Kandel [166]). Fuzzy logic can be applied to control, diagnostics, modelling, and estimation. A fuzzy control, as described in Chapters 4, 5, and 6, essentially embeds the intuition and experience of a human operator, and sometimes those of a designer and researcher. It can be shown that fuzzy control is basically adaptive in nature, and can give improved robustness in systems with unknown or ill-defined plant model, or systems with changing parameters and load. Previous chapters have demonstrated the use of fuzzy tuning schemes for robustness enhancement in many servo drives. This chapter deals with the application of another AI branch, artificial neural networks or neural networks, for this purpose.

The study of artificial neural networks is an attempt to understand the functionality of the brain. Fundamentally, the human brain forms a massive communication network, consisting of billions of nerve cells, also known as neurons. These neurons are interconnected to constitute the biological neural network. The artificial neural network (ANN) tends to simulate the biological one by electronic computational circuits. The ANN technology is the most generic for emulating the human thinking process which is generated by the action of the biological neural network. Gradually evolving since 1950's, the ANN technology has practically captivated the attention of scientific community since the beginning of 1990's (Widrow & Lehr [15]). Neural network applications to engineering problems are many and varied (process control, diagnostics, identification, pattern recognition, robot vision, flight scheduling, and so on). Neural networks can be used for various control and signal processing applications in power electronics and drives. A neural net can be trained for diagnostics of a power electronics and drive system. A nonlinear dynamical system, e.g. in robotics, can be emulated by time-delayed input and output signals with a feedforward network used in identification and control (Narenda & Parthasarathy [27]). In control systems, the use of neural networks is getting increased attention because of many advantages in speed of adaptation, noise rejection, and tracking performance over adaptive control techniques (Kraft & Campagna [167]). The following sections are involved in a brief review on neural network-based control (Hunt *et al.* [168]) and details on some of its applications in servo systems and systems with severe nonlinearity and parameter variation problems (Ha & Negnevitsky [34, 44], Ha [45], Palis, Ha *et al.* [33, 165]).

7.2 Neural networks: basic concepts and application to control

In recent years there has been an increasing interest in studying the mechanisms and structure of the brain. The human brain is said to have around 100 billions neurons or nerve cells, each neuron is interconnected to 1000 to 10 000 other neurons. A biological neuron is a processing element that receives incoming impulses via input paths called dendrites. If the number of incoming impulses within a certain period of time exceeds some threshold, the neuron will "fire," producing an output impulse along the axon that connects to dendrites of many other neurons. When a neuron fires, it transmits its impulse via the axon and synapses. Each synapse is an infinitesimal gap in the dendrite which is filled with neurotransmitter fluid that either accelerates or retards the flow of electrical charges. These electrical signals go to the nucleus or soma of the neurons. The adjustment of the impedance or conductance of the synaptic gap leads to "memory" or "learning process" of the brain (Bose [11]).

7.2.1 Neural network architecture

The artificial neuron (so-called neuron, node, cell, connectionist model, perceptron, or adeline) is a processing element having the standard and unifying architecture shown in Figure 7.1 (Hunt *et al.* [168]). The basic model of a neuron constitutes of three components: a weighted summer, a linear dynamic system, and a nonlinear function. The weighted sum is described by

$$v_i(t) = \sum_{j=1}^{N} a_{ij} y_j(t) + \sum_{k=1}^{M} b_{ik} u_k(t) + w_i, \tag{7.1}$$

where y_j, $j = 1,\ldots,N$, are the neuron outputs; u_k, $k = 1,\ldots,M$, are the external inputs; and a_{ij}, b_{ik}, and w_i are the corresponding weights. The weights are connection strengths whose function are analogous to that of synaptic junctions in a biological neuron. The weights can be positive or negative corresponding to acceleration or inhibition of the flow of electric signals. The transfer function $H(s) = V_i(s)/X_i(s)$ for the linear dynamic system have the following common forms:

$$H(s) = \frac{1}{\alpha_0 s + \alpha_1} \quad \text{or} \quad H(s) = e^{-sT}, \tag{7.2}$$

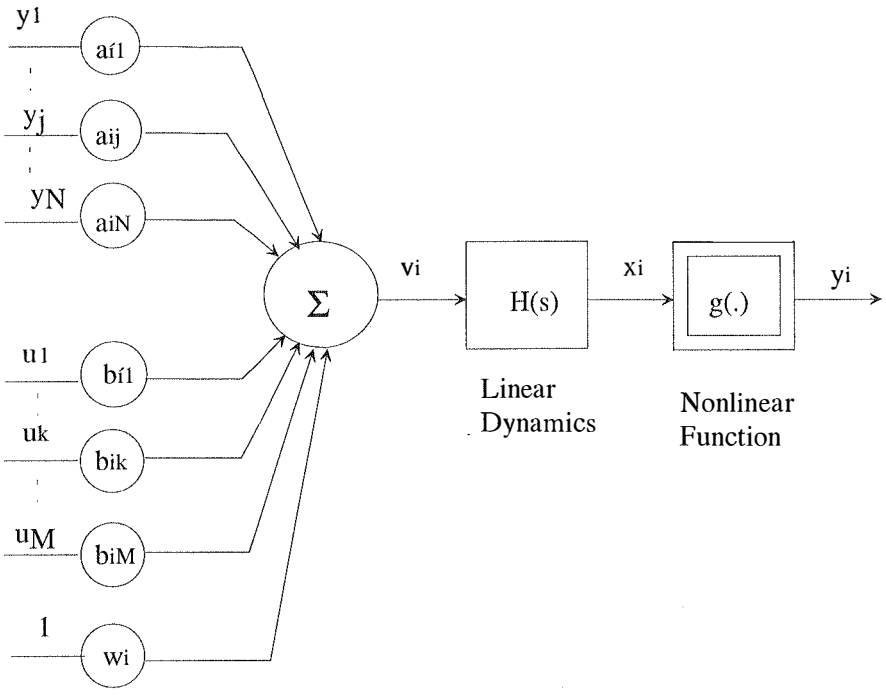

Figure 7.1. Architecture of an artificial neuron.

where α_0, α_1 are constants. The non-dynamic nonlinear function $y_i = g(x_i)$ can be classified as differentiable or non-differentiable, pulse like or step like, and positive (bound to the range (0,1)) or zero mean (bound to the range (-1,1)). Some standard functions are threshold, signum, sigmoid, Gaussian, and hyperpolic tangent, respectively:

$$\begin{aligned} &g(x) = +1 \text{ if } x > 0 \text{ else } 0, \quad g(x) = +1 \text{ if } x > 0 \text{ else } -1, \\ &g(x) = 1/(1+e^{-x}), \qquad g(x) = e^{-x^2/\sigma^2}, \\ &\text{and } g(x) = \tanh(x) = (e^{x} - e^{-x})/(e^{x} + e^{-x}). \end{aligned} \tag{7.3}$$

The sigmoid is positive, monotonic, differential, and step-like having the largest incremental gain at zero signal. Thanks to these particularly interesting properties, it is most commonly used in neuron models.

The three components of the neuron shown in Figure 7.1 can be combined in various ways. The behaviour of networks resulting from such a combination depends on the connection matrix $\mathbf{A} = (a_{ij})_{N\times N}$ and on the form of $H(s)$. The interconnection of neurons allows us to encode relations between the variables giving different powerful processing capabilities. Neural networks can generally be classified as feedforward or

feedback types. In multilayer feedforward networks, the connection of several layers gives the possibility of complicated nonlinear mapping between the inputs and the outputs. This capability can be used to implement classifiers or to represent complex nonlinear relations among the variables. Such networks are typically static, that is $H(s) = 1$. The connection matrix **A** is such that the outputs are partitioned into layers so that a neuron in one layer receives as inputs only from neuron outputs in the previous layer (or only from the network inputs in case of the first layer) as shown in Figure 7.2.

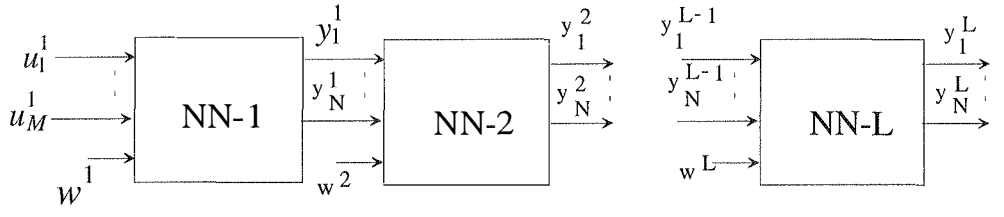

Figure 7.2. Multi-layer feedforward networks

Dynamic or recurrent networks are qualitatively different from static ones, because their structure incorporates feedback. The introduction of feedback produces a dynamic network with several stable points. The general equation can be expressed as

$$\begin{aligned} \dot{\mathbf{x}}(t) &= F(\mathbf{x}(t),\ \mathbf{u}(t),\ \theta), \\ \mathbf{y}(t) &= G(\mathbf{x}(t),\ \theta), \end{aligned} \tag{7.4}$$

where $\mathbf{x}(t)$ is the vector of the state variables, $\mathbf{u}(t)$ the external inputs, $\mathbf{y}(t)$ the outputs, θ the parameters of the network, F is a function that represents the network feedback structure, and G represents the nonlinear relation between the state variables and the outputs. In Kohonen [169], feedback networks were introduced in the context of associative memory (CAM) problems for pattern recognition. There exist numerous neural network architectures, however, at present, the majority of power electronics and motion control applications use the feedforward architecture ($H(s) = 1$) with backpropagation algorithm (Bose [11]). Figure 7.3 shows a typical feedforward network with three inputs and two outputs, having three layers: input layer I, hidden layer J, and output layer K. The number of hidden layers and the number of neurons in each hidden layer (four in Figure 7.3) depend on the design considerations.

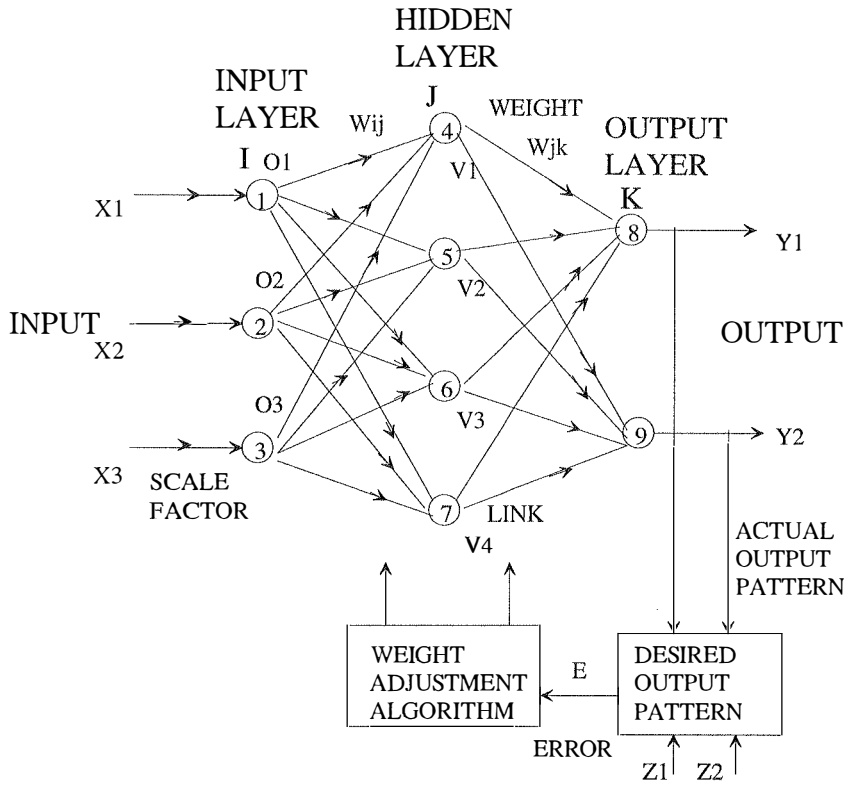

Figure 7.3. A three-layer feedforward network

7.2.2 Learning in neural networks

The application of artificial neural networks normally proceeds in two phases: the recall phase and the training phase. In the recall phase, the networks, which have been trained with appropriate data with constant coefficients, provide a fixed behaviour with constant coefficients in their architecture as described above. The training phase presents algorithms for automatic adjustment of network coefficients, a process called learning. A learning algorithm, associated with any change in memory as represented by the weights, is a parametric adaptation algorithm. If an input set of data corresponds to a definite signal pattern, the network can be trained to give a correspondingly a desired pattern at the output. the capability of learning is explained by the distributed intelligence contributed by the weights. The input-output pattern matching is possible if proper weights are selected. The supervised learning process incorporates an external reference signal (learning by a teacher) or global information about the system. The unsupervised learning process incorporates no external reference signal and relies only on local information and internal signals (learning with a critic). In supervised learning, the actual output pattern can be compared with

the desired output pattern and the weights can be adjusted by an algorithm until the pattern matching occurs. At the end of training when the error is adequately small, the network can recall all the trained output patterns (look-up table function), and interpolate and extrapolate the trained patterns as well.

In multi-layer non-dynamic networks, *backpropagation* algorithm is commonly used. In the beginning, the network is assigned random weights (w_{ij} and w_{jk} in Figure 7.3). For a given input-signal pattern, the output pattern is calculated step-by-step in the forward direction. A cost function given by the squared error between the net output for the set of input patterns is generated and this is minimised by gradient descent method adjusting the weights one at a time. The net input to the j th neuron (node) in layer J (hidden layer) is:

$$net_j = \sum_{i=1}^{M} w_{ij} o_i , \tag{7.5}$$

where j is the processing unit under consideration, o_i is the output of the i th neuron connected to the j th neuron, w_{ij} is the connection weight between the i th and j th neurons, and M is the number of neurons feeding the j th neuron (M=3 in Figure 7.3). The output of the j th node is:

$$v_j = g(net_j), \tag{7.6}$$

where g is the nonlinear activation function, usually a sigmoid:

$$v_j = \frac{1}{1+e^{-(net_j+\theta_j)/\theta_0}}, \tag{7.7}$$

where the net parameter θ_j serves as a threshold or bias and the effect of θ_0 is to modify the sigmoid shape (Figure 7.4). Similarly, for the input and output of the k th node in layer K are:

$$\begin{aligned} net_k &= \sum_{j=1}^{N} w_{jk} v_j , \\ y_k &= g(net_k), \end{aligned} \tag{7.8}$$

respectively, where N is the number of neurons in the hidden layer (N=4 in Figure 7.3).

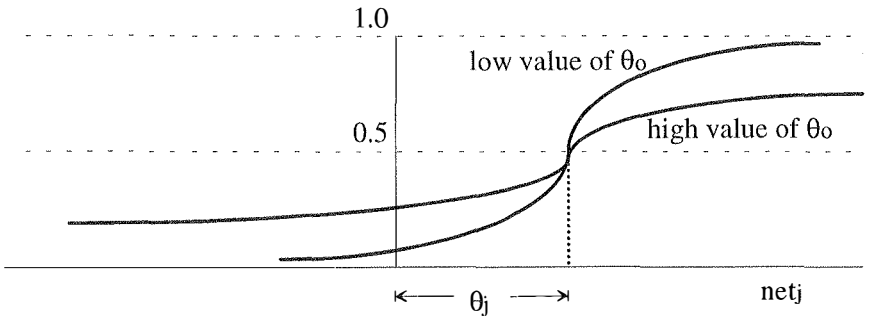

Figure 7.4. Sigmoid with bias and shape modification.

In the learning phase, the pth pattern is presented as input ($p = 1,2,..,P$), and the weights in all connecting links together with the thresholds are adjusted such that the target or desired output t_k^p is obtained at the kth output node ($k = 1,2,..,S$). Once this adjustment has been accomplished by the net, another pair of patterns and targets is presented, and the net is asked to learn that association also. Ideally, the net will find a single set of weights and biases that will satisfy *all* the (pattern, target) pairs presented to it. However, the outputs y_k^p and the desired values t_k^p are generally not the same. For the pth input pattern, the square of the error for all the output-layer neurons is given by

$$E_p = \frac{1}{2}(\mathbf{t}^p - \mathbf{y}^p)^T(\mathbf{t}^p - \mathbf{y}^p) = \sum_{k=1}^{S}(t_k^p - y_k^p)^2 . \tag{7.9}$$

The average system error for the set of P patterns is written as

$$E = \frac{1}{2P}\sum_{p=1}^{P}\sum_{k=1}^{S}(t_k^p - y_k^p)^2 . \tag{7.10}$$

The weights are changed to reduce the cost functional to a minimum value as rapidly as possible by the gradient steepest-descent algorithm. Starting from the output layer, the gradient method leads to the update equation:

$$w_{jk}(n+1) = w_{jk}(n) - \eta\frac{\partial E_p}{\partial w_{jk}(n)} = w_{jk}(n) + \Delta w_{jk}(n), \tag{7.11}$$

where $w_{jk}(n+1)$ is the new weight, $w_{jk}(n)$ is the old weight, $\eta>0$ is the learning rate, and $\Delta w_{jk}(n)$ is the weight incremental change. The partial derivative $\partial E_p/\partial w_{jk}$ can be evaluated using the chain rule:

$$\frac{\partial E_p}{\partial w_{jk}} = \frac{\partial E_p}{\partial net_k}\frac{\partial net_k}{\partial w_{jk}} = \frac{\partial E_p}{\partial net_k} v_j .$$

By defining

$$\delta_k = -\frac{\partial E_p}{\partial net_k}$$

we obtain the delta rule of the weight change for any kth output-layer neuron:

$$\Delta w_{jk} = \eta \delta_k v_j . \tag{7.12}$$

Applying the chain rule to δ_k yields

$$\begin{aligned}\delta_k &= -\frac{\partial E_p}{\partial net_k} = -\frac{\partial E_p}{\partial y_k^p}\frac{\partial y_k^p}{\partial net_k} \\ &= (t_k^p - y_k^p) g_k'(net_k)\end{aligned},$$

where the pth subscript denotes the pattern number. Using sigmoid of the form (7.7) for the nonlinear activation function, we have $\frac{\partial y_k^p}{\partial net_k} = g_k'(net_k) = y_k^p(1 - y_k^p)$, thus the delta δ_k in (7.12) is given by the following expression:

$$\delta_k = (t_k^p - y_k^p) y_k^p (1 - y_k^p). \tag{7.13}$$

If the weights do not link with the output neurons directly, the update equation is written as

$$w_{ij}(n+1) = w_{ij}(n) - \eta \frac{\partial E_p}{\partial w_{ij}(n)} = w_{ij}(n) + \Delta w_{ij}(n), \tag{7.14}$$

where the incremental change Δw_{ij} for hidden layer units is calculated by

$$\begin{aligned}\Delta w_{ij} &= -\eta \frac{\partial E_p}{\partial w_{ij}} = -\eta \frac{\partial E_p}{\partial net_j}\frac{\partial net_j}{\partial w_{ij}} \\ &= \eta(-\frac{\partial E_p}{\partial v_j}\frac{\partial v_j}{\partial net_j}) o_i = \eta(-\frac{\partial E_p}{\partial v_j}) g_j'(net_j) o_i\end{aligned}$$

or

$$\Delta w_{ij} = \eta \delta_j o_i . \tag{7.15}$$

The factor $\partial E_p / \partial v_j$ can be rewritten for its evaluation in terms of known quantities (Pao [170]):

$$-\frac{\partial E_p}{\partial v_j} = -\sum_k \frac{\partial E_p}{\partial net_k}\frac{\partial net_k}{\partial v_j} = \sum_k (-\frac{\partial E_p}{\partial net_k})\frac{\partial}{\partial v_j}\sum_m w_{mk} v_m$$
$$= \sum_k (-\frac{\partial E_p}{\partial net_k}) w_{jk} = \sum_k \delta_k w_{jk} .$$

In this case, since

$$\delta_j = g_j'(net_j)\sum_k \delta_k w_{jk} ,$$

when using sigmoid (7.7) for the nonlinear activation function, the expression for the delta δ_j in (7.15) can be obtained as

$$\delta_j = v_j^p (1 - v_j^p)\sum_k \delta_k w_{jk} . \tag{7.16}$$

The iterative process propagates the error backward in the network (backpropagation) following (7.12), (7.13) and (7.15), (7.16) is called the learning procedure with the generalised delta rule formulated by Rumelhart, Hinton, and Williams [171]. Note that the thresholds θ_j are learned in the same manner as the weights. The weights are iteratively updated for all the P training patterns. In a successful learning exercise, the system error will decrease with the number of iterations, and the procedure will converge to a stable set of weights. The choice of a large value for the learning rate η leads to rapid learning but might also result in oscillations. To avoid local error minima, a *momentum* term $\alpha[w_{ij}(n) - w_{ij}(n-1)]$ is added to the right of (7.14), thus the weight change at the $(n+1)$th step is given by

$$\Delta w_{ij}(n+1) = \eta(\delta_j o_i) + \alpha \Delta w_{ij}(n), \tag{7.17}$$

where α is a proportional constant. A finite momentum constant α tends to dampen oscillations but can also serve to slow the rate of learning. The speed of backpropagation can be increased by the use of adaptive learning rate which attempts to keep η as large as possible while keeping learning stable:

$$\eta(n+1) = u\eta(n), \text{ with } u > 1 \tag{7.18}$$

Normally, training static neural networks is very time-consuming and accomplished off-line with the help of a computer simulator program. Qualitatively different from static networks, dynamic or recurrent networks incorporate feedback in their structure. Thus, in learning phase, the output of every neural is fed back with varying weights to the inputs of all neurons. The network architecture is inherently dynamic and usually one-layered, since its complex dynamics gives it powerful representation capabilities. Therefore, when a pattern is applied at the input, the signals reverberate back and forth until they settle down to an equilibrium. There are two general concepts relating to learning in dynamic neural networks. The purpose of *fixed points learning* is to make the network reach the prescribed equilibria or perform steady-state matching. On the other hand, *trajectory learning* trains the network to follow the desired trajectories in time (Zbikowski & Gawthrop [172]). The convergence of a dynamic network to a final answer is defined by a mathematical function called *computational energy*. This energy function reaches a minimum as the solution is obtained. The design and training of a dynamic network is more complicated than a static one. However, dynamic networks offer a universal and powerful approach to nonlinear adaptive control techniques.

7.2.3 Neural networks for control

A neural network can be used for various control and signal processing applications in power electronics and motion control. The use of neural networks in this area is mainly based on their nonlinear functional mapping properties. One straight forward application is one- or multidimensional function generation with the capability of interpolation between the sample data values. An example of this application is found in a vector control system of a permanent magnet synchronous motor, where neural networks are used to closely mimic nonlinear relationships given in look-up tables (Krishnan *et al.* [173]). A network can be trained for on-line or off-line condition monitoring of power electronic systems, for example, an AC-drive system, where a neural network can receive the sensor signals or fast Fourier transform patterns and be trained to draw important conclusions. Neural networks may be useful for control purposes because they have the capability of learning a nonlinear control law. The application of neural networks to the control of dynamic systems can be explained by regarding the conventional approach, depicted in the control system of Figure 7.4.

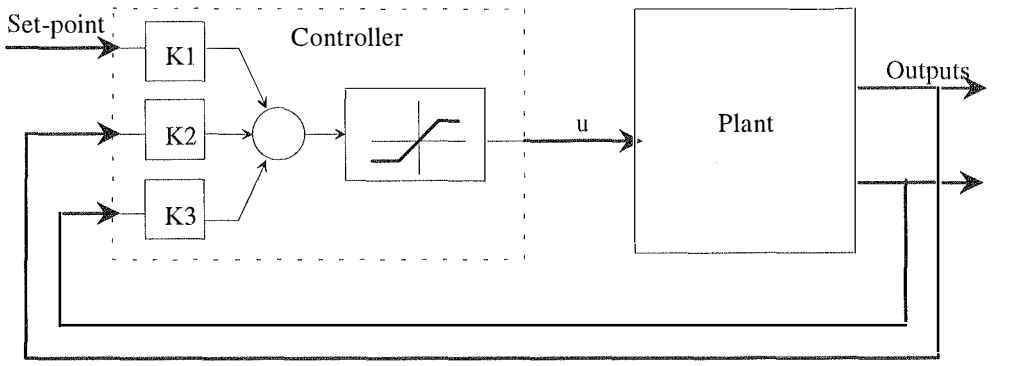

Figure 7.4. Conventional control system.

The control structure can be a modal controller for a DC-motor servo drive with position and speed feedback (Figure 3.1). Note that this conventional controller has much in common with the net architecture in the neural network controller shown in Figure 7.5. A reference trajectory, specifying the desired process outputs, may be used as a performance measure for training the neural net. The question is how to translate the output error into a control error. A possible scheme, using the error between the desired and actual outputs and training rules to adjust the weights of a feedforward network (Figure 7.5), is very close to adaptive control.

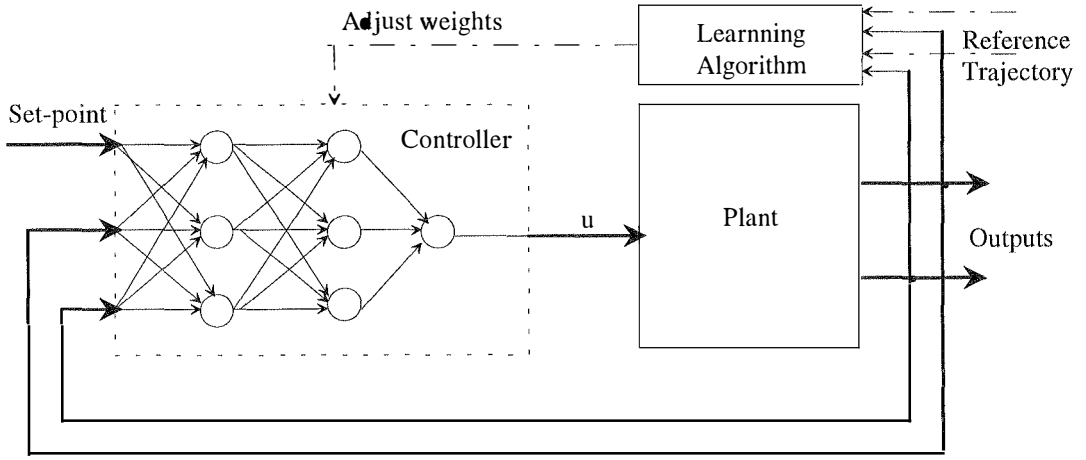

Figure 7.5. Neural network control system.

In the literature on the neural network application to control, a large number of structures have been proposed. Among these techniques, supervised control and direct inverse control are two direct approaches to control. In *supervised control*, the

controller output mimics the action of an expert or operator. Training the network is similar to learning a system forward model. In the structure of Figure 7.6, the teacher (i.e. the system) provides target values directly in the output coordinate system of the learner (i.e. the network model). The network target outputs used for training correspond to the human control input to the system.

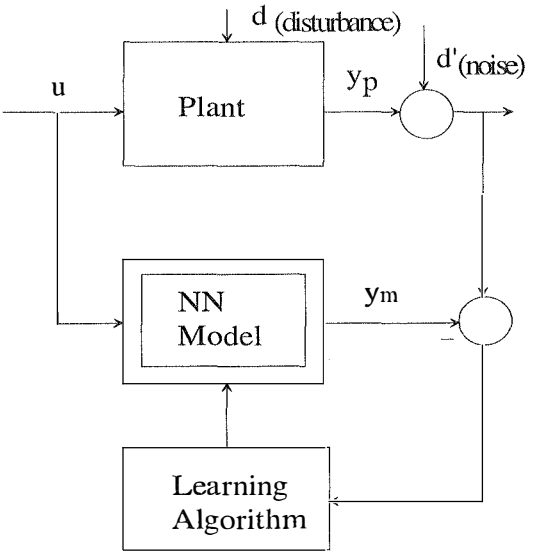

Figure 7.6. Supervised control

In *direct inverse control*, the inverse model, obtained from the neural net NN, is simply cascaded with the plant in order that the composed system results in an identity mapping between desired response (i.e. the network inputs) and the controlled system output. In this case, the network plays directly the role of a controller in the configuration shown in Figure 7.7.

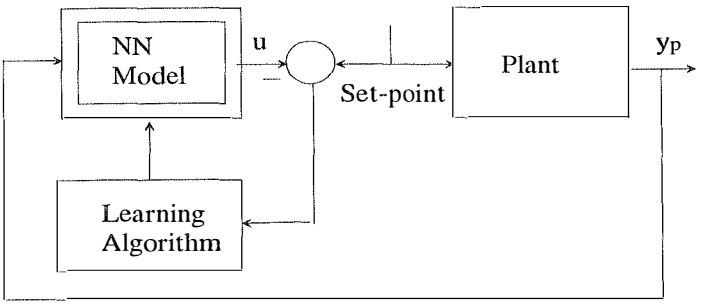

Figure 7.7. Direct inverse control

The other control structures using neural networks combined with a stable reference model (*model reference control*) or with a system model (*internal model control*) are outlined in Hunt *et al.* [168]. While recurrent networks are universal, parametric systems that can be used as identifiers and dynamic controllers, the complexity of their analysis and design is a challenging problem. At present, most of neural network-based applications in power electronics and drives exploit static networks possessing proven capabilities of arbitrary nonlinear approximation.

7.3 Neural network implementation of a fuzzy logic controller

As stated in the section above, a neural network can closely approximate any control relationship of practical interest, to learn such a relationship through a training process, and also to interpolate the controller outputs the inputs do not belong to the training set of the inputs. Essentially, a neural network controller is a nonlinear parametric system which can be easily worked out because of its mathematical rather than linguistic nature of a fuzzy logic controller. A straightforward approach is to implement a fuzzy logic controller in a neural network and expect the system performance with neural control will be as good as with fuzzy control. This approach is motivated by the work described in Buja & Todesco [174]. In this section, it is illustrated through the control of a laboratory crane model. The plant dynamics and the design of a fuzzy logic controller was described in Section 4.4.2.

7.3.1. General system description

A common task for motion control of a swinging load, e.g. in crane, pendulum, and cart-pole systems, is to move a load from an initial position to a specified final one. The loads are usually varying. The inertial parameters of the crane are also uncertain. On the other hand, when a load is transported by a crane, it often exhibits oscillatory swings. The back and forth swinging of the load during the transfer motion can cause considerable problems, especially in bounded places, and in the presence of uncertainties in the system dynamics. Conventional techniques can be applied to address this subject, for example, optimal control in Yoshida & Kawabe [175], adaptive control in Soussi & Koivo [176], and robust modal control as described in Chapter 3. Fuzzy logic has recently arisen as an attractive tool to control ill-defined or parameter-variant plants. A fuzzy logic controller (Negnevitsky, Ha *et al.* [134]) or a robust modal controller with fuzzy tuning (Ha & Negnevitsky [42]) can be used for positioning a swinging load. However, fuzzy logic controllers usually suffer from a

heavy computation burden when implemented. Moreover, its performance relies on the soundness of knowledge acquisition techniques and the availability of human experts. In the following a neural network controller is used to implement the fuzzy logic controller described in Section 4.4.2 for positioning the load of an overhead crane model. The validity of the proposed methods are verified through simulation and experimental results.

The plant block diagram is shown in Figure 7.8 (Ha & Negnevitsky [34]) where analog/digital (A/D) and digital/analog (D/A) converters are used at the interface (see Section 4.4.2). The neural network (NN), shown in Figure 7.9, has two inputs e and θ, a hidden layer, and an output u of one linear neuron, where e is the trolley position error, θ is the chain angle, and u is the control signal.

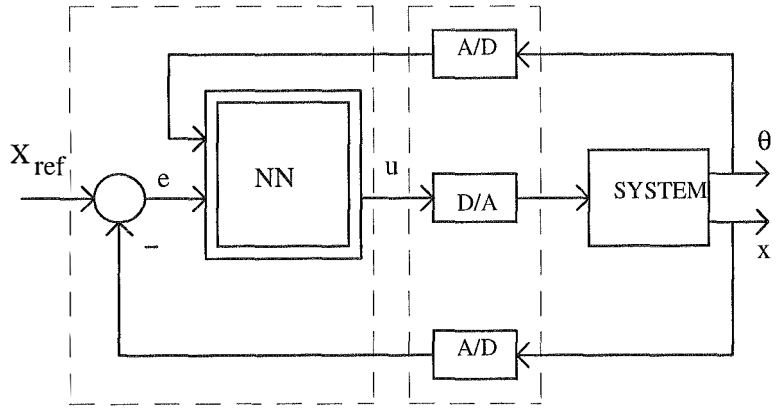

Figure 7.8. Block diagram of the control system.

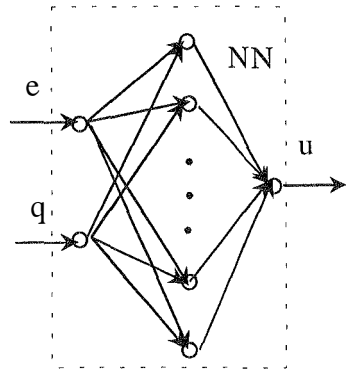

Figure 7.9. Network schematic diagram

In order to obtain a good approximation and to reduce the training time, radial basis function networks (see, e.g., Chen *et al.* [177]) are chosen in the hidden layer. Radial basis networks are non-dynamic networks with a better approximation property in comparison with the other feedforward networks. An approximation scheme is said to have the property of *best approximation* if in the set of approximating functions there is one which has minimum distance from the given function (Poggio & Girosi [178]). The structure of a radial basis neuron with N inputs is shown in Figure 7.10. Its output is a Gaussian function of the Euclidean distance between the input vector $\mathbf{p}_i$ and its weight vector (the centre of the basis function) $\mathbf{w}_i$, multiplied by the bias b_i:

$$y_i = \exp(-\|\mathbf{p}_i - \mathbf{w}_i\|^2 b_i^2). \tag{7.19}$$

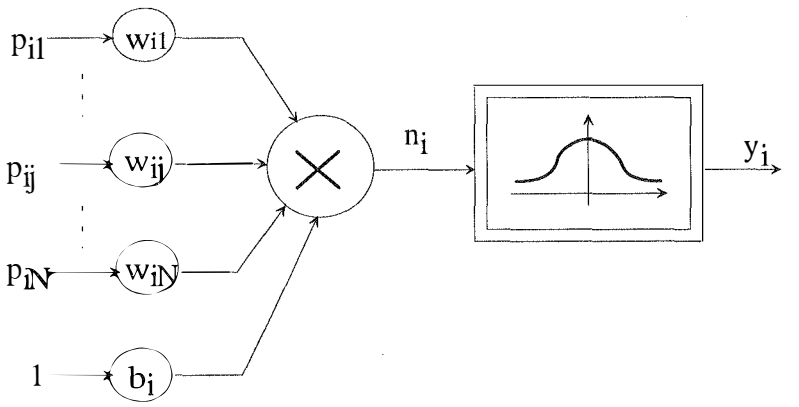

Figure 7.10. Radial basis neuron.

The bias b_i, which is the inverse of the radial arm or spread constant σ_i ($b_i = 1/\sigma_i$), allows the sensitivity of the radial basis to be adjusted. As with the sigmoidal feedforward networks, the number of neurons depends on the size of the training data. and the choice of the basis function centres. Radial basis networks may require more neurons than feedforward backpropagation networks, but they can be trained in a fraction of the time it takes to train standard static networks.

7.3.2. Simulation and experimental results

For implementing the non-linear relationship $u = G(e, \theta)$ obtained from the fuzzy logic controller inputs and output (see Section 4.4.2), the neural network undergoes a supervised two-stage training (Ha & Negnevitsky [34]). In the first stage, the neural

net learns the desired input-output relationship in the transient process. A pattern of 500 two-element input vectors and a target of the associated one-element output vector are used for training. The net error goal is set at 10^{-4} in the transient stage and 10^{-10} in the steady-state stage. The maximal number of neurons in the hidden layer depends on the appropriate choice of the radial basis function spread constant to avoid underlapping and overlapping. Table 7.1 summarises the network parameters obtained to achieve the given error goal. Figure 7.11 depicts the sum-squared network error in two training stages.

Process	Spread constant	Error goal	No. neurons in the hidden layer
Transient	10^{-3}	10^{-4}	110
Steady-state	10^{-6}	10^{-10}	287

Table 7.1. Network parameters.

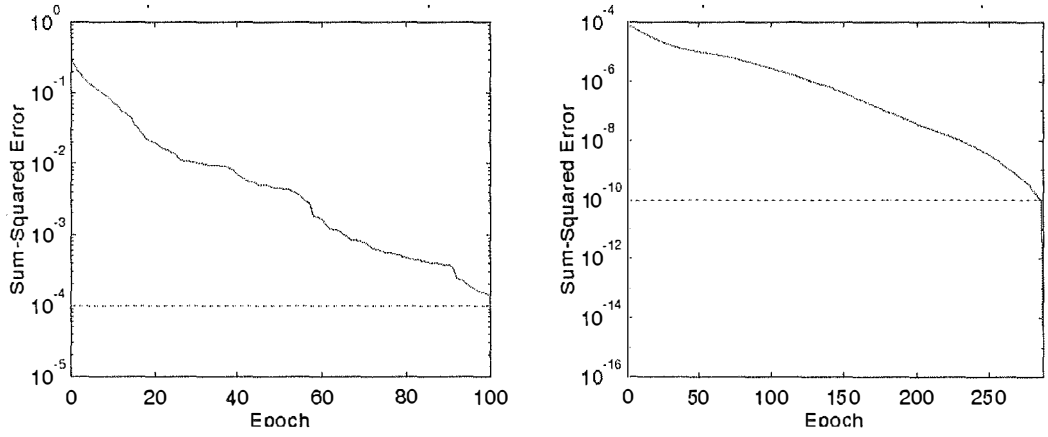

(a) (b)

Figure 7.11. The sum-squared in (a) the transient stage, and (b) the steady-state stage.

The simulated swing and position responses with a step input reference are shown in Figure 7.13 and Figure 7.14, respectively, where the dot-dashed line represents the response obtained from a fuzzy logic controller and the solid line from its neural net implementation.

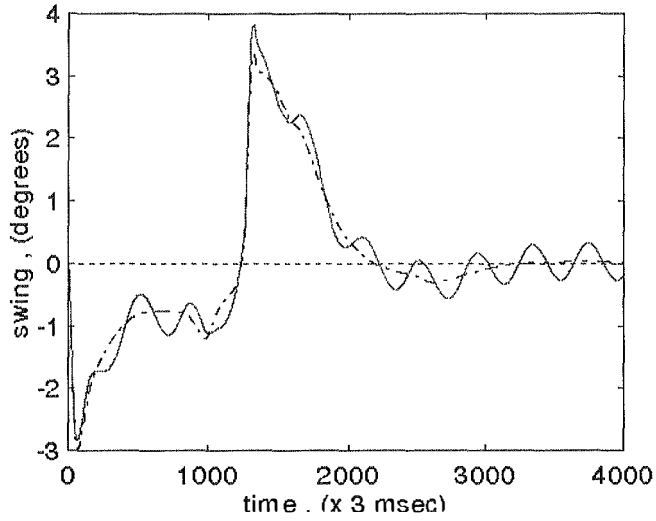

Figure 7.13. Swing responses with fuzzy and neural controllers.

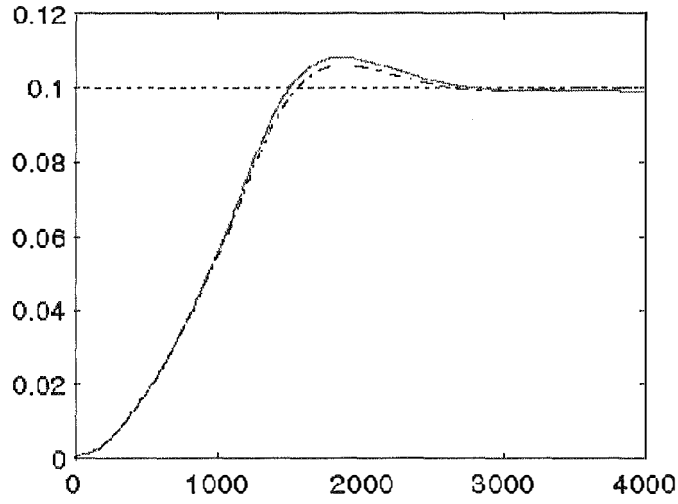

Figure 7.14. Position responses with fuzzy and neural controllers.

Figure 7.15 plots the experimental swing responses obtained from the proposed neural network implementation of the fuzzy logic controller described in Section 4.4.2, and from conventional P and PI controllers. These response practically coincide with those shown in Figure 4.27. The results demonstrate that a neural network can learn the fuzzy logic controller input-output relationship to achieve practically the same control performance as obtained from fuzzy control.

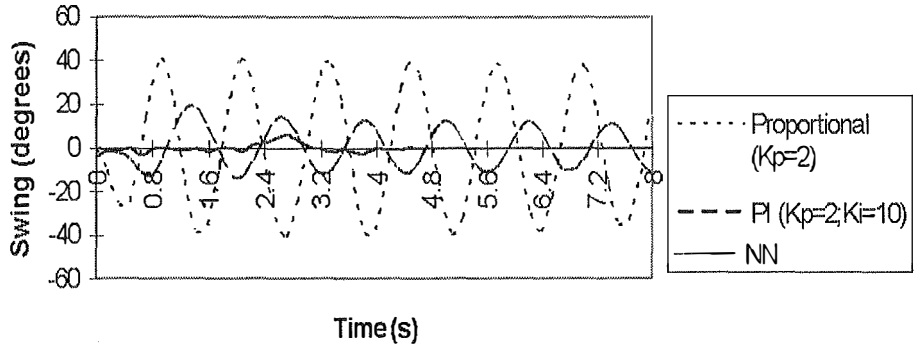

Figure 7.15. Experimental swing responses

7.4 Neural network-based controller for tracking systems

Tracking a given trajectory is a common task in industrial drives. As noted in Dote [65] modern control techniques such as the sliding mode, adaptive controls, robust control can be successfully applied to obtain high quality tracking performance. However, the effectiveness of these techniques diminishes when the servo drives are excessively affected by structured and/or unstructured uncertainties. Even in a well-structured setting for an industrial use, some electromechanical objects, such as robotic manipulators, are subject to structured and/or unstructured uncertainties. Structured uncertainty originates from the imprecision of the system description, parameter variations, and unknown load torques. Unstructured uncertainty is characterised by the unmodelled dynamics resulting from the presence of high-frequency mode, time-delays, and severe nonlinearities. For improving robustness, several control techniques are evolving such as the sliding mode in variable structure systems (Utkin[7], DeCarlo *et al.* [70]), self-tuning and model reference adaptive controls (Astrom [69], Egami *et al.* [102]). Sliding mode control is efficient dealing with structured uncertainty such as changing parameters and load. However, the observation noise and the chattering phenomena due to large control gains are challenging issues and there is a trade-off between robustness and chattering. Moreover, sliding mode control requires a valid model and/or dynamics of the controlled object. Thus, the controller is, mainly due to the structured uncertainty, sensitive to large parameter variation and noise. Conventional adaptive control schemes require information about the plant structure and may not guarantee the system stability in the presence of unmodelled dynamics. In addition, adaptive control algorithms are usually complicated and thus, need excessive computation effort for real-time implementation. Although the adaptive controls are effective in

compensating the influence of the structured uncertainty, it is not clear that adaptive means can overcome the unstructured uncertainty.

Recently, there has been increasing interest in designing and implementing an intelligent controller which can adopt skills of an experienced operator. Artificial intelligent tools such as expert system, fuzzy logic, and neural network have advanced significantly in recent years and are believed to find wide applications in industrial electronics and motion control (Bose [11]). Fuzzy logic controllers (Lee [110]), which are capable of providing an effective solution to most complex systems, can be designed with a minimum understanding of the controlled object. Fuzzy tuning has been demonstrated to be a rigorous tool to deal with uncertainties in servo drives (Ha [148], Ha & Negnevitsky [37]). However, fuzzy logic controllers may suffer from a heavy computational burden required to translate the fuzzy inference into a control action. As mentioned in Section 7.2, artificial neural networks, which have the ability to mimic the adaptive distributed architecture in the human brain, provide potential alternatives to tackle the problem mentioned above. The error backpropagation algorithm (Werbos [25]) is widely used to train neural networks. Most of the neural networks applied to servomechanism learn the inverse dynamics of the controlled object (Lee *et al.* [32], Saad *et al.* [179]), based on an observation of its inputs and outputs. In practice, training neural networks in some cases may take time in order to achieve the error goal, and thus, make on-line training infeasible. For trajectory tracking control, neural networks can also be applied to generate the proper control action without the necessity to identify or learn the plant dynamics. Tai *et al.* [180] proposed a neural network used as an classifier to recognise the patterns of the error signal between the plant output signal and the reference signal. An appropriate control action is calculated proportionally to the control error for each pattern. In fact, a proportional type controller cannot adequately meet high quality servo requirements. In fuzzy control systems, proportional-derivative type controllers are usually applied to increase stability and reduce overshoot (Malki *et al.* [159]). In this section, the tracking performance is improved by using the neural network that can be trained to cluster the groups of both the control error and its derivative which an appropriate control action would correct. The control signal is generated without *a priori* knowledge of the plant dynamics. Thus, it can be implemented in a variety of servo drive applications. The proposed scheme is verified through the control of an overhead crane model of the previous section. Simulation results demonstrate the servo robustness with respect to parameter and load variations, and to nonlinear

dynamics (Ha & Negnevitsky [44]). The application of this approach can be extended to multi-mass servo systems (Ha [45]).

7.4.1. Network architecture and learning

A three-layer feedforward neural network is utilised with the error backpropagation learning method. For learning the plant inverse dynamics, a multilayer neural network with sigmoidal nonlinearities can approximate any arbitrary functions representing the plant input-output relationship. However, it is believed that in some tracking systems, identifying or learning the plant dynamics is not necessary as long as a proper control signal can be generated to make the output closely, quickly, and robustly follow any prescribed reference signal. In the following, the neural net is used as a pattern classifier to learn decision functions for patterns of the control error and its derivative, based on training set examples. The net consists of input, hidden, and output layers as shown in Figure 7.16.

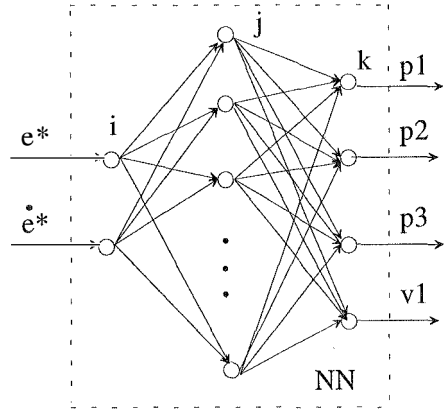

Figure 7.16. Neural network schematic diagram.

The input layer contains R=2 units (nodes or neurons) corresponding to the scaled modulii of the control error e^* and its time derivative $\dot{e}^*$. The hidden layer has a certain number of S units. The value of S will be chosen for an effective training process to achieve the error goal without overlearning. The output layer consists of K=4 neurons corresponding to the error patterns p_1 (e^* is *large*), p_2 (e^* is *medium*) and p_3 (e^* is *small*), and derivative-of-error pattern v_1 ($\dot{e}^*$ is *large*). The log-sigmoidal transfer function (7.7) is used for each neuron. Using the subscripts *i*, *j* and

k for input, hidden and output layers, respectively, the output of the k-th node (unit, or neuron) in the output layer is

$$o_k = f(net_k) = \frac{1}{1+\exp[-(net_k + \theta_k)/\theta_o]}, \tag{7.20}$$

where θ_k serves as a bias (or threshold) of unit k and θ_o determines the slope of sigmoid (here θ_o=1),

$$net_k = \sum_{j=1}^{S} w_{kj} o_j \tag{7.21}$$

is the input to the k-th node ($k = 1,2,3,4$) in the output layer, and w_{kj} is the weight from unit j in the hidden layer to unit k in the output layer.

Similarly, the output of the s-th node in the hidden layer is

$$o_j = f(net_j) = \frac{1}{1+\exp[-(net_j + \theta_j)/\theta_o]}, \tag{7.22}$$

where

$$net_j = w_{j1} e^* + w_{j2} \dot{e}^* \tag{7.23}$$

is the total inputs to unit j ($j = 1,2,\ldots,S$) in the hidden layer, and w_{ji} is the weight from unit r in the input layer to unit s in the hidden layer.

The network is trained by a number of pattern pairs. Each pair consists of an input pattern and a corresponding desired output pattern. Through the learning process, an energy function

$$E = \frac{1}{2} \sum_p \sum_j (t_{pj} - o_{pj})^2, \tag{7.24}$$

which is the mean squared error between the actual outputs o_{pj} and the desired outputs (target) t_{pj} due to an input pattern P, is minimised by changing the weights and biases in a gradient descent manner. Using the generalised delta rule for the net with backpropagation of error, described in Section 7.2, the deltas are given by the following expressions

$$\delta_k = (t_k - o_k)o_k(1 - o_k), \tag{7.25}$$

$$\delta_j = o_j(1 - o_j)\sum_k \delta_k w_{kj}, \tag{7.26}$$

for the output layer and hidden layer, respectively, where t_k is the target. In order to avoid a shallow local minimum, momentum is added to backpropagation learning by making weight changes equal to the sum of a fraction of the previous weight change and the new change suggested by the backpropagation rule (7.17):

$$\Delta w_{rs}(n+1) = \eta\delta_r o_s + \alpha\Delta w_{rs}(n), \quad (r= k, j;\ s=j, i), \tag{7.27}$$

where η is the learning rate, α is the momentum constant, and n is the iteration step for which a set of input patterns are presented to the net.

7.4.2. Neural-network based controller design

The main idea behind this approach is to classify regions from input-output measurements and use them as feedforward rules to generate an appropriate control signal. Control knowledge confirms that in order to improve robustness not only the control error but also the change of error should be taken into account. Here, similarly to a fuzzy logic controller, the control signal is calculated from a look-up table rather than by self-tuning or model reference approaches. The block diagram of the control system is shown in Figure 7.17 (Ha & Negnevitsky [44]).

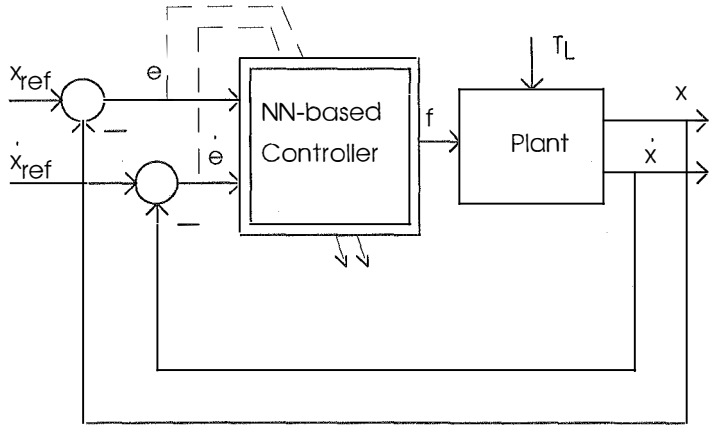

Figure 7.17. Block diagram of the control system.

The neural network-based controller consists of a preprocessing unit, a neural network classifier, a look-up table, and a servo drive unit. The preprocessing unit recognises the signs of the control error $e = x_{ref} - x$ and its time derivative $\dot{e} = \dot{x}_{ref} - \dot{x}$, scales their values into the range [0,1], and partitions them into several groups. The three-layer neural network classifier, as shown in Figure 7.16, has two inputs, the scaled modulii of the control position error e^* and velocity error $\dot{e}^*$, and four output neurons corresponding to the patterns p_1, p_2, p_3, and v_1. Assuming that the values of e^* and $\dot{e}^*$ are frequently found in the vicinity of 0, 0.2, 0.475, 0.85 and 0, 0.65, respectively, the ranges of e^* and $\dot{e}^*$ corresponding to the patterns p_1, p_2, p_3, and v_1 are specified as in Table 7.2.

Group index	e^* and $\dot{e}^*$ ranges	Output patterns				Control action, u_a
		p_1	p_2	p_3	v_1	
1	[0.7, 1] ; [0.3, 1]	1	0	0	1	$k_{p3}sign(e) + k_v sign(\dot{e})$
2	[0.7, 1] ; [0., 0.1]	1	0	0	0	$k_{p3}sign(e)$
3	[0.35, 0.6] ; [0.3, 1]	0	1	0	1	$k_{p2}sign(e) + k_v sign(\dot{e})$
4	[0.35, 0.6] ; [0., 0.1]	0	1	0	0	$k_{p2}sign(e)$
5	[0.1, 0.3] ; [0.3, 1]	0	0	1	1	$k_{p1}sign(e) + k_v sign(\dot{e})$
6	[0.1, 0.3] ; [0., 0.1]	0	0	1	0	$k_{p1}sign(e)$
7	[0., 0.05] ; [0.3, 1]	0	0	0	1	$k_{po}sign(e) + k_v sign(\dot{e})$
8	[0., 0.05] ; [0., 0.1]	0	0	0	0	$k_{po}sign(e)$

Table 7.2. Look-up table for e^* and $\dot{e}^*$ ranges, output patterns, and control action.

Within each group, three points are randomly chosen as the training patterns. With S=30 hidden neurons, the learning rate η=0.1 and momentum α= 0.9, the error goal, which is set equal to 0.01, is reached after 25310 iteration cycles. The sum-squared error of the training process is shown in Figure 7.18.

Figure 7.19 describes in details the network structure and the feedforward training process.

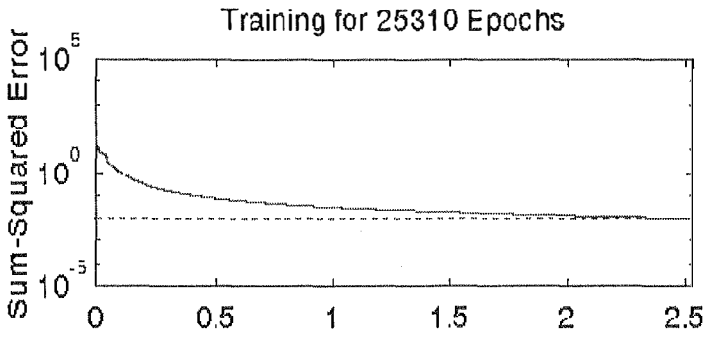

Figure 7.18. Sum-squared network error.

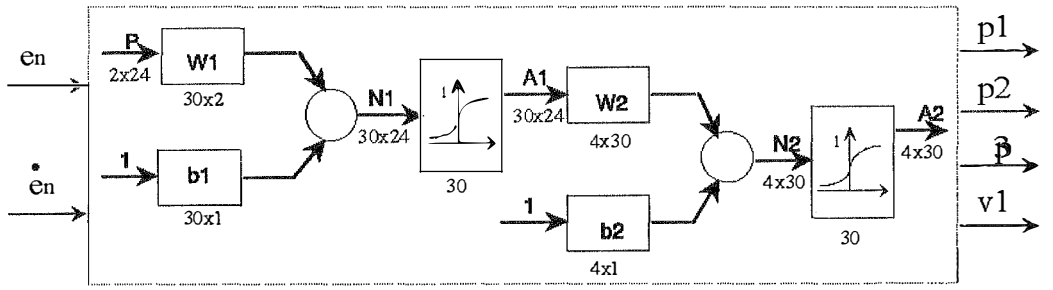

Figure 7.19. Network architecture and feedforward learning.

The possible input patterns for the scaled modulii of the control position error e^* and velocity error $\dot{e}^*$ are written in the language form:

$$\mathbf{P} = [EL\,EL \;\; EM\,EM \;\; ES\,ES \;\; EZ\,EZ$$
$$DL\,DZ \;\; DL\,DZ \;\; DL\,DZ \;\; DL\,DZ],$$

where EZ, ES, EM, and EL stand for *the error* e^* *is zero*, *small*, *medium*, and *large*, respectively, and DZ and DL for *the derivative of error* $\dot{e}^*$ *is zero* and *large*, respectively. The targets for the output patterns p_1, p_2, p_3, and v_1, which correspond to the input patterns above, can then be represented as

$$\mathbf{T} = [U\,U \;\; Z\,Z \;\; Z\,Z \;\; Z\,Z$$
$$Z\,Z \;\; U\,U \;\; Z\,Z \;\; Z\,Z$$
$$Z\,Z \;\; Z\,Z \;\; U\,U \;\; Z\,Z$$
$$U\,Z \;\; U\,Z \;\; U\,Z \;\; U\,Z],$$

where $U = [1\ 1\ 1]$ and $Z = [0\ 0\ 0]$.

In comparison with the approach proposed in Tai *et al.* [180] the self organising capability of the controller is enhanced by adding a signal proportional to the velocity error as in a proportional-derivative type controller. Moreover, in order to improve the servo accuracy the control action is made still maintained in the range from 0 to +0.05 of the scaled error e^*. After the off-line learning process it can be implemented for real-time classification with low computation requirements and memory. The network outputs are rounded off into "1" and "0" in which "1" in p_1, p_2, p_3, and v_1 indicates some level of deviation in the control position error e^* and velocity error $\dot{e}^*$, respectively. The look-up table will determine the appropriate control action depending on the servo position and velocity errors. The controller output is

$$u = w.u_a, \tag{7.28}$$

where w is a scaling factor and the computed signal u_a depends on the proportional coefficients k_{pi}, $i = 0,1,2,3$ and k_v. For example, if e^* and $\dot{e}^*$ fall in group 6, the net will classify it to pattern (0010) and the controller will look up the table to generate the control signal $w.k_{p1}sign(e)$. Parameters k_{pi} and k_v play an important role in the tracking process. For good tracking performance the values of k_v, k_{po}, k_{p1}, k_{p2}, k_{p3} obtained through our simulation process are in an ascending proportion 0.3 : 0.5 : 1 : 2 : 3. The control performance when positioning a load of an overhead crane model verifies this choice. It should be noted that the proposed controller design results in a fuzzy logic-like controller utilising certain expert rules without requirements of membership functions of the controller input/output labels and fuzzy logic operations.

7.4.3. Simulation results for a crane model

The overhead crane model described in Section 4.4.2 is employed as the controlled object. In order to investigate the response with large swing, the non-linear state equation (4.49) is used. The load mass m and the chain length L are time varying parameters. Friction, external disturbances can be considered as an unknown load torque T_L. The system specifications are given in Table 4.6. In our investigation, when the scaled error is between 0 and +0.05 the control system suffers some steady-state error if the there is no control action as proposed in Tai *et al.* [180]. As an attempt to find the thumb of rule for the choice of the proportional coefficients k_{po}, k_{p1}, k_{p2} and k_{p3}, after some trials, they were found to give best results when chosen in the proportion 0. 5: 1: 2: 3. The tracking response to an optimal trapezoidal

trajectory of the reference speed is considered. The scaled modulii of the control error e^* and its derivative $\dot{e}^*$ are calculated as:

$$e^* = \frac{|e|}{X_r}, \; \dot{e}^* = \frac{|\dot{e}|}{V_r}, \tag{7.29}$$

where $X_r = 0.5m$ and $V_r = 0.2m$ / sec. Figure 7.20 shows the position responses with $w = 0.2$, and $k_v = 0$, $k_{po} = 0$, $k_{p1}=1$, $k_{p2}= 2$, and $k_{p3}= 3$, as in the method of Tai *et al.* [180], by a solid line, and with $w = 0.2$, and $k_v= 0$, $k_{po}= 0.5$, $k_{p1}= 1$, $k_{p2}= 2$ and $k_{p3}= 3$ by a dash-dotted line. The results indicate that the latter trajectory is quite close to the position reference (dotted line).

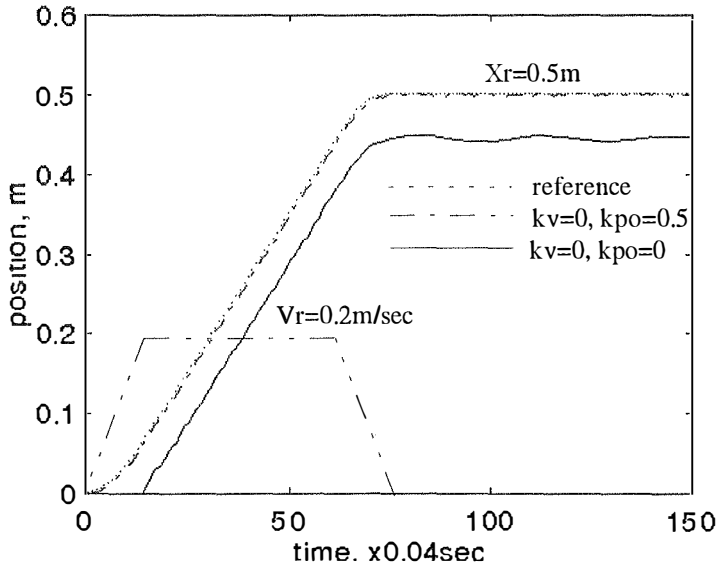

Figure 7.20. Position responses, $T_L = 0$.

The choice of the additional coefficient k_v in the control action is justified by the load response in Figure 7.21 ($T_L = 2T_o$ at 2 sec, where T_o is the nominal motor torque) with the cases k_v=0, k_{po}=0.5, $k_{p1}= 1$, $k_{p2}= 2$ and $k_{p3}= 3$ (solid line), and k_v=0.3, k_{po}=0.5, $k_{p1}= 1$, $k_{p2}= 2$ and $k_{p3}= 3$ (dash-dotted line) at nominal values of the plant compared to the reference curve (dotted line). By adding the derivative type proportional coefficient k_v, it is evident that the response becomes less sensitive to a load disturbance.

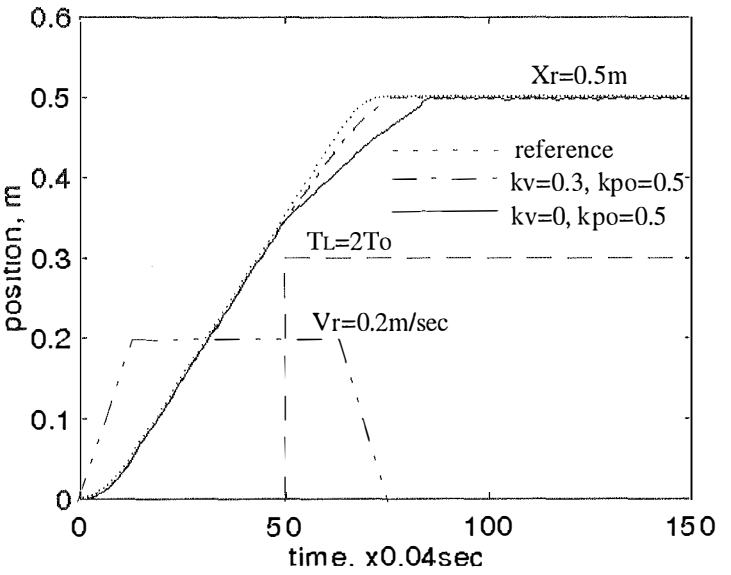

Figure 7.21. Position responses, $T_L = 2T_o$ at 2 sec.

Robustness of the proposed approach is verified through the cases of structured and unstructured uncertainties. The tracking responses to the optimal trajectory of the reference speed where $m = 2m_0$, $L = 0.5L_0$, and $T_L = 0.5T_o(1+\sin 10t)$, (m_0 and L_0 are nominal values of the load mass and chain length), are shown in Figure 7.22, and where an initial swing Φ_o of 75 degrees is applied to the crane model, in Figure 7.23.

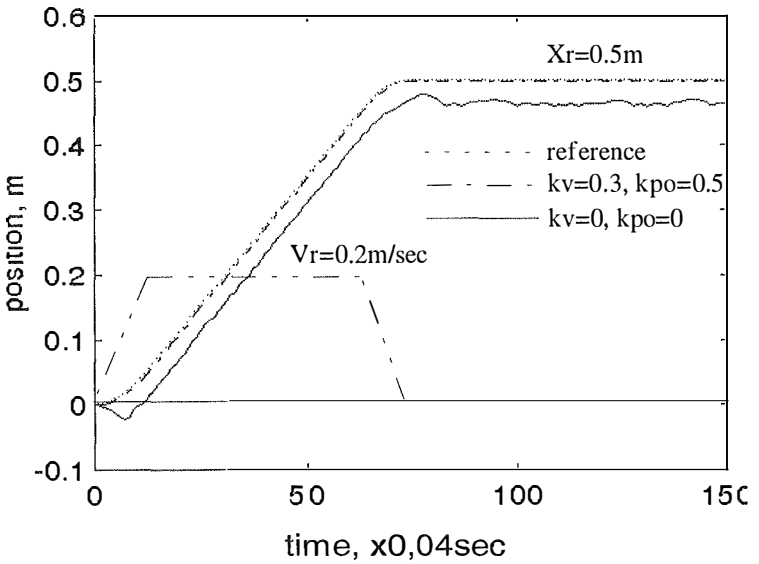

Figure 7.22. Position responses, $m = 2m_0$, $L = 0.5L_0$, and $T_L = 0.5T_o(1+\sin 10t)$;

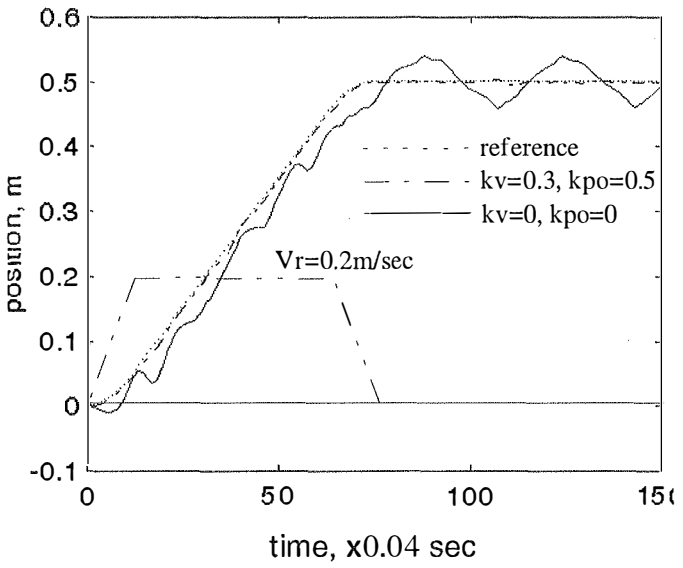

Figure 7.23. Position responses, $\Phi_o = 75^0$.

The responses with this controller (dash-dotted line) and with the controller in Tai *et al.* [180] having six output neurons with three coefficients k_{p1}, k_{p2} and k_{p3} (solid line) are compared with the position reference (dotted line). It is observed that the tracking performance with our proposed scheme is less sensitive to any changing environments.

7.4.4. Application in multi-mass electromechanical systems

The problem of vibration suppression and disturbance rejection is very important in motion control of multi-mass flexible systems. For example, in spatial mechanisms, a reduction in the total weight lowers the stiffness of a manipulator and leads to undesirable oscillations. The same issue is taken up in an industrial steel rolling mill. Uncertainties, such as parameter and load variations, and nonlinearities make the problem more challenging. Observer-based approaches have been reported to tackle the problem (Hori *et al.* [64], Nomura *et al.* [57], Ha & Negnevitsky [41]). The sliding mode or $H\infty$ method can generally be used to increase control system robustness but their application to multi-mass systems is not straightforward. Conventional proportional-integral controllers with fuzzy tuning can improve parameter- and load-insensitivity. However, when applied to flexible structures with cascade control principles (Ha *et al.* [38]), mechanical vibrations are not suppressed as well as with the observer-based state feedback method. In the following, the neural network-based controller described in this section is employed for enhancing both

robustness and the capability of vibration suppression (Ha [45]). An interesting feature of the proposed neural network-based method is that the net plays the role of a classifier to cluster the groups of the control error e and its time derivative $\dot{e}$ without having to learn the system inverse dynamics. Correspondingly, an appropriate command signal is generated to cause the servo output to follow a prescribed trajectory. The two-mass servo system of Example 3.2 is used here as the controlled object. Simulation results verify the validity of the proposed approach when applied to flexible structure systems. The system block diagram including the neural network-based controller is shown in Figure 7.24. The speed reference is an optimal trapezoidal trajectory. The load speed and acceleration feedback signals can be indirectly estimated by an observer.

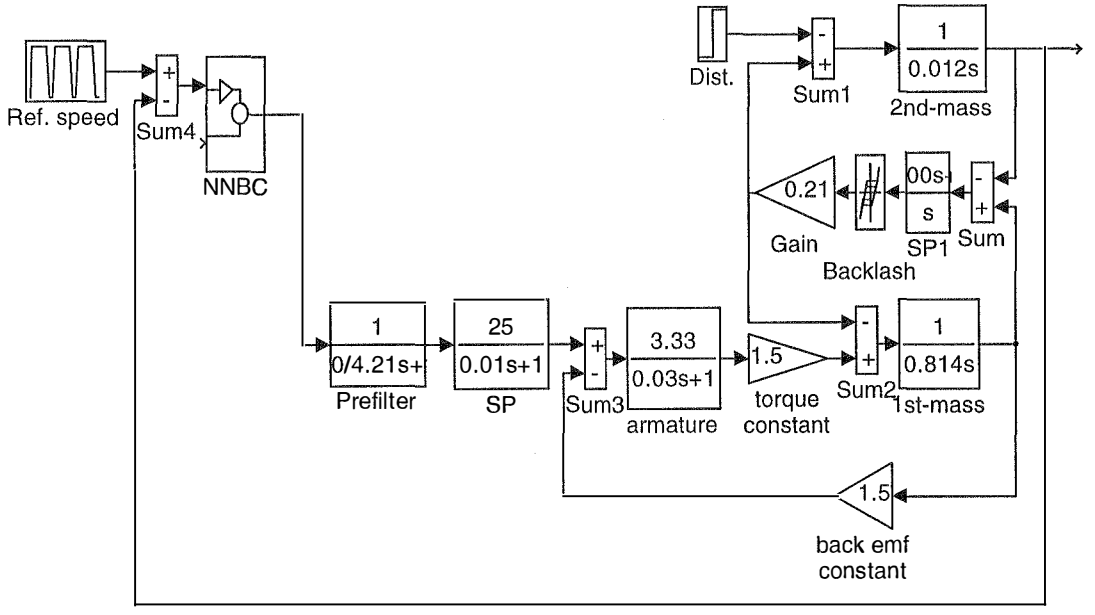

Figure 7.24. Block diagram of a two-mass servo system with a neural network-based controller (NNBC).

Simulation results are shown in Figures 7.25 - 7.27 where the reference and actual speed is represented by a dash-dotted and solid line, respectively. Parameter insensitivity is verified in the case of load inertia variation, $J_L = 2J_{L,nom}$. Figure 7.25 plots the time optimal process of the load speed response in this case.

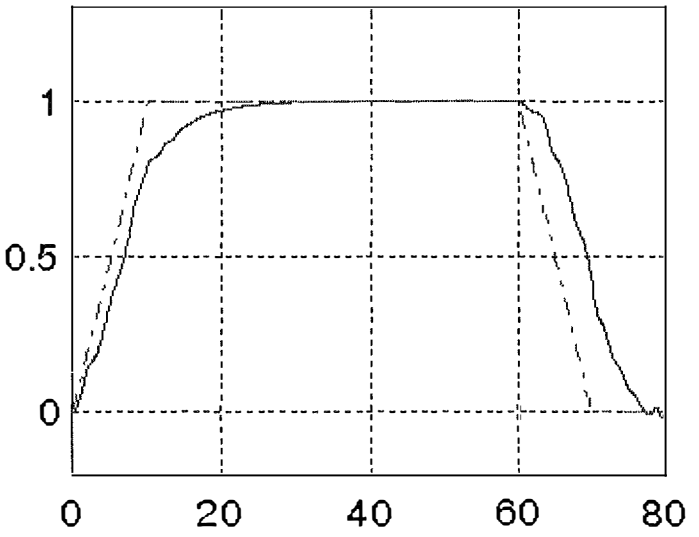

(a)

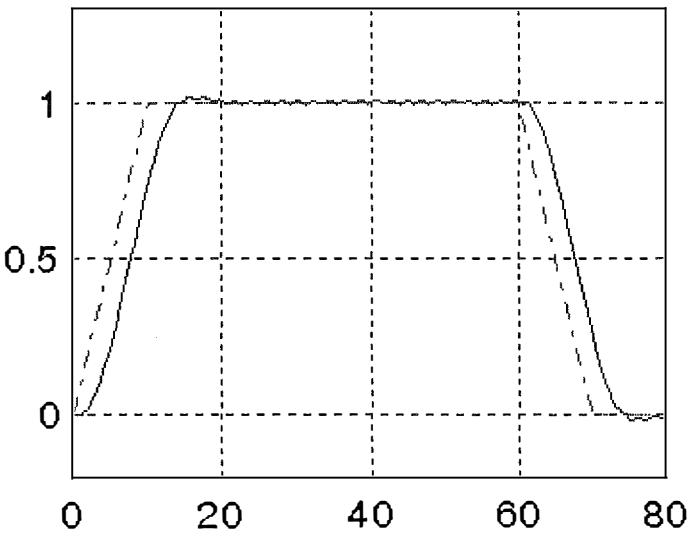

(b)

Figure 7.25. Speed response with load inertia variation, $J_L = 2J_{L,nom}$: (a) NN-based control, and (b) PI control.

The time optimal process of the speed response when a load torque disturbance, $T_L = T_{L,nom}$ exerted at $t = 40\,\text{sec}$, is shown in Figure 7.26 to demonstrate the system robustness against a load variation.

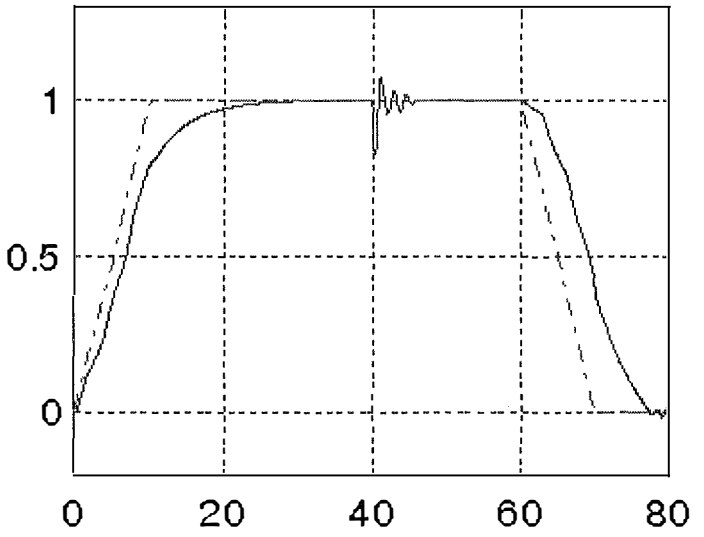

(a)

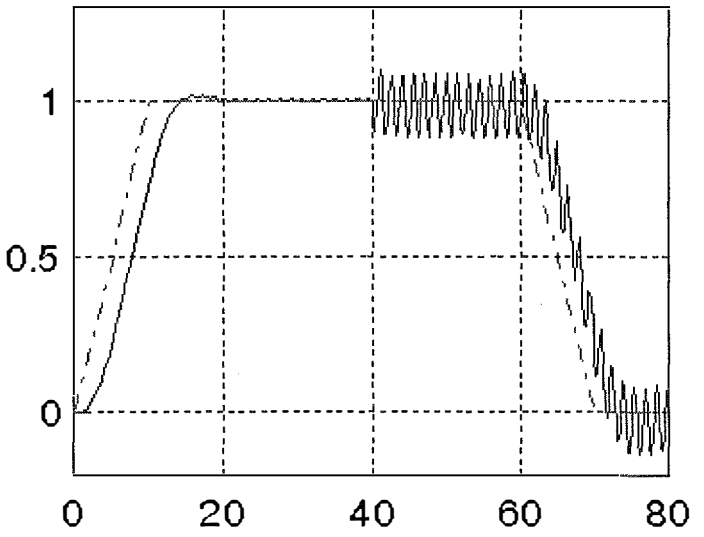

(b)

Figure 7.26. Speed response when $T_L = T_{L,nom}$ at $t = 40\,\text{sec}$:
(a) NN-based control, and (b) PI control.

Finally, Figure 7.27 indicates that good tracking performance can be obtained with the proposed neural network-based controller even in the presence of nonlinearity such as a backlash of a dead-band width $2D = 0.004$.

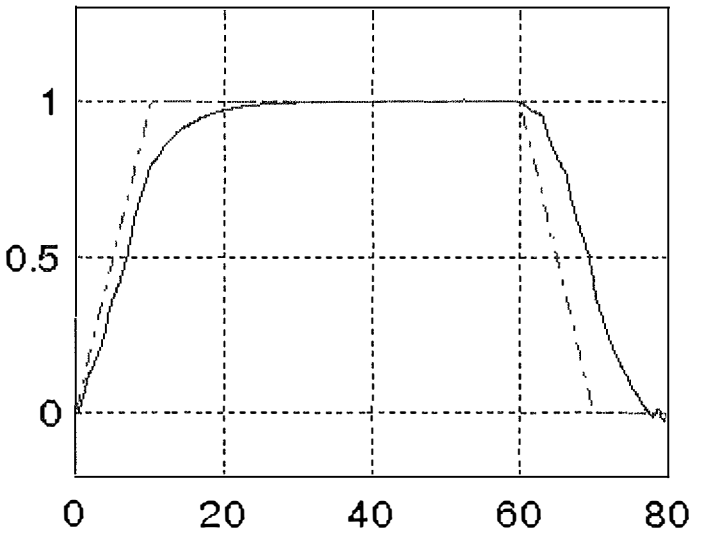

(a)

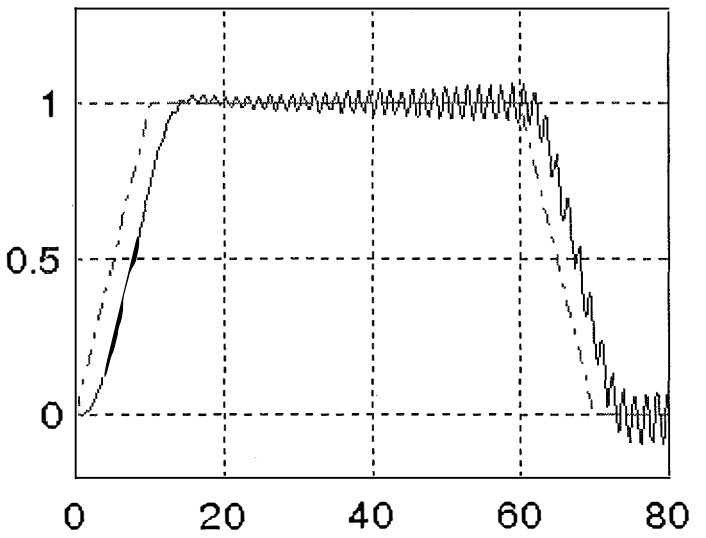

(b)

Figure 7.27. Speed response with backlash $2D = 0.004$:
(a) NN-based control, and (b) PI control.

Comparing the responses obtained by the proposed method (Figures 7.25(a), 7.26(a), and 7.27(a)) and the conventional cascade control with proportional-integral (PI) controllers (Figures 7.25(b), 7-26(b), and 7.27(b)) at the same conditions demonstrates its feasibility in applications to flexible systems for vibration suppression and high tracking performance even in the presence of parameter and load variations, and nonlinearity.

Note that the proposed neural network-based controller is designed like a proportional-derivative fuzzy logic controller. This explains the robustness of the control system. The attraction here is that no fuzzy logic operations and no *a priori* knowledge of the plant dynamics are required. Further research may focus on the application of an additional feedforward compensation, or some adaptive schemes for tuning the coefficients k_{pi}, $i = 0, 1, 2, 3$, and k_v to cope well with severe uncertainties in flexible structures.

A neural network-based controller has been proposed for servo tracking with high accuracy and robustness. The neural net serves as a classifier to cluster the control error and change of error groups instead of acting as the inverse of the plant. Control knowledge is embedded into the representation of the net and helps to generate the appropriate control signal for tracking systems that can cope well with uncertainties. By noticing the symmetry in the control actions and taking the rate of change of error into account, the neural network structure obtained is rather simple and the tracking process is robust against any uncertainties. The attraction of the proposed controller is that no *a priori* knowledge of the controlled object and its dynamics is required, thus it can be applied to a variety of linear or nonlinear servo applications. Simulation results are provided for the control of an overhead crane model. The proposed approach can be applied to the control of a two-mass servo system. Simulation results indicate the capability of vibration suppression and high tracking performance even in the presence of parameter variation, load torque disturbance, and backlash nonlinearity combined with the gear torsion. A learning scheme for the choice of the controller coefficients and the proposed approach application to industrial servo systems working in severely changing environments can be subjects for future extension.

7.5 Robust control using neuro-fuzzy approach

In some motion applications, controlled systems are subject to inertia variations and load torque disturbances. In robot drive systems, several motion axes are mechanically coupled and the position of one axis usually affects the inertia of the others. It is known that the dynamic model of a manipulator is highly non-linear and requires a knowledge of the kinematic dynamics and inertia parameters. Normally, the inertia parameters are not available from manufacturers. On the other hand, in robotics, the plant model, depending on inertia parameters, is highly nonlinear and the values of inertia parameters are required for most modern control schemes that

incorporate inverse dynamics. There are several approaches for identifying the inertia parameters of manipulators and to minimise the number of the inertia parameters appearing in their mathematical equations. A survey on approaches based on this technique is given in Lin [181]. However, the inconvenience of these methods are that the closed form of the system with the inverse dynamics is difficult to analyse, and a large number of off-line experiments are needed to find the required parameters. Recently, there has been increasing interest to implement neural network and fuzzy techniques to address these problems, with robot drive systems as the controlled object. In Lee *et al.* [182], an inverse nonlinear controller using neural networks is applied to treat the position control problem in servomechanisms with nonlinear dynamics. An additional parallel neural network is used in Lee *et al.* [32] to enhance adaptive properties of the basic fixed neural network-based inverse nonlinear controller described in [182]. These techniques were shown to be capable of providing high performance closed-loop control for several classes of servomechanisms with nonlinearities. Here, a training data set consisting of the system output vector $(q(t)\ \dot{q}(t)\ \ddot{q}(t))^T$ and the control input $u(t)$ is used for modelling the dynamic behaviour of the nonlinear system, where q represents an appropriate output of the system such as an angular signal if the described system is a position control servomechanism. For this case, neural networks of the radial basis function type are utilised. Döschner & Schneider [183] proposed a neural network approach for learning the inverse dynamics of a robot, using Kohonen feature maps [184] based on the training data set of all available robot coordinates.

In real time control with neural network applications, it is assumed that the modelled system characteristics are accurately approximated by the net. However, this assumption can be made only after appropriate training and with a sufficiently large number of neurons. When learning the inverse characteristics of the plant from zero, the neural net must be trained off-line, applying the plant input and output signals. For this, we need a robust system which is able to cope with all nonlinearities in order to provide the required training data set. This section is devoted to a technique developed in Palis, Ha *et al.* [33], [165] using :

- fuzzy logic control to guarantee stability during off-line training operations,
- a neural network approach to identify the inverse characteristics of the nonlinear dynamics in order to compensate for nonlinearities in the feedforward channel, and
- a feedforward neural network model to cope with parameter variations due to an inaccurate approximation of mechanical parameters.

7.5.1. Robustness against parameter variations with fuzzy control

Let us assume that the plant consists of p axes of motion which are influenced by the interaction of forces dependent on the co-ordinates of the other axes. The load torque, T_L, and moment of inertia, J, can then be generally written by

$$T_L = T_L(\mathbf{x}) \text{ and } J = J(\mathbf{x}), \tag{7.30}$$

where $\mathbf{x} = (x_1, x_2, \ldots, x_p)^T$ is the state vector. Considering the *i-th* axis with the coordinate

$$x_i = \varphi \text{ and } \dot{x}_i = \omega, \tag{7.31}$$

and using the second equation of Lagrange

$$\frac{d}{dt}\left(\frac{\partial W_{kin}}{\partial \dot{x}_i}\right) - \frac{\partial W_{kin}}{\partial x_i} = -\frac{\partial W_{pot}}{\partial x_i} + T_i, \tag{7.32}$$

the following equation can be obtained:

$$J\frac{d\omega}{dt} = T_{gen} - \omega\sum_j \frac{\partial J}{\partial x_j}\frac{dx_j}{dt} - T_L, \tag{7.33}$$

where $T_i = T_{gen} - T_L$, T_{gen} is the generating torque, and W_{kin} and W_{pot} are the kinetic and potential energy, respectively.

It is obvious that the speed control has to cope with considerable parameter variations. When compensating for these influences, the drive system can be decoupled and optimal dynamic behaviours of the speed loop can be achieved. For this purpose, an adaptive fuzzy observer is proposed in Palis & Ha *et al.* [33] and an observer-based fuzzy tuner in Palis & Ha *et al.* [165].

A. Decoupling of the motion axes using adaptive fuzzy observers

In electrical drives, it can be assumed that the torque generating a current component is controlled by means of an inner current loop. Therefore, we have a similar structure for the cascaded speed loop of DC- and AC-drives. The proposed control system is

based on the idea that the speed controller parameters are set to a medium value of $J(\mathbf{x})$ and the total load torque $(T_L + \omega \sum_j \frac{\partial J}{\partial x_j} \frac{dx_j}{dt})$ is determined by a disturbance observer as proposed in Palis & Schmied [185]. The load torque influence is compensated for by means of a corresponding feedforward correction to the current reference value. However, in order to achieve complete parameter insensitivity and disturbance rejection, we have to overcome the following disadvantages:

- The actual value of $J(\mathbf{x})$ is unknown or only approximately given. Consequently, the load torque cannot be accurately evaluated by the disturbance observer.
- When the load torque is rapidly changing we must cope with an increase of the observer's dynamic error due to the limited rise time both of the current control loop and the digital observer.

Therefore, ideal dynamic performances of the real system in practice cannot be obtained. An adaptive fuzzy observer (AFO), proposed in Palis & Schmied [185] for speed control systems, is used to provide a feedforward compensation for the load torque influence. The system configuration is shown in Figure 7.28.

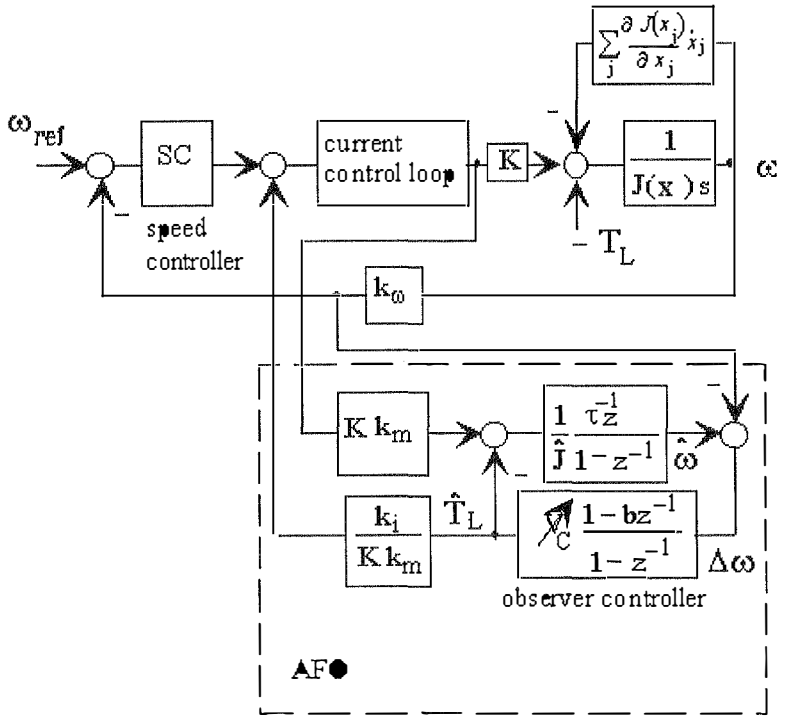

Figure 7.28. Speed control structure with an adaptive fuzzy observer.

Obviously, due to the aforementioned shortcomings the actual speed of the drive system will differ from the optimal speed response. This difference $\Delta\omega$ and its derivative $\Delta\dot{\omega}$ provide the information for correcting the observer controller gain V_c (Figure 7.28) in order to minimise the speed error $\Delta\omega$. The fuzzy rules for tuning this gain are summarised in Table 7.2, where the language labels NB, NS, Z, PS, and PB stand for negative big, negative small, zero, positive small, and positive big, respectively.

$\Delta\omega$ / $\Delta\dot{\omega}$	NB	NS	Z	PS	PB
NS	PS	Z	NS	NS	NS
NS	Z	NS	NB	NB	NS
Z	Z	NS	NB	NS	Z
PS	NS	NB	NB	NS	Z
PB	NS	NS	NS	Z	PS

Table 7.2. Fuzzy rules for tuning V_c.

An improvement in the dynamic behaviour of a speed control system using this approach can be verified through simulation results shown in Figures 7.29 (Palis & Ha *et al.* [33]).

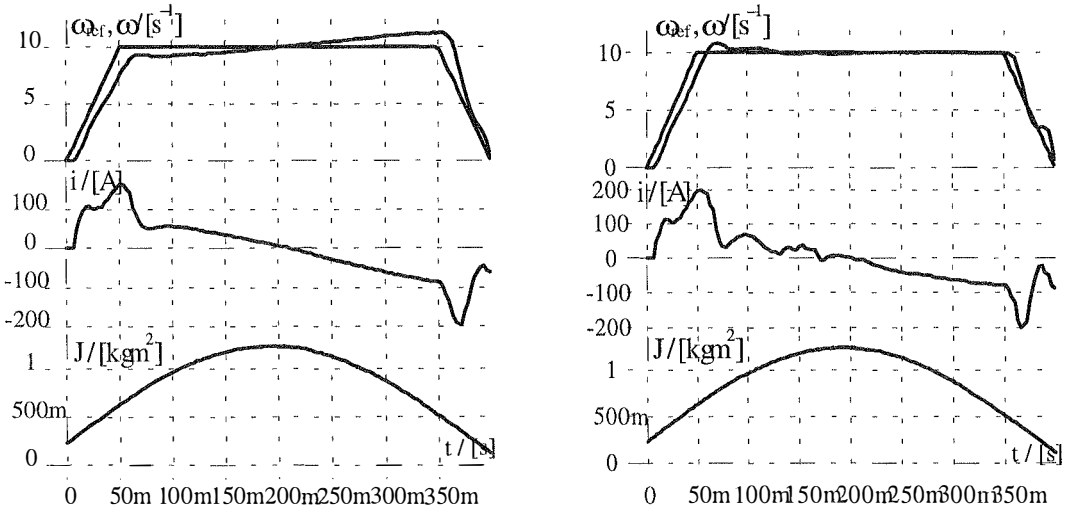

(a) (b)

Figure 7.29. Time optimal positioning process of a robot axis with changing moment of inertia: (a) without AFO, and (b) with AFO.

Here, the time optimal positioning process of a robot axis is considered when the load torque and moment of inertia are changing. The speed response with AFO achieves better performance thanks to the compensation for the disturbance influence in the observer control loop which is adaptively adjusted by a fuzzy logic rule set.

B. Decoupling of the motion axes using observer-based fuzzy tuning

In the previous chapter, fuzzy tuning of the feedforward compensation signal from a disturbance observer has been shown to offer good possibilities for improving load-and- parameter insensitivity. As an alternative to the adaptive fuzzy observer mentioned above, fuzzy tuning schemes can be incorporated to improve robustness against parameter and load variations in the system of Figure 7.28. Here the parameters of the PI controller in the observer control loop will be tuned according to some simple fuzzy logic schemes, proposed in Ha [112]. Figure 7.30 shows the drive system including a PI controller with fuzzy tuning in the observer feedforward loop. The total load torque is compensated for using a disturbance observer-based fuzzy tuner (DOFT).

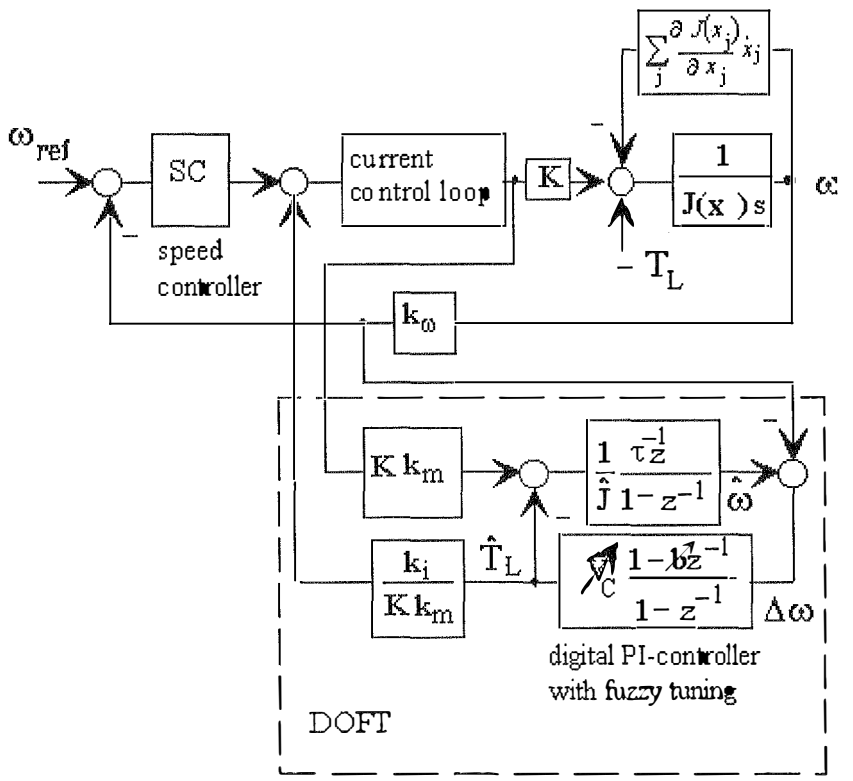

Figure 7.30. Speed control with disturbance observer-based fuzzy tuner (DOFT).

The tuning expressions (5.8)-(5.10) are applied for adjusting the parameters V_c and b of the PI controller in the system of Figure 7.30. The salient features of the use of the disturbance observer-based fuzzy tuner approach are:

- fuzzy logic can be introduced to continuously change the controller gain and time constant, depending on the control error and its rate of change,
- the rule base for tuning is based on human expert experience rather than on precise information of the plant dynamics and allows an easy modification,
- tuning schemes result in explicit expressions which allow low computational cost and a simple implementation.

High performance of a speed control system using this approach can be verified through simulation results shown in Figure 7.31 and 7.32 (Palis & Ha *et al.* [165]). The time optimal positioning process of a robot axis is considered when the load torque and moment of inertia are changing. Comparing the speed responses of Figure 7.31 and Figure 7.32 demonstrates the priority of fuzzy tuning schemes for robust tracking improvement.

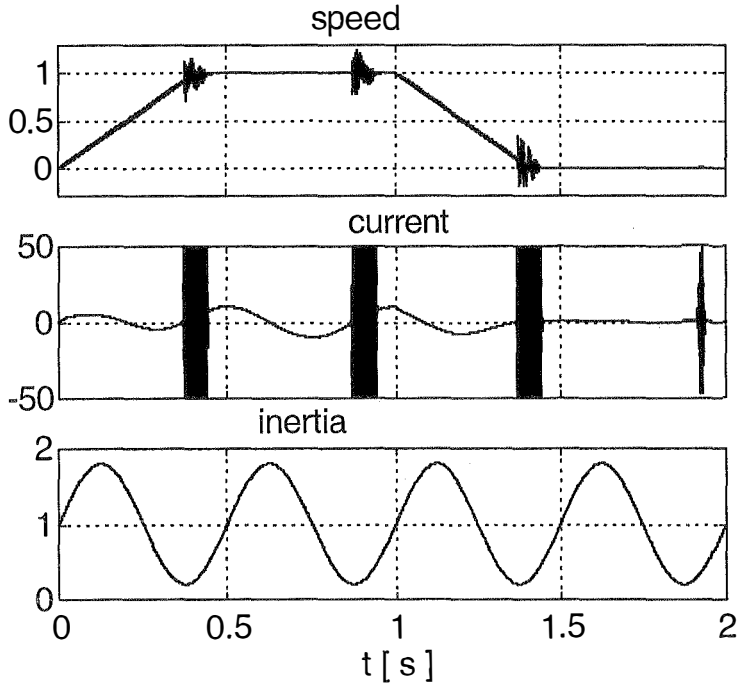

Figure 7.31. Time optimal positioning without fuzzy tuning.

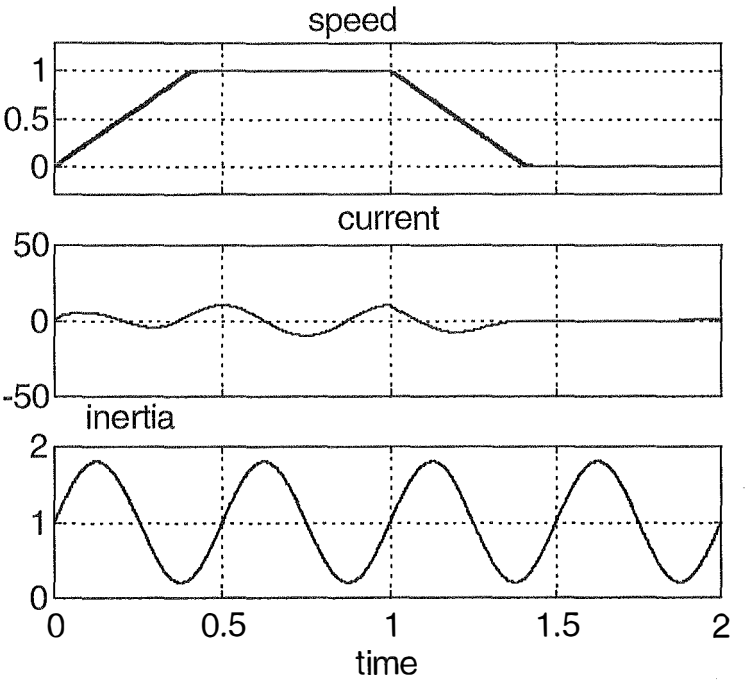

Figure 7.32. Time optimal positioning with fuzzy tuning.

7.5.2. Robustness enhancement using a neural network model for the inverse dynamics

As shown in the section above, fuzzy logic controllers are able to cope with non-linearities and to guarantee stability in a wide range of parameter variations. However, it should be clearly pointed out that both large and fast changes of inertia lead to an increasing error in the estimated torque value from the observer. A neural network identifier can be incorporated in order to alleviate the influence of the nonlinear mechanism characteristics due to inertia variations. Here, a parallel neural network model for the inverse dynamics (NNMID) is applied to the system with AFO or DOFT to provide information of the system input depending on the output. The following approach is proposed:

(i) Set up a neural network with the set

$$[x_1,\ x_2,\ x_3,\ x_4] = [\omega(k),\ \omega(k-1),\ \omega(k-2),\ u_N(k-1)] \tag{7.34}$$

as inputs and the control signal $u_N(k)$ as the desired output of the NNMID, and train the net using real data sets of the system.

(ii) Once a good fit is obtained, the resulting neural network actually realises the function

$$u_N(k) = f(\omega(k),\ \omega(k-1),\ \omega(k-2),\ u_N(k-1)), \tag{7.35}$$

and inserts it into the system to calculate the control signal $u_N(k)$.

A schematic diagram of the described control system is given in Figure 7.33

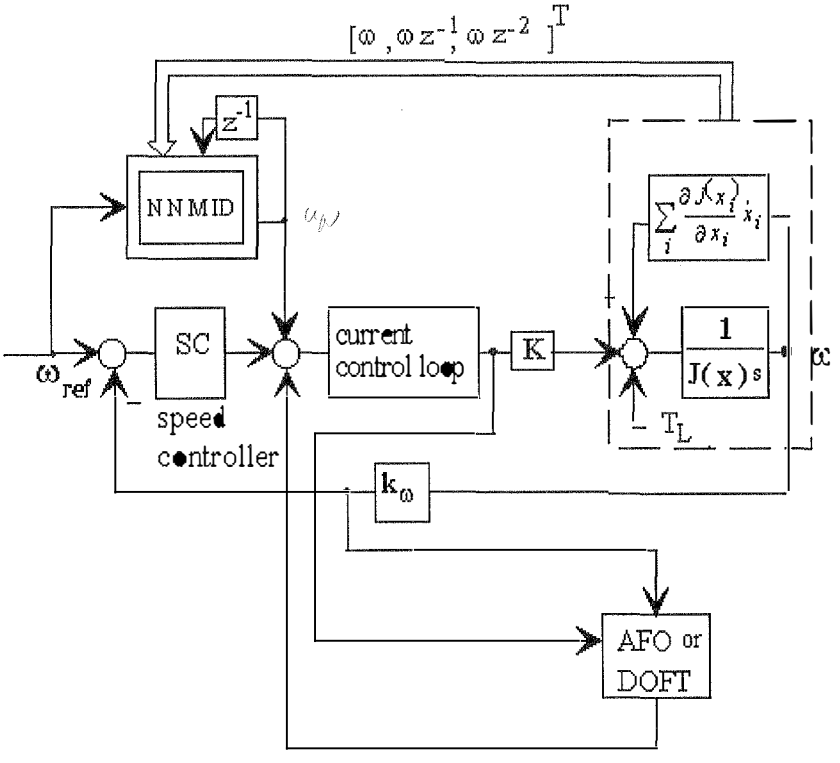

Figure 7.33 Speed control structure with an additional neural network model.

In recent literature, for example Hunt *et al.* [168], Widrow & Lehr [15], Pham & Xing [23], a variety of neural networks have been proposed. Among non-dynamic networks, radial basis function (RBF) ones seem to be very promising. As noted in Section 7.3, an important advantage of RBF networks is that they can be trained in a fraction of the time it takes to train back-propagation networks or multilayer perceptrons with similar power and generality (Van den Bout & Miller [186], Peterson [187]). Furthermore, Lyapunov based updating laws as used in Lee *et al.* [32] can be designed for network training to guarantee asymptotic convergence of the

approximation error to zero. Therefore, a non-linear control law can be injected into a RBF neural network. Further details on RBF networks can be found in Poggio & Girosi [178] and Cichocki & Unbehauen [188].

Here in order to learn the relations (7.34) and (7.35), a neural network, consisting of three layers: the input layer, the hidden layer with a radial basic function and the output layer, is used as configured in Figure 7.34. The net computes a linear combination of radial basis functions which can mathematically be described by

$$y = w_0 + \sum_{i=1}^{4} w_i \Phi_i(\|\mathbf{x} - \mathbf{c}_i\|), \tag{7.36}$$

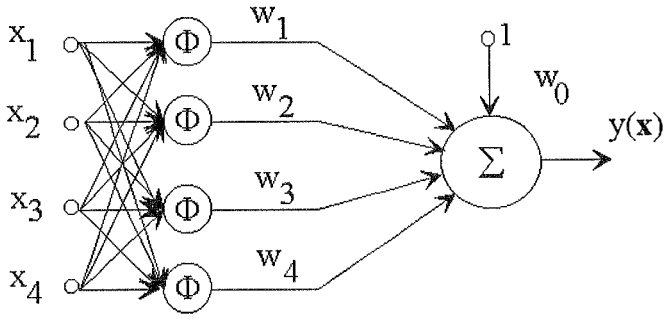

Figure 7.34. Structure of the radial basic function network.

where the expression $\|\mathbf{x} - \mathbf{c}_i\|$ denotes the Euclidean distance or a vector norm between the input vector $\mathbf{x}$ and the chosen centre $\mathbf{c}_i$, and Φ_i is the most widely used Gaussian function (7.19):

$$\Phi_i(\|\mathbf{x} - \mathbf{c}_i\|) = \exp(-\|\mathbf{x} - \mathbf{c}_i\|^2 / \sigma^2). \tag{7.37}$$

The centres $\mathbf{c}_i$ and the spread constant σ are fixed while the weights w_i are adjusted during the learning process.

Simulation results for a robot axis with the compensation from an adaptive fuzzy observer signal and an additional signal from the neural network model (NNMID) in the system are depicted in Figure 7.35 (Palis, Ha *et al.* [33]). The time optimal process of the speed response shows its parameter insensitivity.

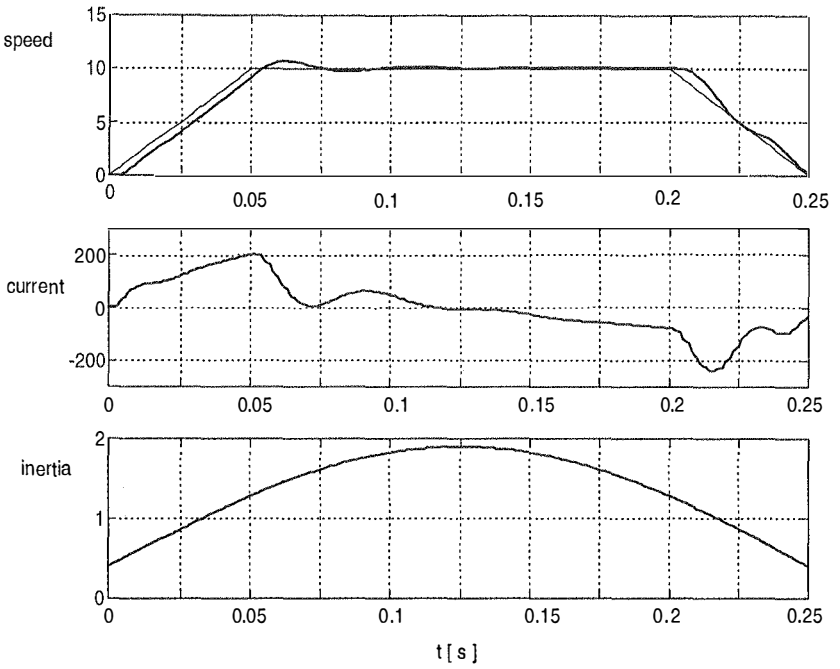

Figure 7.35. Time optimal positioning process with a changing moment of inertia when using AFO and NNMID.

Robustness enhancement can also be verified with the use of DOFT augmented with NNMID as shown in the simulation results of Figure 7.36 (Palis, Ha *et al.* [165]). The time optimal speed response exhibits good tracking performance in a wide range of inertia variation. It is observed that the network output signal dominates the speed controller output. Thus in the presence of severe parameter variations, the main correction is accomplished by the neural network model. The results obtained indicate that the proposed neuro-fuzzy approach can be a promising method to overcome the ill effects of wide ranging parameter variations.

This section has presented a fuzzy and neurocontrol approach for drive systems with changing parameters and load. The influence of load and inertia variations is alleviated using an adaptive fuzzy observer or a digital observer-based fuzzy tuner. Taking into consideration a large range of inertia changes associated with severe nonlinearities, an additional compensation signal from a neural network model for inverse dynamics is added to the control signal. Thus, the closed-loop system is made more robust. Simulation results of a time optimal positioning process verify the validity of the proposed method.

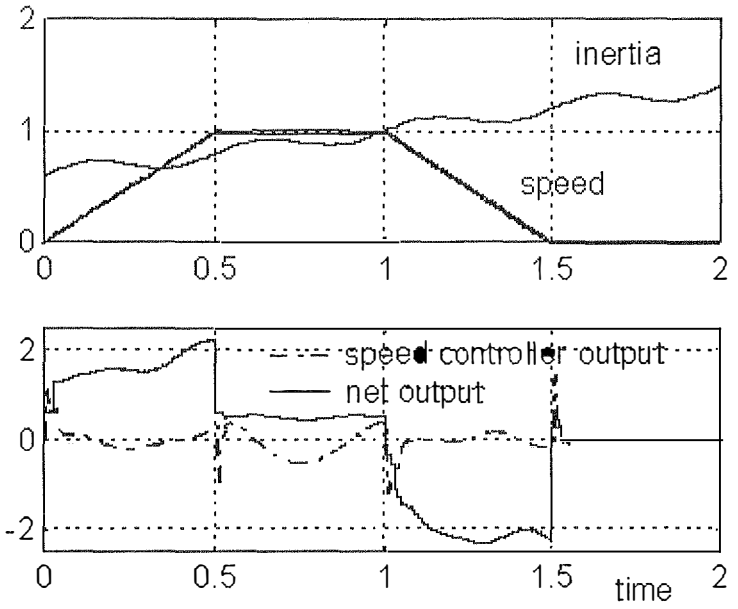

Figure 7.36. Time optimal positioning process with changing moment of inertia when using DOFT and NNMID.

7.6 Summary and discussion

Artificial neural networks, inspired by biological nervous systems, are composed of many elements operating in parallel. The network function is determined mainly by the connection between elements. A neural network can be trained to perform a particular functions by adjusting the values of the connection weights between elements. In this chapter, the basic concept of artificial neural networks was briefly introduced and their applications to motion control system has been outlined. Its content focused mainly on the use of a neural network to mimic a nonlinear controller, e.g. a fuzzy logic controller; or to cluster the groups of both the servo control error and its derivative which an appropriate control action would correct. The combination of fuzzy and neurocontrol was proposed as a promising approach to the problem of severe sensitivity when system parameters and load varying a wide range.

Since a neural network can approximate and learn any control relationship of practical interest, it is worth exploring the implementation of a fuzzy logic controller's input-output relationship in a neural network to ease the control system of computation burden. The solution is investigated with reference to the position control of a

swinging load of an overhead crane model. A radial basis function network, undergoing a two-stage (transient and steady-state) training process, approximates the control action from a fuzzy logic controller for that model. Simulation and experimental results, compared with those of the system with the fuzzy logic controller, show the neural network ability to control in the same manner as a fuzzy logic controller. Robustness against parameter and load variations has been verified.

Another contribution of this chapter is an application of the back propagation network to the tracking control of servo drive systems. Based on information of the control error and its time derivative, the neural network can classify the error and change-of-error patterns, and generate the appropriate control action without learning the inverse dynamics of the plant. The merit of the proposed approach lie in the design simplicity and its practicality for real-time implementation with a look-up table. The overhead crane model and the two-mass servo drive, mentioned in previous chapters, is used as the controlled objects with the standard time optimal trapezoidal trajectory for tracking. Simulation results indicate that the systems exhibit highly robust performance in the presence of uncertainties in the plant parameters and control process. It can be noticed that the proposed approach is conceptually analogous to the proportional-derivative like fuzzy logic control (see Section 4.4.1) without elaboration on membership functions and fuzzy logic operations.

For servomechanisms with severe nonlinearities, the fuzzy neurocontrol technique has been presented. It combines salient features of observer-based fuzzy control for decoupling motion axes, and of additional compensation from a neural network model for inverse dynamics to provide adaptive enhancements. In the observer control loop, the influence of an unknown equivalent load torque is compensated for by an adaptive fuzzy observer controller with the feedforward gain adjusted from a fuzzy rule set. Alternatively, fuzzy tuning schemes can be used to continuously change the gain and time-constant of the disturbance observer-based controller. A radial basis function neural network is trained to provide information of the input (control action) in relation with the system outputs (plant states) in the proportional-integral-derivative manner. The neural net then provides a parallel compensation action for a wide range of system's uncertainties and nonlinearities. The effectiveness of the proposed approach has been demonstrated in simulation results of the time optimal positioning process of a robot axis.

Although the field of neural networks has attraction of some five decades, it has found solid application only since the early 1980's. Thus, it is still very much in its infancy compared with the other fields of control systems. Many questions still have to be answered: determining the best network topology, choosing the net parameters, and number of neurons required, for example. Neural network application to motion control systems needs further exploration. Theoretically, dynamic networks can be used as universal identifiers and sophisticated controllers. However, static networks possess proven capabilities of arbitrary function approximation which can be practically exploited in the context of motion control using state feedback and feedforward compensation. The attraction of using the neural network instead of other model forms within the control strategy is the ability to effectively represent complex nonlinear systems.

Chapter 8

Summary and Future Extensions

8.1 Introduction

This study has encompassed a variety of areas of research relating to robustness issues in analysis and design of motion control systems, particularly electrical drives and robotics. The problems of estimating the dynamic properties as well as damping capability of a generalised electromechanical model, and the development of the robust modal control for linearised drive systems have been addressed, using conventional control approaches. The application of uprising artificial intelligent tools, namely fuzzy logic and neural network, brings new insights into robust enhancement techniques.

Fuzzy logic control and fuzzy logic controllers were discussed with a case study of an overhead crane model. Fuzzy tuning schemes, which result in explicit expressions for continuously changing the PI controller parameters or adjusting the control in the sliding mode, have demonstrated their ability to significantly improve system robustness. Robust modal control can also employ some fuzzy tuning schemes to cope with a wide range of load and parameter variations. Predictive coefficients of an unknown input observer were tuned taking into account the change of the estimated disturbances. Conditional schemes were introduced to tune the dynamic feedforward coefficient according to the signs of error and the change of the estimated load torque. The robust feedback gain were adjusted according to the signs of error and of the change of error. Simulation results for servo drive systems verified the effectiveness of fuzzy tuning in robust modal control.

Some neural network based techniques have been proposed. A radial basis function network was used to closely approximate the input-output relationship of a well designed fuzzy logic controller. A backpropagation feedforward network was trained

to cluster the error and derivative-of-error patterns and correspondingly generate the proper control action in tracking servo systems. Fuzzy and neurocontrol approach was developed for systems with severe nonlinearites, using a neural network model for the inverse dynamics in addition to an adaptive fuzzy observer or and disturbance observer-based controller with fuzzy tuning. The neural network capabilities of learning and approximating have been shown through the simulation and, partially, experimental results. It is believed that neuro technique will be very promising for robust control of motion systems.

In this final chapter, the important points encountered during the course of this study are summarised, and a brief review of the results obtained is presented. A number of extensions and areas of improvement which may be investigated in future work are also outlined. The chapter is ended with some conclusion remarks.

8.2 Summary of main results

When analysing dynamic properties of multi-mass electromechanical systems, it is required to have a common model for a variety of electrical drives with different types of motors. The dynamic stiffness of a generalised electric motor's speed torque characteristics, proposed by Kljuchev [51], has a significant contribution to the construction of such a model. The problem, albeit classic, is still timely when considering flexible structures in robotics or space technology and the increasing number of vector-controlled AC-motors which have a linearised decoupled model. The elaboration on a normalised characteristic equation of an n-mass system was given in Chapter 2. The conditions for maximal damping and complete damping were determined in the general case. The values of the electromagnetic and electromechanical time-constants at maximal damping were found in dependence on the mass ratio (Ha [55]). The results for two-mass systems, which are widely-known in Soviet literature, can be derived as a special case of those obtained for a general n-mass case. The use of multi-parameter root loci allows considering other changing factors, such as the electromagnetic time-constant and the mass ratio, and the influence of viscous friction on the motor, load and coupling shafts. With a given mass ratio, dominant root branches of the system root loci are observed not affected by parameter variations as much as the branches containing other roots. While dynamics of two-mass systems is sensitive to friction on the motor and coupling shaft, maximal damping of the system is seriously affected by friction on the load shaft. The

oscillatory influence of viscous friction on the load and coupling shaft in two-mass systems is reduced at large values of the mass ratio.

In order to design a controller for vibration suppression and load rejection in multi-mass servo systems, robust modal control, first proposed in Ha [9], was developed in Chapter 3. A methodical procedure for designing robust modal controllers was presented. The dominant pole-based technique was proposed for one-mass and two-mass servo systems. When choosing the desired poles for determining the state feedback gain, only the dominant root pair assigns the closed-loop system dynamics. The other poles can be chosen according to additional conditions relating to accuracy or damping capability. This may improve the steady-state performance of systems with modal control. Design equations were given for servo systems to achieve maximum damping. Vibrations due to backlash nonlinearity can be suppressed using the proposed approach. On the other hand, an eigenvalue sensitivity analysis showed a significant increase of the dominant root sensitivities in the vicinity of some critical values of the drive parameters. For simultaneously estimating the unmeasurable states and external disturbances, an observer was constructed on the basis of measurements of the system input and output and some *a priori* information of the unknown inputs. The proposed observer is able to estimate the torsional torque and load speed, and load torque in a multi-mass servo system. Based on load torque estimates, feedforward compensation principles was applied to reject the disturbance influence. Considering the parameter variation problem, a robust feedback signal was added to the modal signal. When satisfying some matching conditions, the asymptotic stability condition was determined via the second method of Lyapunov in dependence on the bounds of uncertain matrices of the state model. Design procedures for the continuous-time and discrete-time robust modal controllers were illustrated in servo drive systems. Simulation results demonstrated the system parameter- and load-insensitivity, and also robustness against nonlinear backlash in the shaft gear of a two-mass servo system.

Fuzzy logic, a new way to represent the vagueness in everyday life, first introduced by Zadeh [12], and its application to control engineering was outlined in Chapter 4. As a powerful tool to grasp the real world complexity, uncertainty, and unpredictability, fuzzy logic has demonstrated its capability of robustness enhancements in many systems including motion control ones. Fuzzy reasoning or approximate reasoning was considered from the engineering viewpoint with IF-THEN fuzzy rules. The design of a fuzzy logic controller was illustrated through the control of a crane model

with two main objectives, load minimal swing and robustness. Simulation and experimental results confirmed the validity of fuzzy logic control in terms of robust performance and advantage over conventional control techniques. The laboratory model can be utilised for teaching fuzzy control issues to university students in electrical engineering (Negnevitsky, Ha *et al.* [134]). Pros and cons of fuzzy control approach were also discussed.

In Chapter 5, simple fuzzy tuning schemes were introduced to continuously change the controller parameters or the control action in order to enhance robustness. The gain and time constant of a conventional proportional-integral (PI) controller were tuned according to some exponential functions, resulting from some engineering heuristics with the use of fuzzy logic (Ha [112]). System robustness was verified through high performance of transient responses in changing environment conditions. The results were extended to multi-loop cascade control with a fuzzy tuned PI controller used in each loop instead of conventional one. Simulation results in a two-mass system indicated that fuzzy tuning can be applied to cascade controllers in flexible electromechanical systems to increase robustness to some extent for parameter and load variations, and nonlinearities. Fuzzy logic schemes were also applied to tune the control action to deal with unmodelled dynamics in sliding mode control. First, the equivalent motion was determined from the desired sliding eigenstructure. The use of a switching gain based on the Lyapunov stability theory guaranteed the reaching condition in the neighbourhood of the sliding surface. Fuzzy tuning schemes were then employed to accelerate the reaching phase, reduce chattering, and hence, improve robust performance (Ha [148]). The proposed technique were applied to the control of a elastic drive system. Simulation results in a servo two-mass drive demonstrated its validity. Here, the explicit expressions for fuzzy schemes facilitated the computational implementation of the proposed controller.

The methodology using fuzzy logic and some engineering heuristics to tune a conventional controller's parameters was extended to robust modal control in Chapter 6. Simple tuning schemes were applied for continuously changing the predictive observer coefficients, the feedforward controller coefficients, and the robust feedback coefficients (Ha & Negnevitsky [37]). The predictive coefficients of an unknown input observer were tuned taking into account the change of estimated disturbances. As illustrated in estimating the load torque of a two-mass servo system, fuzzy tuning improved observer robustness. Conditional schemes were given for tuning the

dynamic feedforward coefficient in relation to the signs of the error and the change of the estimated load torque disturbance. Fuzzy tuned feedforward compensation ameliorated robust performance of the control of a robot arm motion, and a two-mass position drive. Other fuzzy schemes were also proposed to tune the robust feedback gain according to the signs of the error and the change of error. Simulation results obtained through the position control of a two-mass resonant system indicated the feasibility of robust modal controllers with fuzzy tuning in flexible structures for vibration suppression and load rejection.

Chapter 7 was devoted to the application of artificial neural networks to motion control. It focused mainly on the use of a neural network to mimic a nonlinear controller, e.g. a fuzzy logic controller; or to cluster the groups of both the servo control error and its derivative which an appropriate control action would correct. The combination of fuzzy and neurocontrol was proposed as a promising approach to the problem of severe sensitivity when system parameters and load varying a wide range. The implementation of a fuzzy logic controller's input-output relationship in a neural network to ease the control system of computation burden was investigated with reference to the position control of a swinging load of an overhead crane model. A radial basis function network, undergoing a two-stage (transient and steady-state) training process, approximated the control action from a fuzzy logic controller for that model (Ha & Negnevitsky [34]). Simulation and experimental results, compared with those of the system with the fuzzy logic controller, demonstrated the neural network ability to control in the same manner as a fuzzy logic controller. Robustness against parameter and load variations was verified. Another contribution of this chapter is an application of the back propagation network to the tracking control of servo drive systems. Based on information of the control error and its time derivative, the neural network classified the error and change-of-error patterns, and generated the appropriate control action without learning the inverse dynamics of the plant. The merit of the proposed approach lie in the design simplicity and its practicality for real-time implementation with a look-up table (Ha [45]). Simulation results for an overhead crane model and a two-mass servo drive indicated that the systems exhibit highly robust performance in the presence of uncertainties in the plant parameters and control process. For servomechanisms with severe nonlinearities, the fuzzy neurocontrol technique was presented, combining salient features of observer-based fuzzy control for decoupling motion axes, and of additional compensation from a neural network model to provide adaptive enhancements (Palis, Ha *et al.* [33]). In the observer control loop, the influence of an unknown equivalent load torque was

compensated for by an adaptive fuzzy observer controller or a disturbance observer-based fuzzy tuner. A radial basis function neural network was trained to provide information of the input depending on the system outputs in the proportional-integral-derivative manner. The neural net then provided a parallel compensation action for a wide range of system's uncertainties and nonlinearities. Simulation results of the time optimal positioning process of a robot axis demonstrated the effectiveness of the proposed approach.

8.3 Further extensions and developments

This thesis has touched a number of different areas of research including analysis and synthesis of motion control systems. In each of these areas techniques have been developed to address robust issues of electromechanical systems, such as electrical servo drives and robotics. Despite the good achievements obtained from some of these approaches, there is inevitably room for improvements and extensions within or relating to the scope of this study.

8.3.1. Damping estimation

Through the standardisation and generalisation of the model of electromechanical systems using the dynamic stiffness of the drive's speed-torque characteristics, it is worth developing an expert system to help an electromechanical engineer to determine damping and other dynamic properties of his system and provide further guidance on choosing the appropriate controller design for it. Expertise obtained from the results of Sections 2.4 and 2.5 and the electromechanical product catalogue can be embedded in the knowledge base and database which can be easily accessed and updated. This knowledge base can be combined in an expert system for drive product selection (Daoshen & Bose [189]). A topic for further investigation may be the estimation of maximal damping conditions in the presence of viscous friction and its influence on the system dynamic properties. The robust root locus method, proposed by Barmish & Tempo [61], can serve as an effective tool for this purpose. The use of the dominant pole pair leads to many interesting aspects in regards to the design of robust controllers for motion control systems. One of these is the design aimed at achieving maximal damping in electromechanical systems (Ha *et al.* [190]). The approach will be promising if it can be equipped with a self-organising mechanism to assign the dominant roots.

8.3.2. Observer-based control and monitoring

Observer-based control techniques have prevailed their potential not only in control strategies but also in conditions monitoring. Since robust performance of a system with observer-based feedback and feedforward techniques depends much on the accuracy of the recovery from unmeasurable states and external disturbances, observer robustness is an important issue which requires further study. There is a possibility of determining a linear robust control law when the full state cannot be measured and observers are implemented to estimate the state (Jabbari & Schmitendorf [191]). Dynamic feedforward compensation in an adaptive manner may need to be extended when the dynamics of the system subject to an unknown input is complicated. Robust observers can also find applications in non-invasive fault incipient detection, as shown in Ha & Negnevitsky [43] (see Appendix B). It is worth developing this approach for vector-controlled AC drive systems on the basis of off-line or on-line diagnostics. In general, solutions for a robust control strategy depends much on uncertainty bounds, especially in robotics. A more reasonable choice of the bound of the system uncertainty will lead to a less conservative solution. Thus, a study of uncertainty bounds may be an interesting extension to robust control of robotic manipulators (Man, Yu & Ha [192]).

8.3.3. Fuzzy logic control

Since the genesis of fuzzy logic and the "applications pull" of fuzzy logic control, great progress has been made in constructing the mathematical foundation of fuzzy set theory as well as developing tools for and demonstrating applications of fuzzy logic control. However, the utility and role of fuzzy logic control remains controversial because fuzzy logic, in the ordinary sense, is not a control design methodology. As an implementation technique, fuzzy logic control needs more justifications of its use from the user. A taxonomy was provided by Thomas & Armstrong-Helouvry [193] as a contribution towards this purpose. Despite good performance obtained in many simulations and experiments for fuzzy control systems, in fact, some important theoretical and practical problems still have not been solved. For example, error convergence, stability, and robustness have not been fully proven for fuzzy logic control schemes to deal with system uncertain dynamics. Research tendencies aimed at bridging that gap are open and very promising. Other attempts may focus on the combination of fuzzy control with other control strategies, such as sliding mode

control (Ha & Negnevistky [194]) or neuromorphic control as mentioned in the following section.

8.3.4. Neuro-fuzzy approach

A fuzzy inference system can now not only employ linguistic rules from human experts but also adapt itself using numerical input/output data to achieve better performance. In Jang & Sun [128], neural networks and fuzzy inference systems are all special instances of adaptive networks called adaptive network-based fuzzy inference systems. Once a fuzzy controller is transformed into an adaptive network, it can take advantage of all techniques for designing a neural network controller, namely, mimicking another controller, inverse control, backpropagation learning, and others learning techniques. In general, setting up a common framework for unifying both neural networks and fuzzy models will bring certain advantages over fuzzy or neural networks approaches. For single-input single-output linearised systems, the use of a fuzzy radial basis function network (Man, Yu & Ha [195]) to learn the system uncertainty bound can result in an effective control strategy for robust tracking in robotic manipulators. It is believed that by introducing some learning or self-organising algorithms into the disturbance observer-based fuzzy tuner, the neuro-fuzzy approach in Palis, Ha *et al.* [140] can be more flexible in order to cope with a wide range of structured and unstructured uncertainties. Fuzzy tuning has demonstrated its ability to ameliorate robust performance of motion control systems, neuro-fuzzy tuning with its learning capability will bring adaptive enhancements into these robust systems.

8.4 Concluding remarks

A number of analysis and synthesis techniques addressing robustness issues of motion control systems have been developed and verified. The conditions for maximal damping and complete damping were derived from the general characteristic equation of an n-mass system in dimensionless space. The multi-parameter root loci was used to consider other changing factors, such as the electromagnetic time-constant and the mass ratio, and the influence of viscous friction on the motor, load and coupling shafts. The main centre of this study is involved in the application of modern control and intelligent techniques to design robust controllers for electromechanical systems. Robust modal control was examined with the emphasis on dominant pole-based approach. A brief introduction to fuzzy logic control was provided with an illustrative

example for the control of an overhead crane model. Fuzzy tuning highlighted a prominent possibility of robustness enhancements in conventional techniques such as PI control, and also in sliding mode control and robust modal control. Neural network approach was outlined in some applications exploiting the net ability to approximate an input/output relation, to classify patterns of error and its derivative, and to learn the inverse dynamics for an effective compensation.

The results obtained from this study can be directly applied to electrical drive systems, multi-mass servomechanisms with backlash nonlinearity, and robot manipulators with parameter and load uncertainties. However, the strategies proposed here are not limited to electromechanical controlled objects. For example, robust modal control, fuzzy tuning schemes, and neural network approach described in this thesis can find applications in process control, biomedical technology, financial control problems, or any dynamic system with severe uncertainties.

While the developments detailed in this thesis have touched many of the important considerations relevant to robustness issues, especially the application of intelligent tools, in motion control systems, the large scope of this area of research will be never ever exhausted. Nor should the techniques proposed in this work be considered fully complete. A number of possible future extensions and improvements have been suggested in the previous section. More and more contributions to the *pot-pourri* of this field are continually expected.

Appendix A

Normalised closed-loop polynomials

There exist many criteria for choosing the closed loop characteristic equation based on the desired transient response. In the field of electrical drives, e.g., the popular criteria are the binomial expansion, Butterworth polynomials, magnitude optimum, and Graham-Lathrop minimisation of the integral time absolute error (ITAE). This appendix provides a summary of the normalised polynomials by those criteria with the corresponding specifications of overshoot percentage, σ %, and settling time, t_s.

Normalised polynomials	σ %	t_s	Criteria
s^2+2s+1	0	3.2	binomial
s^3+3s^2+3s+1	0	6.3	expansion
$s^4+4s^3+6s^2+4s+1$	0	7.5	
$s^5+5s^4+10s^3+10s^2+5s+1$	0	9.1	
$s^2+\sqrt{2}s+1$	4.5	2.8	Butterworth
s^3+2s^2+2s+1	7.1	5.9	
$s^4+2.6s^3+3.4s^2+2.6s+1$	12	6.9	
$s^5+3.24s^4+5.24s^3+5.24s^2+3.24s+1$	9.5	7.8	
$s^6+3.86s^5+7.46s^4+9.13s^3+7.46s^2+3.86s+1$	12	8	
$s^2+\sqrt{2}s+1$	4.5	2.8	magnitude
s^3+2s^2+2s+1	7.1	5.9	optimum
$s^4+2.82s^3+4s^2+2.82s+1$	6.2	7	
$s^5+4s^4+8s^3+8s^2+4s+1$	5	7.5	
$s^2+\sqrt{2}s+1$	4.5	2.8	ITAE
$s^3+1.75s^2+2.15s+1$	3	3.6	
$s^4+2.1s^3+3.4s^2+2.7s+1$	10	4.7	
$s^5+2.8s^4+5s^3+5.5s^2+3.4s+1$	6	7.8	
$s^6+3.25s^5+6.6s^4+8.6s^3+7.45s^2+3.9s+1$	3	6.6	

Appendix B

A digital predictive observer for incipient fault detection

B1. Introduction

The stability of power systems is affected by generator dynamics and thus by their state variables, which are, in practice, usually subject to completely unknown and time-varying inputs. In instrument fault detection, isolation and identification of power systems, most actuator failures can be generally modelled as unknown inputs to the system. Furthermore, for the control purposes, it is necessary to estimate not only the unmeasurable state variables but also the unknown inputs. The investigation of unknown input observers is important for their application in control and in fault detection of linear system, including power systems. The system parameter values can be derived by using information about the measurable and estimated states variables under unknown inputs. For designing a minimal-order unknown input observer, the procedure presented in Hou & Muller [98] can be reduced to a standard Luenberger observer. Other attempts focus on the problem of simultaneously estimating state variables and unknown inputs. In Park & Stein [97], the state equation is transformed into a special system model for a reduced-order observer. The design procedure in Ha [39] is straightforward with the introduction of a predictive coefficient which can be continuously tuned by fuzzy logic taking into account the rate of change of the unknown input. Observer robustness and the feasibility of its tuning schemes enable a number of its applications (see Chapter 6). This appendix provides an application to the estimation of the damper winding currents of a synchronous generator for on-line non-invasive incipient fault detection. Simulation results are provided for illustration.

B2. Obsever-based incipient fault detection in a synchronous generator

For the reliability and safety improvement in power engineering the early detection and localisation of faults is of high interest. A methodical survey for fault diagnosis of dynamic processes can be found, e.g. in Isermann [196] and Frank [197]. In large

rotating machines such as synchronous generators incipient faults can be detected using radio frequency monitoring (Trimperley [198]) or a set of standstill measurements (Boje *et al.* [199]). Another fault detection technique is the non-invasive parameter estimation using observers and *a priori* knowledge of the process structure. A drawback of this approach is that it requires an accurate mathematical model of the system dynamics. In Keyhani & Miri [200], a recursive algorithm was presented to estimate the machine parameters. To deal with the uncertainty in the machine dynamics, the observer described in Sections 3.4 and 6.2 is proposed instead in order to estimate the unmeasurable damper winding currents under the condition of inaccessible damping torque. The parameter trajectories obtained can then be utilised to detect incipient faults.

B.2.1. Digital Predictive Observer with Fuzzy Tuning for a Synchronous Generator

Exposed to small changes, a synchronous generator can be adequately represented by a linearised model (Anderson & Fouad [201]). Its continuous-time state equation can be written in the form:

$$\dot{\mathbf{x}}(t) = \mathbf{A}_c\mathbf{x}(t) + \mathbf{B}_c\mathbf{u}(t) + \mathbf{D}_c T_d(t), \tag{B.1}$$

where $\mathbf{x} = (i_d \;\; i_F \;\; i_D \;\; i_q \;\; i_Q \;\; \omega \;\; \delta)^{\mathrm{T}}$ is the state vector (i_d, i_q, i_F, i_D, and i_Q are the changes of the direct axis armature current, quadrature axis armature current, field current, direct axis damper winding current, and quadrature axis damper winding current, respectively; and ω and δ are the changes of the p.u. rotor angular velocity and torque angle, respectively); and $\mathbf{u} = (-v_F \;\; T_m)^T$ is the known input vector (v_F and T_m are the changes of the excitation voltage and the mechanical prime mover torque, respectively). The unknown input T_d is considered as a combination of the change of the damping torque and equivalent components due to linearised inaccuracy, perturbations in the change of the mechanical and electromagnetic torque T_e as described in the swing equation [201]:

$$\tau_j \dot{\omega} = T_m - T_e - T_d, \tag{B.2}$$

where τ_j is the normalised constant. The matrices $\mathbf{A}_c$ and $\mathbf{B}_c$ (the subscript c denotes continuous-time system) are constant matrices of corresponding dimensions, and $\mathbf{D}_c^T$ = (0 0 0 0 0 -1 0). The changes of the damper winding currents i_F, i_D and damping torque T_d will be estimated. By rearranging the discrete-time form of equation (B.1)

into the form of equation (3.71) with $\mathbf{x}_1 = (i_d \;\; i_F \;\; i_q \;\; \omega \;\; \delta)^T$ and $\mathbf{x}_2 = (i_D \;\; i_Q)^T$, and augmenting it with the approximation

$$T_d(k+1) = (1+\gamma)T_d(k) - \gamma T_d(k-1), \tag{B.3}$$

the partitioned form of equation (3.75) can be obtained. By choosing the observer gain $\mathbf{L}_1 = \begin{pmatrix} 0 & 0 & l_1 & l_2 & 0 \\ 0 & 0 & l_3 & l_4 & 0 \end{pmatrix}$ and $\mathbf{L}_2 = \begin{pmatrix} 0 & 0 & l_5 & l_6 & 0 \end{pmatrix}$, the observer equation is written as:

$$\begin{aligned} z_i(k+1) &= f_{i1}z_1(k) + f_{i2}z_2(k) + f_{i3}w(k) + g_{i1}i_d(k) + g_{i2}i_F(k) + g_{i3}i_q(k) + g_{i4}\omega(k) + \\ &+ g_{i5}\delta(k) - h_{i1}v_F(k) + h_{i2}T_m(k), \quad i = 1,2 \end{aligned}$$

$$\begin{aligned} w(k+1) &= f_{31}z_1(k) + f_{32}z_2(k) + f_{33}w(k) + g_{31}i_d(k) + g_{32}i_F(k) + g_{33}i_q(k) + g_{34}\omega(k) + \\ &+ g_{35}\delta(k) - h_{31}v_F(k) + h_{32}T_m(k) - \gamma\hat{T}_d(k-1) \end{aligned}$$

$$\hat{i}_D(k) = z_1(k) + l_1 i_q(k) + l_2\omega(k),$$

$$\hat{i}_Q(k) = z_2(k) + l_3 i_q(k) + l_4\omega(k),$$

$$\hat{T}_d(k) = w(k) + l_5 i_q(k) + l_6\omega(k), \tag{B.4}$$

where $z_1(k)$, $z_2(k)$ and $w(k)$ are the observer states, f_{ij}, g_{ij}, and h_{ij} are coefficients calculated from equation (3.76b). For a given coefficient $\gamma = \gamma_0$, a solution for the observer deadbeat condition can be obtained as follows:

$$l_1 = (a_{66}a_{47} - a_{67}a_{46})/\Delta_1,\; l_2 = (a_{67}a_{36} - a_{66}a_{37})/\Delta_1,$$

$$l_3 = (a_{76}a_{47} - a_{77}a_{46})/\Delta_1,\; l_4 = (a_{77}a_{36} - a_{76}a_{37})/\Delta_1,$$

$$l_5 = -(p_0 d_4 + (1+p_0)(f_{13}a_{46} + f_{23}a_{47}))/\Delta_2,$$

$$l_6 = (p_0 d_3 + (1+p_0)(f_{13}a_{36} + f_{23}a_{37}))/\Delta_2, \tag{B.5}$$

with $f_{13} = d_6 - l_1 d_3 - l_2 d_4,\; f_{23} = d_7 - l_3 d_3 - l_4 d_4$,

$$\Delta_1 = a_{36}a_{47} - a_{37}a_{46},$$

$$\Delta_2 = (f_{13}a_{24} + f_{23}a_{25})d_3 - (f_{13}a_{34} + f_{23}a_{35})d_2$$

where the matrix elements a_{ij}, d_i $(i, j = 1,2,\ldots,5)$ found in the form (3.75) of the system discrete-time state equation.

Taking into account uncertainties in the mathematical model of a generator, the observer predictive coefficient γ in equation (B.3) will be tuned, using the fuzzy logic approach as described in Section 6.2. The following membership functions are assigned to γ and the rate of change $r(k)$ of the unknown input $T_d(k)$:

$$\mu(\gamma\_large) = \begin{cases} 1, & \gamma = \gamma_m \\ 0, & \gamma \neq \gamma_m \end{cases},$$

$$\mu(\gamma\_small) = \begin{cases} 1, & \gamma = 0 \\ 0, & \gamma \neq 0 \end{cases},$$

$$\mu_1(r\_small) = e^{-\sigma|r|},$$

$$\mu_2(r\_large) = 1 - e^{-\sigma|r|}. \tag{B.6}$$

where γ_m, σ are some positive constants. By inference and using equation (6.3), the predictive coefficient γ can be expressed in an explicit form as $\gamma = \gamma_m e^{-\sigma|r|}$.

B.2.2. Identification of Machine Parameters

Once the estimates of the unmeasurable states $\hat{i}_D(k)$, $\hat{i}_Q(k)$ and the unknown input $\hat{T}_d(k)$ are obtained, the identification problem is the determination of the discrete-time state matrices of the form (6.1) and then, matrices of the generator state equation (B.1). The least squares identification algorithm (Sinha & Kwong [202], Kreisselmeier [203]) is used. Denoting $\mathbf{X} = (i_d \;\; i_F \;\; \hat{i}_D \;\; i_q \;\; \hat{i}_Q \;\; \omega \;\; \delta)^T$ and $\mathbf{U} = (-v_F \;\; (T_m - \hat{T}_d))^T$, and following the simplified version of the generalised least square algorithm described in Keyhani & Miri [200], we can find the estimates $\hat{\mathbf{A}}$ and $\hat{\mathbf{B}}$ of matrices $\mathbf{A}$ and $\mathbf{B}$ in the state equation

$$\mathbf{X}(k+1) = \mathbf{A}\mathbf{X}(k) + \mathbf{B}\mathbf{U}(k). \tag{B.7}$$

Note that matrix **D** is omitted in equation (B.7) by the use of $T_m - \hat{T}_d$ as the prime torque. If there exists a nonsingular matrix **Q** to diagonalise $\hat{\mathbf{A}}$ or put it into Jordan form $\Lambda = \mathbf{Q}^{-1}\hat{\mathbf{A}}\mathbf{Q}$, then matrices $\mathbf{A}_c$ and $\mathbf{B}_c$ of the continuous-time sate equation corresponding to Equation (18) can be determined as:

$$\hat{\mathbf{A}}_c = \mathbf{Q}\Lambda_c\mathbf{Q}^{-1}, \quad \hat{\mathbf{B}}_c = (\hat{\mathbf{A}} - \mathbf{I})^{-1}\mathbf{Q}\Lambda_c\mathbf{Q}^{-1}\hat{\mathbf{B}}, \tag{B.8}$$

where $\Lambda_c(ii) = \frac{1}{T}\ln\Lambda(ii)$, i=1,2,...,7.

The estimates of the generator damping constant $\hat{D}_w(k)$ and parameter matrices **M** and **K** (Anderson & Fouad [201]) can then be found as:

$$\hat{D}_w(k) = \frac{\hat{T}_d(k)}{w(k)}, \quad \hat{\mathbf{M}} = -(\hat{\mathbf{B}}_c\mathbf{T}_b)^{-1}, \quad \hat{\mathbf{K}} = \hat{\mathbf{B}}_c^{-1}\hat{\mathbf{A}}_c, \tag{B.9}$$

where $\mathbf{T}_b = \begin{pmatrix} 0 & 1 & 0 & 0 & 0 & 0 & 0 \\ 0 & 0 & 0 & 0 & 0 & 1 & 0 \end{pmatrix}$, and **M** and **K** have the following forms, using the notation described in Anderson & Fouad [201]:

$$\mathbf{M} = \begin{pmatrix} L_{d\Sigma} & kM_F & kM_D & 0 & 0 & 0 & 0 \\ kM_F & L_F & M_R & 0 & 0 & 0 & 0 \\ kM_D & M_R & L_D & 0 & 0 & 0 & 0 \\ 0 & 0 & 0 & L_{q\Sigma} & kM_Q & -\lambda_{q0} & 0 \\ 0 & 0 & 0 & kM_Q & L_Q & 0 & 0 \\ 0 & 0 & 0 & 0 & 0 & -\tau_j & 0 \\ 0 & 0 & 0 & 0 & 0 & 0 & 1 \end{pmatrix},$$

$$\mathbf{K} = \begin{pmatrix} R_\Sigma & 0 & 0 & \omega_0 L_{q\Sigma} & \omega_0 kM_Q & \lambda_{q0\Sigma} & -K\cos(\delta_0 - \alpha) \\ 0 & r_F & 0 & 0 & 0 & 0 & 0 \\ 0 & 0 & r_D & 0 & 0 & 0 & 0 \\ -\omega_0 L_{d\Sigma} & -\omega_0 kM_F & -\omega_0 kM_D & R_\Sigma & 0 & -\lambda_{d0\Sigma} & -K\sin(\delta_0 - \alpha) \\ 0 & 0 & 0 & 0 & r_Q & 0 & 0 \\ \frac{\lambda_{q0} - L_d i_{q0}}{3} & \frac{-kM_F i_{q0}}{3} & \frac{-kM_D i_{q0}}{3} & \frac{-\lambda_{d0} + L_q i_{d0}}{3} & \frac{kM_Q i_{q0}}{3} & 0 & 0 \\ 0 & 0 & 0 & 0 & 0 & -1 & 0 \end{pmatrix} \tag{B.10}$$

where $R_\Sigma = r + R_e$, $L_{j\Sigma} = L_j + L_e$, and $\lambda_{j0\Sigma} = \lambda_{j0} + L_e i_{j0}$, $j = d, q$.

The parameter estimates obtained can be used to trace a trajectory for each parameter of the machine as its operating conditions are changing. By comparing the trajectory for a given parameter with earlier trajectories, any deterioration which may cause changes in this parameter can be detected. Possible faults due to temperature rise can also be detected from the estimates of damper winding currents $\hat{i}_D(k)$, $\hat{i}_Q(k)$ and resistances $\hat{r}_D$, $\hat{r}_Q$ by calculating Joule terms ri^2.

B.3 Illustrative example

Simulation results are provided to detect of damper winding currents and the damping coefficient of a synchronous machine taking into account its load variations (values of the machine parameters are taken from Example 6.2 in Anderson & Fouad [201]). With the sampling period $T = 0.01sec$, the actual and estimated damping torque and damper winding currents are shown in Figure B.1 and Figure B.2 when T_m=1, v_F=1, and the damping torque is assumed to be $T_d(k) = 5\times10^{-4}k$ at the system nominal parameters.

The identification error is estimated by

$$e(k) = \max_{i,j}\left|\hat{A}_{c,ij}(k) - A_{c,ij}(k)\right|, \tag{B.11}$$

where $\hat{A}_{c,ij}$ and $A_{c,ij}$ are the *i-th* row and *j-th* column elements of the matrices $\hat{\mathbf{A}}_c$ and $\mathbf{A}_c$. This error *e(k)* is less than 0.1% after 50 sampling periods. Note that as stated in Boje *et al.* discussion of [199], the identification error is sensitive to the initial values of the least squares algorithm.

Figure B.3 depicts the actual (curve 1) and estimated damping torques with fuzzy tuning $\gamma = 0.5e^{-2|r|}$ (curve 2) and without fuzzy tuning $\gamma = 0$ (curve 3) when the total armature resistance is increased 200% ($R_\Sigma = 3R_{\Sigma,nom}$) and the damping torque varies sinusoidally $T_d = 0.5(1-\sin t)$ p.u.

The results obtained indicates that the digital predictive observer with fuzzy tuning is less sensitive to system parameter variations (in this case, the load changes of the synchronous machine R_e). Thus, the identification process is made more robust.

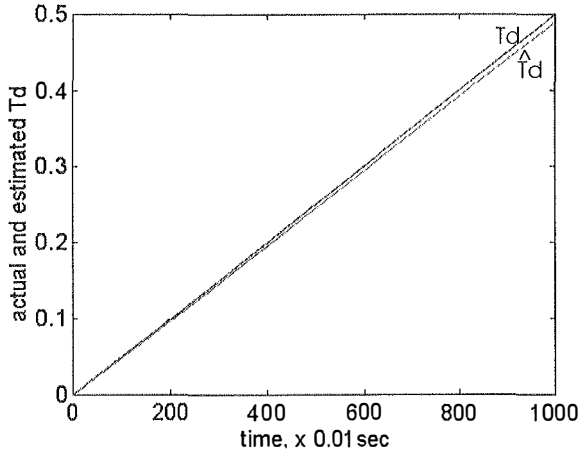

Figure B.1. Actual and estimated damping torque at $R_{\Sigma} = R_{\Sigma,nom}$.

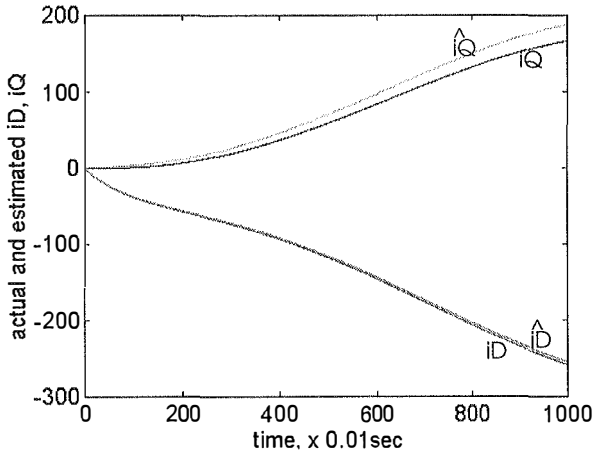

Figure B.2. Actual and estimated damper winding currents.

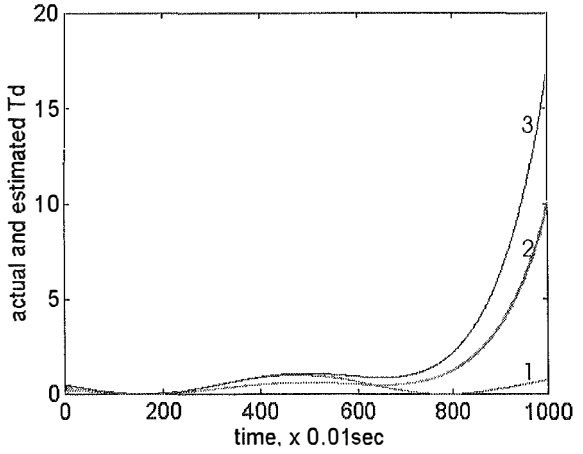

Figure B.3. Actual and estimated T_d when $R_{\Sigma} = 3R_{\Sigma,nom}$.

B.4 Conclusion

A digital predictive observer with fuzzy tuning has been proposed to estimate the damping torque and damper winding currents of a synchronous machine. The advantage of this observer is that it can provide correct estimates of not only the unmeasurable states but also the unknown inputs to the system. Furthermore, with simple tuning schemes the observer is made more robust against any deviation of system parameters. The information about the inaccessible damper winding currents and damping torque is then utilised to identify the continuous-time state matrix of the machine linearised model using a generalised least quare recursive algorithm. The parameter trajectories obtained enable the possibility of detecting incipient faults of a synchronous machine.

References

[1] F. Harashima, "Power electronics and motion control - a future perspective," *Proceedings of the IEEE*, Vol. 82, No. 8, pp. 1107-1110, August 1994.

[2] P. Dorato, "A historical review of robust control," *IEEE Control System Magazine*, Vol. 7, pp. 44-47, April 1987.

[3] P. Dorato, R. Tempo, and G. Muscato, "Bibliography on robust control," *Automatica*, Vol. 29, No. 1, pp. 201-213, January 1993.

[4] Y. Tsypkin, "New approaches to control theory," *Vestnik RAN*, No. 3, pp. 112-115, March 1992. *(In Russian).*

[5] V. A. Kharitonov, "On the asymptotic stability of the equilibrium point of a family of linear differential equation systems, " *Differential Equations*, Vol. 14, No. 11, pp. 2086-2088, November 1978. *(In Russian).*

[6] H. Kwakernaak, "Robust control and H_∞-optimisation - tutorial paper," *Automatica*, Vol. 29, No. 2, pp. 255-273, February 1993.

[7] S. Y. Emelyanov, *Variable structure control systems*, Moscow: Nauka, 1967. *(In Russian).*

[8] V. Utkin, *Sliding modes and their application in variable structure systems*, Moscow: Nauka, 1974. *(In Russian).*

[9] Q. P. Ha, *Design and investigation of a robust modal control system for electric drives of positioning mechanisms*, PhD Thesis, Moscow Power Engineering Institute (MEI), December 1992. *(In Russian).*

[10] V. K. Kumar and N. Mani, "The application of artificial intelligence techniques for intelligent control of dynamical physical systems," *International Journal of Adaptive Control and Signal Processing*, Vol. 8, pp. 379-392, August 1994.

[11] B. K. Bose, "Expert system, fuzzy logic, and neural network applications in power electronics and motion control," *Proceedings of the IEEE*, Vol. 82, No. 8, pp. 1303-1323, August 1994.

[12] L. A. Zadeh, "Fuzzy sets," *Inform. Control*, Vol. 8, pp. 338-353, 1965.

[13] S. S. L. Chang and L. A. Zadeh, "Fuzzy mapping and control," *IEEE Trans. Syst., Man, Cybern.*, Vol. SCM-2, No. 1, pp. 30-34, January 1972.

[14] D. G. Schwartz, G. J. Klir, H. W. Lewis III, and Y. Ezawa, "Application of fuzzy sets and approximate reasoning," *Proceedings of the IEEE*, Vol. 82, No. 4, pp. 482-498, April 1994.

[15] B. Widrow and M. A. Lehr, "30 years of adaptive neural networks: perceptron, madaline and backpropagation," *Proceedings of the IEEE*, Vol. 78, No. 9, pp. 1415-1442, September 1994.

[16] Q. P. Ha and M. Negnevitsky, "New trends in control theory and their reflection in electrical engineering education," *Proceedings of the Pacific Region Conference on Electrical Engineering Education (PRCEEE95)*, Melbourne, Australia, pp. 109-112, February 1995.

[17] K. J. Astrom, C. C. Hang, P. Persson, and W. K. Ho, "Toward intelligent PID control," *Automatica*, Vol. 28, No. 1, pp. 1-9, January 1992.

[18] A. A. Voda and I. D. Landau, "A method for the auto-calibration of PID controllers," *Automatica*, Vol. 31, No. 1, pp. 41-53, January 1995.

[19] Q. P. Ha and V. G. Alferov, "Robust modal controller for position drives," *Preprints of the Electrical Engineering Congress (EEC'94)*, Sydney, Australia, pp. 609-614, November 1994.

[20] H. C. Tseng and V. H. Hwang, "Servocontroller tuning with fuzzy logic," *IEEE Trans. Contr. Syst. Technology*, Vol. 1, No. 4, pp. 262-269, December 1993.

[21] Q. P. Ha and M. Negnevitsky, "Robust controllers with fuzzy tuning", *Australian Journal of Intelligent Information Processing Systems*, Vol. 3, No. 3, pp. 33-40, 1996.

[22] Q. P. Ha, M. Negnevitsky, and Z. Man, "Sliding mode control with fuzzy tuning", in *Proceedings of the 4th IEEE Australian and New-Zealand Conference on Intelligent Information Systems*, Adelaide, Australia, pp. 216-219, 1996.

[23] D. T. Pham and L. Xing, *Neural Networks for Identification, Prediction and Control*, London: Springer-Verlag, 1995.

[24] D. Psaltis, A. Sideris, and A. A. Yamamura, "A multilayered neural network controller," *IEEE Control System Magazine*, Vol. 8, No. 2, pp. 17-21, April 1988.

[25] P. J. Werbos, "Backpropagation through time: what it does and how to do it?," *Proceedings of the IEEE*, Vol. 78, No. 9, pp. 1550-1560, September 1994.

[26] W. T. Miller, R. S. Sutton, and P. J. Werbos, *Neural networks for control*, MIT Press, Cambridge, MA, 1990.

[27] K. S. Narenda and K. Parthasarathy, "Identification and control for dynamic systems using neural networks," *IEEE Trans. Neural Networks*, Vol. 1, No. 1, pp. 4-27, March 1990.

[28] K. J. Hunt and D. Sbarbaro, "Neural networks for non-linear internal model control," *Proceedings of the IEE, Part D, Control Theory Appl.*,Vol. 138, No. 5, pp. 431-438, May 1991.

[29] E. Colina-Morles and N. Mort, "Neural network-based adaptive control design," *Journal of Systems Engineering*, Vol. 2, No. 1, pp. 9-14, January 1993.

[30] G. A. Rovithakis and M. A. Christodoulou, "A robust direct adaptive regulation architecture using dynamic neural network model," *Proceedings of the Int. Conf. on System, Man and Cybernetics*, San Antonio, Texas, USA, pp. 1110-1115, October 1994.

[31] J. T. Evans, J. B. Gomm, J. B. Williams, P. J. G. Lisboa, and Q. S. To, "A practical application of neural modelling and predictive control," in G. F. Page, J. B. Gomm, and J. B. Williams (Eds.), *Applications of Neural Networks to Modelling and Control*, Chapman & Hall, London, 1993.

[32] T. H. Lee, W. K. Tan, and M. H. Ang, Jr., "A neural network control system with parallel adaptive enhancements applicable to nonlinear servomechanisms," *IEEE Trans. Ind. Electronics*, Vol. 41, No. 3, pp. 269-277, June 1994.

[33] F. Palis, A. Buch, U. Ladra, R. Kurrich, Q. P. Ha, and M. Negnevitsky, "Fuzzy and neurocontrol of drive systems with changing parameters and load", in *Proceedings of the 2nd European Power Electronics Chapter Symposium on*

Electric Drive Design and Applications (EPE'96), Nancy, France, pp. 183-186, June 1996.

[34] Q. P. Ha and M. Negnevitsky, "Neural network application for the position drive of a swinging load," in *Proceedings of the IASTED International Conference on Modelling, Simulation and Optimisation (MSO'96)*, Gold Coast, Australia, May 1996.

[35] Q. P. Ha and M. Negnevitsky, "Root locus application for damping capability estimation of multi-mass electromechanical systems," in *Proceedings of the IEEE 21st International Conference on Industrial Electronics, Control, and Instrumentation (IECON'95)*, Orlando, USA, Vol. 1, pp. 633-638, November 1995.

[36] V. G. Alferov and Q. P. Ha, "DC-motor position drives with robust modal control," *Elektrichestvo*, No. 9, pp. 17-24, 1995. *(In Russian).*

[37] Q. P. Ha and M. Negnevitsky, "Fuzzy tuning in motion control", in R. A. Adey, G. Rzevski, and A.K. Sunol (Eds.), *Applications of Artificial Intelligence in Engineering*, Computational Mechanics Publications, Southampton, UK, 1996, 734p.

[38] Q. P. Ha, M. Negnevitsky, and F. Palis, "Cascade PI Controllers with Fuzzy Tuning," to appear in *Proceedings of the IEEE International Conference on Fuzzy Systems (FUZZ-IEEE'97)*, Barcelona, Spain, July 1997.

[39] Q. P. Ha, "A digital predictive observer with fuzzy tuning for multi-mass electromechanical systems," in *Proceedings of the Australian Universities Power Engineering Conference (AUPEC'95)*, Perth, Australia, Vol. 3, pp. 428-433, September 1995.

[40] Q. P. Ha, "A dynamic feedforward controller with fuzzy tuning for electromechanical systems," in *Proceedings of the Australian Universities Power Engineering Conference (AUPEC'95)*, Perth, Australia, Vol. 3, pp. 422-427, September 1995.

[41] Q. P. Ha and M. Negnevitsky, "A robust modal controller with fuzzy tuning for multi-mass electromechanical systems," in *Proceedings of the IEEE 3rd Australian and New Zealand Conference on Intelligent Information Systems (ANZIIS-95)*, Perth, Australia, pp. 214-219, November 1995.

[42] Q. P. Ha and M. Negnevitsky, "Fuzzy tuning in robust modal control," in *Proceedings of the 1st International Discourse on Fuzzy Logic and the*

Management of Complexity (FLAMOC'96), Sydney, Australia, Vol. 2, pp. 160-164, January 1996.

[43] Q. P. Ha and M. Negnevitsky, "A digital predictive observer for incipient fault detection," in *Proceedings of the IEE 3rd International Conference on Advances in Power System Control, Operation & Management (APSCOM-95)*, HongKong, Vol. 1, pp. 183-188, November 1995.

[44] Q. P. Ha and M. Negnevitsky, "Neural network-based controller for servo drives," in *Proceedings of the IEEE 22nd International Conference on Industrial Electronics, Control, and Instrumentation (IECON'96)*, Taipei, Taiwan, Vol. 2, pp. 904-909, August 1996.

[45] Q. P. Ha, "A Neural Network-Based Controller for Multi-Mass Electromechanical Systems," in *Proceedings of the Australian Universities Power Engineering Conference (AUPEC'96)*, Melbourne, Australia, Vol. 1, pp. 31-36, October 1996.

[46] W. Gawronski, "A balanced LQG compensator for flexible structures," *Automatica*, Vol. 30, No. 10, pp. 1555-1564, October 1993.

[47] S. K. Lin, "Minimal linear combinations of the inertia parameters of a manipulator," *IEEE Trans. Robot. and Automat.*, Vol. 11, No. 3, pp. 360-373, June 1995.

[48] V. B. Klepikov and V. A. Samarskii, "Peculiarities of frequency response of electromechanical systems with friction load," *Elektromekhanika*, No. 2, pp. 62-67, May 1990. *(In Russian).*

[49] V. G. Alferov and Q. P. Ha, "Root locus evaluation of the dynamic properties and the pair of dominant roots," *Soviet Electrical Engineering*, No. 64, No. 6, pp. 35-40, June 1993.

[50] R. Dhaouadi, K. Kubo, and M. Tobise, "Analysis and compensation of speed drive systems with torsional loads," *IEEE Trans. Ind. Appli.*, Vol. 30, No. 3, pp. 760-765, June 1994.

[51] V. I. Kljuchev, "Development of the theory of electrical drives with flexible mechanical links: status and perspective," *Elektrichestvo*, No. 7, pp. 28-32, July 1981. *(In Russian).*

[52] B. V. Ol'khovikov, D. A. Kaminskaya, and A. B. Rozenvaig, "Analysis of the dynamics of a two-mass electrical drive system on the basis of the roots of the

characteristic equation," *Elektromekhanika*, No. 5, pp. 98-102, May 1984. *(In Russian).*

[53] N. A. Zadorozhny and V. D. Zemljakov, "Estimating the damping properties of an electrical drive with an elastic mechanical component and viscous friction at the motor shaft," *Elektrichestvo*, No. 4, pp. 70-72, April 1989. *(In Russian).*

[54] V. I. Kljuchev, *Theory of electrical drives*, Moscow: Energoatomizdat, 1985. *(In Russian).*

[55] Q. P. Ha, "Root locus method application for damping capability estimation of multi-mass electromechanical systems," in *Preprints of the CONTROL'95 Conference*, Melbourne, Australia, Vol. 1, pp. 255-259, October 1995.

[56] R. D. Lorenz, T. A. Lipo, and D. W. Novotny, "Motion control with induction motors," *Proceedings of the IEEE*, Vol. 82, No. 8, pp. 1215-1240, August 1994.

[57] S. Nomura, T. Murakami, and K. Ohnishi, "Vibration control of multiple mass system by estimated reaction torque," in *Proceedings of the IEEE 21st International Conference on Industrial Electronics, Control, and Instrumentation (IECON'95)*, Orlando, USA, Vol. 2, pp. 1091-1095, November 1995.

[58] M. Matsuoka, T. Murakami, and K. Ohnishi, "Vibration suppression and disturbance rejection control of a flexible link arm," in *Proceedings of the IEEE 21st International Conference on Industrial Electronics, Control, and Instrumentation (IECON'95)*, Orlando, USA, Vol. 2, pp. 1260-1265, November 1995.

[59] S. P. Strelkov, *Introduction to theory of oscillations*, Moscow: Nauka, 1964. *(In Russian).*

[60] B. C. Kuo, *Automatic control systems*, Englewood Cliffs, NJ.: Prentice Hall, Inc., 1987.

[61] B. R. Barmish and R. Tempo, "The robust root locus," *Automatica*, Vol. 26, No. 2, pp. 283-292, February 1990.

[62] Y. Tong and N. K. Sinha, "A computational technique for the robust root locus," *IEEE Trans. Ind. Electronics*, Vol. 41, No. 1, pp. 79-85, February 1994.

[63] B. Armstrong-Helouvry, P. Dupont, and C. Canudas de Wit, "A survey of models, analysis tools and compensation methods for the control of machines with friction," *Automatica*, Vol. 30, No. 7, pp. 1083-1138, July 1994.

[64] Y. Hori, H. Iseki, and K. Sugiura, "Basic consideration of vibration suppression and disturbance rejection control of multi-inertia system using SFLAC (State Feedback and Load Acceleration Control)," *IEEE Trans. Ind. Appli.*, Vol. 30, No. 4, pp. 889-896, August 1994.

[65] Y. Dote, "Application of modern control techniques to motor control," *Proceedings of the IEEE*, Vol. 76, No. 4, pp. 438-454, April 1988.

[66] F. N. Bailey and C. H. Hui, "Loop gain-phase shaping for single-input-single-output robust controllers," *IEEE Contr. Syst. Mag.*, Vol. 11, No. 1, pp. 93-101, January 1991.

[67] J. V. De Vegte, *Feedback control systems*, Englewood Cliffs, NJ.: Prentice-Hall, Inc., 1990.

[68] B. D. O. Anderson and J. B. Moore, *Optimal control: linear quadratic method*, Englewood Cliffs, NJ.: Prentice-Hall, Inc., 1990.

[69] K. J. Astrom, "Adaptive feedback control," *Proceedings of the IEEE*, Vol. 75, No. 2, pp. 185-210, February 1987.

[70] R. A. DeCarlo, S. H. Zak, and G. P. Matthews, "Variable structure control of nonlinear multivariable systems: a tutorial," *Proceedings of the IEEE*, Vol. 76, No. 3, pp. 212-232, March 1988.

[71] K. Furuta, "VSS type self-tuning control," *IEEE Trans. Ind. Electronics*, Vol. 40, No. 1, pp. 37-44, February 1993.

[72] N. T. Kuzovkov, *Modal control and observers*, Moscow: Mashinostroenje, 1976. *(In Russian).*

[73] V. G. Alferov and Q. P. Ha, "A digital predictive observer," *Elektromekhanika*, No. 3, pp. 71-76, March 1992. *(In Russian).*

[74] V. G. Alferov, Q. P. Ha, and R. M. Khusainov, "Drive control systems using a disturbance observer," in N. F. Ilynsky (Ed.), *Industrial applications of electric drives on the perspective element base*, Moscow, pp. 93-99, May 1992. *(In Russian).*

[75] V. G. Alferov and Q. P. Ha, "Design of a modal control system for servo drive," *Elektrichestvo*, No. 6, pp. 48-54, June 1993. *(In Russian).*

[76] T. M. Jahns, "Motion control with permanent-magnet AC machines," *Proceedings of the IEEE*, Vol. 82, No. 8, pp. 1241-1252, August 1994.

[77] I. Boldea and S. A. Nasar, *Vector control of AC drives*, Boca Raton, Florida: CRC Press, Inc., 1992.

[78] J. S. Ko, J. H. Lee, S. K. Chung, and M. J. Youn, "A robust digital position control of brushless DC motor with deadbeat load torque observer," *IEEE Trans. Ind. Electronics*, Vol. 40, No. 1, pp. 44-49, February 1993.

[79] Y. Y. Tzou and H. J. Wu, "Multi-microprocessor based robust control of an AC induction servo motor," *IEEE Trans. Ind. Appli.*, Vol. 26, No. 3, pp. 441-449, June 1990.

[80] R. E. Kalman, "On the general theory of control systems," in *Proceedings of the First International Congress IFAC*, Moscow, 1960. *Automatica and Remote Control*. London: Butterworth & Co., Ltd., Vol. 1, pp. 481-492, 1961.

[81] V. M. Terekhov, *Discrete and continuous-time control systems in electrical drives*, Moscow: Power Engineering Institute (MEI), 1989. *(In Russian).*

[82] J. W. Umland and M. Safiudin, "Magnitude and symmetric criterion for the design of linear control systems: What is it and how does it compare with the others?," *IEEE Trans. Ind. Appli.*, Vol. 26, No. 3, pp. 489-497, June 1990.

[83] B. C. Kuo, *Digital control systems*, Holt, Rinehart and Winston, Inc., 1980.

[84] K. Ogata, *Discrete-time control systems*, Englewood Cliffs, NJ.: Prentice-Hall, Inc., 1995.

[85] Y. Stepanenko, "Modal control of fast large-scale robot motions," *Trans. of the ASME- Journal of Dynamic Systems, Measurement and Control*, Vol. 109, pp. 80-87, June 1987.

[86] J. Lu, J. S. Thorp, and H. D. Chiang, "Modal control of large flexible space structures using collocated actuators and sensors," *IEEE Trans. Automat. Contr.*, Vol. 37, No. 1, pp. 143-148, January 1992.

[87] Y. A. Bortsov, N. D. Poljakhov, and V. V. Putov, *Electromechanical systems with adaptive and modal control*, Leningrad: Energoatomizdat, 1984. *(In Russian).*

[88] N. V. Kukharenko, "Modal control for DC electrical drives," *Elektrichestvo*, No. 3, pp. 48-53, March 1990. *(In Russian).*

[89] J. C. Doyle, B. A. Francis, and A. R. Tannenbaum, *Feedback control theory*, Maxwell MacMillan, NY: MacMillan, Inc., 1992.

[90] B. Wu, G. R. Slemon, and S. B. Dewan, "Eigenvalue sensitivity analysis of GTO-CSI induction machine drives," *IEEE Trans. Ind. Appli.*, Vol. 30, No. 3, pp. 767-775, June 1994.

[91] Q. P. Ha and V. G. Alferov, "On the problem of parameter sensitivity in control system of DC motor position drive," *Elektrichestvo*, No. 1, pp. 47-53, January 1996. *(In Russian).*

[92] D. G. Luenberger, "An introduction to observers," *IEEE Trans. Automat. Contr.*, Vol. 16, No. 6, pp. 596-662, December 1971.

[93] J. S. Meditch and G. H. Hostetter, "Observers for systems with unknown and inaccessible inputs," *International Journal of Control*, Vol. 19, No. 3, pp. 473-480, 1974.

[94] P. Kudva, N. Viswanadham, and A. Ramakrishna, "Observers for linear systems with unknown inputs," *IEEE Trans. Automat. Contr.*, Vol. 25, No. 1, pp. 113-115, February 1980.

[95] F. Yang and R. W. Wilde, "Observers for linear systems with unknown inputs," *IEEE Trans. Automat. Contr.*, Vol. 33, No. 7, pp. 677-781, July 1988.

[96] Y. Guan and M. Saif, "A novel approach to the design of unknown input observers," *IEEE Trans. Automat. Contr.*, Vol. 36, No. 5, pp. 632-635, May 1991.

[97] Y. Park and J. L. Stein, "Closed-loop, state and inputs observer for system with unknown inputs," *International Journal of Control*, Vol. 48, No. 3, pp. 1121-1136, 1988.

[98] M. Hou and P. C. Muller, "Design of observers for linear systems with unknown inputs," *IEEE Trans. Automat. Contr.*, Vol. 37, No. 6, pp. 871-875, June 1992.

[99] K. Ohishi, M. Nakao, K. Ohnishi, and K. Miyachi, "Microprocessor-controlled DC motor for load insensitive servo system," *IEEE Trans. Ind. Electronics*, Vol. 34, No. 1, pp. 44-49, February 1987.

[100] P. B. Schmidt and R. D. Lorenz, "Design principles and implementation of acceleration feedback to improve performance of DC drives," *IEEE Trans. Ind. Appli.*, Vol. 28, No. 3, pp. 594-599, June 1992.

[101] F. J. Chang, H. J. Liao, and S. Chang, "Position control of DC motors via variable structure systems: a chattering alleviation approach," *IEEE Trans. Ind. Electronics*, Vol. 37, No. 6, pp. 452-459, December 1990.

[102] T. Egami, H. Morita, and T. Tsuchiya, "Efficiency-optimised model reference adaptive control system for a DC motor," *IEEE Trans. Ind. Electronics*, Vol. 37, No. 1, pp. 28-33, February 1990.

[103] F. Jabbari and W. E. Schmitendorf, "A noniterative method for the design of robust linear controllers," *IEEE Trans. Automat. Contr.*, Vol. 35, No. 8, pp. 954-957, August 1990.

[104] W. C. Yang and M. Tomizuka, "Discrete-time Robust Control via state feedback for single input systems," *IEEE Trans. Automat. Contr.*, Vol. 35, No. 5, pp. 590-598, May 1990.

[105] T. S. Perry, "Lotfi A. Zadeh," *IEEE Spectrum*, pp. 32-35, June 1995.

[106] L. A. Zadeh, *Industrial applications of fuzzy control*, M. Sugeno, Ed. Amstterdam: North Holland, 1985.

[107] L. A. Zadeh, "Outline of a new approach to the analysis of complex systems and decision processes," *IEEE Trans. Syst., Man, Cybern.*, Vol. SCM-3, No. 1, pp. 28-44, January 1973.

[108] L. A. Zadeh, "Computing with words - a paradigm shift," in *Proceedings of the 1st International Discourse on Fuzzy Logic and the Management of Complexity (FLAMOC'96)*, Sydney, Australia, Vol. 1, pp. 3-10, January 1996.

[109] E. H. Mamdani, "Application of fuzzy algorithms for control of a simple dynamic plant," *Proc. of the IEE*, Vol. 121, No. 12, pp. 1585-1588, 1974.

[110] C. C. Lee, "Fuzzy logic in control systems: fuzzy logic controller- Part I & II," *IEEE Trans. Syst., Man, Cybern.*, Vol. SCM-20, No. 1, pp. 404-435, March 1990.

[111] T. T. Truong and W. Hofmann, "A new speed controller with fuzzy tuning," in *Proceedings of the IEEE 21st International Conference on Industrial Electronics, Control, and Instrumentation (IECON'95)*, Orlando, USA, Vol. 2, pp. 1484-1489, November 1995.

[112] Q. P. Ha, "PI controllers with fuzzy tuning," *IEE Electronics Letters*, Vol. 32, No. 11, pp. 1043-1044, May 1996.

[113] R. Jager, "Fuzzy logic in control," *Ph.D. thesis, Technische Universiteit Delft*, 1995.

[114] J. M. Mendel, "Fuzzy logic systems for engineering: a tutorial," *Proccedings of the IEEE*, Vol. 83, No. 3, pp. 345-377, March 1995.

[115] R. R. Yager and D. P. Filev, "Template-based fuzzy systems modeling," *J. Intell. and Fuzzy Syst.*, Vol. 2, pp. 39-54, 1994.

[116] L. A. Zadeh, "The concept of a linguistic variable and its application to approximate reasoning," *Inf. Sciences*, Vol. 8, pp. 199-249, 1975.

[117] E. Cox, *The fuzzy systems handbook*, Cambridge, MA: AP Professional, 1994.

[118] H.-J. Zimmermann, *Fuzzy set theory and its applications*, Norwell, MA: Kluwer Academic Publishers, 1985.

[119] B. Kosko, *Neural networks and fuzzy systems: a dynamical systems approach to machine intelligence*, Englewood Cliffs, NJ: Prentice-Hall, 1992.

[120] D. Dubois and H. Prade, "Fuzzy logic and the generalised modus ponens revisited," *Cybern. Syst.*, Vol. 15, No. 1, pp. 3-4, 1984.

[121] P. M. Larsen, "Industrial applications of fuzzy logic control," *Int. J. Man, Mach. Studies*, Vol. 12, No. 1, pp. 3-10, 1980.

[122] L. A. Zadeh, "The rationale for fuzzy control," *J. Dynamic Syst. Meas. Contr.*, pp. 3-4, 1972.

[123] M. Sugeno and M. Nashida, "Fuzzy control of a model car," *Fuzzy Sets Syst.*, Vol. 16, pp. 103-113, 1985.

[124] S. G. Cao, N. W. Rees, and G. Feng, "Stability analysis of fuzzy control systems," in *Proceedings of the IEEE 2nd Australian and New Zealand Conference on Intelligent Information Systems (ANZIIS-94)*, Brisbane, Australia, pp. 219-223, November 1994.

[125] T. Procyk and E. H. Mamdani, "A linguistic self-organising process controller," *Automatica*, Vol. 15, No. 1, pp. 15-30, 1979.

[126] S. Shao, "Fuzzy self-organising controller and its application for dynamic processes," *Fuzzy Sets Syst.*, Vol. 26, pp. 151-164, 1988.

[127] W. A. Kwong, K. M. Passino, E. G. Laukonen, and S. Yurkovich, "Expert supervision of fuzzy learning systems for fault tolerant aircraft control," *Proccedings of the IEEE*, Vol. 83, No. 3, pp. 466-482, March 1995.

[128] J.-S. R. Jang and C.-T. Sun, "Neuro-fuzzy modelling and control," *Proceedings of the IEEE*, Vol. 83, No. 3, pp. 378-406, March 1995.

[129] E. H. Mamdani and S. Assilian, "An experiment in linguistic synthesis with a fuzzy logic controller," *Int. J. Man Machine Studies*, Vol. 7, No. 1, pp. 1-13, 1975.

[130] R. R. Yager and D. P. Filev, *Essentials of fuzzy modeling and control*, NY: John Wiley & Sons, Inc., 1994.

[131] L. I. Larkin, "A fuzzy logic controller for aircraft flight control", in *Industrial Applications of Fuzzy Control*, M. Sugeno (Ed.), Amsterdam: North Holland, 87-104, 1985.

[132] H. Hellendoorn and C. Thomas, "Defuzzification in fuzzy controllers," *J. Intell. Syst.*, Vol. 1, pp. 109-123, 1993.

[133] J.-S. R. Jang and N. Gulley, *Fuzzy logic toolbox for use with MATLAB*, Natick, MA: The MathWorks, Inc., 1995.

[134] Negnevitsky, M., Ha, Q.P., L.P. Chee, and T.H. Ting, "A Fuzzy Logic Controller for an overhead crane," in *Proceedings of the 1st International Discourse on Fuzzy Logic and the Management of Complexity (FLAMOC'96)*, Sydney, Australia, Vol. 2, pp. 171-175, January 1996.

[135] *Fuzzy Inference Development Environment FIDE*, Ver. 2.0, User's Manual, Aptronix, 1994.

[136] J. B. Kiszka, M. M. Gupta, and P. N. Nikiforuk, "Energetistic stability of fuzzy dynamic systems," *IEEE Trans. Syst., Man, Cybern.*, Vol. SCM-15, No. 5, pp. 783-792, September 1985.

[137] V. G. Moudgal, W. A. Kwong, K. V. Passino, and S. Yurkovich, "Fuzzy learning control for a flexible-link robot," *IEEE Trans. Fuzzy Syst.*, Vol. 3, No. 2, pp. 199-210, May 1995.

[138] Y. M. Park, U. C. Moon, and K. Y. Lee, "A self-organising fuzzy logic controller for dynamic systems using a fuzzy auto-regressive moving average model," *IEEE Trans. Fuzzy Syst.*, Vol. 3, No. 1, pp. 75-82, February 1995.

[139] D. A. Linkens and H. O. Nyongesa, "Genetic algorithms for fuzzy control - Part 1&2," *Proceedings of the IEE, Part D, Control Theory Appl.*, Vol. 142, No. 3, pp. 161-185, May 1995.

[140] F. Palis, A. Buch, U. Ladra, R. Kurrich, Q. P. Ha, and M. Negnevitsky, "Robust control using neuro-fuzzy approach", in *Proceedings of the International Conference on Electrical Drives and Power Electronics (EDPE'96)*, Kosice, Slovakia, Vol. 1, pp. 194-198, October 1996.

[141] D. McNeil and P. Freiberger, *Fuzzy logic*, NY: Simon & Schuster, 1993.

[142] C. Kessler, "Das symmetrische optimum", *Regelungstechnik*, Vol. 6, pp. 395-400, 1958.

[143] J. G. Ziegler and N. B. Nichols, "Optimum setting for automatic controllers", *Trans. of the ASME- Journal of Dynamic Systems, Measurement and Control*, Vol. 64, pp. 759-768, 1948.

[144] C. C. Hang, K. J. Astrom, and W. K. Ho, "Refinements of the Ziegler-Nichols tuning formula", *Proceedings of the IEE, Part D, Control Theory Appl.*,Vol. 138, No. 2, pp. 111-118, February 1991.

[145] K. J. Astrom and T. Hagglund, "Automatic tuning of simple regulators with specification on phase and gain margin," *Automatica*, Vol. 20, No. 5, pp. 645-651, May 1984.

[146] Y. Dote, "Stability analysis of variable-structured PI controller by fuzzy logic for servo systems", in *Proceedings of the 30th IEEE Conference on Decision and Control* CDC/91, pp. 1217-1218, Brighton, UK, 1991.

[147] A. Suyitno, J. Fujikawa, H. Kobayashi, and Y. Dote, "Variable-structured robust controller by fuzzy logic for servomotors," *IEEE Trans. Ind. Electronics*, Vol. 40, No. 1, pp. 80-87, February 1993.

[148] Q. P. Ha, "A robust sliding mode controller with fuzzy tuning," *IEE Electronics Letters*, Vol. 32, No. 17, pp. 1626-1628, August 1996.

[149] D. Graham and R. C. Lathrop, "The sythesis of 'optimum' transient response: criteria and standard forms," *Trans. AIEE*, Vol. 72, Part 2, pp. 273-288, 1953.

[150] H. Ying, W. Siler, and J. J. Buckley, "Fuzzy control theory: A nonlinear case," *Automatica*, Vol. 26, No. 5, pp. 513-520, May 1990.

[151] H. Ying, "The simplest fuzzy controllers using different inference methods are different nonlinear proportional-integral controllers with variable gains," *Automatica*, Vol. 29, No. 6, pp. 1597-1589, Jun 1993.

[152] J. -J. E. Slotine and S. S. Sastry, "Tracking control of nonlinear systems using sliding surface, with application to robot manipulators", *Int. J. Contr.*, Vol. 38, No. 2, pp. 465-492, 1983.

[153] S. K. Spurgeon, "Choice of discontinuous sliding mode control", *Int. J. Contr.*, Vol. 53, No. 1, pp. 161-179, 1991.

[154] F. Zhou, and D. G. Fisher, "Continuous sliding mode control", *Int. J. Contr.*, Vol. 55, No. 2, pp. 313-327, 1992.

[155] H. T. Nguyen and D. K. Nguyen, "Continuous sliding mode control", in *Preprints of the Control 95*, Melbourne, Australia, Vol. 1, pp. 57-60, October 1995.

[156] Y. S. Lu and J. S. Chen, "A self-organising fuzzy sliding-mode controller design for a class of nonlinear servo systems", *IEEE Trans. Ind. Electron.*, Vol. 41, No. 5, pp. 492-502, October 1994.

[157] S. Y. Wang, C. M. Hong, C. C. Liu, and W. T. Yang, "Design of a static reactive power compensator using fuzzy sliding mode control", *Int. J. Contr.*, Vol. 63, No. 2, pp. 393-412, 1996.

[158] G. C. Hwang and S. C. Lin, "A stability approach to fuzzy control design for nonlinear systems", *Fuzzy sets and systems*, Vol. 48, pp. 279-287, 1992.

[159] H. A. Malki, H. Li, and G. Chen, "New design and stability analysis of fuzzy proportional-derivative control systems", *IEEE Transactions on Fuzzy Systems*, Vol. 2, No. 4, pp. 245-254, Nov 1994.

[160] A. Hansson, B. Gruber, and J. Todli, "Fuzzy anti-reset PID controllers", in *Preprints of the 12th IFAC Congress*, Sydney, Australia, Vol. 10, pp. 389-392, July 1993.

[161] J. -J. E. Slotine and W. Li, *Applied nonlinear control*, Prentice Hall: Englewood Cliffs, NJ, 1990.

[162] T. Eisaka, Y. Zhong, S. Bai, and R. Tagawa, "Evaluation of robust model matching for the control of a DC servo motor", *Int. J. Control*, Vol 50, No.2, pp. 479-493, 1989.

[163] Q. P. Ha and F. Palis, "Fuzzy logic application in a robust modal controller for position drives," in *Proceedings of the 30th Universities Power Engineering Conference (UPEC'95)*, London, UK, Vol. 1, pp. 85-89, September 1995.

[164] ABB, *Asea Brown Boveri Service Manual*, January 1984.

[165] F. Palis, A. Buch, U. Ladra, R. Kurrich, Q. P. Ha, and M. Negnevitsky, "Robust control using neuro-fuzzy approach", in *Proceedings of the International Conference on Electrical Drives and Power Electronics* (EDPE 96), Kosice, Slovakia, Vol. 1, pp. 194-198, October 1996.

[166] L. O. Hall and A. Kandel, "The evolution from expert systems to fuzzy expert systems", in *Fuzzy Expert Systems*, A. Kandel (Ed.), CRC Press, Inc., 1992.

[167] L. G. Kraft and D. P. Campagna, "Comparison between CMAC neural network and two traditional adaptive control systems", *IEEE Contr. Syst. Mag.*, pp. 36-43, April 1990.

[168] K. J. Hunt, D. Sbarbaro, R. Zbikowski, and P. J. Gawthrop, "Neural networks for control systems- A survey," *Automatica*, Vol. 28, No. 6, pp. 1083-1112, Jun 1992.

[169] T. Kohonen, *Self-Organisation and Associative Memory*, Springer-Verlag, Berlin, 1987.

[170] Y. H. Pao, *Adaptive pattern recognition and neural networks*, Addison-Wesley Publishing Company, Inc., 1989.

[171] D. E. Rumelhart, G. E. Hinton, and R. J. Williams, "Learning internal representations by error propagation", in D. E. Rumelhart and J. McClelland (Eds.), *Parallel Data Processing*, Vol. 1, M.I.T. Press, Cambridge, MA, 1986.

[172] R. Zbikowski and P. J. Gawthrop, " A survey of neural networks for control", in K. Warwick, G. W. Irwin, and K. J. Hunt (Eds.), *Neural networks for control and systems*, Peter Peregrinus Ltd., London, UK, 1992.

[173] R. Krishnan, R. Monajemy, and N. Tripathi, "Neural control of high performance drives: an application to the PM synchronous motor drive," in *Proceedings of the IEEE 21st International Conference on Industrial Electronics, Control, and Instrumentation (IECON'95)*, Orlando, USA, Vol. 1, pp. 38-43, November 1995.

[174] G. S. Buja and F. Todesco, "Neural network implementation of a fuzzy logic controller," *IEEE Trans. Ind. Electron.*, Vol. IE-41, No. 6, pp. 663-665, 1994.

[175] K. Yoshida and H. Kawabe, "A design of saturating control with a guaranteed cost and its application to the crane control system," *IEEE Trans. Automat. Contr.*, Vol. AC-37, No. 1, pp. 121-127, 1992.

[176] R. Soussi and A.J. Koivo, "Adaptive control of cranes," in *Preprints of the 12th IFAC Congress,* Sydney, Australia, Vol. 8, pp. 237-240, July 1993.

[177] S. Chen, C.F.N. Cowan, and P.M. Grant, "Orthogonal least squares learning algorithm for radial basis function networks," *IEEE Trans. Neur. Networks,* Vol. 2, No. 2, pp. 302-309, 1991.

[178] T. Poggio and F. Girosi, "Networks for approximation and learning," *Proceedings of the IEEE,* Vol. 78, pp. 1481-1497, 1990.

[179] M. Saad, P. Bigras, L. A. Dessaint, and K. Al-Haddad, "Adaptive robot control using neural networks", *IEEE Trans. Ind. Electron.*, Vol. IE-41, No. 2, pp. 173-180, Apr 1994.

[180] H. M. Tai, J. Wang, and K. Ashenayi, "A neural network-based tracking control system", *IEEE Trans. Ind. Electron.*, Vol. IE-39, No. 6, pp. 504-510, Dec 1992.

[181] S. K. Lin, "Minimal linear combinations of the inertia parameters of a manipulator", *IEEE Trans. Robot. and Automat.*, Vol. 11, No. 3, 360 - 373, 1995.

[182] T. H. Lee, C. C. Hang, L. L. Lian, and B. C. Lim, "An approach to inverse non-linear control using neural networks", *Mechatronics,* Vol. 2, No. 6, pp. 595 -611, 1992.

[183] Ch. Döschner and R. Schneider, "Ein neuronales Netz für das Erlernen der Dynamik eines Roboters", *Preprints of Otto-von-Guericke-Universität Magdeburg*, No 1, 1995.

[184] T. Kohonen, *Self-organising Maps*, Series in Information Sciences, Vol. 30, Heidelberg: Springer-Verlag, 1995.

[185] F. Palis and Th. Schmied, “Robust current and speed control of electrical drives using fuzzy set theory”, in *Proc. of the International Conference on Electrical Drives and Power Electronics*, Kosice, Slovakia, Vol. 2, pp. 237-242, 1994.

[186] D. E. Van den Bout and T. K. Miller, III, "Graph partitioning using annealed neural networks", *IEEE Trans. Neur. Networks*, Vol. 1, pp. 192-203, 1990.

[187] C. Peterson, "Parallel distributed approaches to combinatorial optimisation: Benchmark on travelling salesman problem", *Neural Computation*, Vol. 2, pp. 261-269, 1990.

[188] A. Cichocki and R. Unbehauen, *Neural networks for optimization and signal processing*, B.G. Teubner Stuttgart, John Wiley & Sons Chichester: New York, 1993.

[189] C. Daoshen and B. K. Bose, "Expert system based automated selection of industrial AC drives," in *IEEE/IAS Annu. Meet. Conf. Rec.*, pp. 387-392, 1992.

[190] Q. P. Ha, M. Negnevitsky, and Z. Man, "Dominant pole-based controller for maximal damping of multi-mass systems", to appear in *Proceedings of the 2nd Asian Control Conference (ASCC-97)*, Seoul, Korea, July 1997.

[191] F Jabbari and W. E. Schmitendorf, "Robust linear controllers using observers," *IEEE Trans. Automat. Contr.*, Vol. 36, No. 12, pp. 1509-1514, Dec 1991.

[192] Z. Man, X. Yu, and Q. P. Ha, "A study of uncertainty bound for rigid robot control systems", to appear in *Proceedings of the 2nd Asian Control Conference (ASCC 97)*, Seoul, Korea, July 1997.

[193] D. E. Thomas and B. Armstrong-Helouvry, "Fuzzy logic control - Taxonomy of demonstrated benefits," *Proceedings of the IEEE*, Vol. 83, No. 3, pp. 407-421, March 1995.

[194] Q. P. Ha and M. Negnevitsky, "Continuous variable structure systems with fuzzy tuning", submitted to *the IEEE 5th Australian and New Zealand Conference on Intelligent Information Processing Systems (ANZIIS 97)*, Dunedin, New-Zealand, November 1997.

[195] Z. Man, X. Yu, and Q. P. Ha, "Adaptive control using fuzzy basis function expansion for SISO linearisable nonlinear systems", to appear in *Proceedings of the 2nd Asian Control Conference (ASCC 97)*, Seoul, Korea, July 1997.

[196] R. Isermann, "Fault diagnosis of machines via parameter estimation and knowledge processing - tutorial paper", *Automatica*, Vol. 29, No.4, pp. 815-835, April 1993.

[197] P. M. Frank, "Fault diagnosis in dynamic systems using analytical and knowledge-based redundancy - a survey and some new results", *Automatica*, Vol. 26, No. 3, pp. 459-474, March 1990.

[198] J. Trimperley, "Incipient fault detection through neutral RF monitoring of large rotating machines," *IEEE Trans. PAS*, Vol. PAS-102, No.3, pp. 693-698, 1983.

[199] E. S. Boje, J. C. Balda, R. G. Harley, and R. C. Beck, "Time-domain identification of synchronous machine parameters from simple standstill tests," *IEEE Trans. Energy Conversion*, Vol. EC-5, pp.164-175, 1990.

[200] A. Keyhani and S. M. Miri, "Observers for tracking of synchronous machine parameters and detection of incipient faults," *IEEE Trans. Energy Conversion*, Vol. EC-1, pp.184-190, 1986.

[201] P. M. Anderson and A. A. Fouad, *Power system control and stability*, Vol. I, The IOWA State University Press, Ames, Iowa, USA, 1977.

[202] N. K. Sinha and Y. H. Kwong, "Recursive estimation of the parameters of linear multivariable systems", *Automatica*, Vol. AC-15, No. 3, pp. 471-475, 1981.

[203] G. Kreisselmeier, "Stabilized least-squares type adaptive identifiers," *IEEE Trans. Automt. Control,* Vol. AC-35, No. 3, pp. 306-310, 1990.